NASA Contractor Report 2959

High Heat Flux Actively Cooled Honeycomb Sandwich Structural Panel for a Hypersonic Aircraft

L. C. Koch and L. L. Pagel

CONTRACT NAS1-12919
DECEMBER 1978

NASA Contractor Report 2959

High Heat Flux Actively Cooled Honeycomb Sandwich Structural Panel for a Hypersonic Aircraft

L. C. Koch and L. L. Pagel
McDonnell Douglas Corporation
St. Louis, Missouri

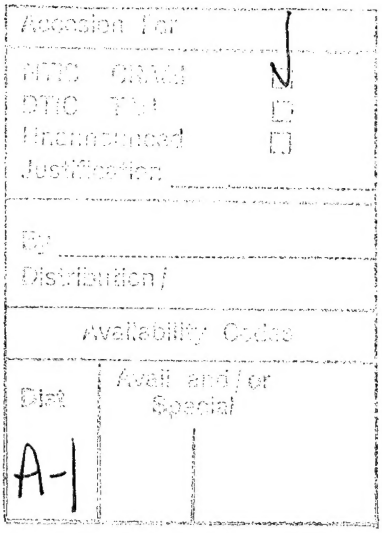

Prepared for
Langley Research Center
under Contract NAS1-12919

National Aeronautics
and Space Administration

Scientific and Technical Information Office

1978

FOREWORD

The purpose of this program was to design and optimize an actively cooled panel for a hypersonic transport aircraft; and to fabricate six fatigue specimens and a test panel for testing by NASA. The program was conducted in accordance with the requirements and instructions of NASA RFP 1-15-3785 with minor revisions mutually agreed upon by NASA and MCAIR. Customary units were used for the principal measurements and calculations. Results were converted to the International System of Units (SI) for the final report.

Mr. Leland C. Koch was the MCAIR Program Manager and Mr. David A. Ellis was Principal Investigator. Mr. L. L. Pagel was responsible for thermodynamic analyses.

TABLE OF CONTENTS

LIST OF TABLES

LIST OF ILLUSTRATIONS

LIST OF ILLUSTRATIONS (CONTINUED)

LIST OF ILLUSTRATIONS (CONTINUED)

LIST OF ILLUSTRATIONS (CONTINUED)

LIST OF ILLUSTRATIONS (CONTINUED)

SUMMARY

This program consisted of the design and optimization of a full scale, 0.61 x 6.1m (2 x 20 ft), actively cooled structural panel for a hypersonic aircraft; fabrication of six fatigue specimens (about 13 x 28 cm (5 x 11 in.)); and design and partial fabrication of a 0.61 x 1.22m (2 x 4 ft) test panel. Problems encountered in plating and soldering the coolant passages to the outer skin prevented fabrication of the test panel.

The actively cooled panel was designed to sustain for 20000 cycles (5000 x a scatter factor of 4), cyclic in-plane limit loading of ±210 kN/m (±1,200 lbf/in.) combined with a uniform panel pressure of ±6.9 kPa (±1.0 psi) while being subjected to a uniform heat flux of 136 kW/m^2 (12 BTU/ft^2sec).

The actively cooled panel configuration is a 2.95 cm (1.16 in.) thick adhesively bonded aluminum honeycomb sandwich with a 6061-T6 brazed manifold/Dee shaped (half circle) coolant tube assembly soldered to the inner surface of the 2219-T87 outer moldline skin. The inner and outer skin thicknesses are 0.041 cm (0.016 in.) and 0.102 cm (0.040 in.), respectively. The Dee coolant tubes have an 0.089 cm (0.035 in.) wall thickness and a 0.97 cm (0.38 in.) inside diameter. The skins are adhesively bonded to 49.7 kg/m^3 (3.1 lbm/ft^3) 5056-H39 aluminum honeycomb core with FM-400 film type adhesive. The honeycomb core is bonded to the Dee tubes and the manifolds with FM-404 foaming type adhesive.

Manifolds located at each end of the panel distribute the coolant into 24 Dee tubes which are parallel to the longitudinal panel edges and are spaced 2.54 cm (1.0 in) apart. The coolant, a 60/40 mass solution of methanol/water with an inlet temperature of 256K (0^oF), is pumped through the Dee tubes at a flow rate of 98.4 g/s (780 lbm/hr) per tube.

The dry mass of the optimized full scale panel is 12.78 kg/m^2 (2.62 lbm/ft^2), and the coolant inventory mass plus the auxiliary power system mass required to circulate the coolant in the panel is 2.0 kg/m^2 (.41 lbm/ft^2), for a total panel mass of 14.78 kg/m^2 (3.03 lbm/ft^2).

Fatigue specimens were fabricated by MCAIR and tested at room temperature by NASA to evaluate critical design areas and identify potential manufacturing problems. During fabrication, the silver-filled Eccobond 58C adhesive

(hereinafter referred to as "elevated temperature curing silver-filled adhesive") used to attach the coolant tubes to the outer skin was found to have unacceptably low thermal conductivity and it was replaced by a low temperature solder (91 Sn - 9 Zn). Fatigue tests confirmed that the 20,000 cycle design life could be satisfied using either solder or elevated temperature curing silver-filled adhesive.

Although fabrication and testing of the soldered fatigue specimen were successful, attempts to solder a 0.61 x 1.22m (2 x 4 ft) test panel were unsuccessful. Development of a suitable plating/soldering process was considered by NASA to be beyond the scope of the program, and test panel fabrication was terminated.

INTRODUCTION

Design of efficient structures capable of long life operation in the severe thermal environment experienced by hypersonic cruise aircraft is a difficult problem. High potential exists for structural mass reduction and cost savings if low cost and low density materials, which operate efficiently at low temperature, are used. Actively cooled structural panels have been proposed (References 1-4) as a means of achieving these goals since they are conceptually capable of handling the severe thermal environment encountered by hypersonic cruise aircraft. The active cooling concept uses a coolant which circulates, in a closed loop, though the structure then through a heat exchanger where the absorbed heat is transferred to hydrogen fuel enroute to the engines. Long life can be achieved by cooling the structure to temperatures which permit use of conventional materials such as aluminum. Although several different concepts can be configured to incorporate active cooling, the only concept considered indepth in the present study was a honeycomb sandwich with coolant passages contacting the moldline skin.

Program objectives were: (1) to add to the technology base of actively cooled hypersonic aircraft structures by designing and optimizing a representative full scale 0.61 x 6.1m (2 x 20 ft) panel for a hypersonic transport aircraft; (2) to fabricate six fatigue specimens and one 0.61 x 1.22m (2 x 4 ft) test panel for testing by NASA; and (3) to identify critical engineering and manufacturing parameters for actively cooled structures.

Design requirements were established for a panel of a hypersonic transport aircraft and trade studies conducted to determine the aluminum alloy and the coolant that would meet those criteria with minimum total mass, i.e., structural mass, plus coolant inventory mass, plus auxiliary power system mass for circulating the coolant in the panel. Several candidate aluminum alloys (2014-T6, 2024-T81, 2219-T6, 2219-T87, 6061-T6, 7075-T6, and 7475-T761) and several coolants (alcohols, glycols, coolanols, freons, and fluorochemicals) were evaluated.

The requirements, trade studies and optimizations, methods of analysis, fatigue test results, and fabrication problems for the actively cooled panel

design are summarized in the body of this report and supporting details are presented in appendices.

Certain commercial materials are identified in this paper to specify adequately which materials were used in the research effort. In no case does such identification imply recommendation or endorsement of the product by NASA, nor does it imply that the materials are necessarily the only ones or the best ones available for the purpose. In many cases equivalent materials are available and would probably produce equivalent results.

SYMBOLS AND PARAMETERS

APS	Auxiliary Power System
b	Length of panel edge, m(in.)
C_P	Specific heat, J/kg·K (Btu/lbm ^oF)
$\mathbb{C}_L$	Centerline
D	Tube inside diameter, m(in.)
da/dn	Crack growth rate, m/cycle (μin/cycle)
E	Young's Modulus of Elasticity, Pa(psi)
E'	Effective modulus of elasticity of face sheet, Pa(psi)
E_c	Effective modulus of core, Pa(psi)
F	Allowable stress, Pa(psi)
F_c	Core flatwise compression strength; or compression stress, Pa(psi)
F_{cy}	Compression yield stress, Pa(psi)
F_I	Allowable stress of inner face sheet, Pa(psi)
F_o	Allowable stress of outer face sheet, Pa(psi)
F_{tu}	Tensile ultimate stress, Pa(psi)
F_{ty}	Tensile yield stress, Pa(psi)
F_w	Face wrinkling stress, Pa(psi)
f	Fanning friction factor
G	APS conversion factor, kg/W·s (lbm/Hp-hr)
H	Distance between skin centroids m(in.)
H_D	Hydraulic diameter, m(in.)
HP	Horsepower
h	Heat transfer coefficient $W/m^2 \cdot K$ ($BTU/ft^2 \cdot hr \cdot {}^oF$)
hr	Hour
I	Moment of Inertia, $m^4(in^4)$
in.	Inch
K	Panel buckling coefficient; or stress intensity factor, $Pa\sqrt{m}$ ($ksi\sqrt{in.}$)
K_c	Critical stress intensity factor, $Pa\sqrt{m}$ ($ksi\ \sqrt{in.}$)
K_T	Loss coefficient; or stress concentration factor
k	Thermal conductivity, W/m·K ($BTU \cdot in./hr \cdot ft^2\ {}^oF$)

ksi	Thousand pound force per square inch
L	Length, m(in.)
lbf	Pounds force
lbm	Pounds mass
ML	Mold Line
$\dot{m}_c$	Coolant mass flow rate, kg/s (lbm/hr)
N	Compression load per unit length of edge N/m (lbf/in.); or cycles to fatigue failure
P	Pitch, m(in.); or pressure, Pa(psi)
Pr	Prandtl number
$\dot{q}$	Heat flux, W/m^2 (Btu/ft^2 sec)
R	Stress ratio - minimum stress divided by maximum stress
Re	Reynolds number
S	Honeycomb cell size, m(in.)
Sn	Tin
T	Temperature, K(^oF)
T_c	Local temperature of coolant, K(^oF)
$T_{M\ D}$	Temperature of outer skin midway between Dee tubes, K(^oF)
T_o	Temperature in outer skin, K(^oF)
t	Thickness, m(in.)
t_I	Thickness of inner skin, m(in.)
t_o	Thickness of outer skin, m(in.)
t_t	Thickness of Dee tube wall, m(in.)
V	Velocity of fluid m/s (ft/sec.)
W	Mass per unit area, kg/m^2 (lbm/ft^2)
Zn	Zinc
α	Coefficient of thermal expansion, m/m·K(in./in. ^oF)
δ	Initial deflection of face skin, m(in.)
Δ	Delta; or difference
μ	Poisson's ratio; or fluid viscosity, Pa·s(lbm/ft·sec)
μ_s	Fluid viscosity evaluated at wall temperature, Pa·s(lbm/ft·sec)
ρ	Density, kg/m^3 (lbm/ft^3)
ψ	Deflection due to combined edgewise and normal loadings, m(in.)
ψ_o	Deflection due to panel normal load only, m(in.)
θ	Time, hour

SUBSCRIPTS

B	Bond
C	Core; compression
c	Coolant
cr	Critical
H/C	Honeycomb
I	Inner
i	Insulation; or inlet
L	Laminar
max	Maximum
s	Skin
STR	Structure
T	Turbulent
1,2,3 etc.	Specific parameters

SI UNITS

kg	Kilogram (Mass)
K	Kelvin (Temperature)
m	Meter (Length)
N	Newton (Force)
Pa	Pascal (Pressure and stress)
s	Second (Time)
W	Watt (Power)

SI PREFIXES

m	Milli (10^{-3})
c	Centi (10^{-2})
k	Kilo (10^{3})
M	Mega (10^{6})
G	Giga (10^{9})

DESIGN REQUIREMENTS

Design requirements were based on NASA specifications, Federal Aviation Regulations (Ref. 5), experience in the design of commercial and military aircraft, and practical considerations. NASA specified design requirements are listed below.

1. Full scale panel size: 0.61 x 6.1m (2 x 20 ft).
2. Test panel size: 0.61 x 1.22m (2 x 4 ft).
3. In-plane limit load: $\pm$210 kN/m ($\pm$1200 lbf/in) parallel to long edge. Panel must withstand 5000 fully reversed load cycles.
4. Uniform pressure load on panel: $\pm$6.9 kPa ($\pm$1.0 psi) (Panel limit loads are shown in figure 1.).
5. Uniform heat flux: 136 kW/m^2 (12 $Btu/ft^2 \cdot sec$).
6. Coolant outlet pressure: at least 344.7 kPa (50 psi).
7. Support frame spacing: 0.61m (2 ft).
8. Panel design must be representative of hypersonic transport structure.
9. Fatigue and crack growth failures must be avoided.
10. Unless otherwise justified, primary structural material shall be aluminum.
11. Attachment to similar panels on all edges and to fuselage frames shall be provided.
12. Coolant manifolds shall terminate at panel edges.
13. Total panel mass (excluding frames) shall be minimized.
14. Redundant panel cooling shall be considered in the concept selection.

Additional design requirements were:

1. A scatter factor of four times the 5000 cycles service life shall be used to protect against fatigue failures in aircraft that experience a more severe than specified service-loads spectrum. A scatter factor of four is consistent with Reference 6.

2. The structure shall be designed to preclude failure and coolant leakage due to propagation of cracks from surface flaws in coolant passages and fastener holes.

3. A life of 10,000 hours exposure to maximum temperature shall be used in the panel design. This life is considerably lower than present day subsonic

transports. However, (1) a significant portion of the total life for a typical hypersonic aircraft will be spent at speeds well below the design speed, hence below the maximum temperature; and (2) the useful productivity of a hypersonic aircraft (total miles traveled during the aircraft life), because of its higher speed, will be comparable to that of a subsonic transport with much longer life.

4. Factors of safety on loads, temperatures and stresses are shown in Table 1. Since Reference 5 does not specify factors of safety for heated structures, the factors of safety for thermal stresses, temperature, and temperature gradients were based on the recommendations of Reference 7. Factors of safety greater than one are applied only to in-plane loads, panel pressures, and coolant pressures when sizing the panel to prevent failure (an ultimate strength check). The panel was designed to sustain any combination of limit loads and temperature conditions without yielding or significant permanent set, and to sustain any combination of ultimate load and temperature conditions without failure.

5. The panel surface deviation from contour of +0.051 cm (0.020 in.) and -0.102 cm (-0.040 in.) are the same as that used for the forward fuselage of the F-15, where a smooth surface is required to minimize aerodynamic drag. This flatness requirement was selected because, although surface smoothness at hypersonic speeds is not as important as it is in the Mach 0.60 to Mach 3.0 range, a hypersonic aircraft is penalized as it passes through the subsonic and supersonic region if the aircraft surface is not reasonably smooth.

FINAL FULL SCALE PANEL CONFIGURATION

A honeycomb sandwich concept with coolant tubes nested in the honeycomb core was selected after evaluating several concepts. These concepts included corrugated passages, bulge formed passages, round and square tubes, and extrusions with integral tubes in various arrangements with stiffening members. The relative masses of the three most attractive concepts are presented in Figure 2. The lower mass of the tube honeycomb concept, its ability to encapsulate the coolant passages and permit the honeycomb core to act as a leak stopper, and the simplicity of attachment to substructure and to adjacent panels resulted in selection of this concept. The Dee shape was selected to provide a large contact area (good heat conduction path) between the tube and the face sheet.

The full scale panel design is shown in Figures 3 and 4. It is a 0.61 x 6.1m (2 x 20 ft) aluminum honeycomb sandwich with coolant manifolds and 0.97 cm (0.38 in) diameter Dee (semicircle) shaped coolant tubes soldered (for good interface conductance) to the outer skin and adhesively bonded to the honeycomb core. The panel is supported by frames at 0.61m (2.0 ft) spacing. The outer face sheet is 2219-T87 aluminum 0.102 cm (0.040 in.) thick. The inner face sheet is 2219-T87 aluminum 0.041 cm (0.016 in.) thick. The distance between centroids of the inner and outer face sheets is 2.87 cm (1.13 in.). The skins are adhesively bonded to 49.66 kg/m^3 (3.1 lbm/ft^3) 5056-H39 aluminum honeycomb core with FM-400 film type adhesive (see Figure 5). FM-404 foaming type adhesive is used to bond the Dee tubes and the manifolds to the honeycomb core. Additional information on the panel materials is in Appendix A.

The manifolds, shown in Figure 6, are machined 6061 aluminum extrusions and have dual chambers. The coolant enters and exits at the panel centerline through the chamber closest to the panel ends. The ends of the manifolds are cooled as the coolant turns the corner into the second chamber and is distributed into the Dee tubes. The 6061 Dee tubes (drawn extrusions) and the end plugs are brazed to the extruded manifolds in one operation using a salt bath brazing technique. The assembly is then heat treated to the T6 condition. Figure 7 shows the tube and tube end plug details and the manifold

with the machined grooves which accept the Dee tubes. The Dee tube wall thickness of 0.089 cm (0.035 in) was picked because it was the thinnest wall available in the tube diameters of interest.

To have a smooth outer panel surface, countersunk bushings and flush fasteners (Figure 8) were used to attach the panel to intermediate frames, and subflush doublers (Figure 9) were used at the panel corners to transfer loads across the manifolds and transverse splice plates. To adequately cool the splice plates, a silver filled adhesive was used to enhance heat transfer across the splice plate/actively cooled panel interface.

The coolant is a 60/40 mass solution of methanol/water, and is pumped through the Dee tubes at a mass flow rate of 98.4 g/s (780 lbm/hr) per tube at an inlet temperature of 256K ($0^{o}F$).

The mass of the panel, including the coolant and auxiliary power system (APS) increment is 55.01 kg (121.28 lbm) or 14.78 kg/m^2 (3.03 lbm/ft^2). (The APS mass includes the hydrogen fuel and oxidizer consumed in pumping the coolant through the panel and the APS hardware). A breakdown of the panel mass is shown in Table 2. Panel temperatures and stresses in critical areas and structural and thermodynamic models are presented in Appendix B.

PANEL COOLANT PASSAGE REDUNDANCY

The need for coolant passage redundancy (two independent coolant loops) was qualitatively assessed. Preliminary investigations indicated it is practical to provide redundancy by using two independent cooling loops. However, safe and reliable operation can also be assured without redundant coolant passages, provided there is an adequate supply of coolant at the manifold inlet and the panel is designed to prevent surface flaw growth through the thickness of the coolant passages in the life of the airplane.

The Dee tube/honeycomb sandwich panel design incorporates many features that provide a high degree of damage tolerance and safety. These include:

1. Encapsulation of the coolant tubes by the honeycomb core and face sheets to prevent unrestricted leakage if a crack or fracture in a tube occurs.

2. With independent tubes (separate from the outer skin), the growth of cracks from skin to tube and from tube to skin is inhibited because the stress intensity at the crack tip is greatly reduced when the crack propagates to the softer material (adhesive or solder) at the tube to skin joint.

3. Low stress levels in the manifolds ensure slow crack growth and increase the probability of detecting leaks before catastrophic failure occurs.

With these features, a panel with nonredundant coolant passages, could be assured of safe and reliable operation if there is an adequate supply of coolant. Therefore, a nonredundant coolant passage approach was selected for the actively cooled panel.

PANEL DESIGN PROCEDURE

1. OPTIMIZATION

The objective of the optimization process was to define the variables shown in figure 10 such that the mass of the inner and outer skins, the Dee tubes, the honeycomb core, the coolant inventory in the passages, plus the auxiliary power system (APS) mass was as low as practical. Additional variables were defined during the optimization process and they are discussed in the following optimization steps. Figure 11 shows, in schematic form, the optimization process. Trend studies used in the optimization process result in a low, but not necessarily a mathematically precise minimum mass configuration. Furthermore, items such as manifolds, splices, and joint details were not included in the optimization process, but were sized for low mass based on practical considerations.

STEP 1. Materials and coolants that met the design criteria were identified and evaluated. (Appendix A gives details of the materials and coolant selection.) The 6061-T6 aluminum alloy was chosen for the cooling passages because it is the highest strength alloy which can be brazed and welded, and it is available in drawn shapes. The 2219-T87 and 2024-T81 aluminum alloys were the best candidates, based on strength requirements for the basic structure. A fracture mechanics analysis showed for a life of 20,000 cycles, 2219-T87 could operate at a higher stress than 2024-T81; thus 2219-T87 was selected for the face sheet material.

Six commonly used heat transport fluids with freezing points below 222K (-60^{o}F) and boiling points above 339K (150^{o}F) were considered to assess the impact of coolant selection on panel mass. Aqueous solutions of glycol or methanol were selected for coolant candidates since a figure-of-merit based on mass of the coolant in the passages plus the APS mass showed that nonaqueous coolants have significant mass penalties compared to glycol or methanol.

STEP 2. Preliminary thermal sizing relations (Figure 11, Step 2) between outer skin thickness, temperature difference in the outer skin, Dee tube pitch (spacing between tube centers), and Dee tube diameter were developed.

The relations were kept simple to rapidly assess trends and screen the many variables. Only one-dimensional heat conduction in the outer skin was modeled, and a relation was derived between diameter and pitch for a specific coolant, and coolant temperature rise and exit velocity. No explicit constraint on outer skin temperature is in the preliminary thermal relations. As seen in Figure 11, Step 2, tube diameter increases with pitch. The relations were refined in Step 4. (Details are given in Appendix B.)

STEP 3. Sensitivities of structural mass (skins, honeycomb, and Dee tubes) to outer skin temperature differences, skin thicknesses, Dee tube diameter and pitch, and honeycomb core height were calculated. A structural optimization program iterated on core height to give a minimum mass configuration with all failure modes satisfied. The failure modes addressed in the analysis include basic strength; local instability, such as face sheet wrinkling and face sheet dimpling; and overall panel buckling, including beam column effects. The beam column analysis included the effects of normal pressures and panel eccentricities, coupled with the uniaxial inplane loading. The allowables and the mechanical stresses were computed using the methods of Reference 8. Thermal stresses were calculated and were superimposed on the mechanical stresses. More refined thermal analyses, Step 4, gave more accurate thermal stresses. (Details of the analyses are discussed in Appendix B.)

Figure 11, Step 3 shows the structural mass trends. Although the mass decreases with decreasing pitch, a 2.54 cm (1.0 in) pitch was selected since it is the practical minimum that left room for fastener penetration.

STEP 4. The mass sensitivity results in Step 3 are functions of the coolant and its inlet and outlet temperatures. The sensitivity of the APS mass plus coolant inventory mass to coolant inlet temperature was determined for three candidate coolants: methanol/water, ethylene glycol/water, and propylene glycol/water (60/40 mass ratios). The sensitivity study showed (shown schematically in Figure 11, Step 4) that methanol/water gave a 33% lower APS and coolant inventory than ethylene glycol/water. Methanol/water also gave a 40% lower flow rate, a 55% lower pressure drop, and resulted in about a 5% lower panel mass than ethylene glycol/water. On these bases, methanol water was selected for the coolant.

For the coolant evaluations, a detailed three-dimensional finite difference model of the outer skin and Dee tube was used instead of the one dimensional conduction assumption used in the Step 2 calculations. The analysis accounted for laminar, transitional, and turbulent flow, and showed that heat conduction in the flow direction was not significant. A two dimensional model of the outer skin, tubes, honeycomb, and inner skin showed that heat transfer through the honeycomb was small and did not significantly change the outer skin temperature. Thermal stresses were calculated from the refined temperature distributions by the methods of Reference 9 and 10. The detailed stresses were used to update the structural optimization routine described in Step 3.

STEP 5. The mass sensitivity of the structure (skins, tubes, and honeycomb), APS, and coolant inventory to outer skin temperature, T_{MID}, are shown schematically in Figure 11, Step 5. For a given t_o, P, and D, the coolant inventory is constant, and the structural mass is nearly constant except for an increase at elevated temperatures due to reduced material allowables. The APS mass decreases rapidly as outer skin temperature increases and results in a minimum total panel mass at the optimum T_{MID}.

Since the total panel mass does not decrease significantly for T_{MID} greater than 422K ($300^{o}F$), this temperature was selected as a maximum outer skin temperature.

STEP 6. With the optimum outer skin temperature, T_{MID}, defined, total panel mass sensitivities to outer skin thickness and Dee tube diameter were calculated. As shown in Figure 11, Step 6 (and in agreement with the results of Step 3), the mass decreases with decreasing outer skin thickness and with decreasing tube diameter. The optimum diameter and outer skin thickness were input to the structural optimization program described in Step 3, and the optimum inner skin thickness and core height were selected. Table 3 shows the panel and operating variables defined during the optimization process.

2. DESIGN OF PANEL DETAILS.

After the honeycomb sandwich panel was optimized, panel details were sized to minimize their mass. Panel details include: (1) transverse splice plates; (2) longitudinal splice plates; (3) honeycomb core bushings to prevent core crushing at attachments; (4) longitudinal edge closures angles;

(5) corner splice plates; (6) intermediate frames; (7) manifolds; (8) adhesives; and (9) fasteners. These details are discussed further in Appendix B.

3. IN-DEPTH ANALYSIS.

In-depth thermal and stress analyses indicated that the final panel design -- optimized configuration and panel details -- met all the design criteria. Items determined in the in-depth analyses included (1) manifold pressure drop and flow uniformity; (2) manifold and splice-plate temperatures; (3) sensitivity of panel temperatures to variations in bondline conductance values; (4) thermal stresses in the panel skin/tube area and near the entrance and exit manifolds of the panel; (5) bolt bearing shear and bending stresses, flange bending stress due to bolt clamp-up, shear stress in the adhesives, honeycomb core crushing stress, and flat plate bending stresses; (6) growth of surface cracks in the tubes and cracks at fastener holes in the skins; and (7) effect of manufacturing eccentricities on panel stability.

A discussion of the indepth analyses techniques is presented in Appendix B with a discussion of the finite element model used to verify the optimized panel configuration.

FATIGUE SPECIMENS

Fatigue specimens were designed and fabricated by MCAIR and tested by NASA to evaluate the structural integrity of critical areas of the panel and to identify any design deficiencies. Six fatigue specimens were fabricated, two each of the three representative areas shown in Figure 12. A basic skin specimen was selected to demonstrate the ability of the aluminum skin to sustain the design stress levels for the life of the panel. A skin/Dee tube/manifold specimen was selected to evaluate the brazed tube/manifold interface area, and to observe crack growth in the outer skin near the Dee tubes. A corner splice specimen was selected because of the complexity of the panel corner area where the transverse and lateral splice plates intersect and transfer loads to adjacent panels.

Some details of the specimens differed from the full scale panel design: (1) the 2024-T81 alloy was substituted for the 2219-T87 aluminum face sheets because of unavailability of 2219-T87; reoptimization using reduced allowables for 2024-T87 led to increasing the inner face sheet thickness, t_I, from 0.041 cm (0.016 in) to 0.064 cm (0.025 in); (2) dee tubes were formed from round tubing (see Figure 13), resulting in a shape not exactly semi-circular; (3) the coolant manifolds were fabricated as a three piece weldment, Figure 14, and not as an extrusion; and (4) on one skin/Dee tube/manifold specimen a low temperature solder was substituted for the adhesive originally specified to bond the outer skin to the Dee tube/manifold assembly.

The fabricated fatigue specimens are shown in Figures 15, 16, and 17. The design limit loads applied to each specimen type are shown in Figure 18. The resulting stresses correspond to the maximum limit stresses that are developed in a full scale panel when subjected to the critical combination of thermal, pressure, and in-plane loads.

All specimens were tested at room temperature. The Dee tube specimens were pressurized with hydraulic fluid to approximate the design pressure, 530. kPa (76.8 psi). All specimens (except one corner splice fatigue specimen that was destroyed by a testing machine failure) successfully sustained 20,000 inplane load cycles without failure. Tests with the corner splice specimen showed that (1) the honeycomb could contain an internal leak, and (2) the

single row of fasteners did not provide adequate clamp-up of the splice plates. (For the test panel design, tolerances were tightened on the fastener holes in the lateral splice plate area, and webs were added between the manifold flanges at the fastener locations, see Figure 4.)

Tests with the skin/Dee tube/manifold specimen showed that (1) cracks in the outer skin propagated past the tubes without penetration for both the bonded and soldered specimens; and (2) the Dee tubes served as crack arrestors, temporarily stopping crack growth. A discussion of the specimens and the tests and the test results, are presented in Appendix C, and a more extensive discussion is presented in Reference 11.

TEST PANEL

A schematic of the test panel, load adapters, and support frames is shown in Figure 19. The test panel is representative of a section at the end of the full scale panel. The test panel is 0.61 x 1.22m (2 x 4 ft) and is supported by three support frames at 0.61m (2 ft) intervals. The in-plane loads are applied to the panel through 2.54 cm (1.0 in.) thick aluminum load adapters attached to the panel's transverse splice plates by a series of titanium links. The links are required to minimize thermal stresses which result from differential expansion between the loading grips and the panel. The load adapters are insulated to ensure proper simulation of the temperatures by minimizing heat loss to the environment and are designed to provide uniform application of the in-plane running loads.

Thermal and structural analyses indicated that the test conditions would simulate the full scale panel inlet and exit conditions if coolant inlet temperatures, pressures, and mass flow rate were modified to compensate for differences between the test panel and the full scale panel design. These differences included (1) use of ethylene glycol/water instead of methanol/water as the coolant; (2) the different interface conductance between the Dee tubes and the outer skin resulting from the higher thermal conductivity of the solder; and (3) the heat sink effects of the large load adapters and the massive test apparatus. Details of these analyses are presented in Appendix D.

Although several components of the test panel were fabricated, the test panel was not completed because of inability to attach the manifolds and Dee tubes to the outer skin using the low temperature soldering process. The fabrication process and photographs of some of the fabricated components are presented in Appendix E.

FABRICATION PROBLEMS

Problems were encountered in fabricating the fatigue specimens and the larger 0.61 x 1.22m (2 x 4 ft) test panel. Specifically, the problems were (1) obtaining an undistorted, leak free, brazed tube-manifold assembly; and (2) providing a high thermal-conductance structural joint between the tube-manifold assembly and the face sheet. These problems were successfully overcome for the fatigue specimens; however, after numerous unsuccessful attempts to fabricate two test panels, the effort was terminated.

The braze problems resulted from temperature differences, hence differential thermal expansion, between the Dee tubes, manifolds, and brazing support fixture as the assembly was removed from the hot brazing salts. The resulting relative motion (in effect) caused poor fit-up during solidification of the braze alloy, and resulted in porous joints and distorted tubes. The porosity problem was overcome by improving the brazing support fixturing. The distorted tubes were hand straightened after heat treating but before aging; however, the distortions degraded the fit-up with the outer skin and compounded the problem of obtaining high thermal conductance in the interface joint.

For bonding the tube-manifold assembly to the outer skin, an elevated temperature curing silver-filled adhesive was initially selected because of its reported high thermal conductivity, (Thermal conductivity greater than 28.8 W/m•K (200 BTU-in/hr-ft^2-^{o}F) see Ref. 12). However, the discovery of voids in the adhesive layer during fabrication of the fatigue specimens led to testing which revealed that the thermal conductivity and peel strength of the adhesive were lower than expected. Appendix A presents the results of these tests and also of attempts to improve the conductivity and peel strength of the adhesive. As a result of the inability to increase the thermal conductivity of the elevated temperature curing silver-filled adhesive to an acceptable value, it was replaced with a low temperature solder (91 Sn-9 Zn).

One skin/Dee tube/manifold specimen, Figure 16, was fabricated using the low temperature solder. Achieving good solder wetting of the surfaces was difficult and required careful control of the plating and the soldering temperature profile. In general, randomly dispersed voids throughout the

solder were expected. The voids resulted from outgassing of the organic flux and were exaggerated in areas with large overlaps. Temperature uniformity in the components during the solder heating cycle was also identified as a critical factor. However, despite the voids, the thermal conductivity of the solder is high enough to maintain panel temperatures within design limits.

Numerous attempts were made to solder two outer skin-tube/manifold test panel assemblies. The parts to be soldered first had to be plated. MCAIR facilities, used to plate the fatigue specimen, were not large enough to accommodate the outer skin and tube/manifold. Therefore, plating was done by local vendors. The vendors plating processes were not identical to the process used by MCAIR on the fatigue specimen. However, after analyzing the vendors process it was concluded that the alternate processes would yield acceptable results.

Lack of success in soldering the first panel was attributed to nonuniform panel temperatures during the soldering heating cycle. An attempt was made to salvage these panel parts by desoldering, cleaning, replating and resoldering. However, the parts were damaged beyond repair during replating operations and they were scrapped. Parts were made for a second panel and a second attempt was made to solder an assembly using a different heating arrangement and plating processes (see Appendix E). The desired temperature uniformity and soldering heating cycle was obtained; however, nondestructive evaluation of the soldered assembly revealed voids in the skin-to-manifold areas (5% to 10% wetting at the inlet manifold and 30% to 40% wetting at the exit manifold), some tubes that were unsoldered, and randomly dispersed intergranular hairline cracks in the Dee tubes. Photomicrographs and metallurgical analyses revealed a breakdown of the alloys used to tin the surfaces of the 6061-T6 aluminum. This was considered as a possible major contributor to the gross lack of wetting. The cause of the intergranular cracking of the 6061 aluminum was never isolated. Several attempts to duplicate the problems with small subscale element specimens were unsuccessful. Appendix E presents a discussion of the soldering procedure, the tinning operation, the method of heating, and post-soldering evaluation of the panel.

CONCLUDING REMARKS

This report presents the results of a program to add to the technology base for active cooling of hypersonic aircraft structure by designing and optimizing a full scale 0.61m by 6.1m (2 ft by 20 ft) panel for a hypersonic transport aircraft and by fabricating and testing small fatigue specimens and a 0.1m by 1.22m (2 ft x 4 ft) panel. Because of fabrication problems, the test panel was not built.

The design goal was a minimum mass full scale panel that would sustain 2000 cycles (5000 x scatter factor of 4) of $\pm$210 kN/m ($\pm$1200 lbf/in.) inplane loading combined with a $\pm$6.89 kPa ($\pm$1.0 psi) uniform pressure while subjected to a 136 kW/m^2 (12 BTU/ft^2 sec) uniform heat flux. The panel concept developed was an adhesively bonded aluminum honeycomb sandwich, with manifolds and Dee shaped coolant tubes nested in the honeycomb core and soldered to the outer mold line skin. The honeycomb was sized to withstand coolant pressure in event of a leak. The panel unit mass is 14.78 kg/m^2 (3.03 lbm/ft^2).

Some specific conclusions derived from this study are as follows:

When an actively cooled structure is subjected to a high heat flux, a structural joint with high interface conductance between the thermally exposed mold line skin and the cooling passages is required. This requirement significantly complicated panel fabrication. Specifically, the peel strength and thermal conductivity of the silver-filled adhesive, initially selected for the skin to cooling passage joint, were found experimentally to be inadequate. Soldering the outer skin to the tube/manifold assembly gave adequate thermal conductivity and peel strength despite voids randomly dispersed throughout the solder.

Small scale components were successfully soldered. However, scaling up to larger components, such as the 0.61m x 1.22m (2 ft x 4 ft) test panel, requires considerably more care in the control of temperature profiles, component temperature uniformity, and control of gaps between the mating surfaces to be soldered. And careful selection of the alloys used to plate panel components, plus close control of the plating process are required to obtain adequately soldered joints.

Total panel optimized mass (skins, honeycomb core, Dee tubes, coolant inventory, and auxiliary power system (APS)) is minimized, for 10,000 hour exposure duration, by operating at approximately a 422K ($300^{o}F$) maximum outer skin temperature. A 60/40 (mass ratio) solution of methanol/water resulted in a 33% reduction in coolant inventory and APS mass, which gives a 5% reduction in total panel mass; a 40% reduction in coolant mass flow rate; and a 55% reduction in panel pressure drop compared to the nearest competing coolant, ethylene glycol/water.

Fatigue tests, at room temperature, on specimens representative of critical design areas of the full scale panel showed excessive motion of the transverse panel joint with a single row of fasteners. The tests led to the design change of tightening fastener hole tolerances, and thickening transverse joint details. The fatigue tests showed that the honeycomb sandwich structure can contain the coolant if a coolant passage fails. The fatigue tests showed that cracks induced in the face sheet propagated past the cooling passages without entering the cooling tube wall for the cooling tubes either adhesively bonded or soldered to the skins. All fatigue specimens (except one that was accidentally destroyed) successfully sustained 20,000 inplane design load cycles at room temperature without failure.

APPENDIX A

MATERIALS

A.1 METALS

Material property data were collected for seven candidate aluminum alloys: 2014-T6, 2024-T81, 2219-T6, 2219-T87, 6061-T6, 7075-T6, and 7475-T761. Plots of the strength efficiencies (F_{tu}/ρ, F_{ty}/ρ, and E_{cy}/ρ), stiffness efficiency (E_c/ρ), crippling efficiency ($E_c^{.225} F_{ty}^{.325}/\rho$), and face sheet wrinkling efficiency ($E_c^{.333}/\rho$) for long time exposure (10,000 hours) at temperatures up to 589K (600°F) are presented in Figures 20 through 25. Figure 26 shows the variation in coefficient of thermal expansion vs temperature for the candidate materials. Room temperature stress intensity factors, K_c, are compared in Figure 27. Elevated temperature K_c data were not available for any of the candidate materials.

Crack growth rates, da/dn, for five of the material candidates are presented in Figure 28 versus ΔK (change in stress intensity factor). These data are for thin sheets at room temperature and a stress ratio (minimum stress divided by maximum stress) of minus one (R=-1).

Fatigue F_{max}-N curves for an R=-1, T=422K (300°F), and stress concentration factors (K_T) of 1.0 and 4.4 are presented in Figure 29. Elevated temperature F_{max}-N curves for K_T = 4.4 were not available for all materials. Consequently, materials could not be compared on a consistent basis.

Table 4 presents a relative rating of the material candidates at four different temperatures: room temperature, 394K (250°F), 422K (300°F), and 533K (500°F). The 394K (250°F) and 422K (300°F) temperatures were representative of probable normal operating temperatures for the panel. The evaluation of 533K (500°F) was made based on short time exposure, corresponding to a failed condition. An index rating of one is the best, and all other ratings were computed by ratioing the allowables to the material with the highest allowable in each category. The advantages and disadvantages are also listed for each material. This table shows that 2024-T81 and 2219-T87 are the most attractive face sheet candidates.

Figure 30 shows the fatigue allowables for R=-1 and a life of 20,000 cycles versus K_T for 2024-T81 and 2219-T87 at room temperature and 422K ($300^{o}F$).

Figure 31 shows the K_c data used for 2219-T87 at different temperatures and extrapolated to a K_c of 69.2 MPa $\sqrt{m}$ (63 ksi $\sqrt{in.}$) at 422K ($300^{o}F$). Since these were the only available K_c versus temperature data, the same shape curve was used for 2024-T81 passing through K_c = 50.6 MPa $\sqrt{m}$ (46 ksi $\sqrt{in.}$) at room temperature and extrapolated to a K_c of 30.8 MPa $\sqrt{m}$ (28 ksi $\sqrt{in.}$) at 422 K ($300^{o}F$).

Maximum allowable stress levels were developed which satisfied the requirement that cracks growing from the edge of fastener holes would not grow to a critical length in 20,000 cycles. The stress levels were developed based on an initial flaw size of 0.013 cm (0.005 in.), an infinitely wide plate and a stress ratio of minus one (R=-1). The initial flaw size was based on the results of a study of probable flaw sizes in holes in F-4 airplane wing skins. The results of the fracture mechanics analysis are presented in Figure 32, and show that the 2219-T87 material achieves the required 20,000 cycle life with a maximum stress level of 124.1 MPa (18,000 psi) and the 2024-T81 material at 106.9 MPa (15,500 psi). As a result of this material evaluation, 2219-T87 was selected as the material for the face sheets.

The selected material for the tubing and manifolds was 6061-T6, because it is weldable, brazable, and resistant to corrosion; has high fracture toughness; and has better mechanical properties than the other weldable tubing material candidates considered, 5052-H32, 5052-H34, and 5086-H34. Aluminum alloy 5056-H39 hexagonal cell honeycomb was chosen because it can be used at higher temperature (up to 478K ($400^{o}F$)) than other aluminum honeycombs that were considered.

A.2 COOLANTS

Six commonly used heat transport fluids with freezing points below 222K ($-60^{o}F$) and boiling points above 339K ($150^{o}F$) were evaluated in assessing the impact of coolant selection on panel mass. These are:

1. 60/40, by mass, methanol/water solution.
2. 60/40, by mass, ethylene glycol/water solution.
3. 60/40, by mass, propylene glycol/water solution.

4. Monsanto "Coolanol 15."

5. 3M fluorochemical "FC-75."

6. DuPont "Freon 114B2."

Coolant property data (density, specific heat, thermal conductivity, viscosity, and vapor pressure) for each of the above coolants is presented in Figures 33 through 37.

Based upon an initial coolant evaluation, it was found that the use of nonaqueous coolants (Monsanto "Coolanol 15", 3M fluorochemical "FC-75" and DuPont "Freon 114B2") result in a 2.93 kg/cm^3 (.60 lbm/ft^2) penalty, relative to aqueous glycol and alcohol solutions and consequently were eliminated from further consideration.

A.3 JOINING MATERIALS

The mechanical and thermal property data for the adhesives and a low temperature solder considered for the actively cooled panel are presented in Table 5. All of the data except the shear and peel strength data for FM-400 and FM-404 were developed in this program. The strength data for FM-400 and FM-404 were obtained from in-house tests.

The FM-400 film type adhesive is used to bond the panel skins to the honeycomb core. The FM-404 foaming type adhesive is used to bond the Dee tubes and manifolds to the honeycomb core. Eccobond 56C, a room temperature curing silver filled paste adhesive, is used under the panel's lateral and longitudinal splice plates to enhance heat conduction away from these areas.

An elevated temperature curing silver-filled paste adhesive, was first selected to attach the outer skin to the coolant passages. However, the adhesive was discarded when it was found to have a low peel strength and a lower thermal conductivity than reported by the vendor (see note 3, table 5). This adhesive was ultimately abandoned after attempts to improve the peel strength and thermal conductivity (see Table 6) by mixing different percentages of a diluent (5% and 25% Methyl Ethyl Keytone) and by adding a fine mesh aluminum or nylon screen failed to eliminate voids in the adhesive. (The voids resulted from entrapped air.) The aluminum screen impregnated with the elevated temperature curing silver-filled adhesive showed the most promise, with the peel strength doubling to 0.35 kN/m (2 lbf/in.) and the thermal conductivity tripling to 3.17 W/m^2K (22 Btu-in/hr $ft^2{}^oF$). However,

the corresponding interface conductance was only 8.34 $kW/m^2 \cdot K$ (1467 $Btu/hr \cdot ft^2 \cdot {}^oF$) compared to the required design value of 18.9 $kW/m^2 \cdot K$ (3333 $Btu/hr \cdot ft^2 \cdot {}^oF$). Analysis showed, reference Table 6, that this would result in the temperature in the outer skin at a location midway between Dee tubes and near the panel exit, of 442K (335°F) which was above the design value of 422K (300°F).

The investigation of alternate means of attaching the outer skin to the coolant passages resulted in the selection of a low temperature solder (91Sn-9Zn) as the most promising candidate. It had, reference Table 6, a thermal conductivity greater than 57.65 $W/m^2 \cdot K$ (400 $Btu/in./hr \cdot ft^2 \cdot {}^oF$) a peel strength of 3.5 kN/m (20 lbf/in.), and good shear strength.

The 91Sn-9Zn solder is classified as a low temperature solder because it melts at 472K (390°F) and wets the faying surfaces at 500K (440°F). This was a major consideration in selecting this solder material. Soldering at higher temperatures would degrade the mechanical properties of the outer skin and the tube/manifold assembly. Additional information on the soldering process is given in Appendix C and Appendix E.

The Dee tubes were salt bath brazed to part of the manifold detail using Alcoa 718 braze foil. The remaining manifold details were welded with 4043 aluminum filler rod. (See Figure 14.)

APPENDIX B

FULL SCALE PANEL DESIGN PROCEDURE

B.1 OPTIMIZATION.

The objective of the optimization process was to define the panel variables such that the mass of the inner and outer skins, the Dee tubes, the honeycomb core, the coolant inventory in the passages, plus the auxiliary power system (APS) increment was as low as possible. (The APS mass includes the hydrogen fuel and oxidizer consumed in pumping the coolant through the panel and the APS hardware). Trend studies used in the optimization process resulted in a low, but not necessarily a mathematically precise minimum mass configuration. Furthermore, items such as manifolds, splices, and joint details were not included in the optimization process, but were sized for low mass based on practical considerations. These details are discussed in B.2 of this appendix.

Figure 11 shows in schematic form the optimization process. STEP 1, Materials Identification, was discussed in Appendix A. In STEP 2, preliminary thermal sizing relations between the outer skin thickness (t_o), temperature difference in the outer skin (ΔT_o) (to approximately account for thermal stresses), Dee tube pitch (P), and Dee tube diameter (D) were developed. The relations were kept simple to rapidly assess trends and screen the many variables.

Equation (1) gives an exact solution for one-dimensional heat conduction in a constant heat flux environment:

$$\left(\frac{P-D}{2}\right) = \sqrt{\frac{2k\ t_o\ \Delta T_o}{\dot{q}}} \qquad (1)$$

This equation accounts for heat conduction in the outer skin between cooling tubes assuming that the inner surface is adiabatic. The term $\left(\frac{P-D}{2}\right)$ is used rather than one-half the pitch (P/2) because it is assumed that the skin is isothermal over the distance (D) where the skin is in contact with the tube.

A relation between P and D is obtained by noting that all the heat which impinges on a panel segment that is P wide and L long must be absorbed by the

coolant. Thus:

$$\dot{q} \cdot P \cdot L = \dot{m}_c \cdot C_p \cdot \Delta T_c \qquad (2)$$

For a semi-circle:

$$\dot{m}_c = \rho_c \cdot V_c \cdot \frac{\pi D^2}{8} \qquad (3)$$

Combining equations (3) and (2) gives:

$$P = \left(\frac{0.393\ \rho_c \cdot V_c \cdot C_p \cdot \Delta T_c}{\dot{q} \cdot L} \right) D^2 \qquad (4)$$

Since $\dot{q}$ and L are specified design requirements, Equation (4) can be evaluated for a particular coolant, given inlet and outlet coolant temperatures, and a given coolant velocity.

The results of the preliminary thermal analysis, given in Figure 38 are for a specific coolant and flow conditions which were not the final conditions. However, the results provided approximate interdependence between P, D, t_o, and ΔT_o suitable for preliminary stress analyses. No explicit constraint on T_{MID} is in Figure 38; however, with V = 3.05 m/s (10 ft/sec), the maximum T_{MID} is approximately 422K (300^{o}F) for $\Delta T_o \leq$ 56K (100^{o}F) (based on previous estimates).

STEP 3. Sensitivities of structural mass (skins, honeycomb, and Dee tubes) to outer skin temperature differences, skin thickness, Dee tube diameter and pitch, and honeycomb core height were calculated.

A computer program was used to aid in the structural optimization (and in the materials evaluation). The failure modes addressed in the analysis include basic strength; local instability, such as face sheet wrinkling and face sheet dimpling; and overall panel buckling, including beam column effects. The beam column analysis included the effects of normal pressures and panel eccentricities, coupled with the uniaxial inplane loading. The allowables were computed using the equations delineated in Reference 8.

Face Sheet Wrinkling:

$$F_w = \frac{0.82\sqrt{\frac{E_c E' t_s}{t_c}}}{1.0 + 0.64\frac{\delta E_c}{t_c F_c}}$$

Panel Buckling:

$$N_{cr} = K\frac{\pi^2 E_s I}{b^2}$$

Face Sheet Dimpling:

$$F_c = \frac{2.0 E_s t_s^2}{S^2(1-\mu^2)}$$

Beam Column Effects:

$$\psi = \frac{\psi_o}{1 - N/N_{cr}}$$

The panel was analyzed as a continuous panel on multiple nondeflecting supports. The strength checks treated the panel as fixed (zero slope) along the loaded edges and free along the unloaded edges. The panel was checked where the maximum stresses occurred, i.e., at the supports and at midspan, for the critical combination of completely reversible inplane loads and normal pressures. Panel beam column checks made for the inplane loading only treated the panel as simply supported at the transverse supports and free along the unloaded edges, with an initial manufacturing eccentricity, at midspan, of 0.102 cm (0.040 in.). For the combination of inplane loading and normal pressures, the beam column analysis treated the panel as fixed at the transverse supports and added the deflections, at midspan, due to the normal pressures to the assumed maximum 0.102 cm (0.040 in.) manufacturing eccentricities.

The basic assumptions used in the analysis of the panel are as follows:

- Poisson's ratio for the face sheets and tubes is 0.3.
- The inplane stiffness of the honeycomb core is neglected.
- The facings and tubes are isotropic materials.
- The panel buckles before plastic behavior occurs.

The mass optimization of the panel was an iterative process in that preliminary thermal stresses were computed, for a given cross section, and superimposed on the mechanical stresses. Thermal stresses were calculated considering the temperature of each element of the thermal stress model. These elements include the outer skin, tubes and inner skin. The resulting

stresses were compared to the allowables and if they were less, the geometry was modified in an attempt to reduce the mass. The thermal stresses were then recalculated for the new geometry and the process was continued until convergence was achieved.

The results are shown in Figure 39 and 40. Figure 39 shows that the mass: (1) decreases with decreasing outer skin thickness for a given pitch and diameter; (2) decreases with decreasing diameter for a given pitch; and (3) decreases with decreasing pitch. A minimum pitch of 2.54 cm (1.0 in.) was selected to leave enough room, even with adverse tolerances, for fastener penetration between Dee tubes (see Figure 8 for size of fasteners). The Dee tube wall thickness of 0.089 cm (0.035 in) was picked because it was the thinnest wall available in the diameters of interest. Thinner tube walls would not reduce mass because the tubes carry their share of the panel load. Thus, skins would have to be made thicker to make up for thinner tube walls. Also, the tube wall had to be thick enough to prevent surface flaw penetration before 20,000 load cycles.

The results in Figure 39 are coolant dependent to the extent that the coolant properties influence T_{MID}. For each P, D, and t_o there exists a unique combination of inner skin thickness (t_I) and panel thickness (H) that yields a minimum mass structure. Figure 40 shows the typical variation of structural unit mass and H versus t_I for a given P, D, and t_o.

STEP 4. The sensitivity of the APS mass plus coolant inventory mass to coolant inlet temperature was determined for three candidate coolants: methanol/water, ethylene glycol/water, and propylene glycol/water (60/40 mass ratios).

Detailed thermal analyses, used in panel optimization and coolant selection studies, employed a three-dimensional finite difference computer program with a fluid flow subroutine. The full scale panel thermal model used in the coolant evaluation study is presented in Figure 41. In addition to the nodes required to define the model an additional node was used to regulate coolant inlet temperatures. Along with the physical dimensions, the thermal model also defined materials, external heating or cooling conditions, and the modes of heat transfer between nodes. Since all thermal resistance and capacitance terms are recomputed for each time step calculation, material property

varia ions with temperature are fully accounted for. Analyses with the therm l model in Figure 41 showed that longitudinal (coolant flow direction) condu tion is less than 0.1% of the lateral conduction and can be neglected.

aminar and turbulent coolant side heat transfer coefficients for each fluid volume element are computed from the expressions of References 13 and 14 respe tively, as follows:

$$\text{aminar:}\quad h_L = 1.86 \frac{k}{H_D} \left[(Re)(Pr)\left(\frac{H_D}{L}\right)\right]^{1/3} \left(\frac{\mu}{\mu_s}\right)^{0.14} \tag{5}$$

$$\text{urbulent:}\quad h_T = 0.027 \frac{k}{H_D} (Re)^{0.8} (Pr)^{1/3} \left(\frac{\mu}{\mu_s}\right)^{0.14} \tag{6}$$

The R ynolds number range of each expression is specified by the user. Analy es performed during the present program were based upon the condition that he flow is laminar at coolant Reynolds numbers below 2100 and fully turbu ent for Reynolds numbers in excess of 3000. No factor of safety was place l upon laminar heat transfer coefficients as defined by Equation (5). Turbu ent values were reduced 20% to ensure conservative predictions of tube wall nd skin temperatures. Heat transfer coefficients in the transition regic n were determined by logarithmically interpolating between the laminar and t rbulent values.

he pressure drop for each fluid element is computed from Equation (7) and s mmed to determine the total pressure drop in the panel.

$$\Delta P = \frac{4fL}{H_D} (1/2\ \rho V^2) \tag{7}$$

Frict ion factors (f) are determined from the correlations of Reference 15 prese ited herein as Equations (8) through (10).

$$f = \frac{16}{Re} \qquad Re < 2100 \tag{8}$$

$$f = \frac{0.0791}{(Re)^{0.25}} \qquad Re = 3000 \text{ to } 10{,}000 \tag{9}$$

$$f = \frac{0.046}{(Re)^{0.2}} \qquad Re = 10{,}000 \text{ to } 200{,}000 \tag{10}$$

Friction factors in the region between a Reynolds number of 2100 and 3000 are determined by linearly interpolating between the corresponding values of f as determined by Equations (8) and (9), respectively. Friction factors determined during the present program were not corrected for viscosity-variation effects. For the condition of interest, heating of a liquid, neglecting the viscosity correction results in conservative predictions of friction factor and pressure drop (see References 13, 16, and 17). As pointed out in the above references, the correction for the condition of most interest (turbulent flow) is small.

The APS mass was determined from the procedure of Reference (3) as follows:

$$\text{APS mass} = \frac{G \cdot \dot{m}_c \cdot \Delta P \cdot \theta}{\rho_c}$$

Where θ is the flight time, defined as one hour, and G is the APS conversion factor. The factor G accounts for the Auxiliary Power System: hydrogen and oxygen, tankage, boil off, and inefficiencies due to combustion, exhaust losses, and pump losses. During the present study, a value of G = 0.84 g/kW•s (5 lbm/HP hr), as specified in Reference 3, was used. A recent in-house study indicates that the above value is in error and that a factor of 0.34 g/kW•s (2 lbm/HP hr) should adequately account for the total mass of the APS system. Even though APS mass was overestimated, it is less than 2% of the total panel mass and does not significantly impact the results and conclusions of this program. Since G and θ are constants, APS mass is directly proportional to the product of coolant mass flow rate ($\dot{m}_c$) and pressure drop (ΔP) and inversely proportional to coolant density (ρ_c).

A fluid penalty, which included the coolant inventory mass plus the APS mass, was used as the figure of merit in evaluating the three candidate coolants. The evaluation was performed with an outer skin/tube interface conductance value of 18.9 kW/m^{2}K (3333 Btu/ft^2 hr ^{o}F). The results of the evaluation are shown in Figure 42. Selection of a 60/40 mass solution of methanol/water results in a 0.78 kg/cm^2 (0.16 lbm/ft^2) coolant inventory and APS mass saving relative to an aqueous ethylene glycol solution; a 40% reduction in coolant mass flow; and a 55% reduction in panel pressure drop

(see insert, Figure 42). Only 60% aqueous solutions were evaluated (glycol concentration required to achieve a 222K (-60°F) freezing point) in this study.

Pertinent characteristics of methanol and ethylene glycol are presented in Table 7. A comparison of these characteristics indicates that the low flash point of methanol, relative to ethylene glycol, is the dominate characteristic which requires special consideration. The impact of using methanol with a flash point of 289K (61°F) versus ethylene glycol with a flash point of 389K (240°F) could not be quantified within the scope of the present study.

Next, the effect of the honeycomb core and the inner face sheet on the panel's temperature distribution was analyzed with a two-dimensional model, see Figure 43, since longitudinal conduction is negligible. An expression was derived to account for solid conduction in the ribbon direction for any hexagon shaped honeycomb. The expression is:

$$k_{H/C} = \frac{9}{16} \cdot \frac{\rho_{H/C\ Core}}{\rho_{Material}} \cdot k_{Material}$$

Heat transfer across the honeycomb, including radiation, gaseous conduction or convection, and solid conduction, was accounted for by the method of Reference 6. The back side of the inner skin was assumed adiabatic. Typical results for aluminum core with a cell size of 0.318 cm (0.125 in.) and a density of 72 kg/m^3 (4.5 lbm/ft^3) at the design coolant flow rate of 354 kg/hr (780 lbm/hr) per tube are presented in Figure 44. The inner skin (T_5) and honeycomb core (T_6) were found to be nearly isothermal, with a maximum variation about the nominal of $\pm$0.3K ($\pm$0.5°F) and $\pm$3K ($\pm$5°F), respectively. The good agreement between maximum outer skin temperature (T_0) as determined by the tube/skin model (dashed curve) and the present honeycomb model (solid curve) demonstrates that conduction within the honeycomb and inner skin has little impact upon maximum outer skin temperatures. Varying the honeycomb core density from 37 kg/m^3 (2.3 lbm/ft^3) to 72 kg/m^3 (4.5 lbm/ft^3) resulted in less than a 1.1K (2°F) change in predicted panel temperatures.

Using the two-dimensional temperature distributions, thermal stresses were calculated by elementary beam bending theory, accounting for elastic

strains. The thermal stresses were computed assuming an infinitely long beam with constant temperature in each element, zero slope over the supports, and freedom to expand in the plane of the panel. The updated thermal stresses were input to the structural optimization program described in STEP 3, with coolant properties for methanol/water, and refined structural masses were calculated.

STEP 5. Figure 45 gives the mass of the skins, tubes, honeycomb, APS, and coolant inventory versus the outer skin temperature. The structural mass (inner and outer skins, tubes, and honeycomb) is essentially constant over the temperature range 339K (150^{o}F) to 422K (300^{o}F), and increases above 422K (300^{o}F). At 442K (300^{o}F) the structure is strength and buckling critical, and at higher temperatures, it is strength critical. The coolant inventory mass is constant for a given pitch and Dee tube diameter, but the APS mass decreases rapidly with increasing outer skin temperature. The resulting total mass (structural, coolant inventory, and APS decreases to T_{MID} = 450K (350^{o}F). However, beyond 422K (300^{o}F) the decrease in total mass is small, therefore 422K (300^{o}F) was selected as the upper limit on T_{MID}.

STEP 6. Using the 422K (300^{o}F) maximum operating temperature, a study was performed to determine sensitivity of panel mass to tube diameter and outer skin thickness. Figure 46 shows that a minimum mass panel is achieved with a 0.965 cm (0.38 in.) tube diameter, and an outer skin thickness of 0.102 cm (0.04 in.). With the optimum pitch, Dee tube diameter, and outer skin thickness defined, the structural optimization program (described in STEP 3) gave optimum inner skin thickness and honeycomb core height of 0.041 cm (0.016 in.) and 2.79 cm (1.10 in.) respectively. Table 3 shows the panel operating variables defined during the optimization process.

B.2 DESIGN OF FULL SCALE PANEL DETAILS

B.2.1 EDGE ATTACHMENTS

The panel was designed to transmit 315 kN/m (1800 lbf/in.) ultimate load across the .61m (2 ft) transverse splice and provisions were made for attaching adjacent panels along the 6.1m (20 ft) longitudinal edge.

The transverse splice (Figure 47) uses a 0.254 cm (0.100 in.) thick 2219-T87 outer splice plate with 0.478 cm (0.188 in.) diameter corrosion

resistant steel shearhead type countersunk fasteners at 2.54 cm (1.00 in.) spacing. These fasteners pass through the solid 6061-T6 aluminum manifold and the flange of the support bulkhead. Consequently, moment continuity is maintained across the splice by the outer splice plate and by the flanges of the support bulkhead. A thin film of Eccobond 56C room temperature curing paste adhesive, less than 0.0254 cm (0.010 in.) thick, is used between the outer 2219-T87 splice plate and the manifold to provide a high interface conductance and prevent the splice plate from overheating.

A longitudinal splice, shown in Figure 48, allows practical placement of the fasteners relative to the coolant tubes. The coolant tubes are as close as possible to the panel edge to prevent overheating of the longitudinal splice plate. Again Eccobond 56C adhesive is used under the splice plate to assure splice plate cooling. Cross-sectional area of the longitudinal splice plates is minimized to assure a more uniform loading across the panel width.

The 0.396 cm (0.156 in.) shear head titanium fasteners are countersunk into the 0.127 cm (0.050 in.) thick 2219-T87 longitudinal splice plate. Crushing of the honeycomb core during fastener installation is prevented by a bushing which is installed in the honeycomb. Thin 0.064 cm (0.025 in.) upper and lower closure angles provide load paths for panel splicing and protect the honeycomb core and coolant tubes from damage during handling. Fastener spacing is based on requirements to prevent inter-fastener buckling of the 0.127 cm (0.05 in.) splice plate.

The corner splice, shown in Figure 9, incorporates a local subflash splice doubler. The longitudinal splice plates are terminated at the transverse splice centerline of the panels. The outer longitudinal splice plate loads are transferred through two 0.397 cm (.156 in.) diameter Hi-Lok fasteners into the subflush 0.178 cm (.070 in.) 2219-T87 splice doubler. The inner longitudinal splice plate loads are transferred through these same Hi-Lok fasteners but into the flange of the support bulkhead. These loads are then reacted by the adjacent panel.

B.2.2 INTERMEDIATE FRAME ATTACHMENT

The intermediate frames stabilize the panel and carry the $\pm$6.89 kPa ($\pm$1 psi) limit normal pressure. The panel is attached to these frames, as shown in Figure 8 with 0.396 cm (0.156 in.) diameter Hi-Lok fasteners, which are

countersunk into special bushings which themselves are countersunk into the thin 0.102 cm (0.040 in.) 2219-T87 outer face sheet. The bushings are required to prevent crushing of the honeycomb core during fastener installation and provide a positive clamping action of the panel to the intermediate frame. The design avoids the use of expensive close-tolerance tooling which would be required to mate predrilled holes in the panel and the intermediate support frames.

B.3 IN-DEPTH ANALYSIS

This section describes the full scale panel detailed thermodynamic and structural analyses.

All possible combinations of design pressures, in-plane loads, and temperatures were evaluated to identify the critical loading conditions for each panel element. The panel was subjected to temperatures associated with a uniform heat flux of 136 kW/m^2 (12 Btu/ft^2-sec), static ultimate in-plane loads of $\pm$3.15 kN/m ($\pm$1800 lbf/in.), and static ultimate pressures of $\pm$10.35 kPa ($\pm$1.5 psi). The effects of mechanical (pressures and in-plane loads) and thermal loads were evaluated separately and combined to ensure that the maximum stress had been used to design the panel.

The panel was also designed to sustain any combination of fully reversed limit (ultimate/1.5) in-plane and normal loads for the 20,000 cycle lifetime while being subjected to the design heat flux.

B.3.1 MANIFOLD THERMAL AND PRESSURE DROP ANALYSIS

Detailed thermal and pressure drop analyses were performed to determine structural temperatures and ensure uniform coolant flow through the panel. The manifold design requirements were to (a) distribute the coolant to the panel uniformly with a minimum pressure loss, (b) provide for attachment to adjacent structure, and (c) cool itself and the transverse splice plates to acceptable levels. A constant area design (Figure 49) did not satisfy cooling requirements, since the flow velocity, and hence the heat transfer coefficient, continually decreases as coolant is distributed to the panel. This results in a rise in outer skin temperature (T_o) as indicated in Figure 49. The flow area could be varied with an insert to keep the flow

velocity and heat transfer coefficient at acceptable levels. This approach was judged to be both heavy and complex, as the shape of the insert would have to conform to the shape of the manifold passage to achieve the area reduction necessary to satisfy heat transfer requirements.

The selected double or "split" manifold design illustrated in Figure 50 satisfies both cooling and flow distribution requirements. With this design, the coolant is routed through the cooling manifold, Chamber (1), before entering the distribution manifold, Chamber (2). Keeping the mass flow, and hence the heat transfer coefficient, constant in Chamber (1) provides nearly uniform cooling of the end of the manifold and lateral splice plate. The selected split manifold design, which can be easily fabricated as an extrusion, minimizes lateral temperature gradients and provides uniform flow (within $\pm$0.6%) of the coolant through the panel.

Manifold pressure drops were computed employing a conventional pressure drop relationship as follows:

$$\Delta P = (4f\ L/H_D + K_T)\ (1/2\ \rho V^2)$$

where friction coefficients (f) and loss coefficients (K_T) were obtained from Reference 7.

Pressure drops for various locations in the inlet and exit manifold are tabulated in Figures 51 and 52. Design temperatures and pressures of the coolant, APS mass for the panel, and the total coolant inventory weight are summarized in Figure 53. As indicated in this figure, the total coolant mass with a 60/40 mass solution of methanol/water as the coolant is 2 kg/m^2 (0.4 lbm/ft^2).

Results of a flow balancing analysis indicates that coolant mass flow rates through the panel will be uniform within $\pm$0.6% of the nominal. Such small variations in mass flow rate have a negligible effect upon panel temperatures.

B.3.2 MANIFOLD AND SPLICE PLATE TEMPERATURES

Manifold and splice-plate temperatures were computed utilizing a three-dimensional thermal model of a section of the manifold and the first 10.2 cm (4 in.) of the face sheet and coolant tube. The model, shown schematically in

Figure 54 accounted for variations in material properties with temperature, and could be easily modified to accommodate dimensional changes due to design refinements or parametric variations when conducting sensitivity studies to calculate effects of variations in bond-line conductance values on temperature.

Design temperatures for the manifolds are presented in Figures 55 through 58. In Figure 55, inlet manifold temperatures are presented as a function of spanwise location. As the flow, and hence the heat transfer coefficient, in the inner (smaller) manifold chamber goes to zero at the panel centerline, a corresponding rise in manifold temperature can be noted. However, with the split manifold design, transverse temperature differences in the manifold are quite small, being less than 20K (36^{o}F). The large variation in outer skin temperatures (T_8) reflects the temperature directly above the midway between coolant tubes.

Longitudinal temperature distributions in the inlet manifold, at the quarter span location, are presented in Figure 56. The cooling effect of the manifold results in the large longitudinal temperature difference in the face sheet at a location midway between tubes and in the area adjacent to the manifold. Similar spanwise and longitudinal temperature plots for the exit manifold are presented in Figures 57 and 58 respectively.

B.3.3 PANEL DESIGN TEMPERATURES

The effect of the honeycomb core and the inner face sheet on the panel's temperature distribution was analyzed with the two-dimensional model, see Figure 43, since longitudinal conduction is negligible. Heat transfer across the honeycomb, including radiation, gaseous conduction or convection, and solid conduction, was accounted for by the method of Reference 6. The back side of the inner skin was assumed adiabatic. Typical results for aluminum core with a cell size of 0.318 cm (0.125 in.) and a density of 72 kg/m^3 (4.5 lbm/ft^3) at the design coolant flow rate of 354 kg/hr (780 lbm/hr) per tube are presented in Figure 44. The inner skin (T_5) and honeycomb core (T_6) were found to be nearly isothermal, with a maximum

vari tion about the nominal of ±0.3K (±0.5°F) and ±3K (±5°F), respectively. The ood agreement between maximum outer skin temperature (T_o) as determined by t e tube/skin model (dashed curve) and the present honeycomb model (solid curv) demonstrates that conduction within the honeycomb and inner skin has litt e impact upon maximum outer skin temperatures. Varying the honeycomb core density from 37 kg/m^3 (2.3 lbm/ft^3) to 72 kg/m^3 (4.5 lbm/ft^3) resulted in less than a 1.1K (2°F) change in predicted panel temperatures.

B.3. BONDLINE INTERFACE CONDUCTANCE

Analyses were performed to determine the sensitivity of panel temp ratures to variations in bondline conductance values. Face sheet temp ratures versus interface conductance between the face sheet and mani old are presented in Figure 59. Face sheet temperatures are less than the design temperature of 422K (300°F) for interface conductance valu s greater than 2.38 kW/m^{2}K (420 Btu/ft^{2}hr°F). (The FM-400/Titanium Lami ated specimen consisted of a stack of six pieces of titanium sheet stoc bonded together with FM-400 adhesive. The laminated stack was used, rath r than two sheets with one bond joint, to increase the temperature diff rence across the specimen. Small instrument errors in measuring small temp rature differences could result in large errors in calculating inte face conductance. Thus, the laminated specimen was expected to resu t in a more accurate estimate of interface conductance. For the same reas n, the FM-400 solid specimen was 1.3 cm (0.5 in.) thick.) The import nce of high interface conductance between the face sheet and coolant tubes is i lustrated in Figure 60, where percent of design of coolant flow rate and APS mass versus interface conductance is given for a panel temperature of 4 2K (300°F). As shown, reducing the design interface conductance value by 5)% increases the coolant flow rate by 50% and the APS mass by 200%

B.3.5 STRUCTURAL FINITE ELEMENT MODEL

Verification of the internal mechanical and thermal loads used to optimize the panel was accomplished by generating a finite element model and using

the design loads and pressures, and the resulting temperatures from the detailed thermal analysis. The model, Figure 61, had 3090 degrees of freedom. The structural idealization of the panel was compatible with the MCAIR Computer Aided Structural Design (CASD) computer program. The model consists of bars and panels to represent the axial and shear stiffness of the skins, tubes, manifolds, and honeycomb core. There were large thermal gradients in the outer skin. Thus, skin bar elements in the actively cooled panel model had to be closely spaced to assure accurate determination of thermal stresses. Consequently, bar elements representing the basic panel, i.e., skins, coolant tubes, and honecomb core, were spaced 1.27 cm (0.50 in.) apart in the transverse direction and approximately 12.7 cm (5.0 in.) apart in the longitudinal direction (thermal gradients are much less severe in the longitudinal direction). To keep the model from becoming too large, the symmetry of the panel was utilized and a portion of the structure spanning three frames was idealized since analysis showed this was sufficient to simulate accurately the stress distributions in the panel.

B.3.6 THERMAL STRESSES

Using the two-dimensional temperature distributions, (see section B.3.3) thermal stresses were calculated by elementary beam bending theory accounting for elastic strains. The thermal stresses were computed assuming an infinitely long beam with constant temperature in each element, zero slope over the supports, and freedom to expand in the plane of the panel.

Thermal stresses in the panel skin/tube area were calculated at both the entrance and exit of the full scale panel. Thermal stresses in the outer skin, the tube, and the inner skin for the basic panel cross-section are shown in Figure 62, for the area near the panel entrance, where the maximum thermal stresses occur. Note the sinusoidal variation of thermal stress in the outer skin, Figure 62, with maximum compressive stress occurring midway between the tubes. The coolant tubes are in tension and the inner skin is in compression.

Thermal stresses were determined in the manifold area at both the entrance and exit of the full scale panel. Thermal stresses in the manifold area are shown in Figure 63 for the area near the panel entrance, where the maximum thermal stresses occur.

B.3. FRACTURE MECHANICS

Surface cracks in the tubes and cracks emanating from fastener holes in the skins were the two types of flaws considered. Flaws were assumed in areas where panel failure was most probable - either due to overheating or overstressing. The operating stress levels for both the mechanical and thermal loadings are shown, Figure 64, separately and combined, to permit identification of the most critical condition.

Crack propagation is more likely in the inner skin, since it is more highly stressed than the outer skin. (Note that for a normal operating condition, the thermal stresses, Figure 62, significantly reduce the maximum tension stress levels in the outer skin and so crack growth from the fastener hole is even less likely.) On the other hand, surface flaws were considered more likely to occur in the outer skin, since it is exposed to foreign object damage. However, analysis showed that surface flaws as large as 1.27 cm (0.500 in.) long and 0.06 cm (0.025 in.) deep would not grow at the operating stress level of 84.4 MPa (12,300 psi).

As a result of the above analysis, the panel was found to have a fatigue life of 20,000 cycles.

B.3.3 PANEL STABILITY

A beam column analysis addressing panel stability and accounting for deflections associated with manufacturing eccentricities and pressure loadings showed panel stability to be the critical failure mode.

The critical loading condition for the beam column analysis, see Table 8, is an outward pressure coupled with a compressive in-plane running load. This results in a maximum compressive stress on the inner face sheet, which is reflected in the reduced moment capability of the cross section due to the lower wrinkling allowable of the inner face sheet.

Table 8 summarizes the results of these analyses, identifying the critical components, stress levels, failure modes, and margins of safety. As shown, the Dee tubes are equally critical, i.e., have zero margins of safety, over the intermediate frames and midway between frames. Cracks growing through the thickness of the 0.089 cm (0.035 in.) wall is the critical failure mode. The inner skin is critical only in the area of the

intermediate frames, and cracks growing from one side of a fastener hole is the critical failure mode.

APPENDIX C

FATIGUE SPECIMENS

Six fatigue specimens were fabricated by MCAIR and tested at room temperature by NASA. These specimens, Figure 12, were representative of three different areas of the full scale panel.

The skin/Dee tube/manifold specimen consisted of manifolds with provisions for pressurizing the Dee tubes, an outer skin, and loading adapters. The honeycomb core and inner skin were omitted to permit access to the Dee-tube-to-manifold and the Dee-tube-to-outer-skin interfaces. The specimen was 12.7 cm x 27.94 cm (5 x 11 in.).

The corner splice specimen represented the corner of the panel and incorporated the inner and outer skin, honeycomb core, manifolds, and lateral and longitudinal splice intersections. Means for pressurizing the specimen were supplied by welding 1.27 cm (.50 in.) diameter fittings to the ends of both the inlet and exit manifolds. The loading adapters were interchangeable with the skin/Dee tube/manifold specimen.

The basic skin specimen consisted simply of an 0.102 cm (0.040 in.) skin with tapered loading doubler bonded to the ends to reduce the stress concentration at the loading adapters. The specimen was 12.7 x 27.94 cm (5 x 11 in.).

Of the four specimens (two skin/Dee tube/manifold specimens and two corner splice specimens) fabricated, only one had the low temperature solder (91Sn-9Zn) attaching the outer skin to the coolant passages and manifolds. The other three specimens were fabricated using the elevated temperature curing silver-filled adhesive. This adhesive had initially been selected to attach the outer skin to the coolant passages. However, it was discarded when it was found to have low peel strength and low thermal conductivity. The low peel strength, 0.18 kN/m (1.0 lbf/in.), was discovered when numerous debonds occurred between the Dee tubes and the outer skin during shop handling of the specimens. Damage could be avoided with special care in handling. However, the low thermal conductivity of the adhesive could not be accepted since it would result in skin temperatures in excess of the design value of 422K (300^{o}F) (see Tables 6 and 7). The decision to use low

temperature solder rather than the elevated temperature curing silver-filled adhesive for attaching the outer skin to the coolant passages was not the result of the fatigue tests. All specimens that used the adhesive satisfied the fatigue requirements.

C.1 FATIGUE SPECIMEN SOLDERING PROCESS

In-house developments of plating, fixturing, and specimen heating cycles were required to obtain successful soldering. The plating process involved zincating, a cyanide copper strike, a copper plate, and a tin plate. Small lap shear coupons were tested to develop solder heating cycles and processing techniques and to establish joint static and fatigue strength.

Selection of the soldering heating cycle was determined to be important since the organic flux begins to outgas as it cleans the oxides from the surfaces at 422K (300^{o}F), and the 91Sn-9Zn solder does not melt until 472K (390^{o}F). Consequently, it is essential that the time span between 422K (300^{o}F) and 472K (390^{o}F) be as short as possible so as not to permit the flux to exhaust itself prior to the solder reaching its 472K (390^{o}F) to 500K (440^{o}F) wetting temperature range. The time at temperature is a function of the ability to achieve uniform temperature throughout the component. Therefore, a soldering heating cycle with temperature rising from 450K (350^{o}F) to 500K (440^{o}F) in 5 minutes, holding at 500K (440^{o}F) for 2 minutes, and then falling from 500K (440^{o}F) to 450K (350^{o}F) in 5 minutes was established. Uniform wetting of the faying surfaces with the solder was difficult to achieve, especially in areas having overlaps greater than 0.636 cm (0.25 in.). This was because of outgassing of the organic flux which was used to remove the oxides from the surfaces to be soldered. Performations in one of the faying surfaces was found to improve wetting. Consequently, the outer skin was perforated, as shown in Figure 65, on one coolant passages/skin/manifold specimen.

Six coupons were tested at room temperature and at 350K (170^{o}F). Five of the coupons were fatigue tested to failure and the sixth was fatigue tested to 20,000 cycles and then loaded statically to failure. The 3.25kN (730 lbf) load corresponded to the maximum limit load that is transferred from the outer skin through the solder to the manifold. The 350K (170^{o}F)

tempe ature corresponds to the maximum bondline temperature which occurs at the e it manifold. Results of the coupon tests are given in Table 9.

older wetting as low as 50% was determined to be acceptable from a therm dynamic standpoint, since the thermal conductivity of the solder was much igher than the design value and the voids in the solder were randomly dispe sed, as shown in Figure 66.

C.2 ATIGUE SPECIMEN TESTS

he fatigue loads applied to each of the three specimens are shown in Figur 18. The loads correspond to the maximum limit loads sustained for 20,00 cycles (5,000 cycles times a scatter factor of 4) without failure. Subse uent sections discuss the applied loads and the results of the fatigue tests for each of the specimens. Additional information is in Reference 11.

C.2.1 BASIC SKIN SPECIMENS

he fatigue loading for the basic skin specimen was varied from 0 to 13.8 N (0 to 3100 lbf). Only tension loads were applied, since the specimen was n t stabilized to prevent buckling. This loading produced 106.9 MPa (15,5 0 psi) in the 0.102 cm (0.040 in.) outer skin and is representative of the s resses, over the intermediate frames, developed in the inner skin of the f ll scale panel when subjected to a tensile 210 kN (1200 lbf/in.) in-plane load coupled with an outward acting 6.89 kPa (1.0 psi) pressure.

he basic skin specimens were tested for 20,000 cycles. Then a crack start r was put in the center of each specimen. The crack starter was produced by dr lling a 0.277 cm (0.109 in.) diameter hole in the skin and sawing a cut 0.079 cm (0.031 in.) long on each side of the hole, resulting in a total crack lengt , tip to tip, of 0.435 cm (0.171 in.). The growth of the cracks versu cycles is plotted in Figure 67 for each of the two specimens tested.

C.2.2 CORNER SPLICE SPECIMENS

he corner splice specimens were subjected to a completely reversible 25.35 kN (5700 lbf) in-plane load. This load is representative of the maximum l ading in the corner of the full scale panel. It produces maximum faste er loads in the outer transverse splice plate and corresponds to a compl tely reversible loading in the full scale panel which results from a

tensile 210 kN/m (1200 lbf/in) in plane loading coupled with an inward acting 6.89 kPa (1.0 psi) pressure loading, or a compressive in-plane load coupled with an outward acting pressure loading.

The first corner splice specimen was pressurized to 517 kPa (75 psi) and subjected to a fully reversed loading of ±25.35 kN (±5700 lbf) for 24,789 cycles with no apparent damage. However, considerable joint motion was observed in the area of the fasteners.

A hole was then drilled through the outer skin and completely through a tube of the first corner splice specimen. The hole in the outer skin was then plugged so that fluid could enter the honeycomb core. The coolant passages were pressurized to 517 kPa (75 psi), and the specimen was cycled for 10,000 cycles at ±25.35 kN (±5700 lbf). No damage or loss in pressure was observed. The cyclic load was increased to ±30.69 kN (±6900 lbf) (121% of the design limit load) and after 3000 cycles a pressure drop was detected. The pressure was gradually increased back to 517 kPa (75 psi) and the testing continued for another 2000 cycles with no apparent damage. Testing was terminated after an additional 571 cycles when a crack approximately 3.80 cm (1.5 in.) long was discovered in the inner face sheet at the skin/manifold interface.

Subsequent non-destructive tests (x-rays) indicated that the pressure drop resulted from fluid entering into 8 to 10 of the adjacent honeycomb cells. The test demonstrates the capability of the 49.66 kg/m^3 (3.1 lbm/ft^3) honeycomb to contain the coolant (for the 5000 cycle design life of the panel) in the event of a crack in a tube.

The second corner splice specimen had excessive joint motion in the fastener areas similar to that observed in the first specimen. Unfortunately, the second specimen was destroyed after being subjected to only 2000 cycles, due to a malfunction in the testing equipment which overloaded the specimen.

C.2.3 - COOLANT PASSAGES/SKIN/MANIFOLD SPECIMENS

The fatigue loading for the skin/Dee tube/manifold specimens was cycled from 0 to 18.1 kN (0 to 4070 lbf). This loading produced a maximum stress of 82.7 MPa (12,000 psi) in the outer skin. This stress is equivalent to the stress level developed in the outer skin of the full scale panel, in the area of the intermediate frames, when the panel is subjected to a 210 kN/m

(1200 lbf/in.) in-plane loading coupled with an inward acting 5.89 kPa (1.0 psi) pressure loading. One of the coolant passages/skin specimens was fabricated using the elevated temperature curing silver-filled adhesive and the other with low temperature solder for attaching the outer skin to the coolant passages.

The specimen having the adhesive was subjected to a total of 78,176 cycles before a leak developed in one of the coolant tubes. First, with zero coolant pressure, it was subjected to a cyclic load of 0 to 18.1 kN (0 to 4070 lbf) for 20,000 cycles with no apparent damage. Second, a 0.277 cm (0.109 in.) diameter hole was then drilled in the skin, midway between tubes, and a saw cut 0.079 cm (.031 in.) long, was made on each side of the hole. With coolant pressure of 517 kPa (75 psi), 16,176 cycles of loading from 0 to 18.1 kN (0 to 4070 lbf) was sustained with no crack growth detected. Thirdly, the simulated crack length was increased to 0.953 cm (0.375 in.) tip to tip. The above pressures and loads were continued for another 20,000 cycles and still no crack growth was detected. Fourth, the maximum load was then increased to 22.69 kN (5100 lbf) (125% of design limit load) and cycled 0 to 22.69 kN (0 to 5100 lbf) for 22,000 cycles before a slow leak developed in one of the tubes near the tube/manifold brazed interface. Fifth, the test was then continued for another 20,866 cycles, without pressure, and the crack in the skin propagated across one of the tubes without propagating into the tube. (The stress in the skin corresponding to the 18.1 and 22.69 kN (4070 and 5100 lbf) applied load was 82.7 MPa (12,000 psi) and 103.7 MPa (15,035 psi), respectively.)

The skin/Dee tube/manifold specimen with the low temperature solder was pressurized to 517 kPa (75 psi) and the load cycled for 20,000 cycles with no apparent damage. Next, a crack starter was cut in the center of the specimen midway between tubes. The crack starter was a saw cut with razor cut V-groves on each end. Tip to tip length of the crack starter was 1.04 cm (0.410 in.). The specimen was again pressurized and cyclic load initiated. After 142,946 additional cycles, the crack grew past one tube without damaging it; Figure 68 shows the results of the test.

The refinements in the full scale panel design resulting from the fatigue tests were: (1) The tolerances between the fasteners and the holes in the lateral splice plate were tightened. The holes in the fatigue specimens had

a specified tolerance of +.0056/-.0000 cm (+.0022/-.0000 in.). The new tolerances are +.0038/-.0018 cm (+.00151/-.0007 in.); and (2) solid aluminum between manifold flanges at each fastener location was provided. These refinements were incorporated because of excessive motion observed in the corner splice specimens at the onset of testing.

APPENDIX D

TEST PANEL DESIGN AND ANALYSIS

The test panel design is based on the full scale panel design and is representative of a section at the end of the full scale panel. Although several components of the test panel were fabricated, the test panel was not completed because of inability to attach the manifolds and Dee tubes to the outer skin using the low temperature solder. Details of the problems are in Appendix E. Figure 19 shows a schematic of the test panel, load adapter, and support frames. The test panel is 0.61 x 1.22m (2 x 4 ft) and is supported by three aircraft type support frames. The details of the test panel, such as attachment to support frames and attachment to adjacent panels along the 1.22m (4 ft) longitudinal edge, are the same as for the full scale panel design, reference Appendix B. NASA had planned on heating the panel with a radiant lamp bank while loading the panel in a fatigue machine.

D.1 TEST PANEL LOAD ADAPTER

Provisions were made along the transverse edges of the panel for application of the in-plane loads and to compensate for the differential thermal expansion between the manifold and the load adapters. This was accomplished by applying and reacting the in-plane loads with a 2.54 cm (1.0 in) thick aluminum load adapter. The load adapter has two rows of fasteners (See Section A-A, Figure 19): one row has close tolerance holes for transferring the axial loads; and the second row, closest to the manifold, has oversized holes to allow for differential thermal expansion between the manifolds and the load adapters. The loads are transferred from the load adapter into a series of titanium (selected because of its low thermal conductivity) links, which in turn transfer the load into the transverse splice plate, on the outer surface, and into the flange of the support frame, on the inner surface. The loads are then transferred from the splice plate and the flange of the support frame to the outer and inner surfaces of the manifold, respectively.

Asbestos insulators were placed between the aluminum load adapters and the titanium links. Insulation was also placed over one side of the load adapter to reduce heat loss to the environment. Thermal and structural analyses showed that this design reasonably simulated temperatures and thermal stresses in the full scale panel.

D.2 THERMAL AND STRUCTURAL ANALYSES

Thermal and structural analyses were required to simulate differences between the test panel and the full scale panel design in order to ensure that the full scale panel inlet and exit conditions could be simulated. The primary differences included use of ethylene glycol/water instead of methanol/water as the coolant, increased interface conductance between the Dee tubes and the outer skin resulting from the high thermal conductivity of the solder, and the heat sink effects of the load adapters and the proposed NASA test apparatus.

D.2.1 FULL SCALE PANEL ANALYSIS WITH ETHYLENE GLYCOL/WATER

A thermal analysis was performed to determine the coolant flow rate required for a 60/40 mass solution of ethylene glycol/water to simulate the full scale panel temperatures. Results of the coolant evaluation presented in Fig. 42 showed that the optimum inlet temperature was 283K (50^{o}F). Utilizing this initial temperature (and the glycol/water properties presented in Figures 33-37) temperatures of the full-scale panel and splice plates were determined as a function of coolant flow rate, as presented in Figure 69. Since the onset of fully developed turbulent flow cannot be rigorously determined, two limiting cases were considered in predicting maximum panel temperatures. The solid line in Figure 69 is based on the assumption that the flow is fully turbulent for the full length of the panel. It is probable that this condition will prevail, due to the high entrance Reynolds number (greater than 3000) and induced turbulence as a result of the flow turning as it enters the coolant tube. However, to ensure conservatism in the prediction of maximum panel temperatures, a second condition was considered (dashed curve) where fully developed turbulent flow is delayed until the Reynolds number reaches 10,000. This latter condition results in maximum

panel temperatures that are approximately 4.4K (8°F) higher, and hence was used in test panel analyses. For the all-turbulent case, the maximum panel temperature (longitudinal splice-plate) occurs at the panel exit, whereas when a critical Reynolds number of 10,000 is used, maximum temperatures occur in the vicinity of the inlet. As shown in Figure 69, a design flow rate of 485 kg/hr (1070 lbm/hr) per tube results in a maximum temperature of 422K (300°F) for the full scale panel. At the design flow rate the inlet coolant temperature is 283K (50°F), the exit coolant temperature is 332K (138°F), and the pressure drop in the full scale panel, excluding manifolds, is 245 kPa (35.5 psi).

D.2.3 TEST PANEL THERMAL ANALYSIS

Predicted test panel temperatures for a simulated full scale inlet and exit condition are presented in Figures 70 and 71, respectively. Since the test panel is only 1.22m (4 ft) long, temperatures increase only 5K (9°F) over the length of the panel. To simulate the inlet condition (Figure 70) the glycol/water coolant enters at 283K (50°F) and exits at 294K (68.3°F). Full scale exit manifold conditions can be simulated (Figure 71) with a coolant inlet temperature of 322.7K (120.0°F), which results in an exit temperature of 332K (138°F). The overall temperature level of the panel increases by about 22 to 28K (40 to 50°F) in the simulated exit condition.

Predicted transverse splice-plate temperatures for the test panel are compared to full scale panel design values in Figure 72. The test panel temperatures will be lower than predicted full scale panel temperatures because of heat transfer to the test panel loading grip, which in turn is dissipated to the ambient environment. The splice-plate temperatures of Figure 72 are based on insulating the first 6.5 cm (2.6 in.) of the loading adapter. Omitting the insulation would increase the heat transfer to the ambient environment and decrease lateral splice-plate temperatures.

Transient analyses were performed to determine if sudden heat-up or shut-down of the heater would result in thermal gradients which would jeopardize the structural integrity of the panel. Analyses were performed for the inlet and exit manifold/load adapter assemblies. Figure 73 shows results for the inlet manifold where the largest temperature difference occurs. Transient temperature differences are less than the steady state values and will not jeopardize the structural integrity of the panel.

Transient analyses were also performed to determine temperature gradients in the basic panel (tube/skin/honeycomb/inner skin) and the results are presented in Figure 74. As shown, transient temperature differences are greater than the design steady state values. Consequently, thermal stresses in the panel were determined using the temperature distributions from Figure 74, considering both a sudden heat-up of the panel and a sudden shut-down of the heater. The results of the analysis are presented in Figure 75 for the worst case, i.e., near the inlet manifold, for the simulated full scale panel entrance condition. This is the area where the maximum ΔT's and consequently the maximum thermal stresses, occur. The stresses for the inner and outer skin and the coolant tube are compared to those predicted for the steady state condition. As was expected, a sudden heat-up condition results in compressive stresses in the outer skin and a tensile stress in the inner skin, due to the outer skin expanding rapidly and being restrained by the inner skin. The reverse is true for a sudden shut-down of the heater. This condition, sudden heater shut-down, was determined to be less critical than a sudden heat-up of the panel.

D.2.3 MANIFOLD PRESSURE DROP ANALYSIS

A detailed pressure drop analysis was performed for the inlet and exit manifolds and the results are presented in Figures 76 and 77, respectively. The pressure drop in manifolds varies from 46.7 kPa (6.78 psi) for a simulated full-scale inlet condition to 27.1 kPa (3.93 psi) for a simulated full scale exit condition. However, the pressure drop in the inner chamber is the only contributor to non-uniformity of flow through the panel, and is less than 10% of the total pressure drop in the manifold. Based on the above computed pressure drops, flow through the test panel has been computed to be within $\pm 5\%$ of the nominal, as shown in Table 10. Analyses indicate a $\pm 5\%$ deviation in coolant flow through the panel results in less than a ± 2.8K ($\pm 5^{o}$F) change in panel temperatures.

APPENDIX E

TEST PANEL FABRICATION/SOLDERING PROBLEMS/EVALUATION

The test panel was not fabricated because of inability to solder the outer skin to the manifold/Dee tubes. Soldering of two assemblies was attempted. This Appendix discusses fabrication of the test panel components, the soldering and plating problems encountered, and the results of the post-soldering failure analysis.

E.1 FABRICATION PROCESS

Fabrication of the tube/manifold/outer skin assembly involved: (1) salt bath brazing the Dee tubes to the manifold detail using Alcoa 718 braze foil; (2) welding the remaining manifold details with 4043 aluminum filler rod to complete the tube-manifold subassembly; (3) heat treating the 6061-0 tube/manifold subassembly to the T6 condition; (4) straightening the Dee tubes; (5) plating the tube/manifold subassembly and the outer skin; and (6) low temperature soldering the outer skin to the tube/manifold subassembly. Figures 78 through 83 show the subassemblies in various stages of fabrication. The Dee tubes, the Dee tube end plugs, and the manifold details are shown in Figure 78. These components comprise the manifold/Dee tube subassembly. This subassembly was brazed in one operation.

Figure 79 shows the Dee tubes in position in the machined manifold detail and a close-up of the corner area, showing the recess and the slot machined into the manifold detail and the corresponding slot in the Dee tube. Inconel 625 "C"-clamps were used to maintain pressure between the manifold and the Dee tubes during brazing. The brazing fixture shown in Figure 79 was subsequently discarded when it was found that differential expansion between the Dee tubes and the brazing fixture created gaps between the ends of the tubes and the manifold detail. The final brazing operation used a 1.27 cm (0.50 in.) thick aluminum plate located directly under each manifold to permit the Inconel "C"-clamp to clamp more directly. Figure 80 shows the salt bath brazing operation. Figure 81 shows the completed (brazed tubes and welded manifolds) tube/manifold assembly.

Figure 82 shows the 0.10 cm (0.040 in.) outer skin and the 0.64 cm (.025 in.) closure angles with the 0.160 cm (0.063 in.) diameter holes that were added in an attempt to improve the solder wetting (reference Appendix C). Perforation of the outer skin and closure angles was eliminated because the perforations did not markedly improve wetting. Subsequently, capillary action was depended on to draw in the solder and force out the flux gases. The tube/manifold assembly and outer skin are plated and tinned in order to improve the solder wetting of the faying surfaces. The plated tube/manifold assembly and outer skin parts are shown in Figure 83 with the masking applied in order to provide clean surfaces for the subsequent bonding operations. The masking is removed after the soldering operation.

E.2 PLATING AND SOLDERING PROBLEMS

The plating process, developed in house, for the successfully soldered fatigue specimen was a combination of zincating, a copper strike, copper plating, and tin plating (zincate/copper/tin), reference Appendix C. (Reference 18 has a discussion of the above plating technique). MCAIR facilities for plating the tube/manifold subassembly were not large enough.

Local vendors could not zincate/copper/tin plate the panel details. However, they could provide an adequate nickel/copper/tin plating on small coupons. Successful in-house soldering and testing of lap shear coupons proved the adequacy of the nickel/copper/tin plating.

The first tube/manifold subassembly was nickel/copper/tin plated and the panel was soldered in a large heat-treat furnace after some initial trail runs had been made to minimize panel temperature variations. The soldered joints were determined, after reviewing the x-rays, to be strength deficient over the manifolds due to excessive voids. Excessive voids were attributed to the long heating cycle. The furnace heat-up rate was too slow to match the desired thermal cycle. It was decided to desolder the specimen and to solder it again in another facility.

Several attempts to reapply the nickel/copper/tin plating were unsuccessful because blisters developed in the plating. Another vendor attempted to plate the parts using the Alstan 70 process (see Reference 18). In this process the oxides were removed from the aluminum parts in a special

st nnate bath. A bronze strike was then applied to serve as a base for the ti plate which was electro-deposited on the unmasked surfaces.

Bend tests and tape tests of plated 6061-T6 and 2024-T81 coupons in icated excellent adhesion of the bronze/tin plating and the 0.61 x 1.22m (2 x 4 foot) panel details were plated. Problems were encountered immediately wi h blisters and poor adhesion, especially in the area of the manifolds. Se eral unsuccessful attempts were made to plate the parts. A hole, ap roximately .076 cm (.03 inch) diameter, developed in one tube. It was su pected to be a burn-through due to electrical arcing during electroplating. Th hole was weld repaired and the tube/manifold assembly was then pressure te ted. Many very small leaks were found in the tubes. Most of these leaks we e so small that they could only be detected during pressure test or with a 10 power magnifying glass. In the process of attempting to weld repair th se leaks the tubes were further damaged by thermal distortions. The panel wa judged unrepairable and it was scrapped.

At the time the panel was scrapped, the aluminum surfaces were so co ntaminated from repeated exposure to chemicals that mechanical means would ha e been required to remove enough of the surface to get down to a clean su face for tin plating. Chemical attack was also blamed for the leaks in th tube. Subsequent examination of the inside of the tubes confirmed that co rosion due to exposure to sulfides (probably sulfuric acid entered the tu es when the first leak developed) was responsible for the leaks. The in side surfaces of the tubes and manifolds were severely corroded. There was no evidence of chlorides in the corrosion products or on the corroded inner su faces. Chlorides could have been present if the corrosion was due to ex posure to brazing salts.

Detail parts were fabricated for a second actively cooled panel. The de tails were the same as for the first panel except that the cover skin was no t perforated for soldering. The tube/manifold assembly, outer cover skin, an d outer closure angles were plated using the Alstan 70 process. Blisters de veloped in the plating over the manifolds. Plating on all other areas pa ssed the tape peel test and was accepted. Another unsuccessful attempt was m de to plate the manifolds. The vendor suggested that the problem was p obably due to the 4 to 5% silicon content of the weld filler material in

the manifold. The basic 6061 material in the manifold has in the order of 1% silicon. MCAIR decided to strip the manifolds only and replate them as follows:

1. Vendor apply a nickel/copper plating.
2. MCAIR Laboratory tin plate as done previously on the development test coupons and on the soldered fatigue test specimens. (This was possible since only the manifolds were being tinned and existing MCAIR tanks and associated apparatus were large enough to do the job.)

Plating thus applied passed the plating acceptance tests and the panel details were prepared for soldering by MCAIR.

During soldering, the panel assembly was sandwiched between two 1.72 cm (0.50 in.) thick stiffened aluminum plates, as illustrated in Figure 84. These thick aluminum plates were required to react the 24.1 kPa (3.5 psi) bladder pressure used to hold the Dee tubes in contact with the outer skin. A hard insulation board was provided to thermally isolate the panel from the lower pressure plate. The honeycomb core and bladder similarly restricted heat transfer between the panel and upper pressure plate. The panel assembly was heated by blowing hot air through the tube/manifold assembly, and around the soldering fixture as shown in Figure 84. Thermocouples, located on the panel, were monitored and the air temperature, pressure, and flow rate was varied in order to achieve the required soldering thermal cycle. This cycle involved increasing the panel temperature from 450K ($350^{o}F$) to 505K ($450^{o}F$) in five minutes, holding at 505K ($450^{o}F$) for two minutes, and then cooling to 460 ($370^{o}F$) in less than five minutes (reference Appendix C). Examination of the panel after soldering revealed some areas were not soldered, some areas had many voids, soldered joints had very low strength, and that extensive intergranular cracking occurred in the coolant tubes.

E.3 EVALUATION OF FAILURE OF SECOND PANEL

X-rays of the second soldered assembly revealed voids in the manifold areas (5% to 10% wetting at the inlet manifold and 30% to 40% wetting at the exit manifold) and some unsoldered tubes. Pressure tests revealed leaks through randomly dispersed hairline cracks in the Dee tubes. Figure 85 shows the location of the cracks along the Dee tubes. Photomicrographs and metallurgical analysis of several dissected areas were made in an attempt to identify

the cause of the cracking. Figures 86 through 92 show the results of this ana ysis. A photomicrograph of a typical crack in a Dee tube is shown in Fig ıre 86, with the results of the metallurgical analysis shown in Figure 87. The solder, which is 91Sn-9Zn, migrated into the crack in the tube.

Figures 88 through 90 show the results of the evaluation of three dif erent areas of a typical Dee tube cross section. As shown in Figure 88, the Scanning Electron Microscope (SEM) showed Area 3, the flat portion of the tub : in contact with the outer skin, to be covered with solder. Figure 89, sho /s that the solder migrated along the tube wall up to Area 2 half way up the tube. No evidence of solder was found in Area 1, as shown in Figure 90.

A photomicrograph of a cross section in the tube/manifold area is shown in igure 91. This figure compares a "sound" soldered joint to an unsoldered joi ıt. This was typical of several areas where poor solder wetting was ide ıtified. Note the separation of the copper strike at the tube boundary. Fig ıre 92 shows a photomicrograph of the 2024-T81 skin in an area where voids exi ;ted. In this area there was no evidence of the bronze strike, tin plate or ;older, which indicated complete erosion due to the solder penetrating the pla ;ing on the 2024-T81.

As a result of this analysis, it was speculated that the primary cause of :he gross lack of aluminum wetting was a breakdown of the plating during sol dering. The intergranular cracking of the Dee tubes was also attributed to :he breakdown of the plating, which permitted the solder to come into dir ect contact with the bare aluminum. The exact cause of the plating bre ıkdown and the intergranular cracking of the Dee tubes was never isolated. Sev eral attempts to duplicate the problems with small subscale element cou ons, by using different soldering temperature profiles and prestressing the coupons as high as 100% of yield, were unsuccessful.

REFERENCES

1. W. A. McConarty and F. M. Anthony, Design and Evaluation of Active Cooling Systems for Mach 6 Cruise Vehicle Wings, NASA CR-1916, December 1971.
2. R. G. Helenbrook, W. A. McConarty and F. M. Anthony, Evaluation of Active Cooling Systems for a Mach 6 Hypersonic Transport Airframe, NASA CR-1917, December 1971.
3. R. G. Helenbrook and F. M. Anthony, Design of a Convective Cooling System for a Mach 6 Hypersonic Transport Airframe, NASA CR-1918, December 1971.
4. R. J. Nowak and H. N. Kelly, Actively Cooled Airframe Structures for High-Speed Flight, J of Aircraft, Vol. 14, No. 3, pp. 244-250, March 1977.
5. Federal Aviation Regulations, Volume III, Part 25 Airworthiness Standards: Transport Category Airplanes, June 1974.
6. Anon: Military Specification, Airplane Strength and Rigidity Reliability Requirements, Repeated Loads and Fatigue (MIL-A-008866A USAF). Department of Defense, March 1971.
7. E. W. Brogren, A. L. Brown, B. E. Clingar, V. Deriugir and C. L. Jaeck, Thermal-Structural Combined Loads Design Criteria Study, NASA CR-2102, October 1972.
8. Anon: Military Standardization Handbook, Structural Sandwich Composites (MIL-HDBK-23A). Department of Defense, December 1968.
9. S. P. Timoshenko and S. Woinowsky-Krieger, Theory of Plates and Shells, McGraw-Hill, Second Edition, 1959.
10. B. E. Gatewood, Thermal Stresses, McGraw-Hill, 1957.
11. Sharpe, E. L. and Elber, W.: Ambient Temperature Fatigue Tests of Elements of an Actively Cooled Honeycomb Sandwich Structural Panel, NASA TM X-3557, September, 1977.
12. Technical Bulletin 3-2-5A, Eccobond Solder 58C, Emerson & Cumming, Inc., rev. Jan. 1, 1966.
13. W. H. McAdams, Heat Transmission, McGraw-Hill, Third Edition, 1954.
14. W. M. Rohsenow and J. P. Hartnett, Handbook of Heat Transfer, McGraw-Hill, 1973.
15. SAE Aerospace Applied Thermodynamics Manual, Second Edition, October 1969.

16. W. M. Kays and A. L. London, Compact Heat Exchanges, McGraw-Hill, First Edition, 1958.
17. W. M. Kays and A. L. London, Compact Heat Exchanges, McGraw-Hill, Second Edition, 1964.
18. Aluminum Soldering Handbook, The Aluminum Association, 2nd Edition, December 1974.

TABLE 1
FACTORS OF SAFETY

Static Strength Design Conditions	Factor of Safety	
	Limit	Ultimate
In-Plane Axial Load	1.0	1.5
Lateral Pressure	1.0	1.5
Thermal Stress	1.0	1.0
Temperature	1.0	1.0
Temperature Gradient	1.0	1.0
Coolant Pressures	1.0	1.5(1)

(1) Burst pressure (acting alone) factor of safety for coolant passages, manifolds and fittings is 4.0.

TABLE 2
MASS OF FULL SCALE PANEL DETAILS

Component	Unit Mass	
	kg/m^2	lbm/ft^2
Skins (2219-T87)	3.77	(0.77)
Dee Tubes (6061-T6)	2.75	(0.56)
Honeycomb (5056-H39)	1.34	(0.27)
Closure Angles (2219-T87)	0.85	(0.18)
Manifolds (6061-T6)	0.69	(0.12)
Splice Plates (2219-T87)	0.89	(0.18)
Adhesives	2.09	(0.43)
Bellmouth	0.04	(0.01)
Connectors	0.01	(0.01)
Bushings/Fasteners	0.50	(0.10)
Subtotal	12.80	(2.62)
Residual Coolant (1)	1.60	(0.33)
APS	0.39	(0.08)
Total	14.78	(3.03)

(1) 60/40 Methanol/Water

TABLE 3
OPTIMIZED PANEL VARIABLES

1. OUTER SKIN THICKNESS	0.102 cm (0.040 in.)
2. INNER SKIN THICKNESS	0.041 cm (0.016 in.)
3. DEE TUBE INNER DIAMETER	0.965 cm (0.38 in.)
4. DEE TUBE WALL THICKNESS	0.089 cm (0.035 in.)
5. DEE TUBE PITCH	2.54 cm (1.0 in.)
6. HONEYCOMB CORE DENSITY	49.66 kg/m^3 (3.1 lb/ft^3)
7. COOLANT	60/40 Methanol/Water
8. COOLANT INLET TEMPERATURE	256 K (0^o F)
9. COOLANT OUTLET TEMPERATURE	321 K (117^o F)
10. COOLANT MASS FLOW RATE FOR PANEL	2.35 kg/sec (18720 lb/hr)
11. PRESSURE DROP IN DEE TUBES	140.7 kPa (20.4 psi)
12. MAXIMUM OUTER SKIN TEMPERATURE	422 K (300^o F)
13. MAXIMUM OUTER SKIN DELTA TEMP.	296 K (72^o F)
14. SKIN MATERIAL	2219-T87
15. TUBE MATERIAL	6061-T6
16. CORE MATERIAL	5056-H39
17. ALLOWABLE STRESSES	124.1 MPa (18,000 psi)
18. CORE HEIGHT (between skins' centroids)	2.87 cm (1.13 in.)
19. APS MASS FOR PANEL	0.293 kg/m^2 (0.06 psf)
20. PANEL STRUCTURAL MASS	7.81 kg/m^2 (1.60 psf)
21. COOLANT INVENTORY IN DEE TUBES	1.42 kg/m^2 (0.29 psf)
22. OPTIMIZED PANEL MASS (TOTAL)	9.52 kg/m^2 (1.95 psf)

TABLE 4

COMPARISON AND RATING OF ALUMINUM MATERIAL CANDIDATES

(INDEX OF 1.00 INDICATES BEST RATING)

Material	T = 300 K (80°F)								T = 422 K (300°F) T = 394 K (250°F) (10,000 hr)						T = 533 K (500°F) (10 hr)						Advantages	Disadvantages
	Fatigue (20,000 Cycles)	K_c	$\Delta K = 33\ MPa\sqrt{m}$ ($\Delta K = 30\ psi\sqrt{in}$)	da/dn	F_{tu}/ρ	F_{ty}/ρ	F_{cy}/ρ	$E_c^{0.333}/\rho$	$(E_c^{0.225} F_{cy}^{0.325})/\rho$	Fatigue (20,000 Cycles)	F_{tu}/ρ	F_{ty}/ρ	F_{cy}/ρ	$E_c^{0.333}/\rho$	$(E_c^{0.225} F_{cy}^{0.325})/\rho$							
2014-T6	1.00 (1)	0.67		0.72 0.92	0.66 0.84	1.00 0.99	1.00 0.99	1.00 1.00	0.86	0.52	0.61	0.54	0.95	0.79		Susceptible to Corrosion, Exfoliation, and Stress Corrosion Cracking
2024-T81	1.00	0.47	0.34	1.00 1.00	1.00 1.00	0.99 1.00	1.00 1.00	1.00 1.00	1.00	1.00	1.00	0.85	0.97	0.93	Good Corrosion Resistance, Good Elevated Temperature Mechanical Properties	Low Fracture Toughness at Room Temperature. No Elevated Temperature Fracture Toughness Data
2219-T6	0.64	0.92		0.83 0.75	0.64 0.58	0.67 0.63	0.98 0.98	0.87 0.86	0.55	0.75	0.72	0.83	0.95	0.91	Stable for Long Time Exposure at Elevated Temperature	Low Initial Strength, i.e., at Low Temperatures. No Elevated Temperature K_c Data
2219-T87	1.00	0.98	1.00	0.86 0.79	0.80 0.77	0.81 0.82	0.98 0.98	0.92 0.95	0.91	0.82	0.82	1.00	0.95	1.00	High Fracture Toughness. Stable for Long Time Exposure to Elevated Temperature. Good Corrosion Resistance Weldable, Property Data Readily Available at Elevated Temperature	Low Initial Strength, i.e., at Low Temperatures. No Elevated Temperature K_c Data
6061-T6	0.69	1.00	0.41	0.66 0.59	0.63 0.57	0.65 0.61	1.00 1.00	0.87 0.85	0.59	0.51	0.54	0.47	1.00	0.85	High Fracture Toughness. Excellent Corrosion Resistance	Low Strength. No Elevated Temperature K_c Data
7075-T6	0.91	0.60	0.76	0.55 0.84	0.60 0.82	0.62 0.80	0.97 0.98	0.84 0.95		0.39	0.40	0.35	0.91	0.67		Susceptible to Corrosion, Exfoliation, and Stress Corrosion Cracking. Low Fracture Toughness. Temperature Limited. No Elevated Temperature K_c Data
7475-T761	0.78	0.89	1.00	0.52 0.59	0.49 0.76	0.50 0.85	0.96 0.97	0.78 0.88		0.32	0.35	0.27	0.91	0.62	High Fracture Toughness	Sole Source, Premium Price, Temperature Limited. No Elevated Temperature K_c Data

(1) Index rating - highest value indicates best rating

TABLE 5
MECHANICAL AND THERMAL PROPERTY DATA FOR ADHESIVES AND LOW TEMPERATURE SOLDER

Bonding Material	Exposure	Test Temp	Peel Strength	Shear Strength	Thermal Conductivity
	Time K (°F)	K (°F)	kN/m (lbf/in.)	MPa (ksi)	W/m-K $\left(\frac{\text{Btu-in.}}{\text{hr-ft}^2\text{-}^\circ\text{F}}\right)$
FM-400 (1)	None	297 (75)	3.3 (19.0)	23.7 (3.44)	0.37 (2.6)
	10 min at 218 (–67)	218 (–67)	– –	24.6 (3.56)	0.37 (2.6)
	18 hrs at 458 (365)	297 (75)	– –	27.8 (4.03)	0.37 (2.6)
	18 hrs at 458 (365)	458 (365)	1.3 (7.2)	21.2 (3.08)	0.37 (2.6)
	3 hrs at 489 (420)	489 (420)	– –	12.6 (1.82)	0.37 (2.6)
FM-400 Paste (5)	None	297 (75)	0.88 (5.0)	22.9 (3.32)	1.89 (13.1)
FM-404 (2)	None	297 (75)	– –	3.4 (0.50)	– –
Eccobond 58C	None	297 (75)	0.18 (1.0)	8.6 (1.25)	1.24 (8.6)
Eccobond 58C	None	297 (75)	0.18 (1.0)	11.4 (1.65)	28.83 (200) (3)
	None	297 (75)	0.18 (1.0)	11.4 (1.65)	1.08* (7.5)*
	10 min at 366 (200)	366 (200)	– –	13.9 (2.02)	1.08* (7.5)*
	3 hrs at 366 (200)	366 (200)	– –	12.9 (1.87)	1.08* (7.5)*
	18 hrs at 366 (200)	366 (200)	– –	11.9 (1.73)	1.08* (7.5)*
	10 min at 422 (300)	422 (300)	– –	6.1 (0.88)	1.08* (7.5)*
Eccobond 58C (5) (5% Diluent, Al. Screen)	None	297 (75)	0.35 (2.0)	11.7 (1.70)	3.17 (22.0)
Eccobond 58C (5)	None	297 (75)	0.26 (1.5)	14.4 (2.09)	2.22 (15.4)
Eccobond 58C (5) (5% Diluent, Nylon Scrim)	None	297 (75)	0.44 (2.5)	13.2 (1.91)	0.59 (4.1)
Eccobond 58C (5) (25% Diluent)	None	297 (75)	0.26 (1.5)	– –	– –
Low Temp Solder (91% Sn + 9% Zn)	None	297 (75)	3.5 (20.0)	19.6 (2.84)	>57.7 (>400)
	None	350 (170)	– –	13.3 (1.93	– –
	None	375 (215)	– –	9.0 (1.31)	– –

NOTES:

(1) Peel and shear strength data generated in-house

(2) Peel and shear strength data generated in-house

(3) This value of thermal conductivity obtained from technical bulletin 3-2-5A, Eccobond solder 58C, Emmerson and Cuming, Inc., Dielectric Materials Division, Canton, Massachusetts, January 1, 1966.

(4) All other data were generated during this program.

(5) The addition of the methyl ethyl keytone diluent, the aluminum screen, and the nylon scrim cloth in the adhesive was an attempt to reduce and/or control voids in the adhesive and thus improve its thermal conductivity and its peel strength.

TABLE 6
SKIN/COOLANT PASSAGES JOINT MATERIALS CHARACTERISTICS

Bonding Media	Bondline Thickness cm	(in.)	Thermal Conductivity $\frac{W}{m \cdot K}$ $\left(\frac{Btu\text{-}in.}{hr\text{-}ft^2\text{-}^oF}\right)$		Interface Conductance $\frac{kW}{m^2 \cdot K}$ $\left(\frac{Btu}{hr\text{-}ft^2\text{-}^oF}\right)$		Skin Temperature Manifold/Skin K	(^{o}F)
ull Scale Panel esign Values	0.0150	(0.006)	2.88	(20.0)	18.9	(3,333)	374/416	(214/290)
ccobond 58C	0.0254	(0.010)	1.08	(7.5)	4.25	(750)	400/489	(260/420)
% Diluent 58C	0.0254	(0.010)	2.22	(15.4)	8.74	(1,540)	383/441	(230/335)
% Diluent 58C lylon Scrim	0.0229	(0.009)	0.59	(4.1)	2.58	(456)	416/553	(290/535)
% Diluent 58C luminum Screen	0.038	(0.015)	3.17	(22.0)	8.34	(1,467)	383/442	(230/335)
ccobond 56C	0.0254	(0.010)	1.24	(8.6)	4.88	(860)	394/478	(250/400)
hin FM-400 ilm Type	0.0130	(0.005)	0.37	(2.6)	2.95	(520)	411/533	(280/500)
M-400 Paste luminum Screen	0.0380	(0.015)	1.88	(13.06)	4.95	(871)	393/474	(248/393)
ow Temp Solder 91% Sn + 9% Zn)	0.0254	(0.010)	>57.65	(>400)	227	(40,000)	<366/396	(<200/254)

TABLE 7
COMPARISON OF COOLANT PROPERTIES - 60% AQUEOUS SOLUTIONS OF METHANOL AND ETHYLENE GLYCOL

	Coolant Property	Methanol	Ethylene Glycol
I	Temperatures, K (^{0}F)		
	• Normal Inlet	256 (0)	283 (50)
	• Normal Outlet	321 (117)	323 (122)
	• Freezing Point	199 (−101)	289 (−60)
	• Boiling Point at 101.3 kPa (14.7 psia)	348 (166)	384 (231)
II	Pressures, kPa (psi)		
	• ΔP of Panel	185 (26.9)	410 (59.4)
	• Normal Maximum	552 (80)	758 (110)
	• Normal Minimum	345 (50)	345 (50)
	• Vapor Pressure at T_{out}	32 (4.7)	0.14 (0.02)
III	Flammability, K (^{0}F)		
	• Flash Point (Open Cup)	289 (61)	389 (240)
	• Autoignition	743 (878)	749 (888)
IV	Toxicity[1]		
	• Single Oral LD_{50} Dose for Rats	Slight Hazard (12.9 gm/Kg)	7.4 ml/Kg
	• Repeated Oral Feeting (Rats), Acceptable Level in Diet and Duration[2]	–	0.18 gm/Kg/Day (30 Days)
	• Single Skin Penetration LD_{50} Dose (Rabbits)	Slight Hazard	>20 ml/Kg
	• Single Inhalation Concentrated Vapor (Rats	Slight Hazard (Killed None of 6 in 4 hrs; 5 of 6 in 8 hrs)	8 hrs Killed None of 6
	• Primary Skin Irritation (Rabbits)	–	None
	• Eye Injury (Rabbits)	(No More Severe Than Liquid Hand Soap)	None
V	Suffocation,[3] kPa (psia)		
	• Potential at 300 K (80^{0}F)	12.4 (1.8)	≈0.014 (0.002)
VI	Material Compatibility		
	• Aluminum	Requires Inhibitor	Requires Inhibitor
	• Braze Material (Aluminum)	Requires Inhibitor	Requires Inhibitor
	• Elastomers	OK	OK
VII	Lubricity (at Normal Inlet Temperature)	5.4 cps	7.3 cps
VIII	Thermal Expansion, per K (^{0}F)	0.00119 (0.00066)	0.00115 (0.00064)
IX	Relative Leakage Factor	1.00	1.20
X	Development Status	Developed	Developed
XI	Availability	Readily Available	Readily Available

(1) Toxicity
- The term LD_{50} refers to that quantity of chemical which kills 50 percent of dosed animals within 14 days. For uniformity, dosage is expressed in grams or milliliters per kilogram of body weight.
- Single skin penetration refers to a 24 hour covered skin contact with the liquid chemical.
- Single inhalation refers to the continuous breathing of a certain concentration of chemical for the stated period of time.
- Primary irritation refers to the skin response 24 hours following application of 0.01 ml amounts to uncovered skin.
- Eye injury refers to surface damage produced by the liquid chemical.

(2) Methanol is commonly labeled as a poison for statutory reasons even though it does not meet the definition of a poisonous substance. This practice results form the too common and ill-advised use of methanol for beverage purposes.

(3) Vapor pressures above 17.2 kPa (2.5 psia) are unsafe.

TABLE 8
FULL SCALE PANEL COMPONENT STRESS LEVELS

Panel Loading	Location	Component/Stress MP_a (ksi)	Critical Mode	Allowable MP_a (ksi)	Margin of Safety
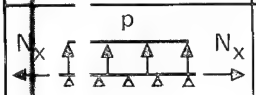 lus Temp	Over Frame Between Frames	Inner Skin/118.0 (17.1) Dee Tube/159.0 (23.0)	Crack Growth Crack Growth	124.0 (18.0) 159.0 (23.0)	0.05 0.00
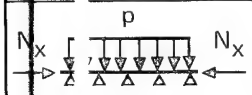 lus Temp	Over Frame	Inner Skin/−188.0 (−27.0)	Face Sheet Wrinkling	250.0 (36.3)	0.33
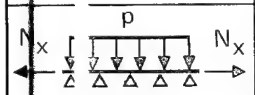 lus Temp	Over Frame	Dee Tube/159.0 (23.0)	Crack Growth	159.0 (23.0)	0.00
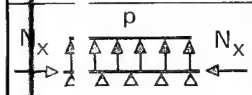 lus Temp	Over Frame Between Frames	Outer Skin/−225.0 (−32.0) Stability/−134.0 (−19.5)	Face Sheet Wrinkling Beam Column	292.0 (42.4) 135.0 (19.6)	0.30 0.00

Note: 1 N_x = 0.210 MN/m (1200 lb/in.), p = 6.9 kP_a (1.0 psi) [Limit Loads]
2 Limit stresses shown for crack growth failure mode
3 Ultimate stresses shown for face sheet wrinkling failure mode
4 Ultimate average stress shown for beam column failure mode
5 Minus Indicates Compression Stress

TABLE 9
TEST RESULTS FOR SOLDERED LAP SHEAR COUPONS

Specimen Number	Temp K	Temp (°F)	Fatigue Loading kN	Fatigue Loading (lbf)	Cycles to Failure	Static Load kN	Static Load (lbf)	Comments
1	297	(75)	0 to 3.25	(730)	36,220	—		Skin Failed at Loading Hole
2	297	(75)			58,260	—		Skin Failed at Solder Fillet
3	297	(75)			56,340	—		Skin Failed at Solder Fillet
4	350	(170)			72,250	—		Skin Failed at Loading Hole
5	350	(170)			96,010	—		Skin Failed at Solder Fillet
6	350	(170)	0 to 3.25	(730)	20,000[1]	12.88	(2895)	Shear Failure in Solder

Note: 1. Fatigue testing stopped after 20,000 cycles and static tested to failure.

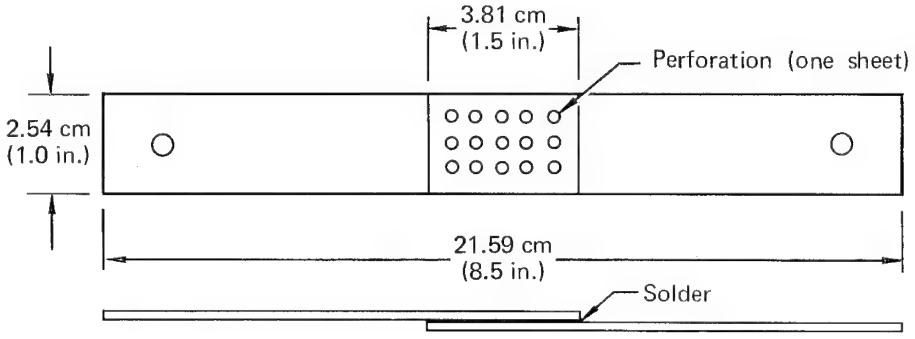

TABLE 10
SUMMARY OF PANEL PRESSURES

Parameter	Units	Full - Scale Panel	Test Panel Simulated Inlet	Test Panel Simulated Exit
Coolant Temperature	K (^{o}F)			
In		283.3 (50)	283.3 (50)	322.7 (120.9)
Out		332.7 (138)	293.5 (68.3)	332.7 (138)
Pressure Drop	kPa (psi)			
Inlet Manifold		46.7 (6.8)	46.7 (6.8)	31.0 (4.5)
Panel		234.4 (34.0)	49.6 (7.2)	37.9 (5.5)
Exit Manifold		28.9 (4.2)	42.7 (6.2)	28.9 (4.2)
Total		310.0 (45.0)	139.0 (20.2)	97.8 (14.2)
Coolant Pressure	kPa (psi)			
In		654.7 (95.0)	654.7 (95.0)	442.5 (64.2)
Out		344.7 (50.0)	515.7 (74.8)	344.7 (50.0)
Mean Flow Deviation	–	± 1.2%	± 4.2%	± 5.0%

Ethylene Glycol/Water (60/40) by Mass
$\dot{m}_c$ = 3234 g/s (7.13 lbm/sec)

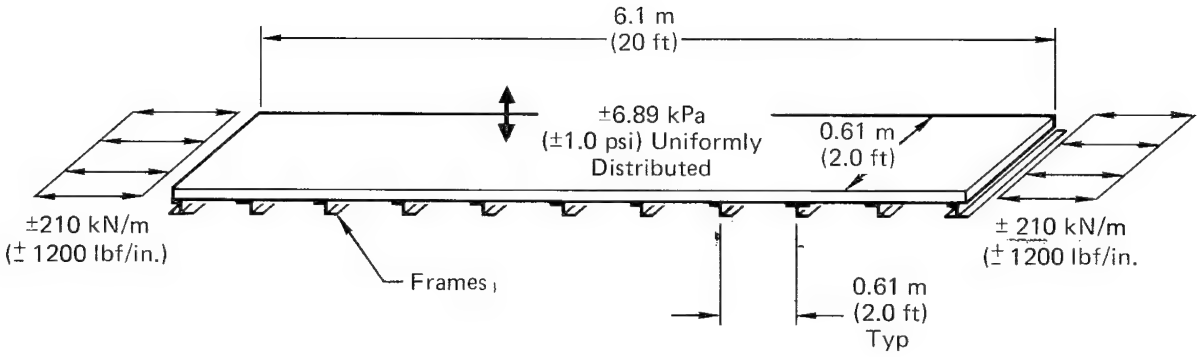

FIGURE 1
FULL SCALE PANEL DESIGN LIMIT LOADS

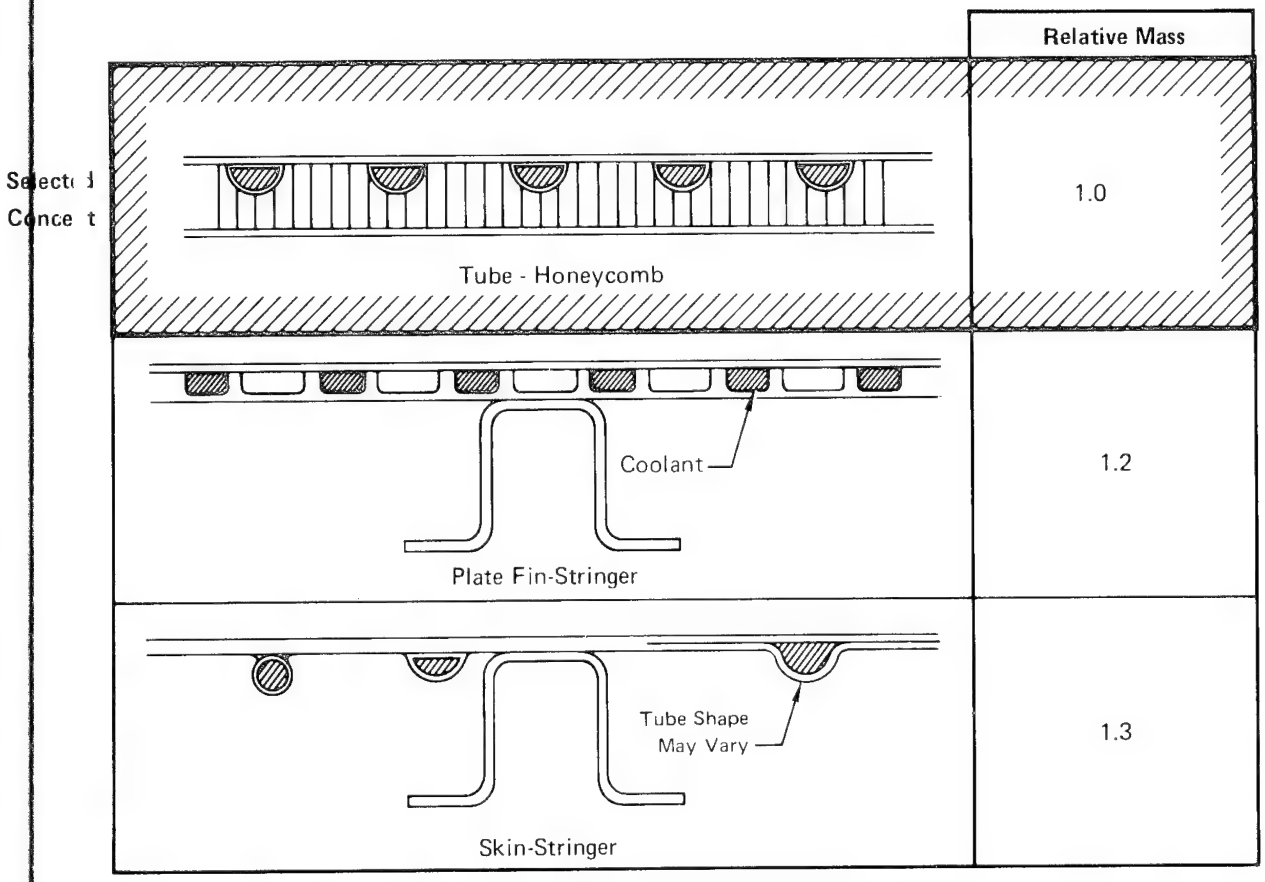

(Mass Components Are Coolant And Structural Elements)

FIGURE 2
RELATIVE MASS OF ACTIVELY COOLED PANEL CONCEPTS

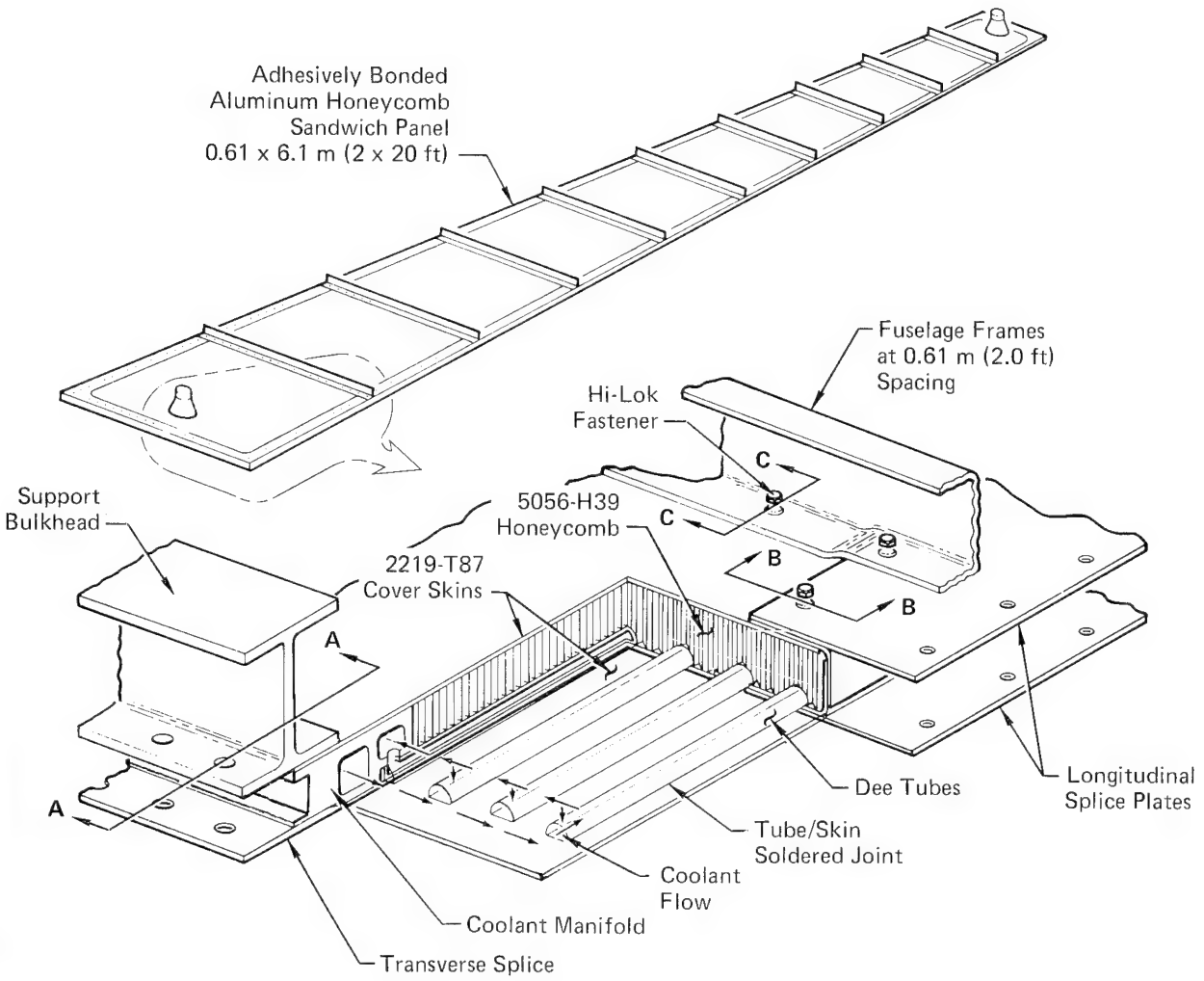

SECTION A-A IS SHOWN ON FIGURE 47
SECTION B-B IS SHOWN ON FIGURE 48
SECTION C-C IS SHOWN ON FIGURE 8

FIGURE 3
ILLUSTRATION OF FULL SCALE ACTIVELY COOLED PANEL DETAILS

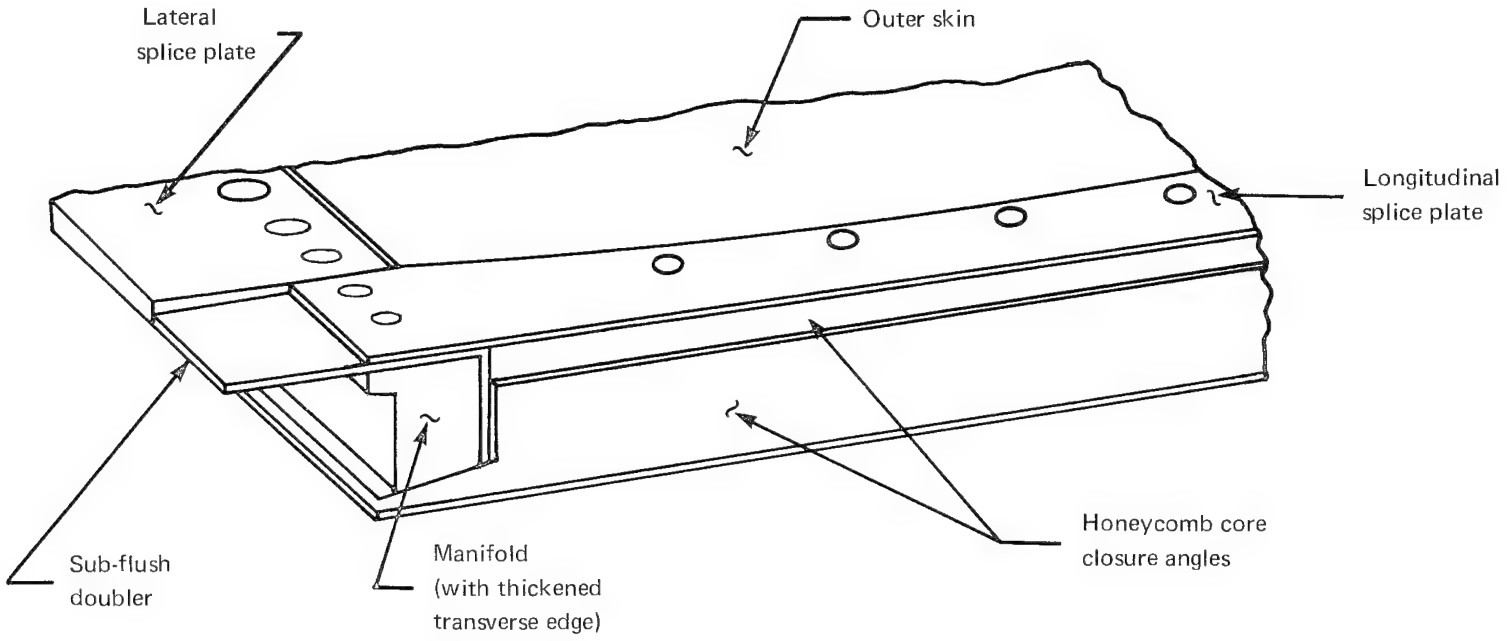

FIGURE 4
TOP VIEW OF PANEL

1. 2219-T87 Concept
   W_{STR} = 8.01 kg/m^2 (1.64 lbm/ft^2)
2. 2219-T87 Skins, 6061-T6 Dee Tubes, 5056-H39 Aluminum Honeycomb

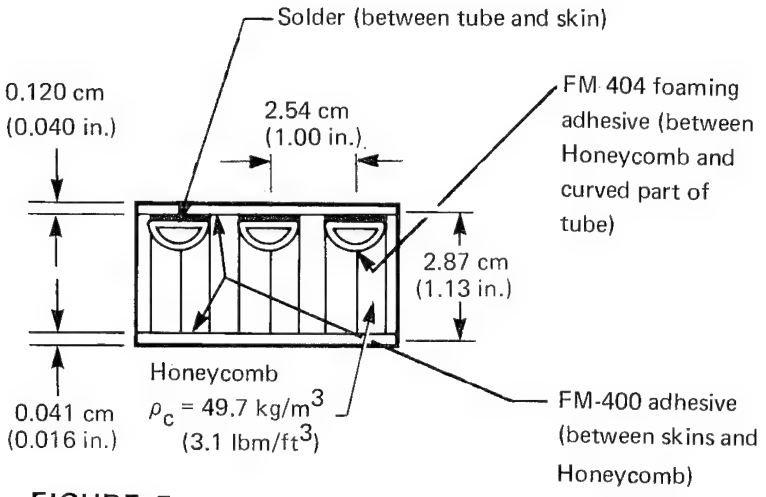

FIGURE 5

DETAILS OF FULL SCALE PANEL SKINS, TUBES AND HONEYCOMB CORE

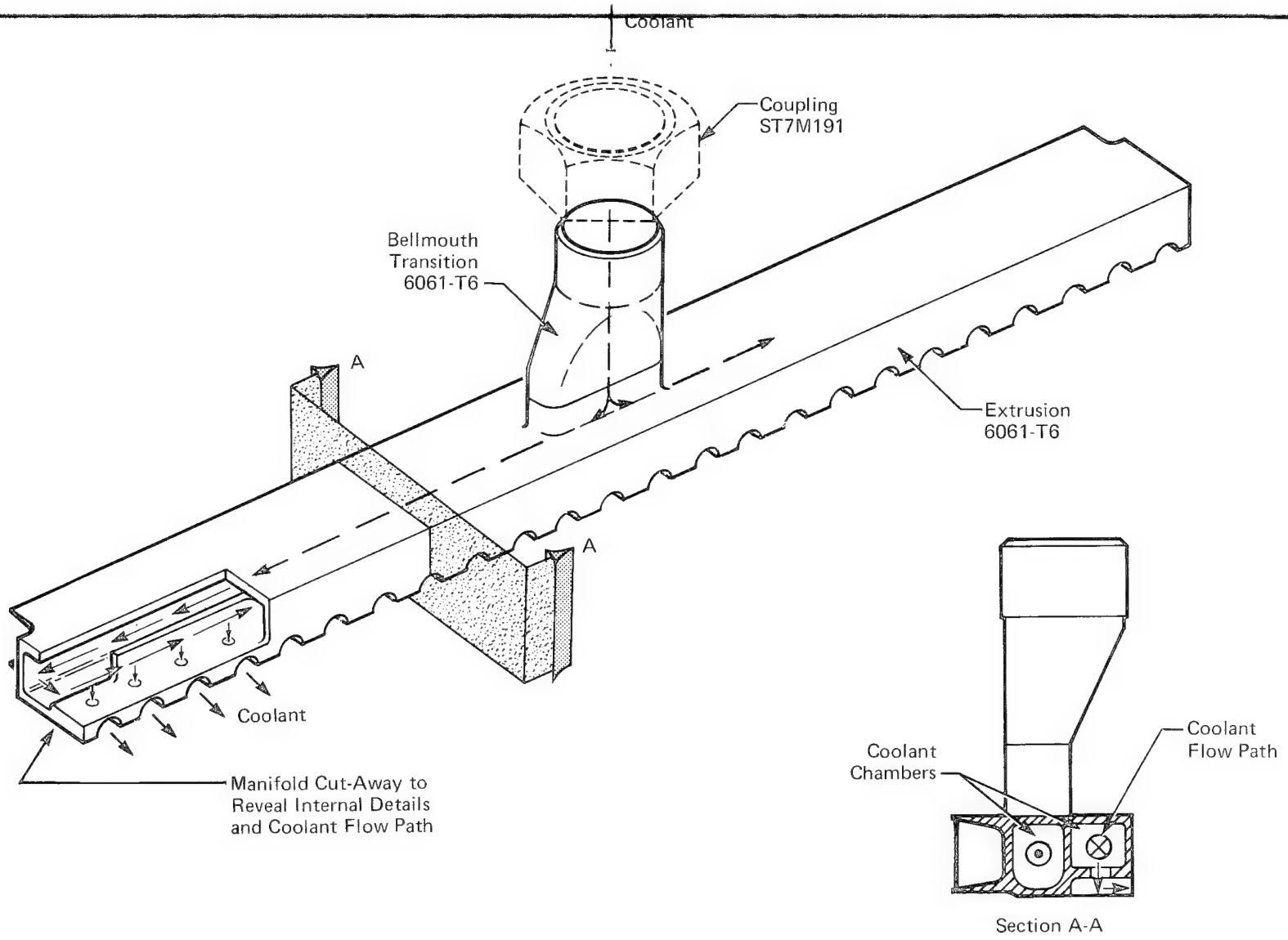

FIGURE 6
ACTIVELY COOLED PANEL MANIFOLD

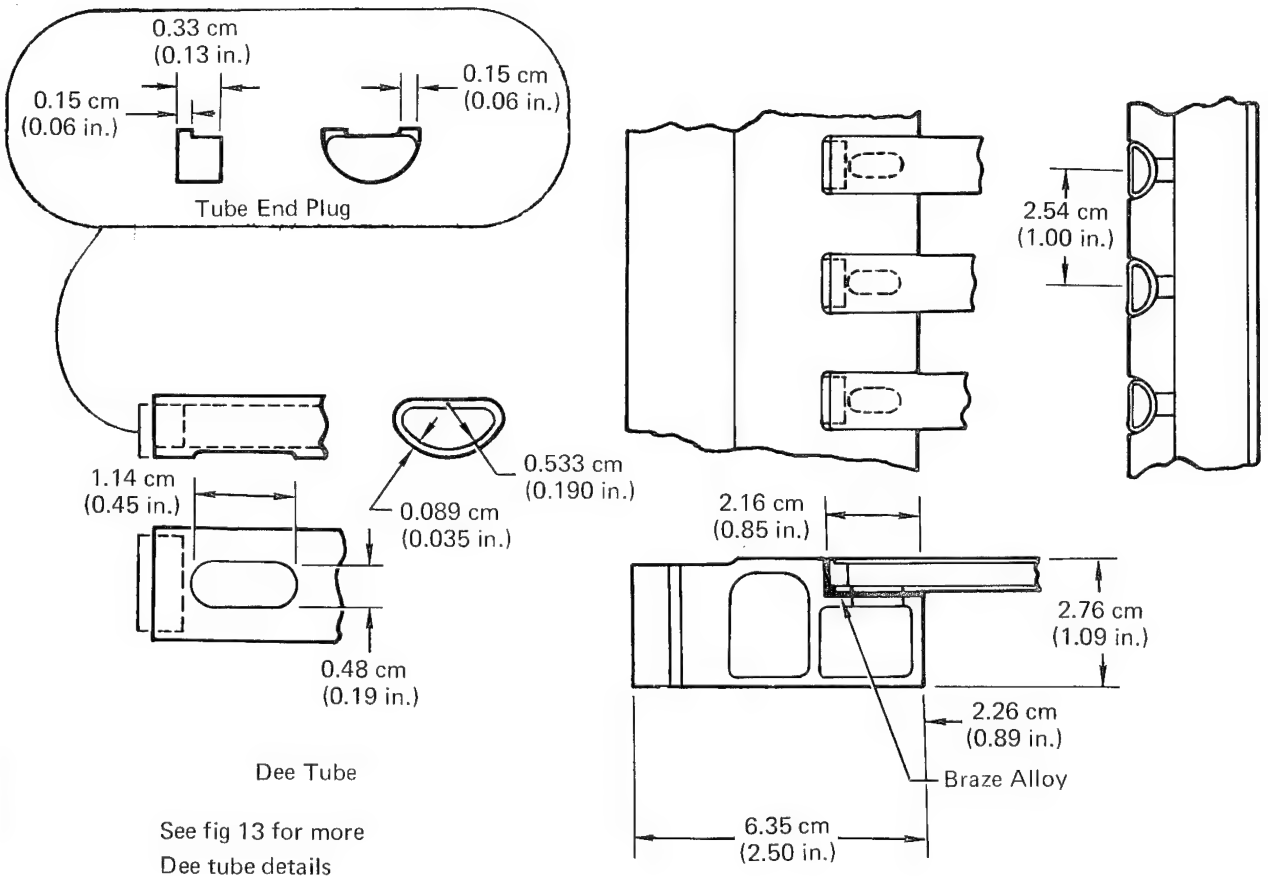

FIGURE 7
DEE TUBE/MANIFOLD JOINT DETAILS

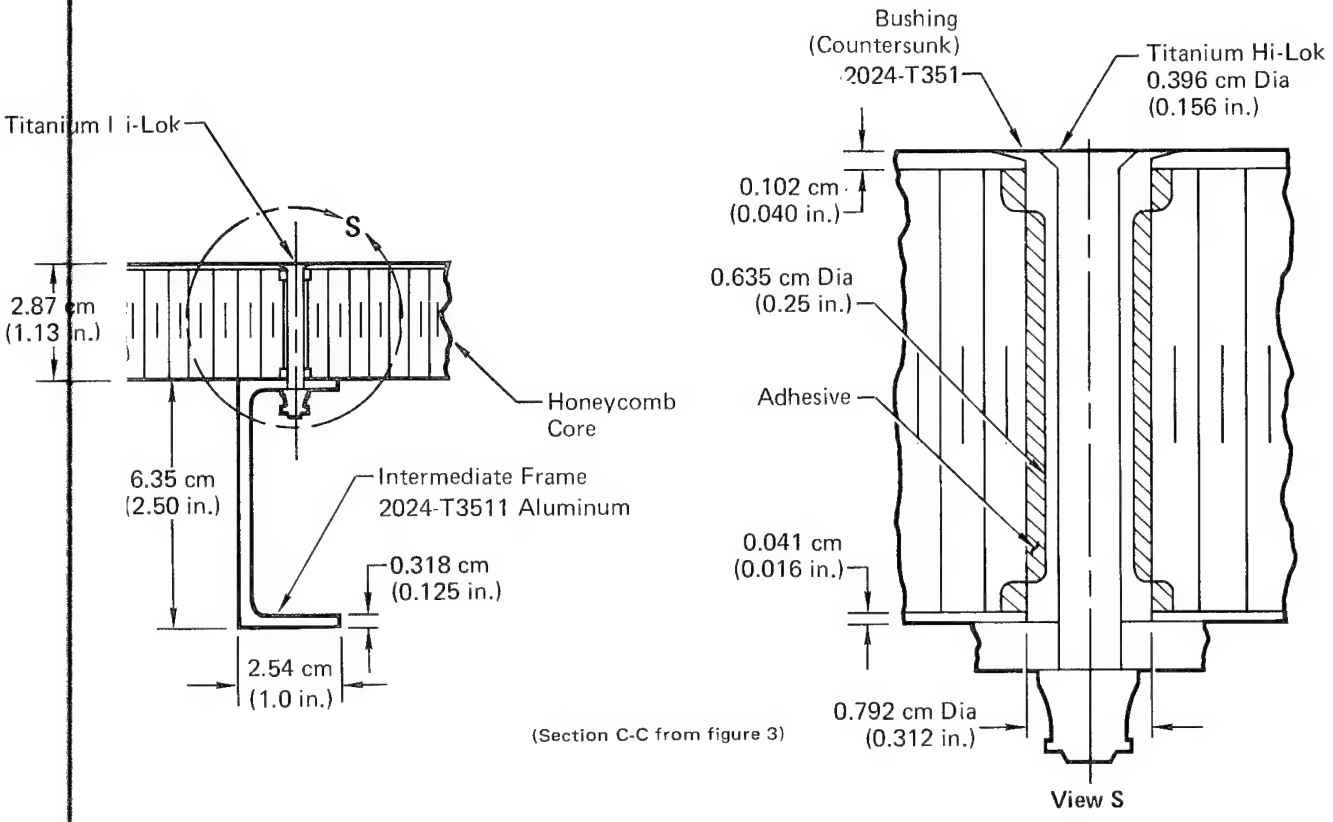

FIGURE 8
INTERMEDIATE FRAME ATTACHMENT

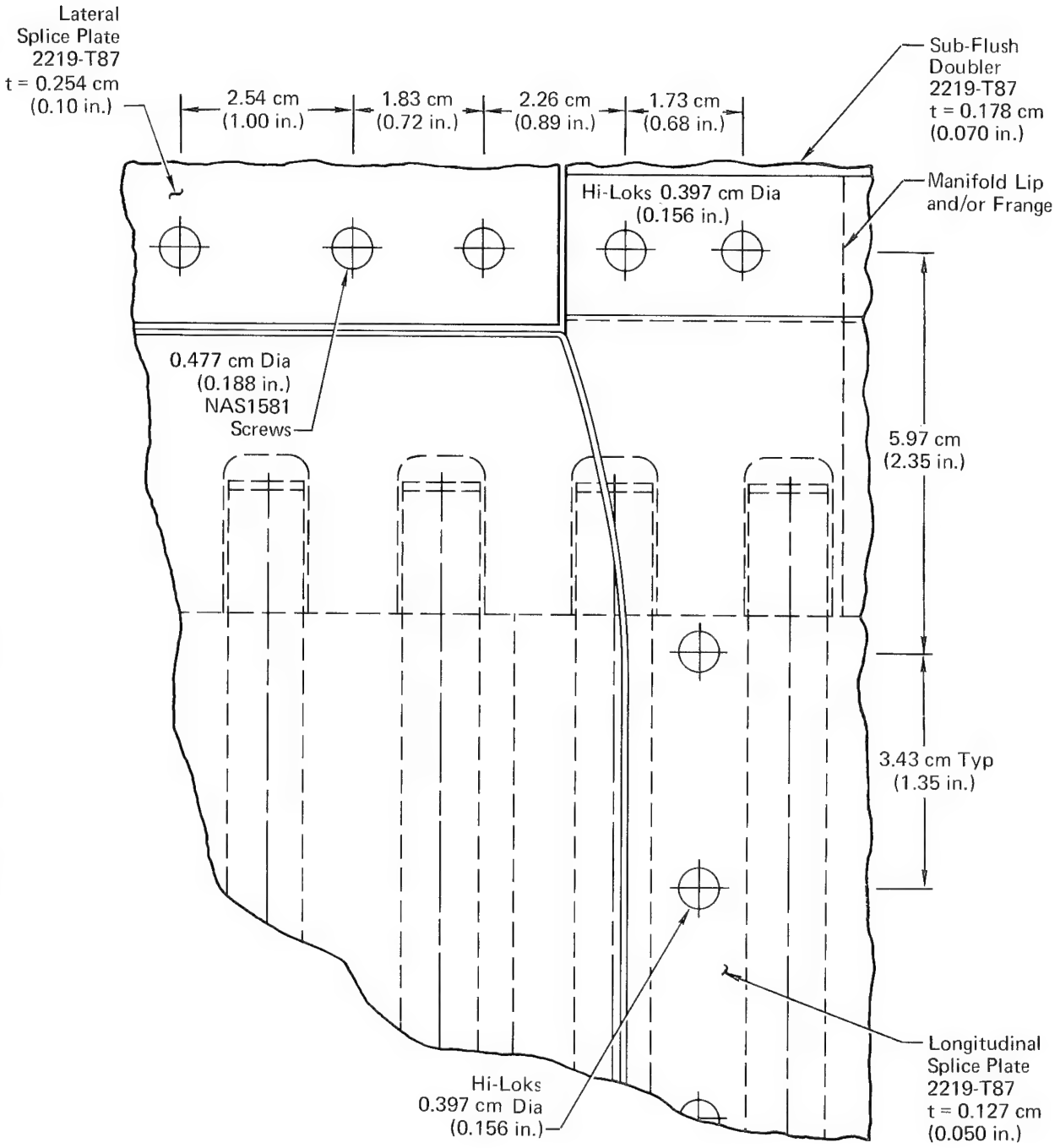

FIGURE 9
PANEL CORNER DESIGN

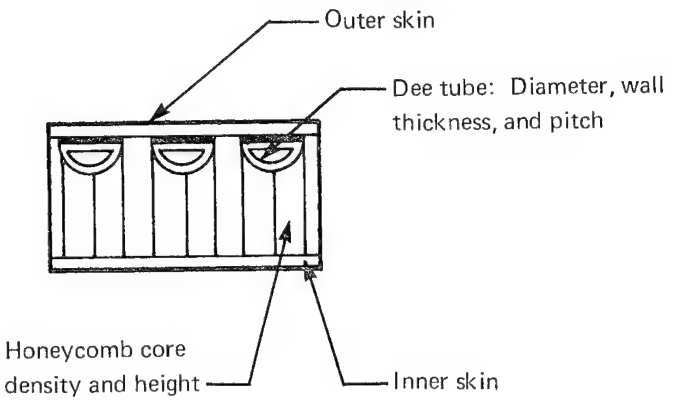

FIGURE 10
PANEL OPTIMIZATION VARIABLES

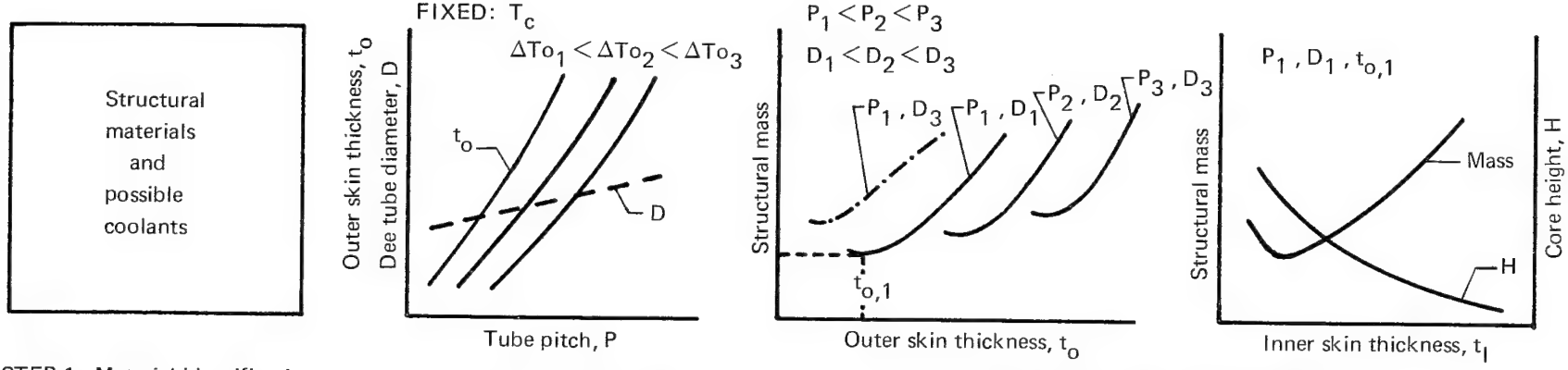

STEP 1 - Material identification

STEP 2 - Preliminary sizing relations

STEP 3 - Structural mass sensitivity

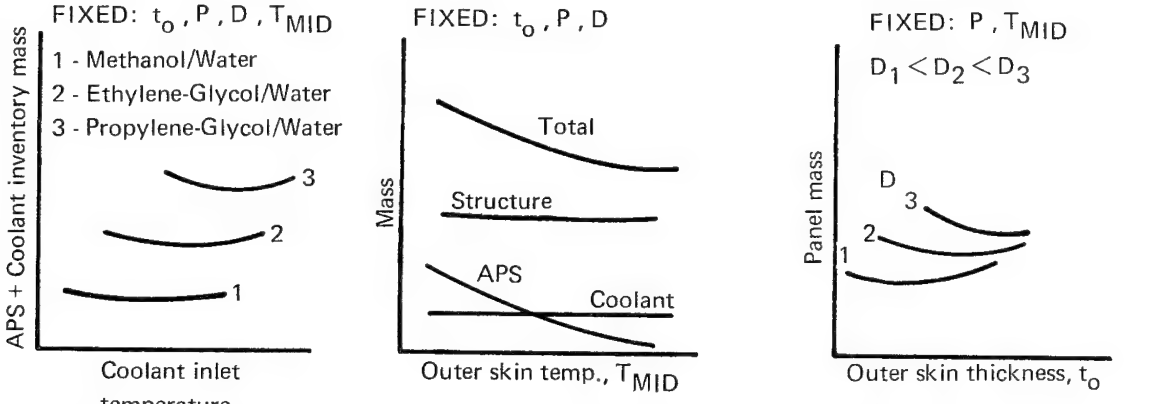

STEP 4 - Coolant mass sensitivity

STEP 5 - Panel mass sensitivity to outer skin temp.

STEP 6 - Mass sensitivity to skin thickness and tube dia.

FIGURE 11
OPTIMIZATION PROCESS

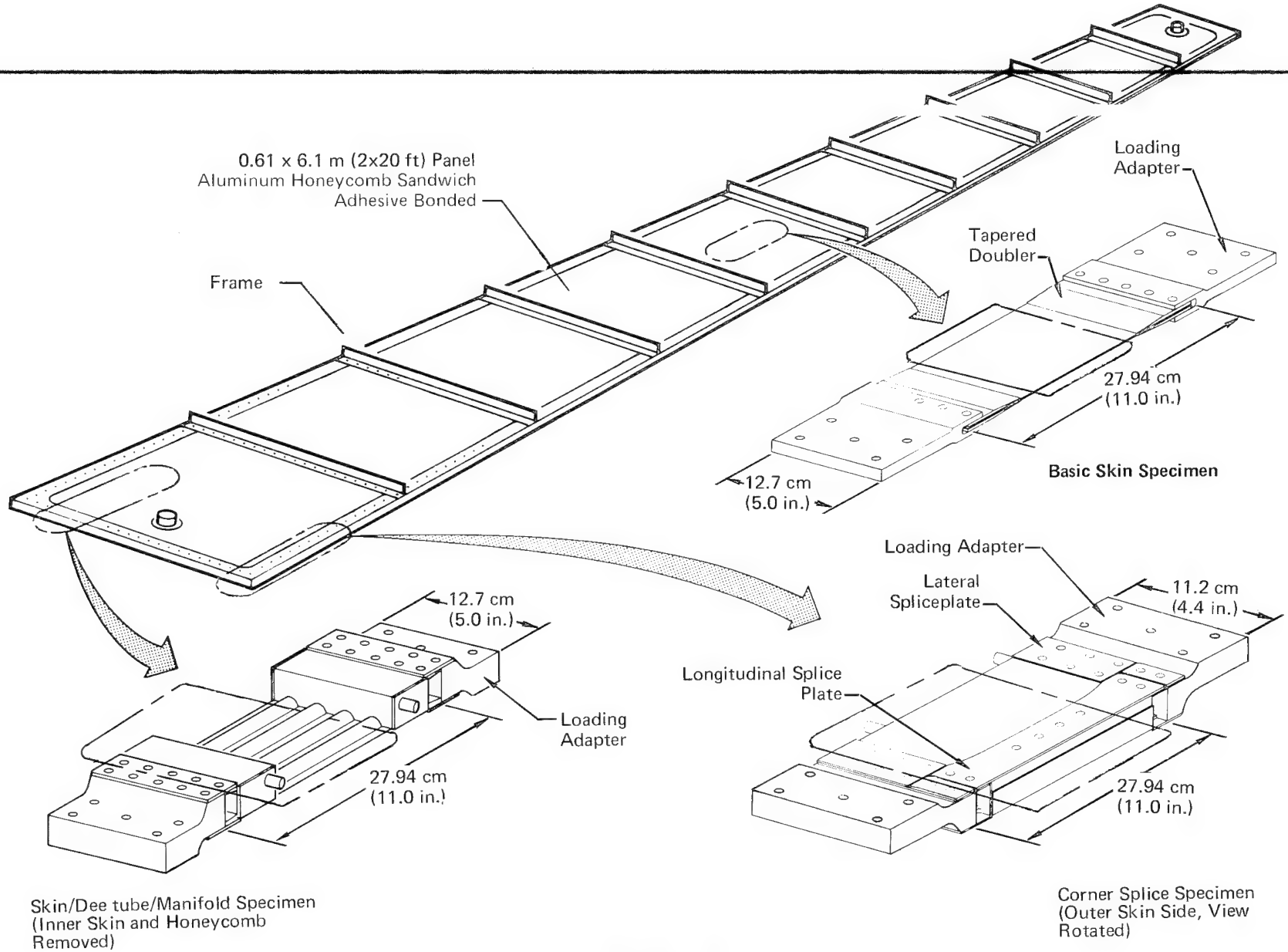

FIGURE 12
FATIGUE SPECIMENS ARE DESIGNED TO EVALUATE THREE AREAS
OF FULL SCALE PANEL

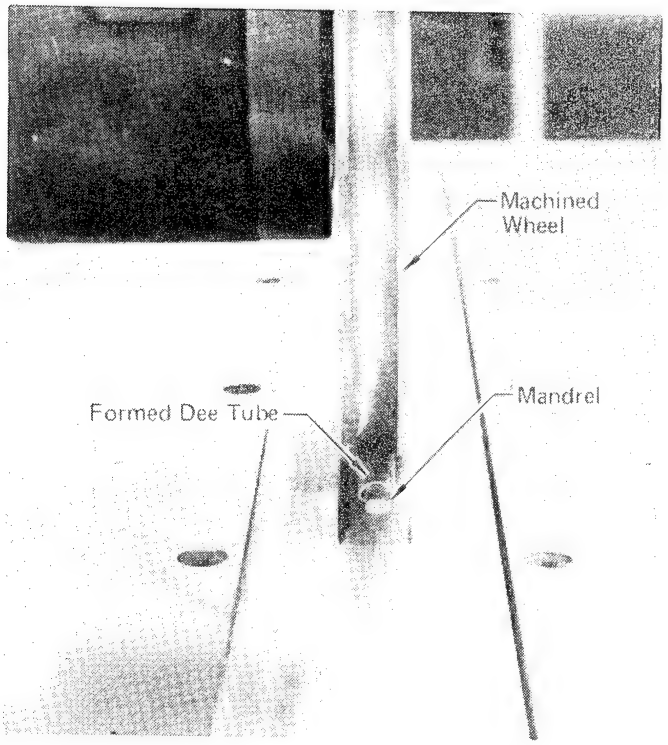

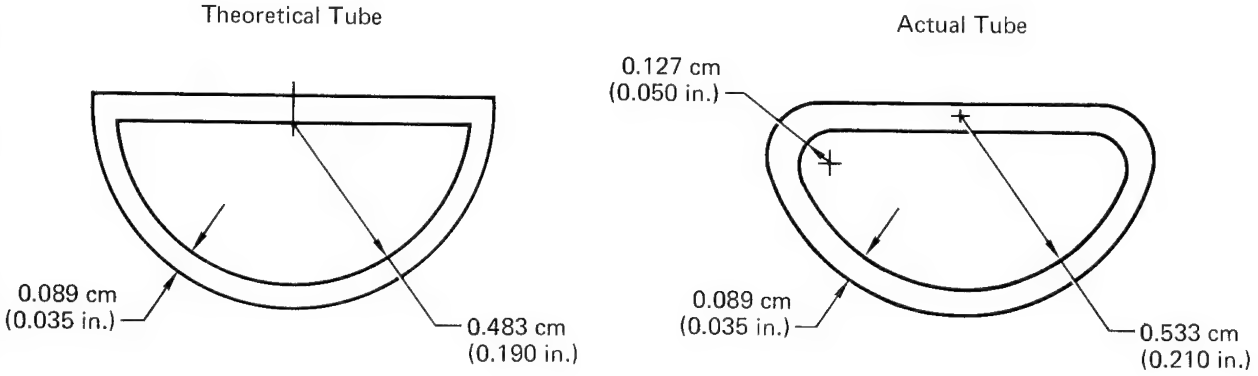

$$0.365\ cm^2\ (0.0566\ in.^2) = A_{flow} = 0.387\ cm^2\ (0.060\ in.^2)$$

$$0.235\ cm^2\ (0.0365\ in.^2) = A_{tube} = 0.243\ cm^2\ (0.0377\ in.^2)$$

$$0.031\ cm^4\ (0.000745\ in.^4) = I_{tube} = 0.031\ cm^4\ (0.000747\ in.^4)$$

FIGURE 13
DEE TUBE FORMING PROCEDURE AND SIZE

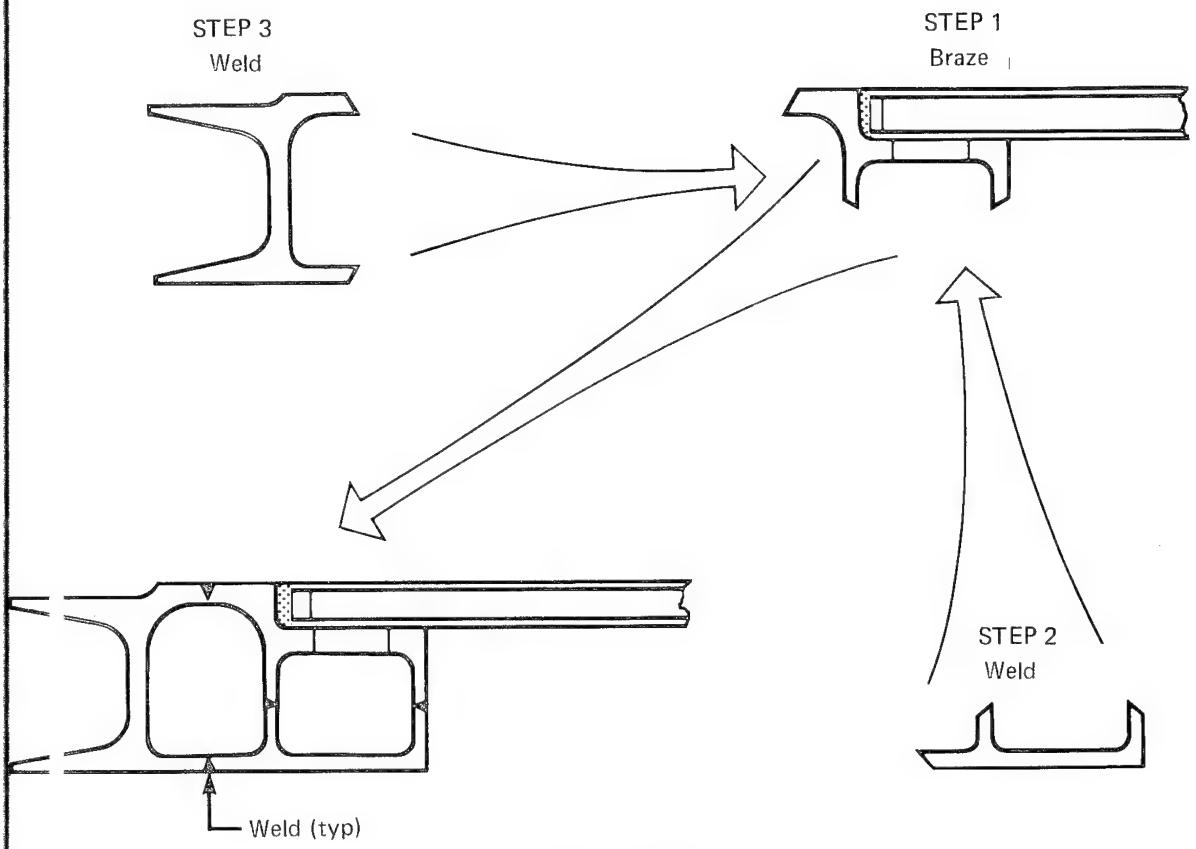

FIGURE 14
MANIFOLD/TUBE ASSEMBLY WELDING SEQUENCE

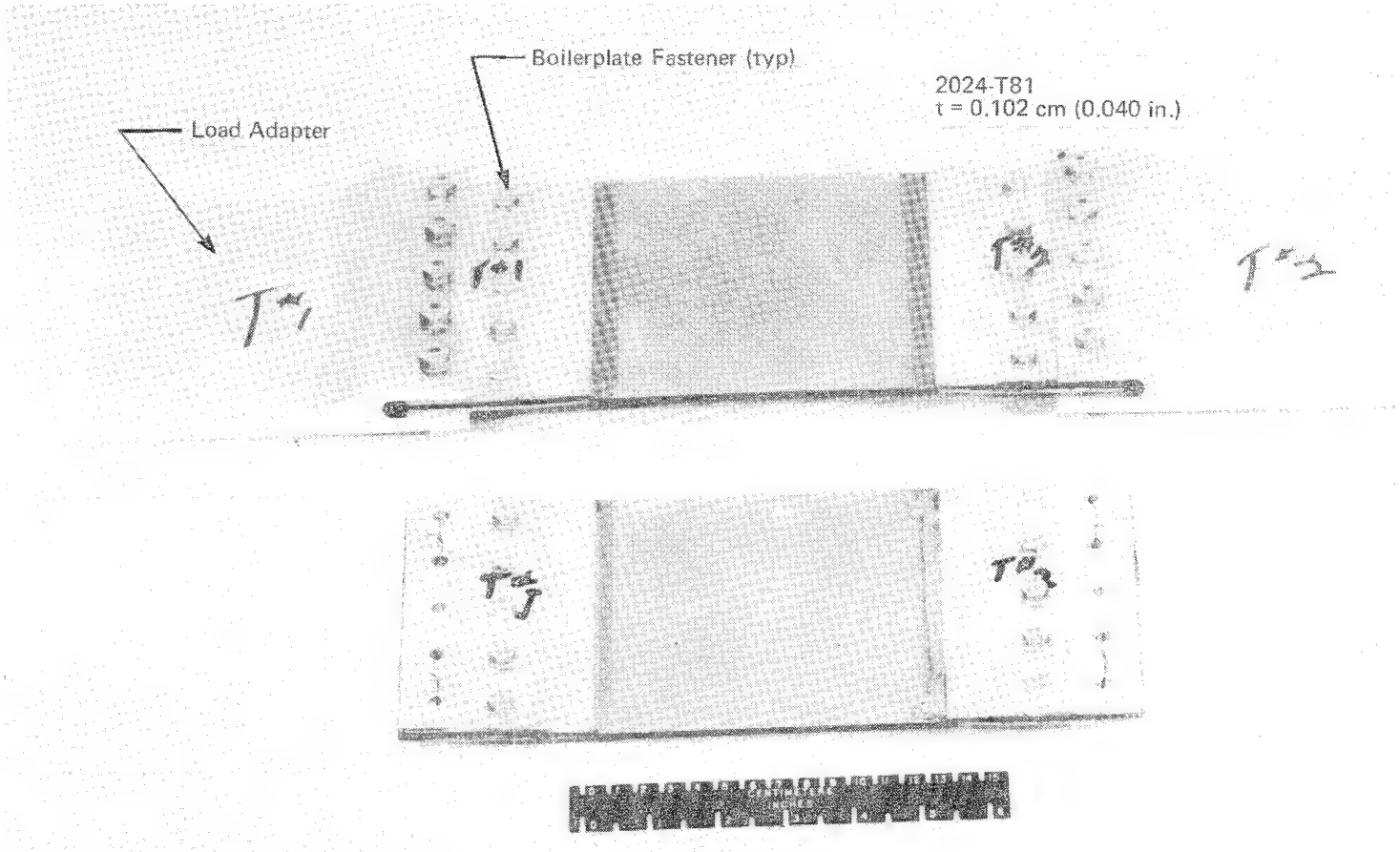

FIGURE 15
BASIC SKIN SPECIMEN

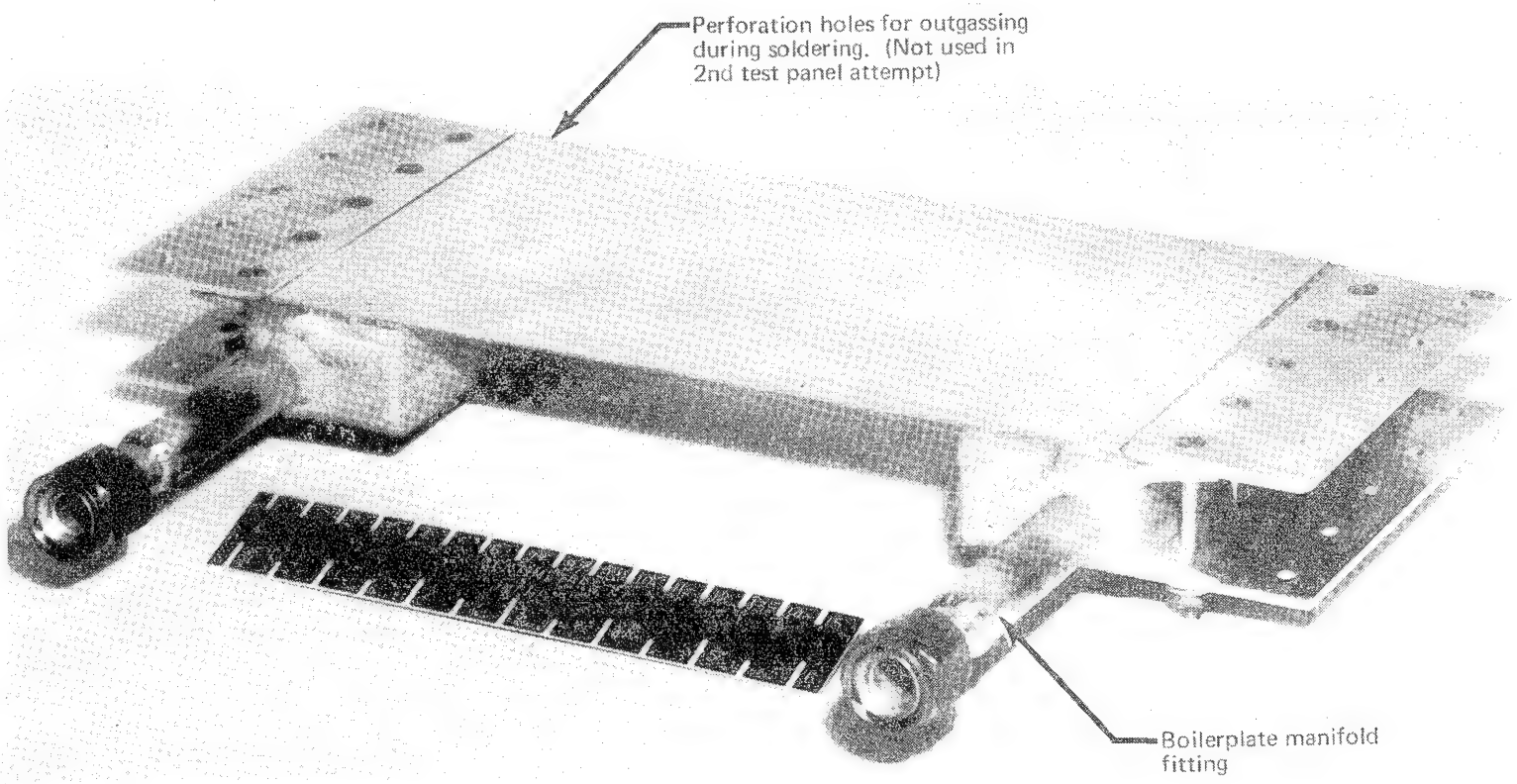

FIGURE 16
SKIN/DEE TUBE/MANIFOLD SPECIMEN
(SOLDERED SPECIMEN)

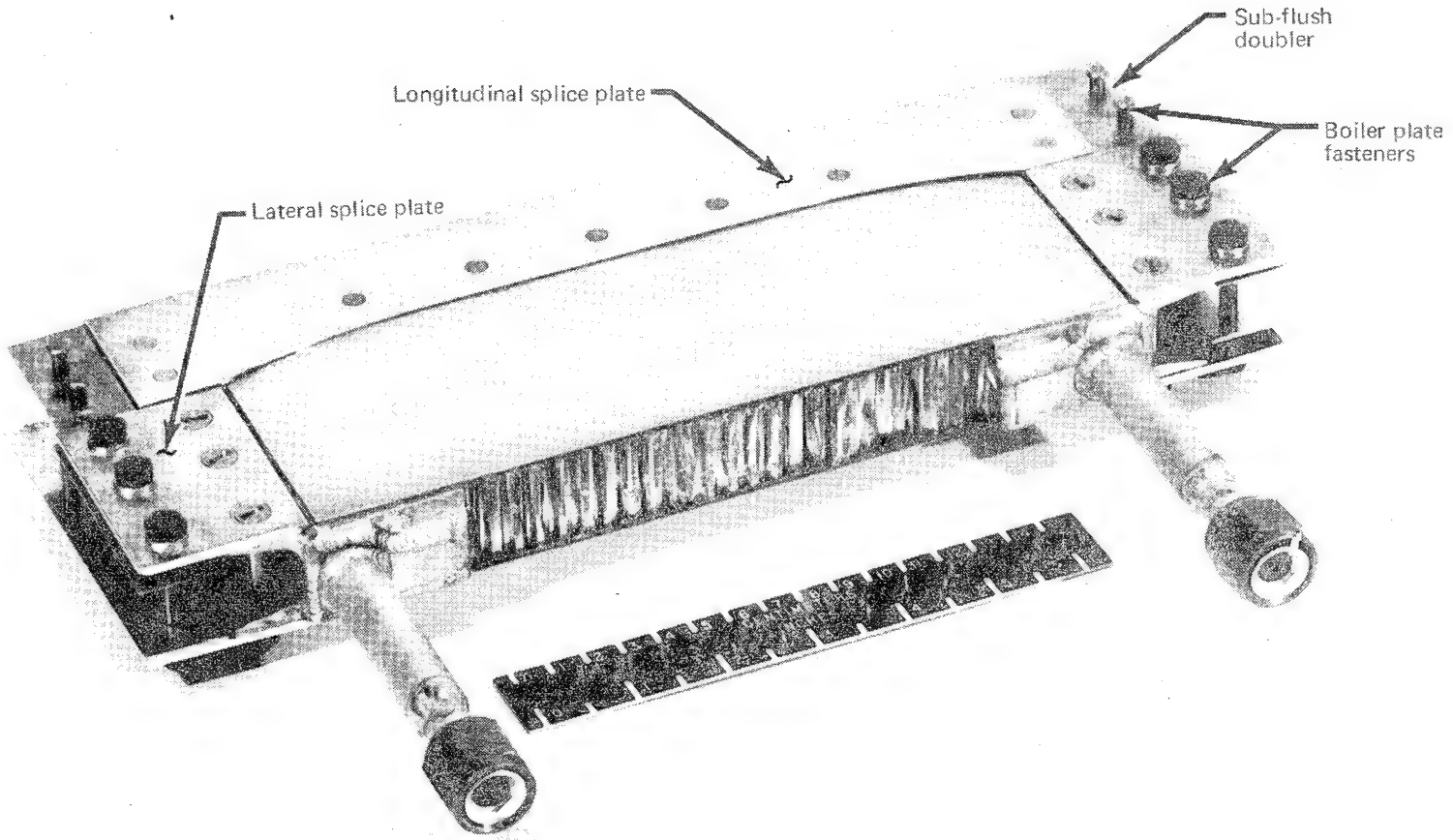

(See figure 9 for details)

FIGURE 17
CORNER SPLICE FATIGUE SPECIMEN

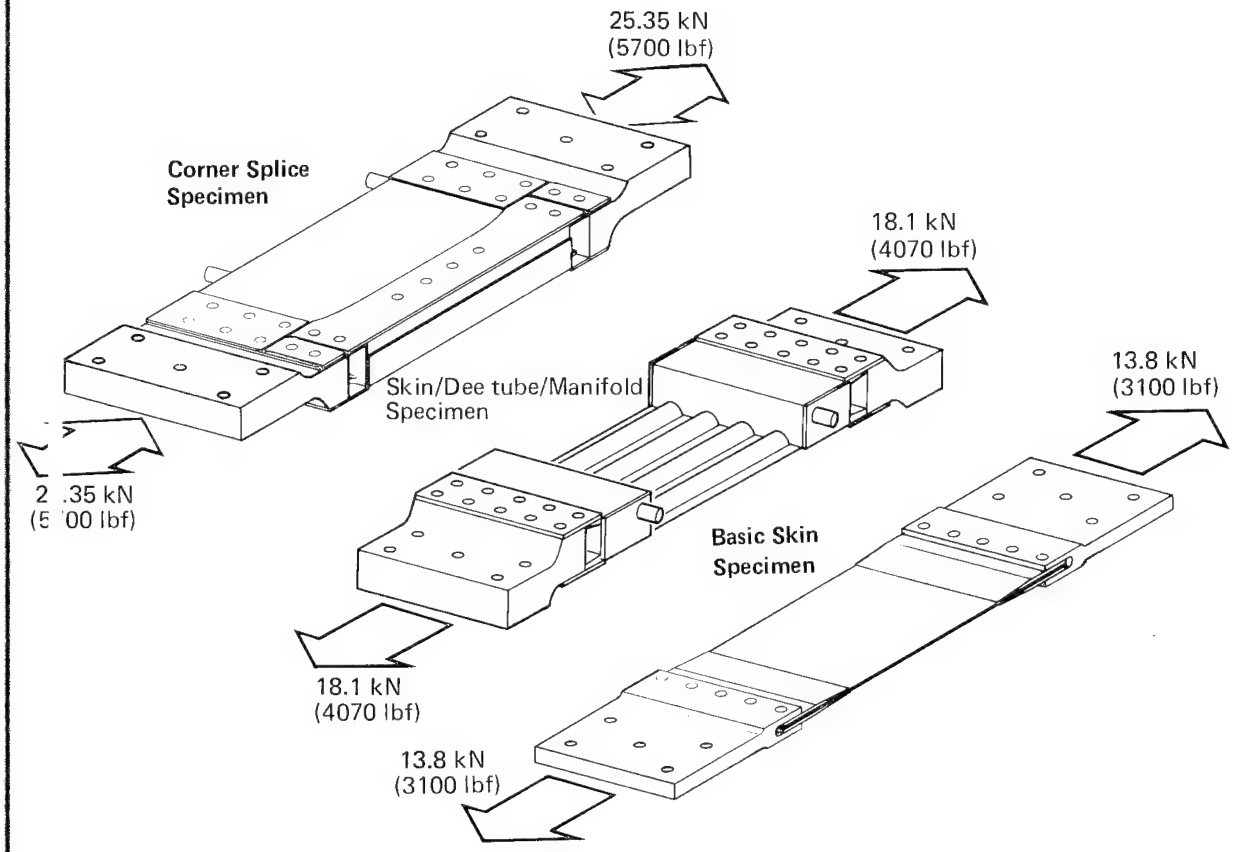

FIGURE 18
FATIGUE SPECIMEN TEST LOADS

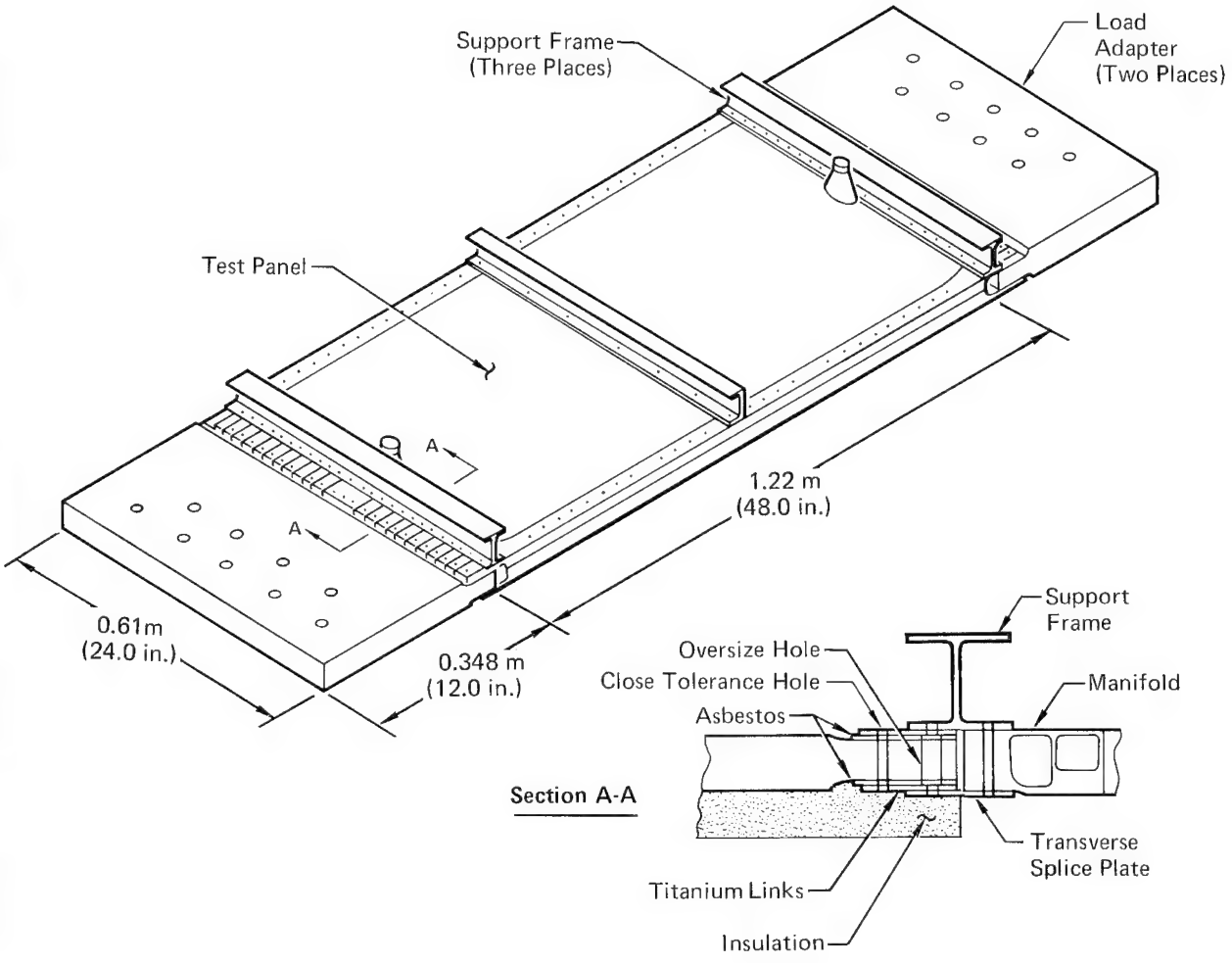

FIGURE 19
ACTIVELY COOLED TEST PANEL, SUPPORT FRAMES, AND LOAD ADAPTERS

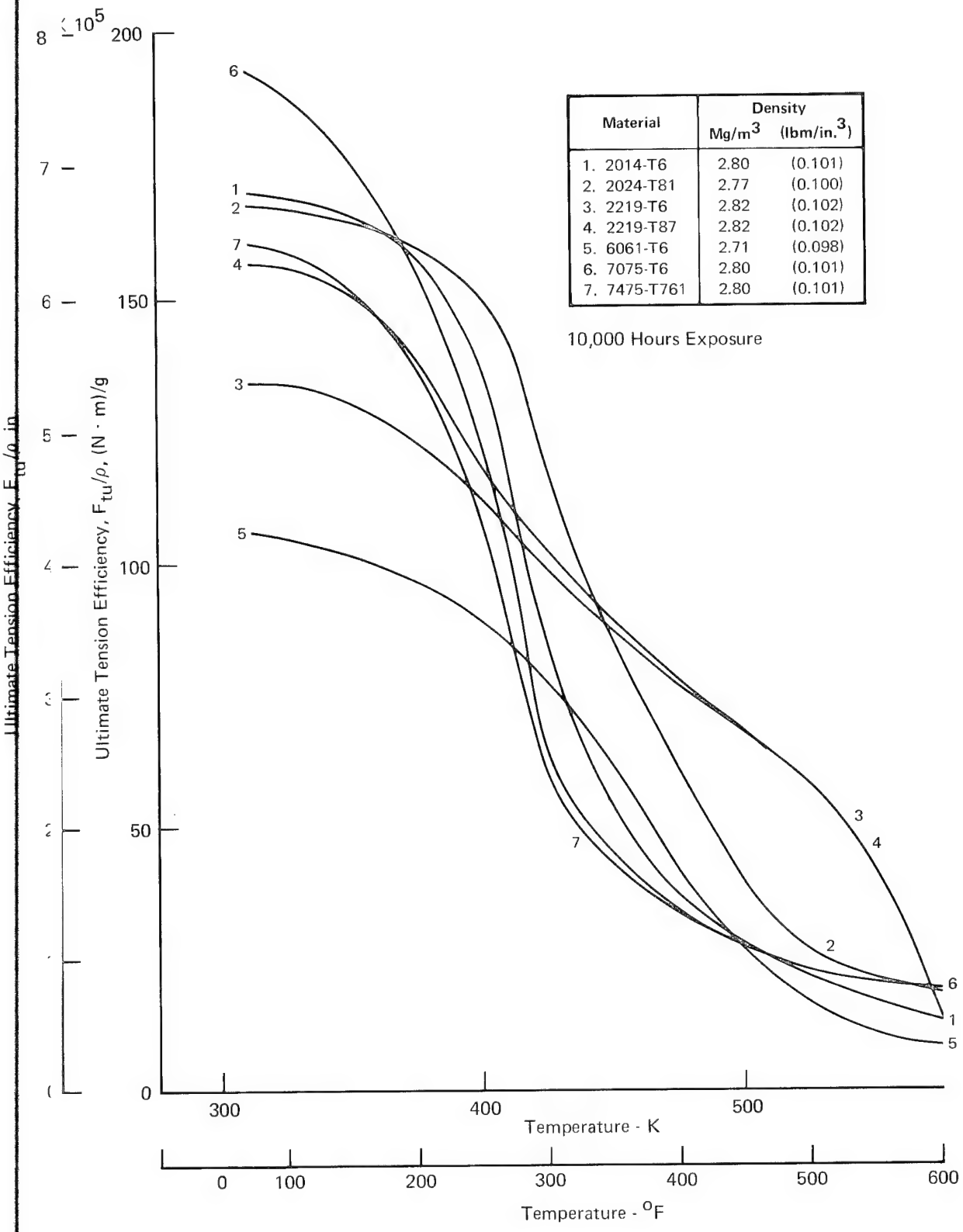

FIGURE 20
ALUMINUM ULTIMATE TENSION EFFICIENCY vs TEMPERATURE

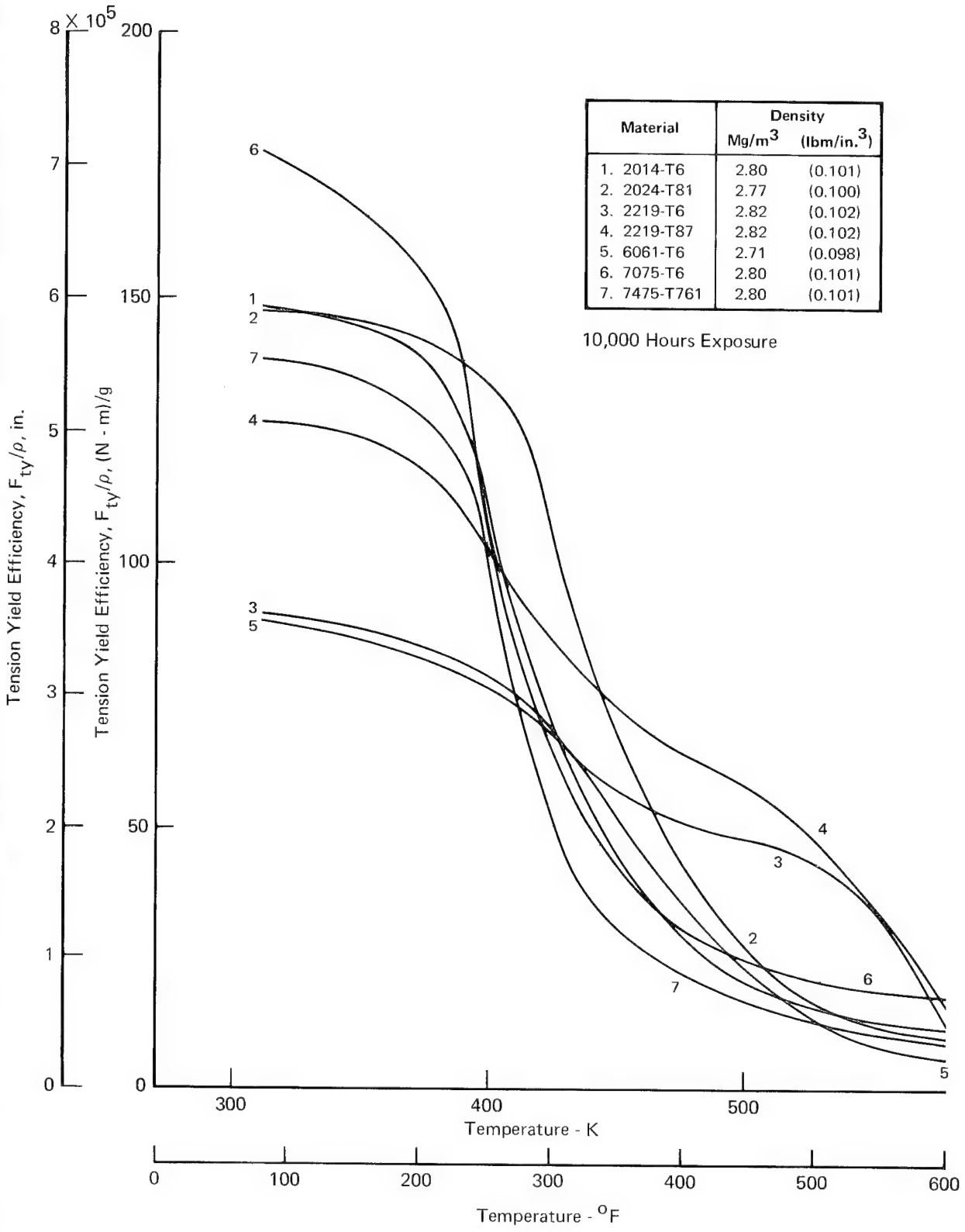

FIGURE 21
ALUMINUM TENSION YIELD EFFICIENCY vs TEMPERATURE

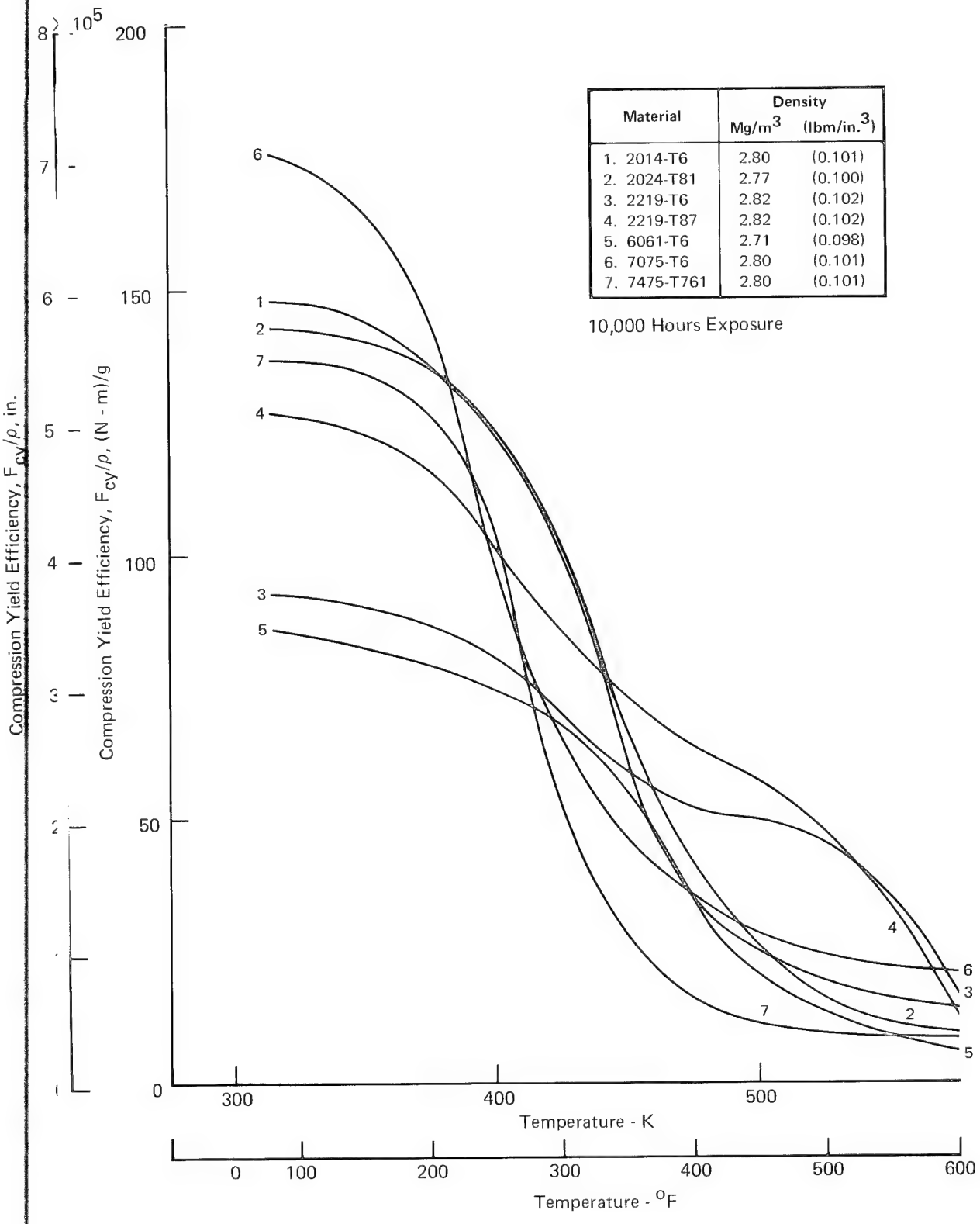

FIGURE 22
ALUMINUM COMPRESSION YIELD EFFICIENCY vs TEMPERATURE

Material	Density	
	Mg/m^3	$(lbm/in.^3)$
2014-T6	2.80	(0.101)
2024-T81	2.77	(0.100)
2219-T6	2.82	(0.102)
2219-T87	2.82	(0.102)
6061-T6	2.71	(0.098)
7075-T6	2.80	(0.101)
7475-T761	2.80	(0.101)

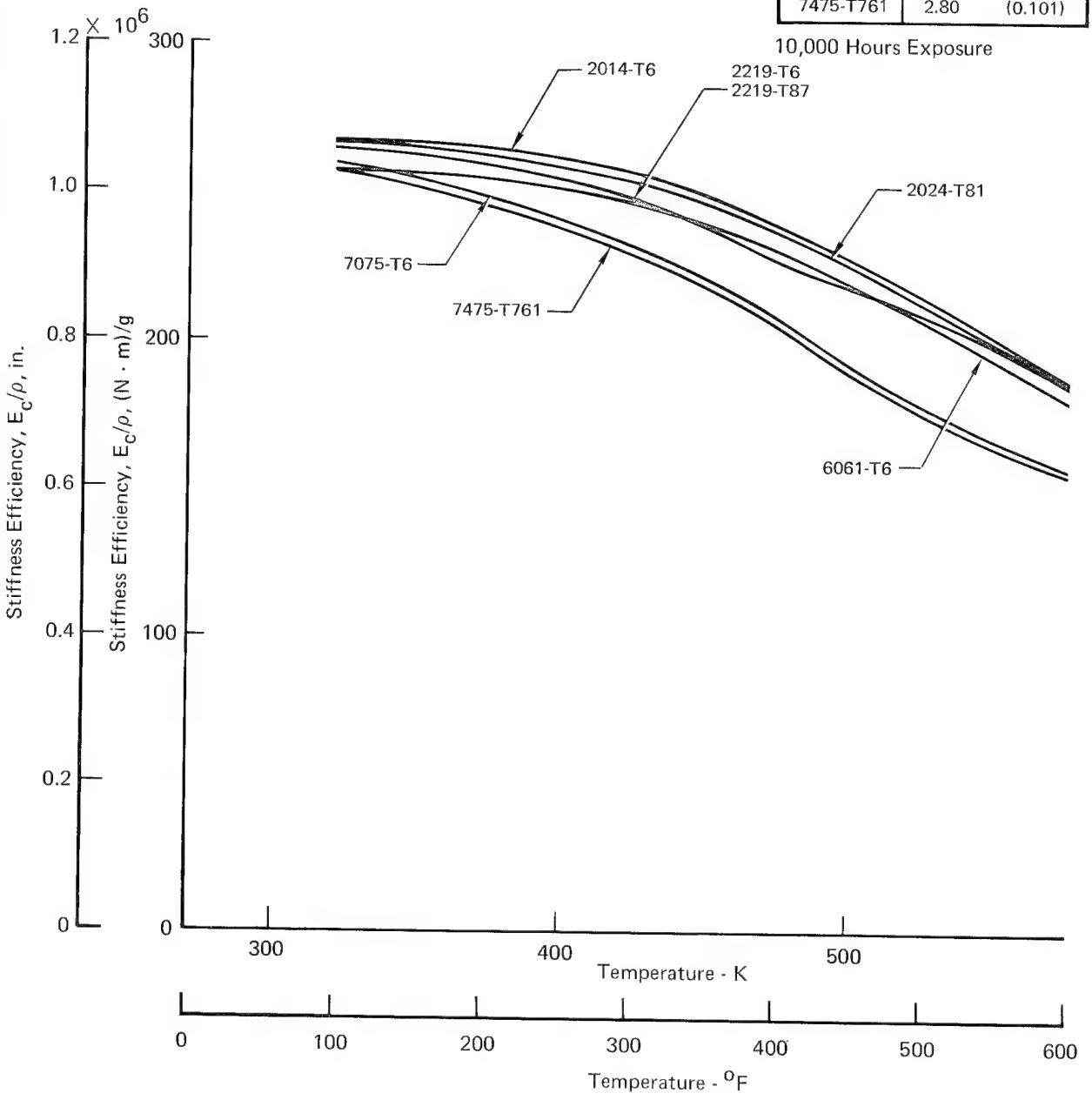

FIGURE 23
ALUMINUM STIFFNESS EFFICIENCY vs TEMPERATURE

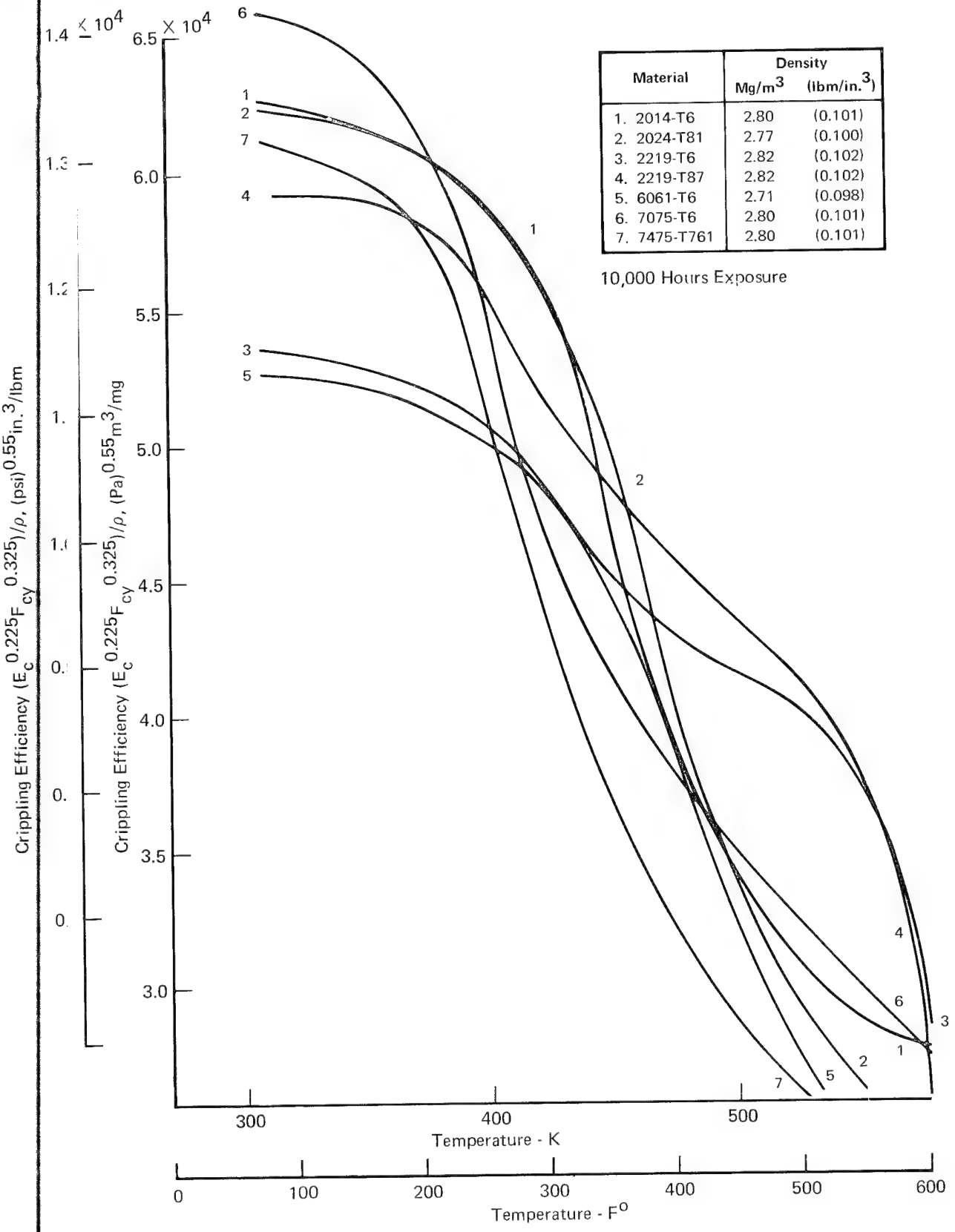

FIGURE 24
ALUMINUM CRIPPLING EFFICIENCY vs TEMPERATURE

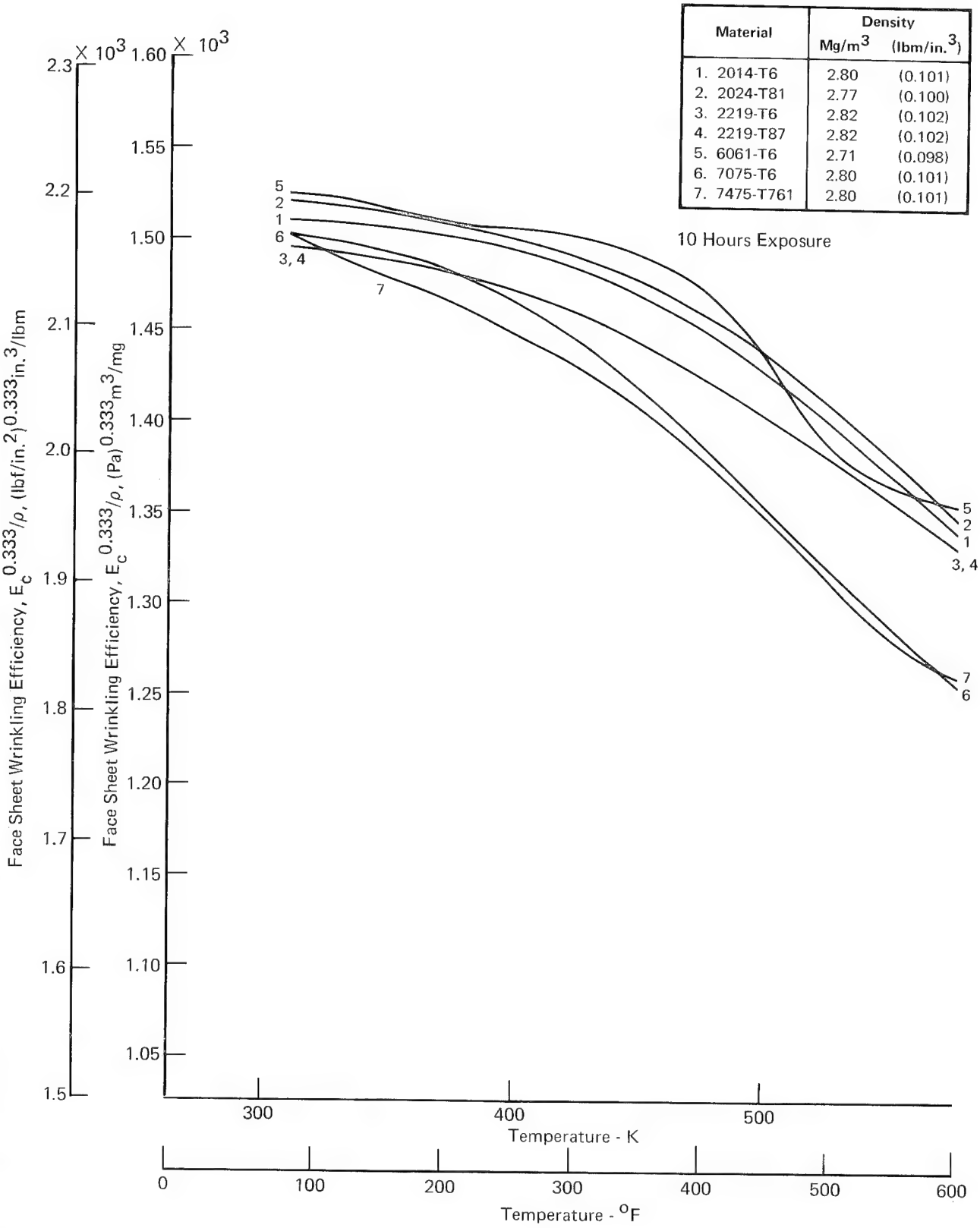

FIGURE 25
ALUMINUM FACE SHEET WRINKLING EFFICIENCY vs TEMPERATURE

Material	Density	
	Mg/m^3	$(lbm/in.^3)$
1. 2014-T6	2.80	(0.101)
2. 2024-T81	2.77	(0.100)
3. 2219-T6	2.82	(0.102)
4. 2219-T87	2.82	(0.102)
5. 6061-T6	2.71	(0.098)
6. 7075-T6	2.80	(0.101)
7. 7475-T761	2.80	(0.101)

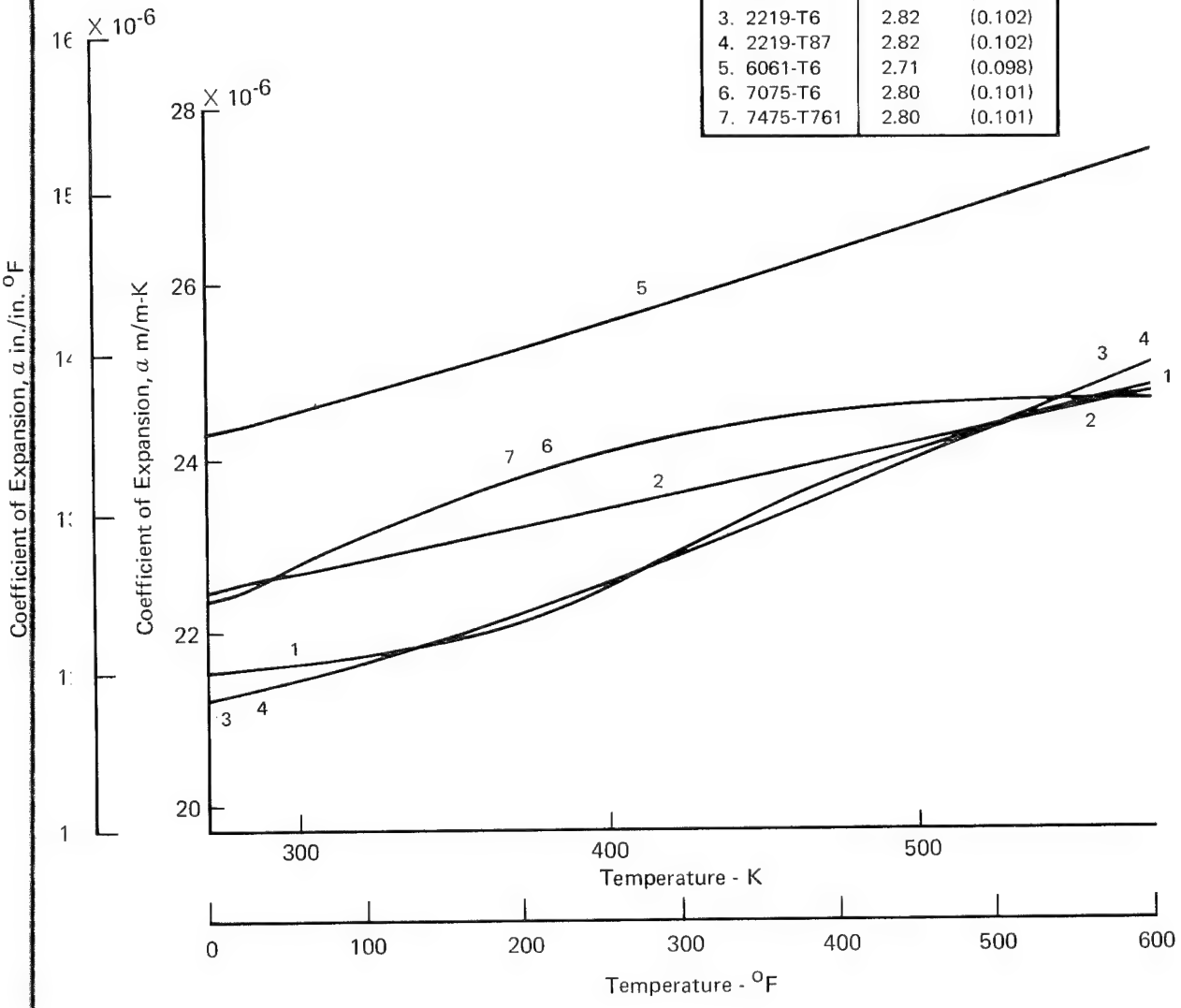

FIGURE 26
ALUMINUM COEFFICIENT OF EXPANSION vs TEMPERATURE

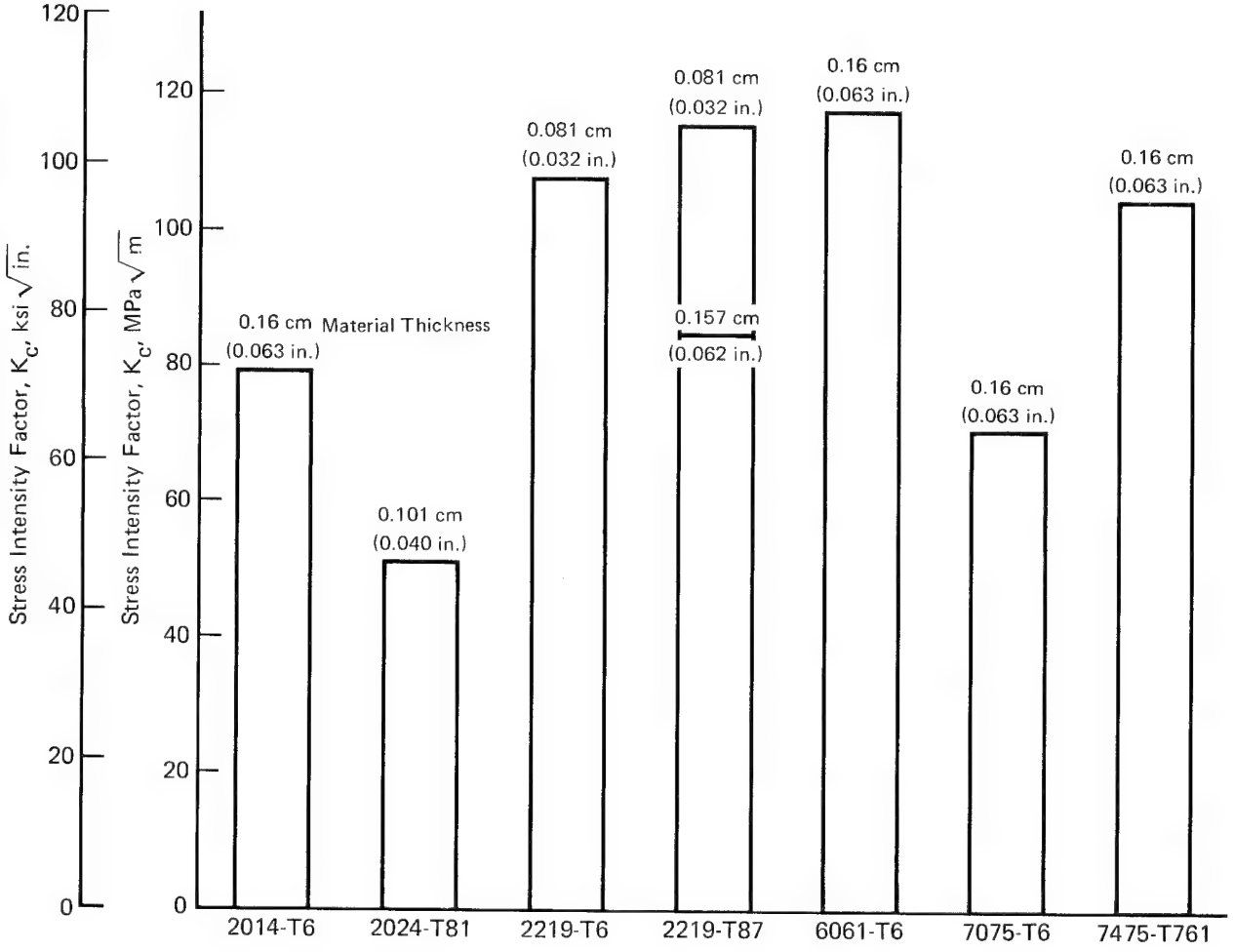

FIGURE 27
ALUMINUM STRESS INTENSITY, K_c AT ROOM TEMPERATURE

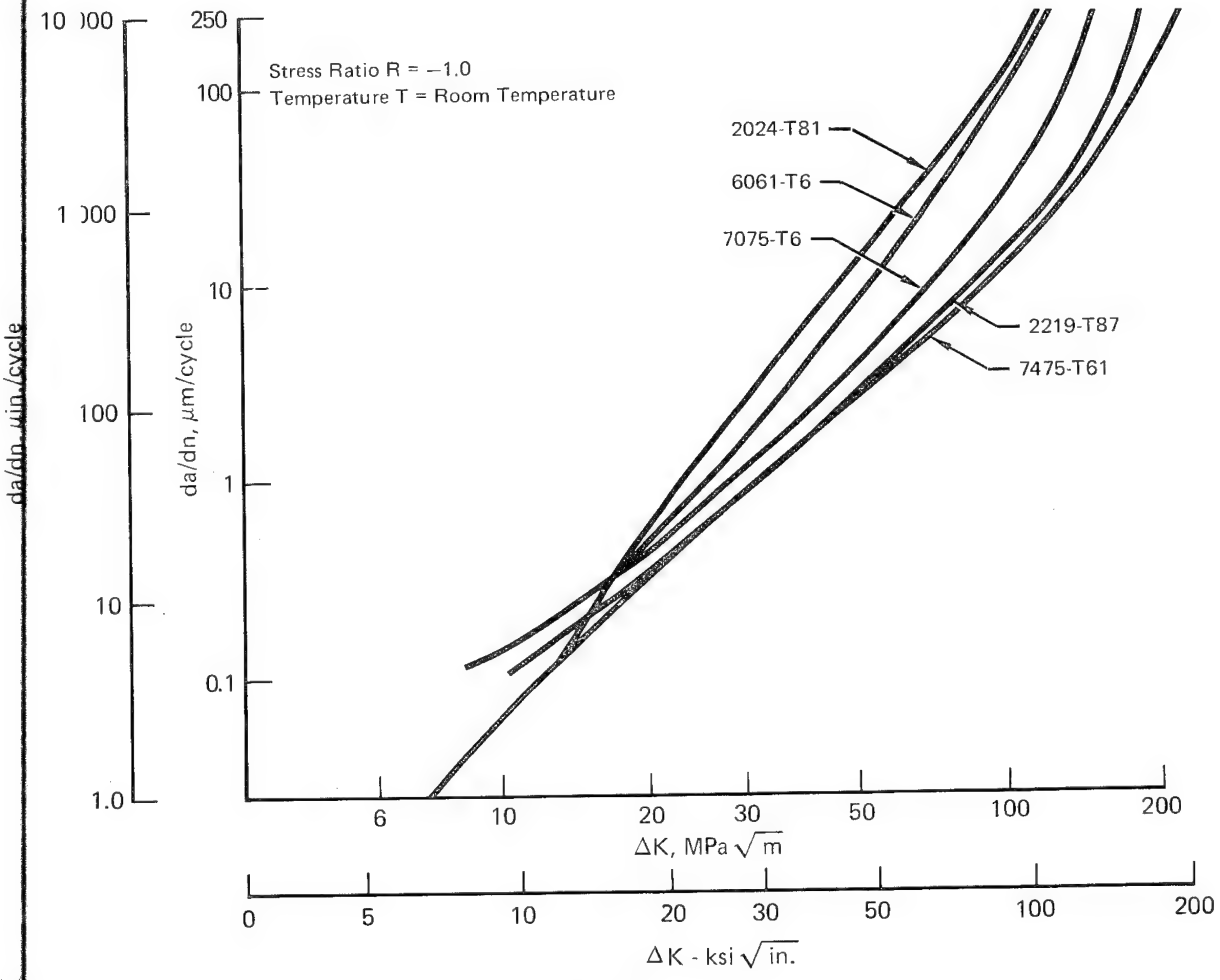

FIGURE 28
COMPARISON OF CRACK GROWTH RATE vs STRESS INTENSITY RANGE

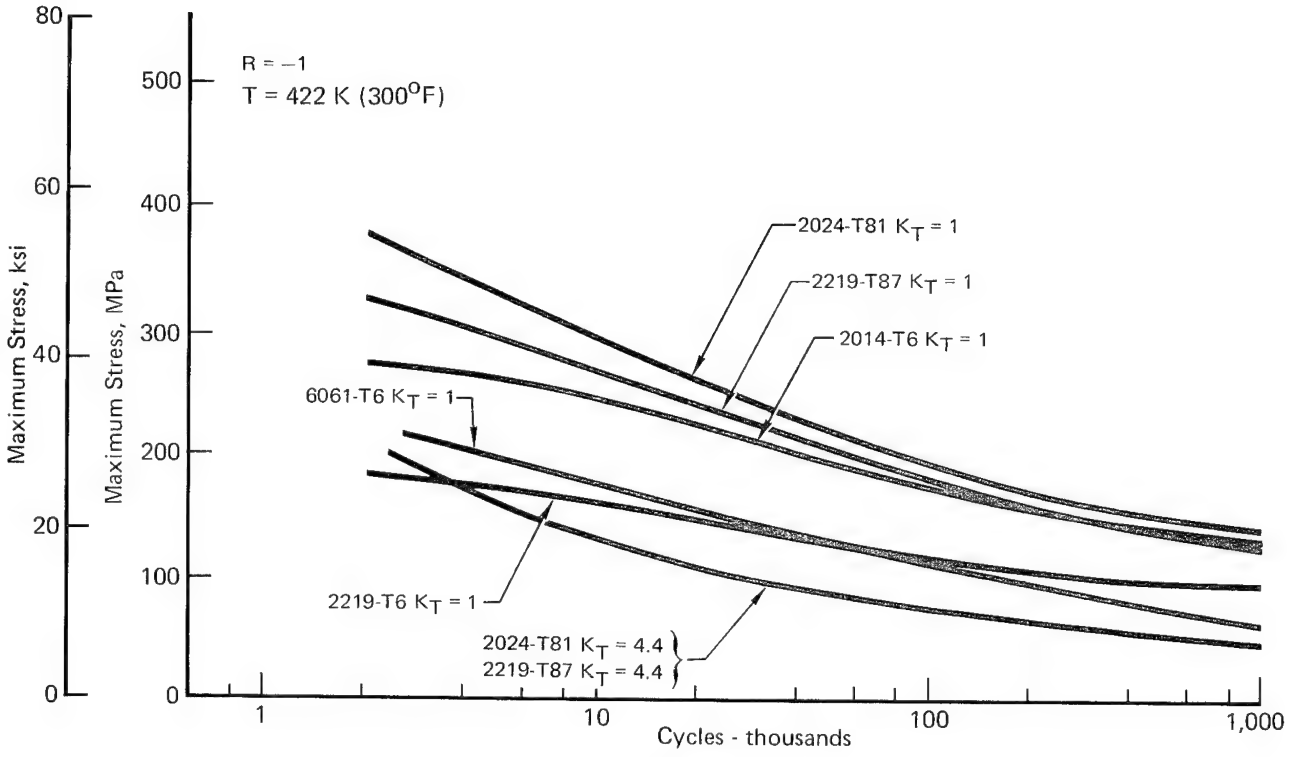

FIGURE 29
MAXIMUM FATIGUE STRESS vs CYCLES TO FAILURE

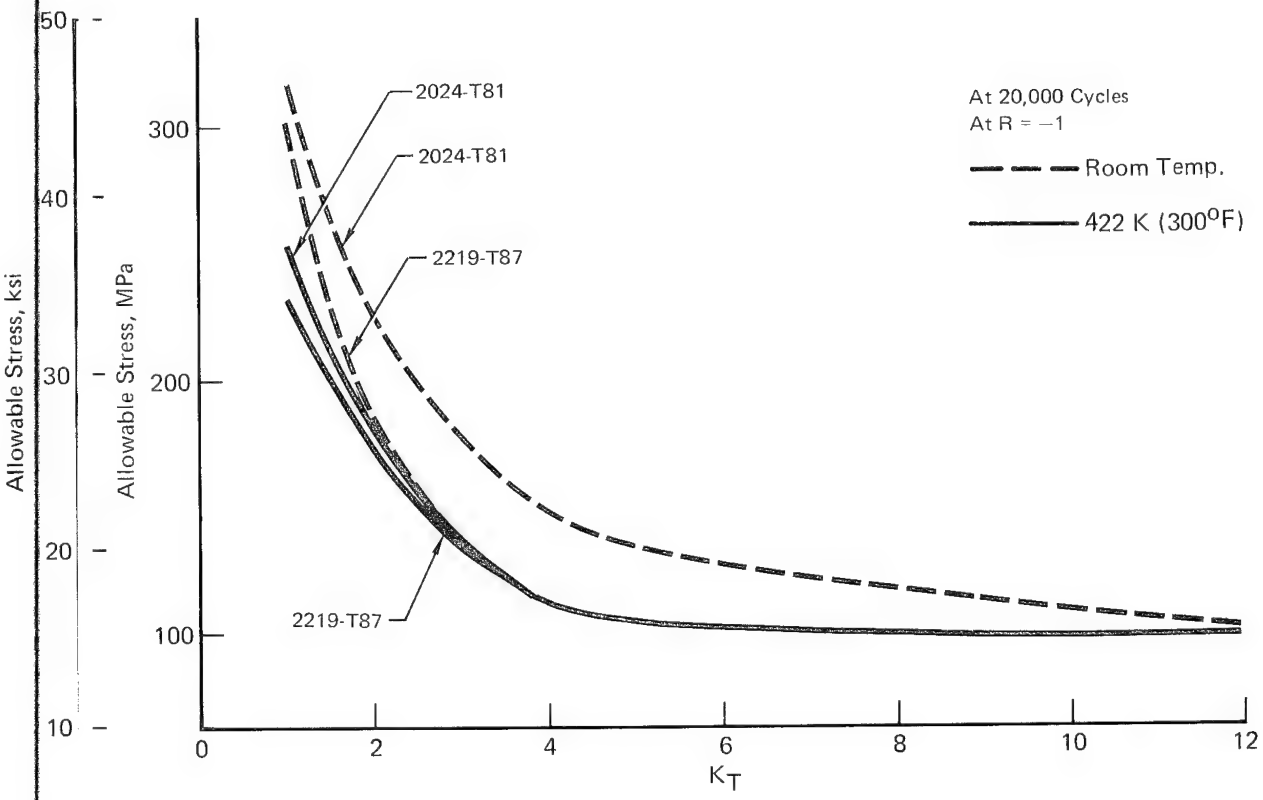

FIGURE 30
ALLOWABLE TENSION STRESS vs STRESS CONCENTRATION FACTOR

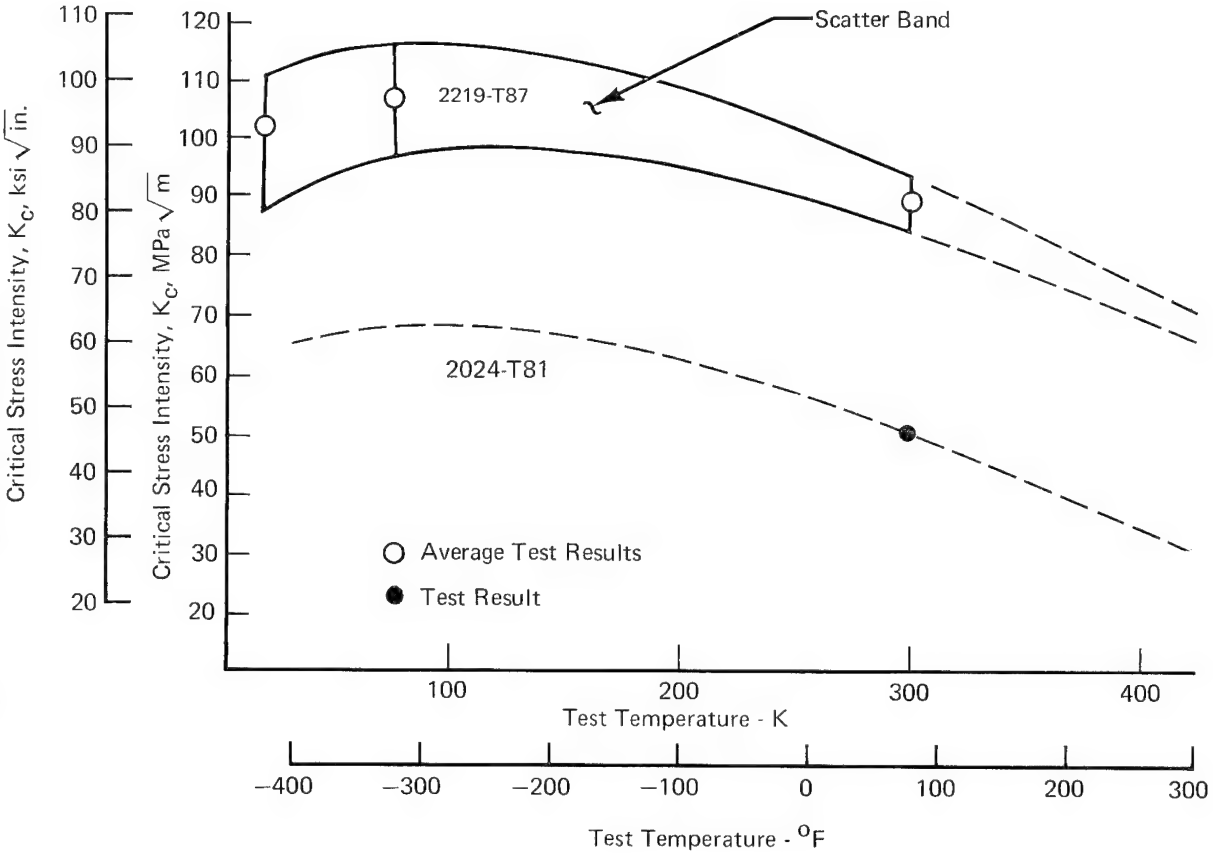

FIGURE 31
CRITICAL STRESS INTENSITY, K_c, RANGE FOR 2219-T87
AND ESTIMATED K_c FOR 2024-T81

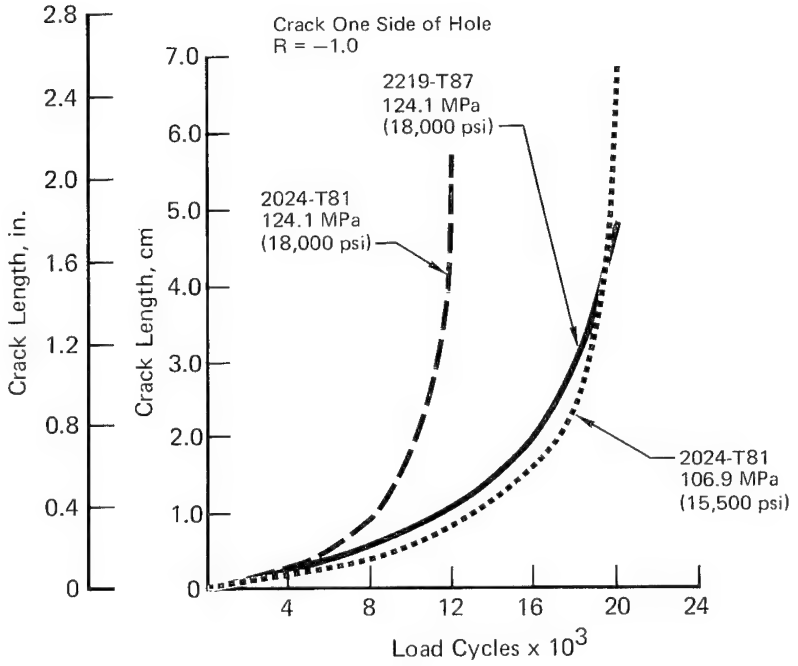

FIGURE 32
COMPARISON OF 2219-T87 AND 2024-T81 FACE SHEET CRACK GROWTH

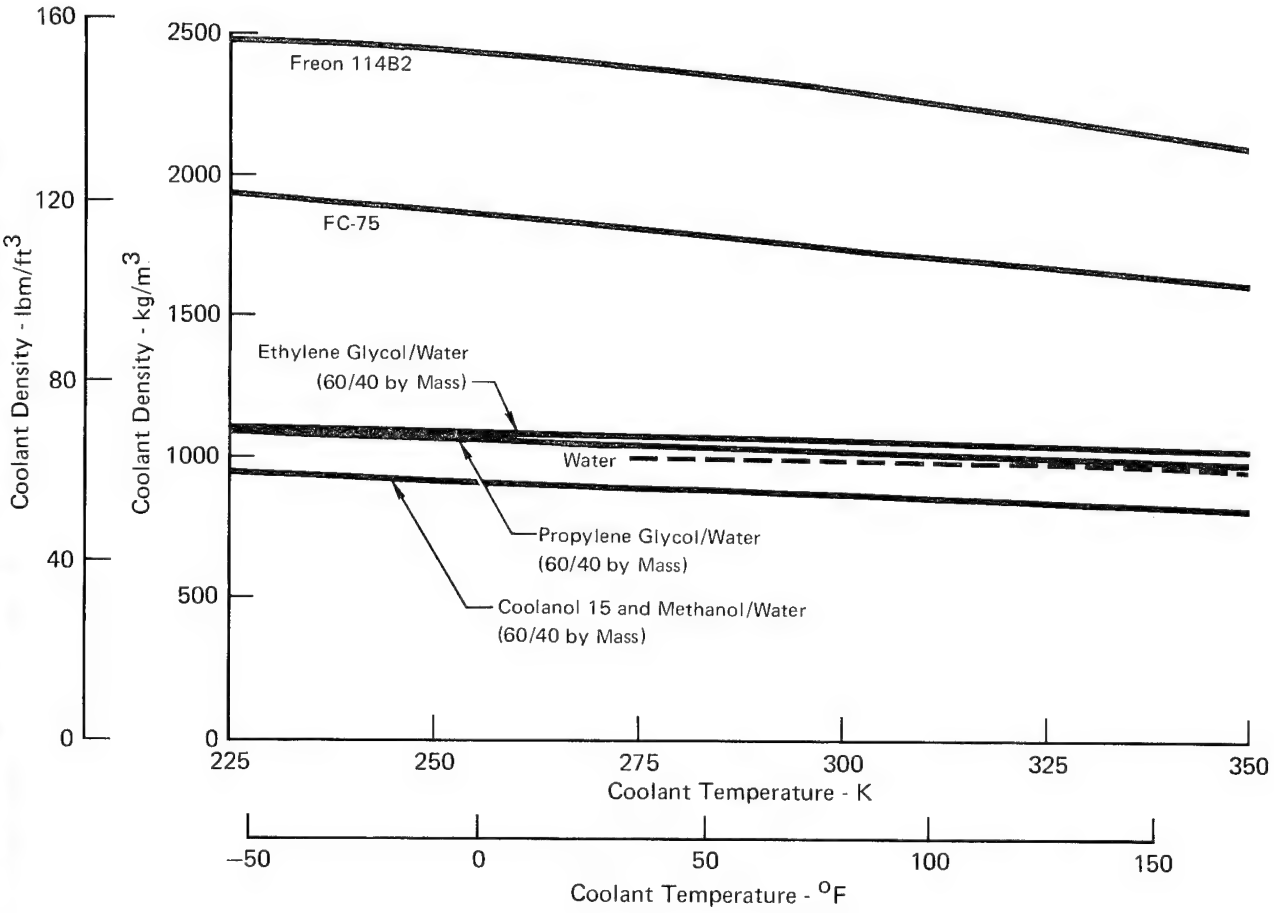

FIGURE 33
COOLANT DENSITY vs TEMPERATURE

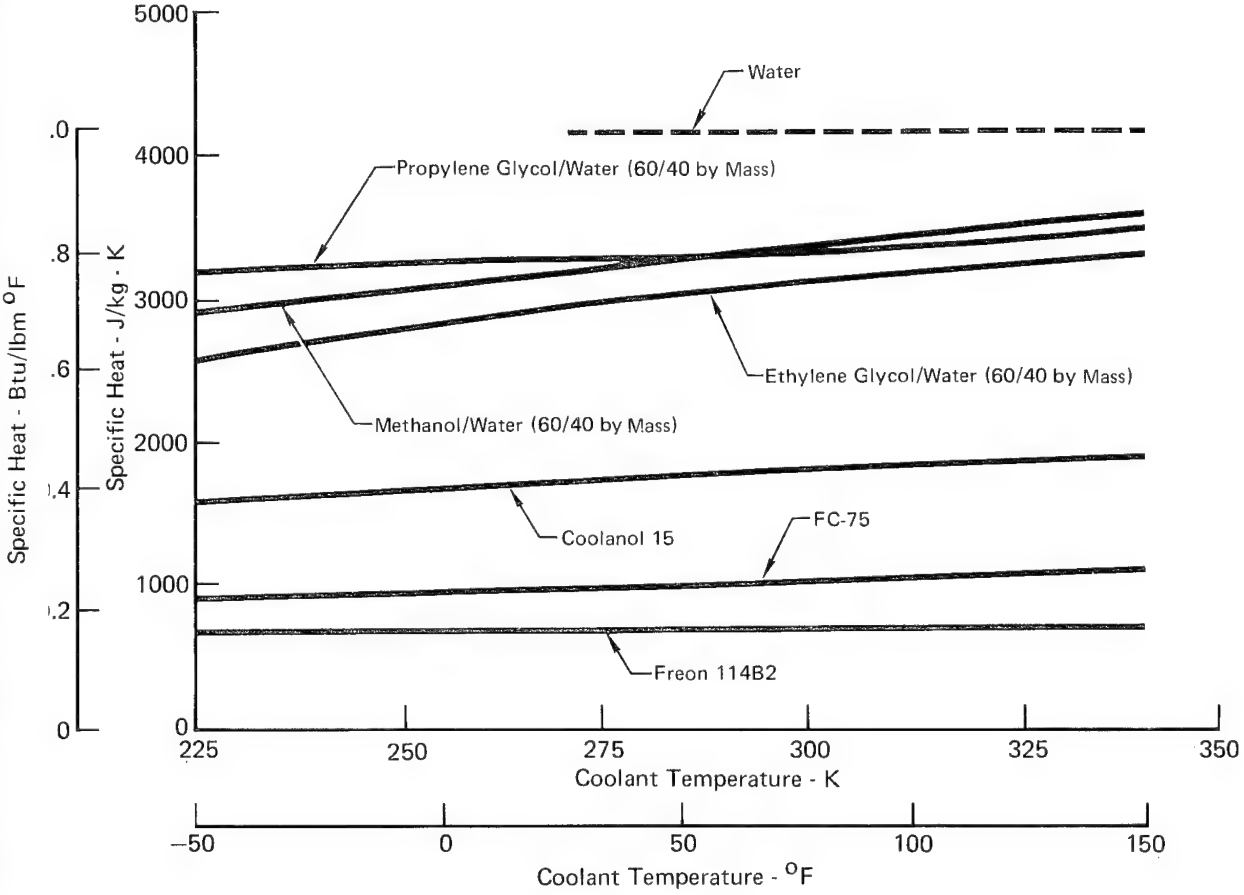

FIGURE 34
COOLANT SPECIFIC HEAT vs TEMPERATURE

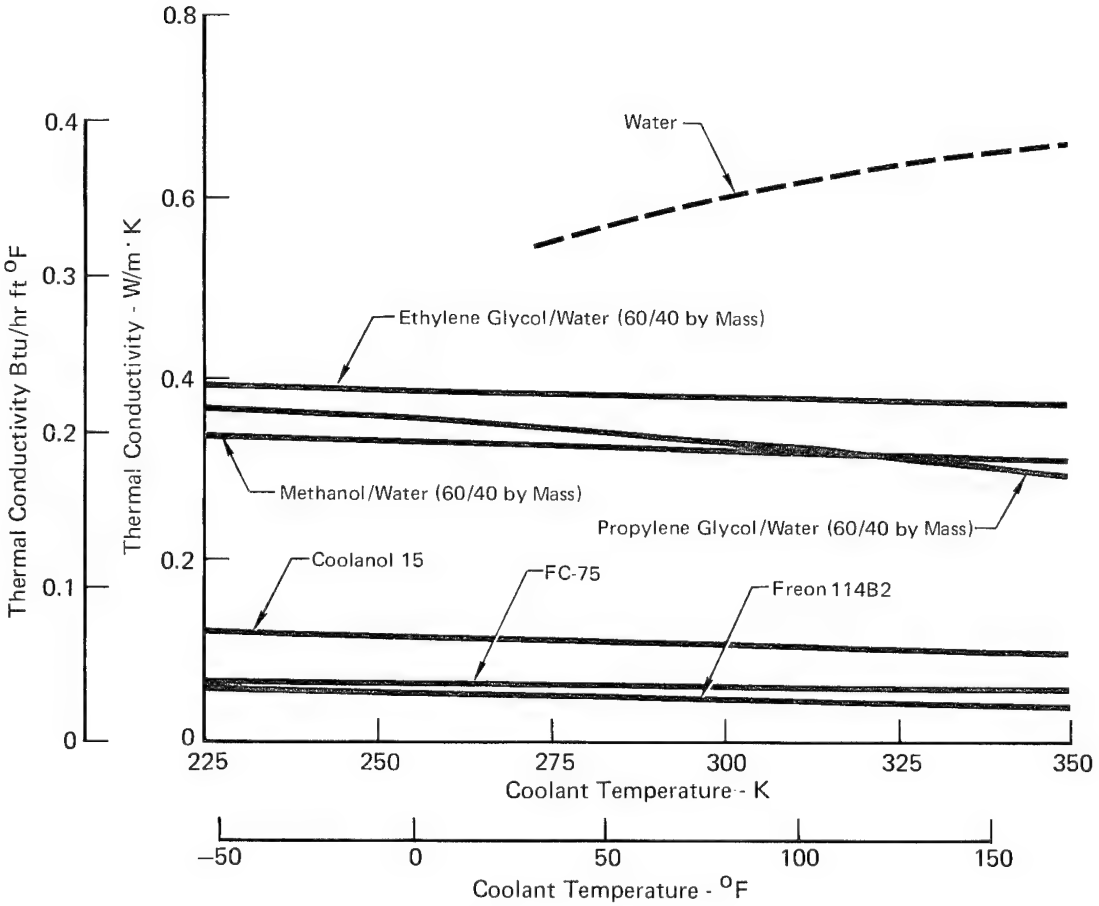

FIGURE 35
COOLANT THERMAL CONDUCTIVITY vs TEMPERATURE

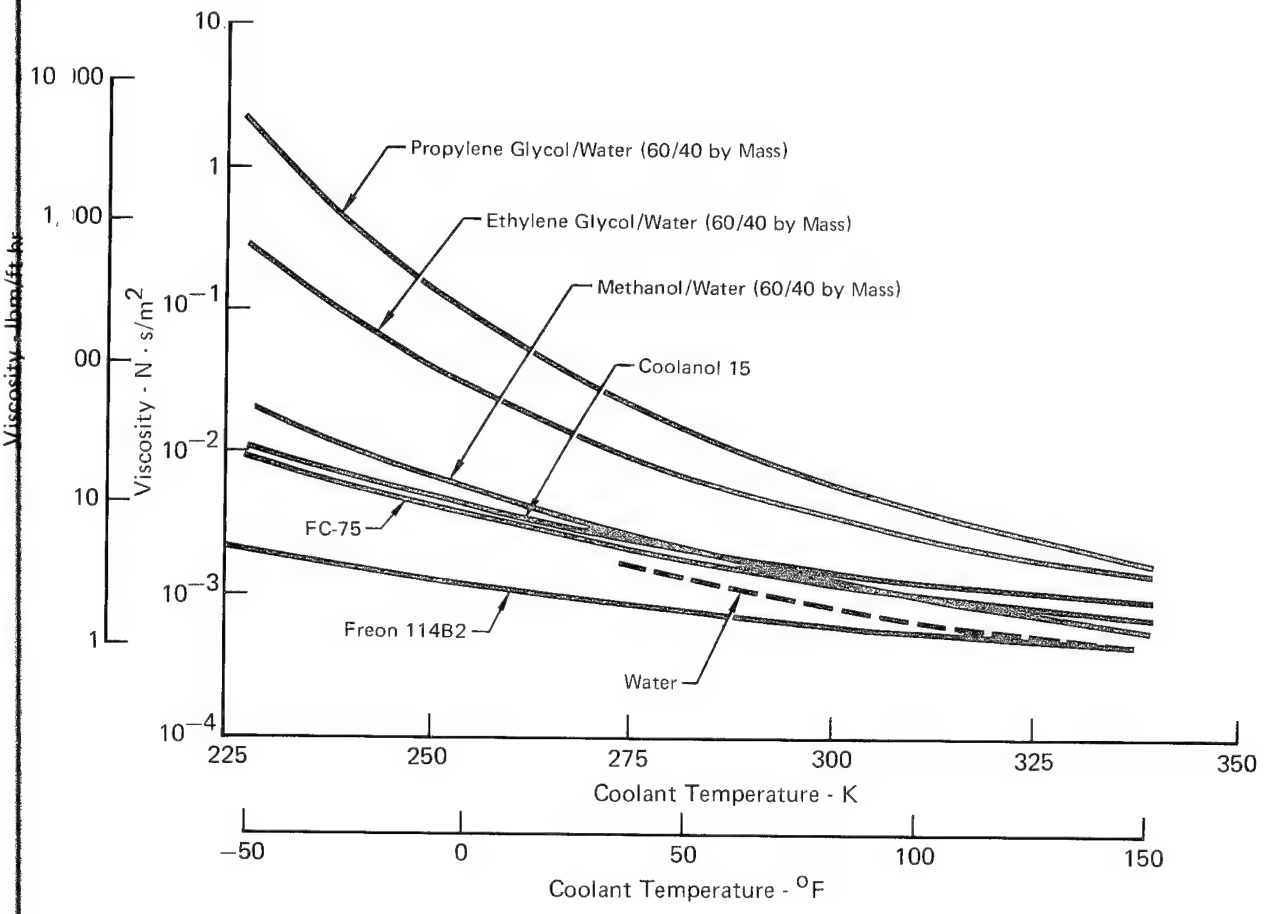

FIGURE 36
COOLANT VISCOSITY vs TEMPERATURE

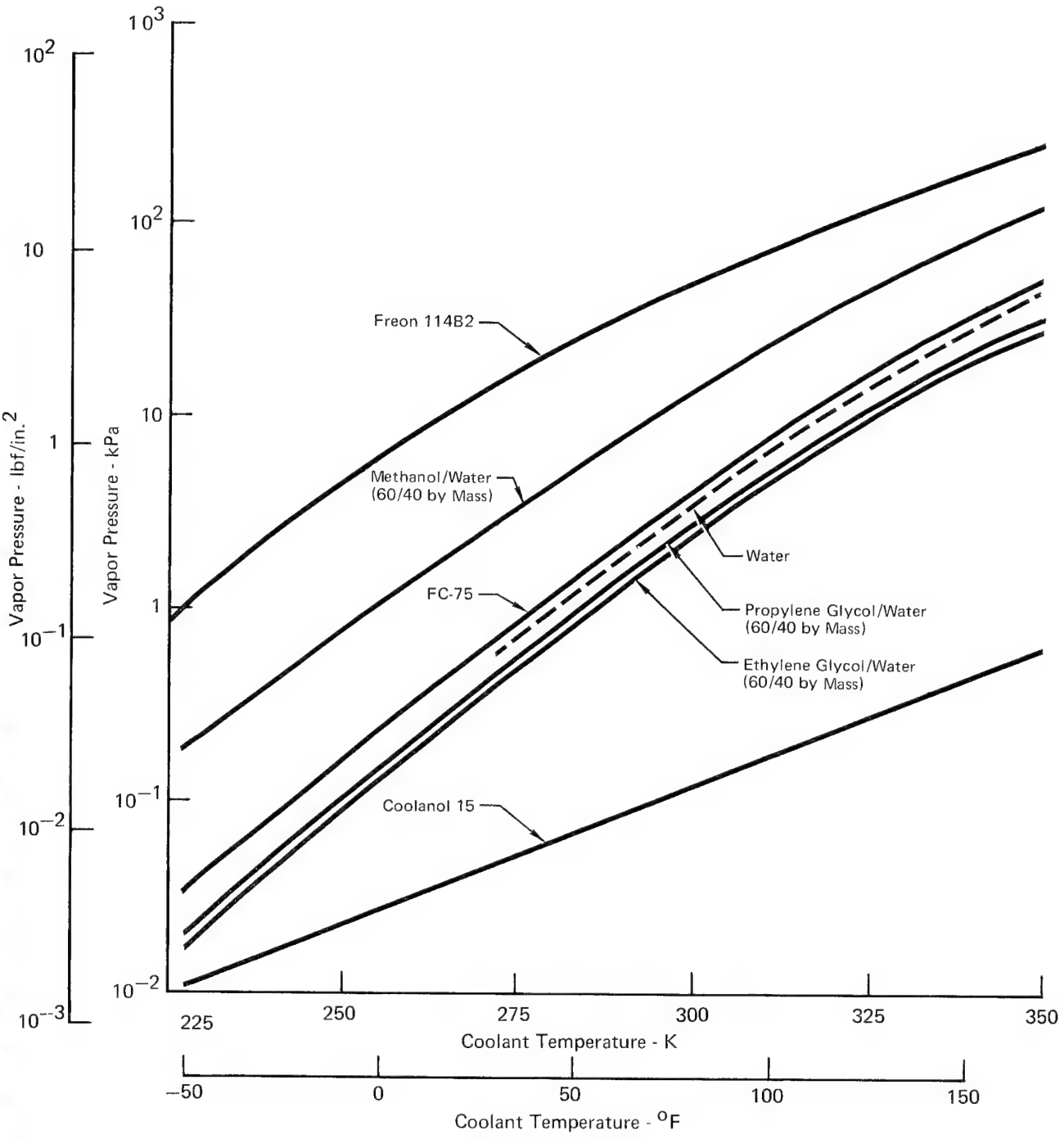

FIGURE 37
COOLANT VAPOR PRESSURE vs TEMPERATURE

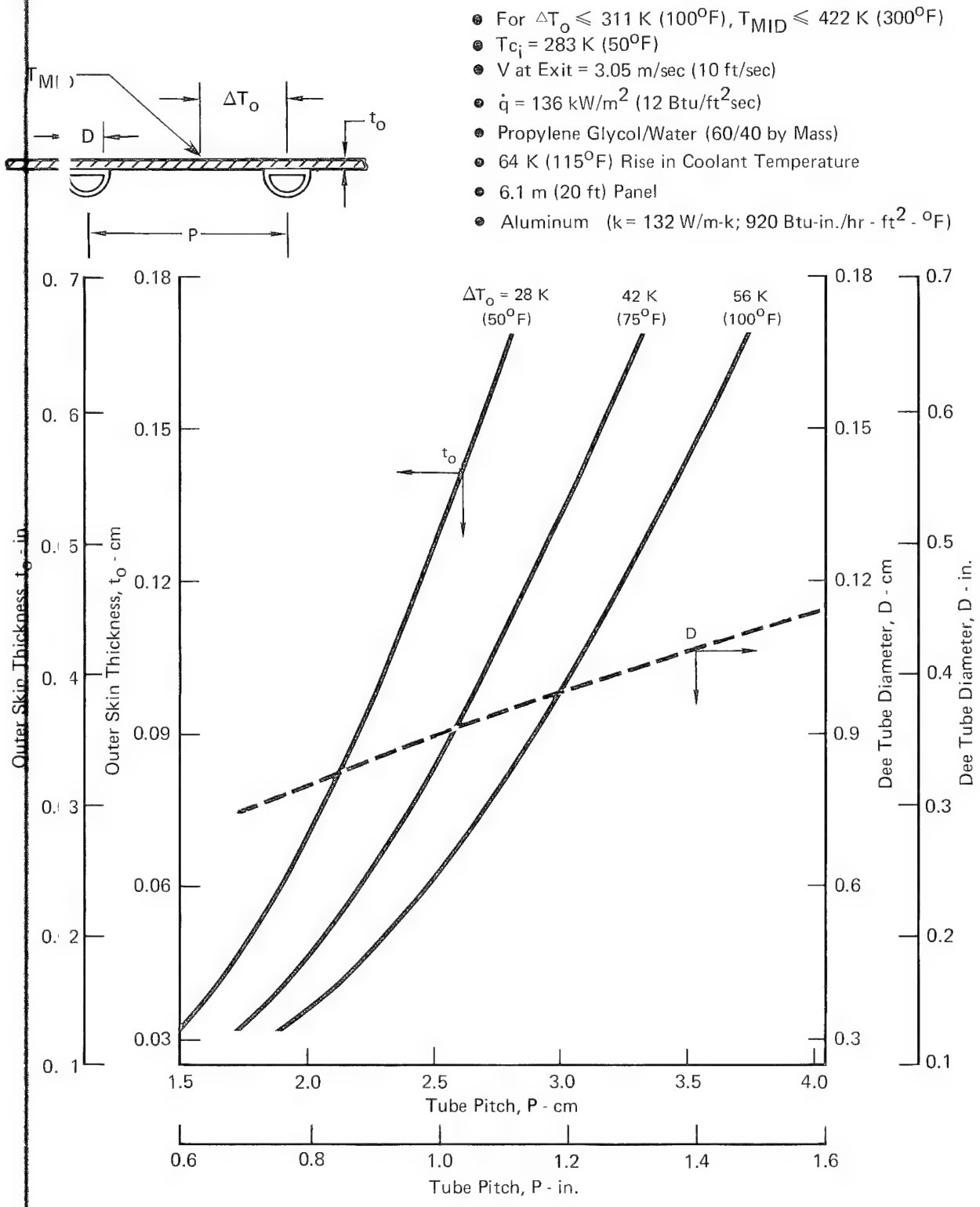

FIGURE 38
OUTER SKIN THICKNESS AND TUBE DIAMETER vs TUBE PITCH

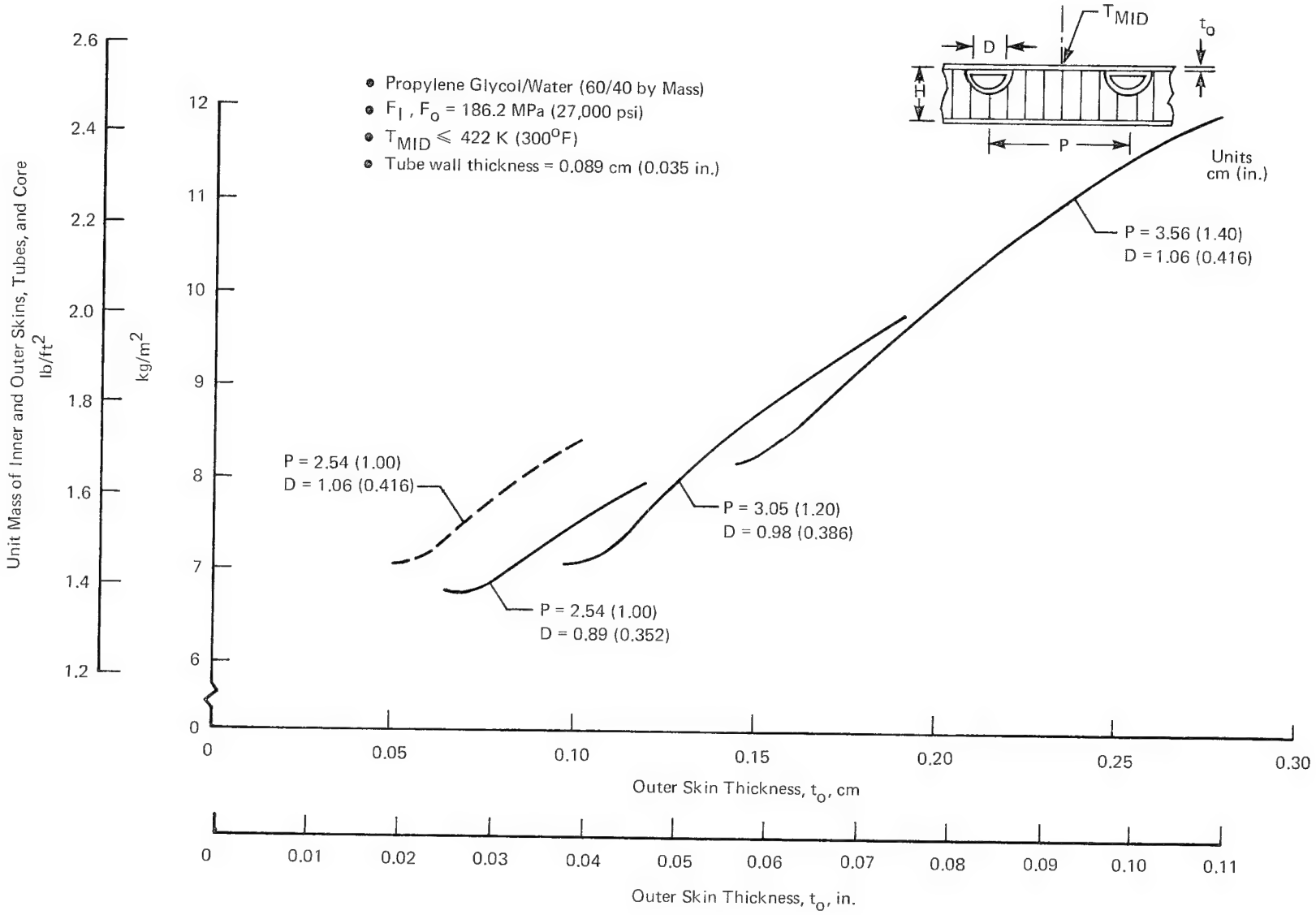

FIGURE 39
STRUCTURAL UNIT MASS vs OUTER SKIN THICKNESS

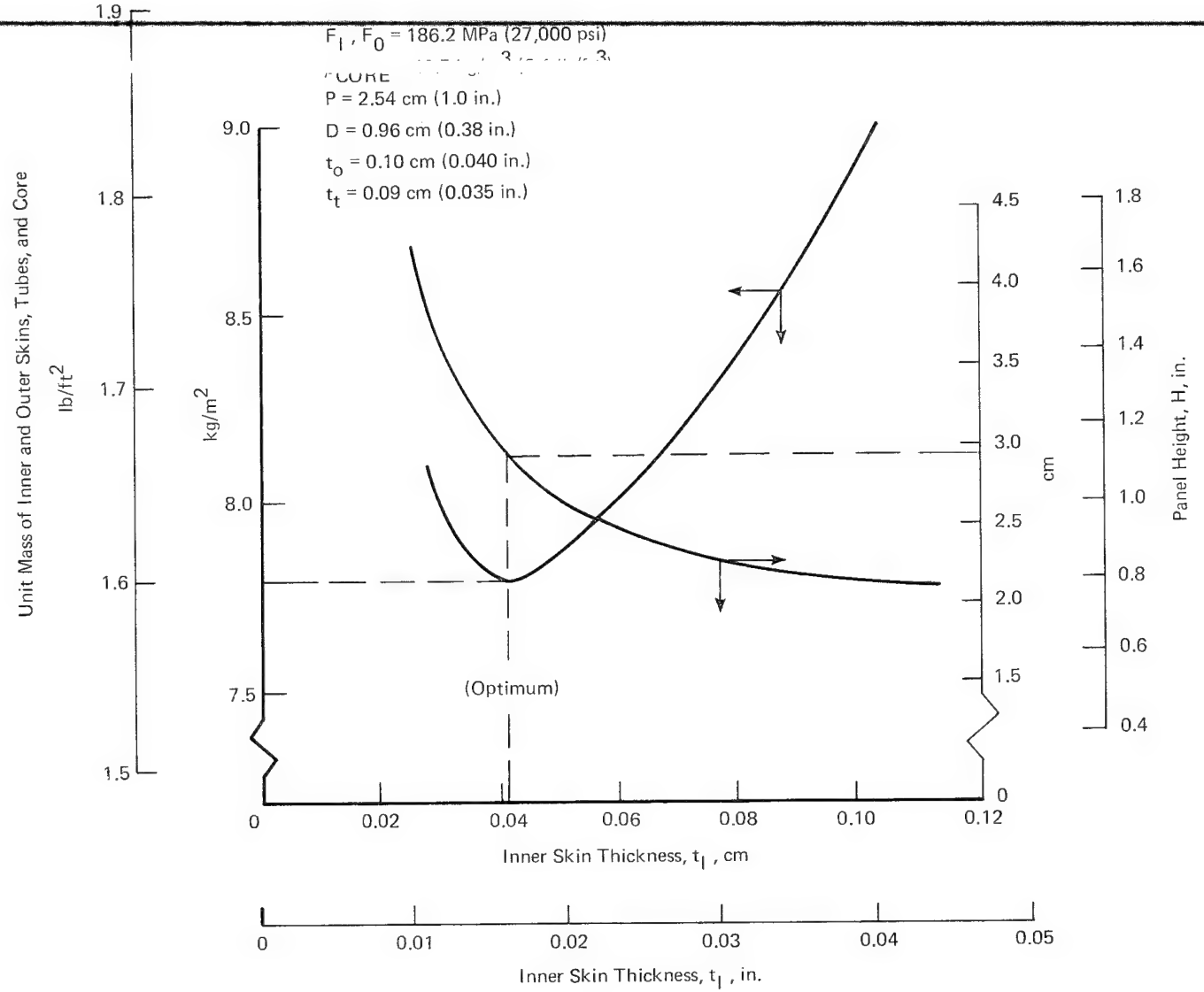

FIGURE 40
STRUCTURAL MASS vs INNER SKIN THICKNESS

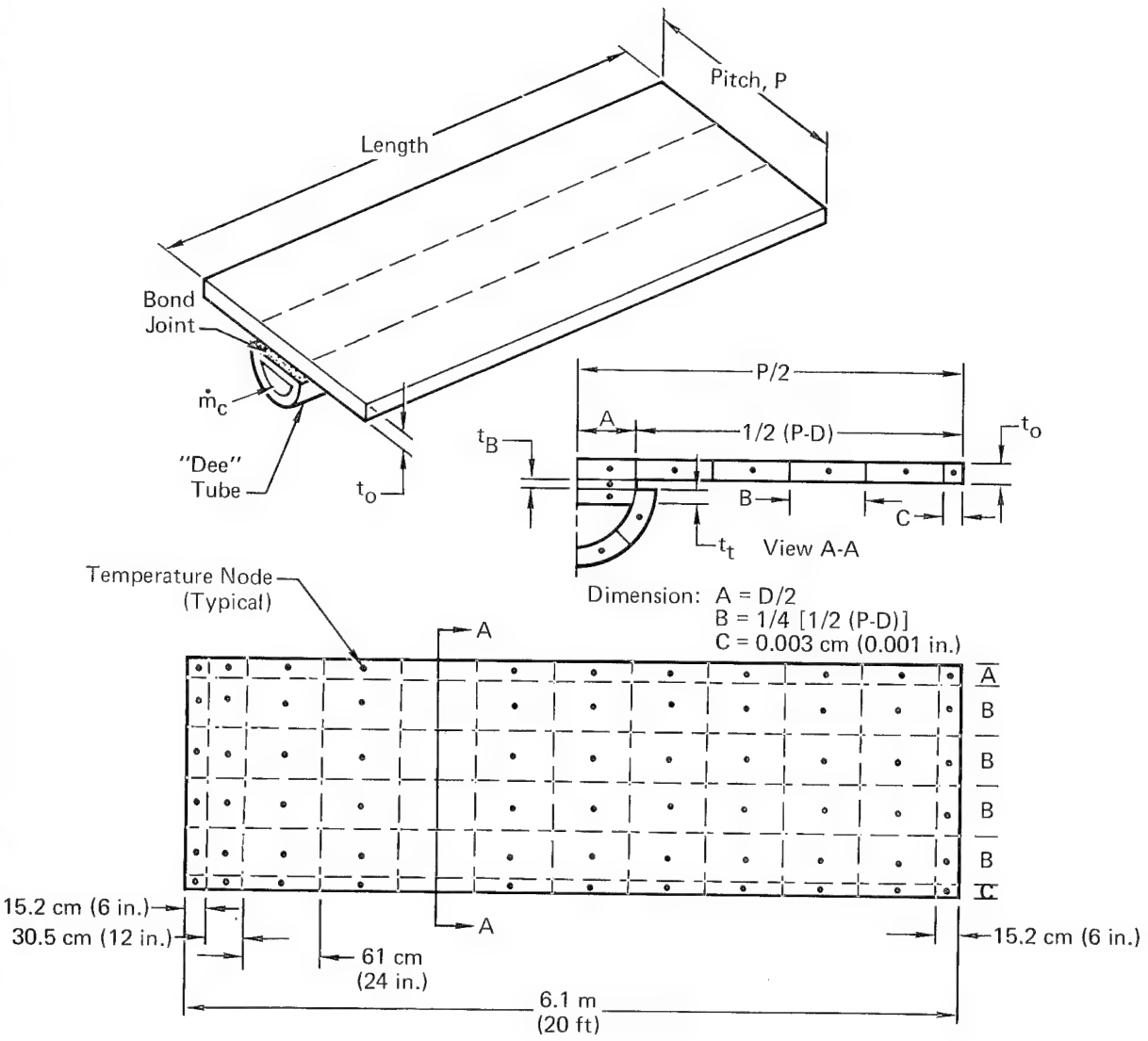

Includes Coolant Property Variations with Temperature
Laminar, Turbulent, and Transitional Heat Transfer of Coolant, and
Pressure Drop

FIGURE 41
TUBE/SKIN THERMAL MODEL USED IN COOLANT EVALUATION ANALYSIS

Coolant*	Optimum Values					
	T_i		Flow Rate		Pressure Drop	
	(K)	(^{o}F)	(g/s)	(lbm/hr)	(kPa)	(psi)
Methanol	256	0	98	780	141	20.4
Ethylene-Glycol	283	50	164	1300	310	45.0
Propylene-Glycol	289	60	224	1780	565	82.0

* 60/40 Coolant/Water (By Mass)

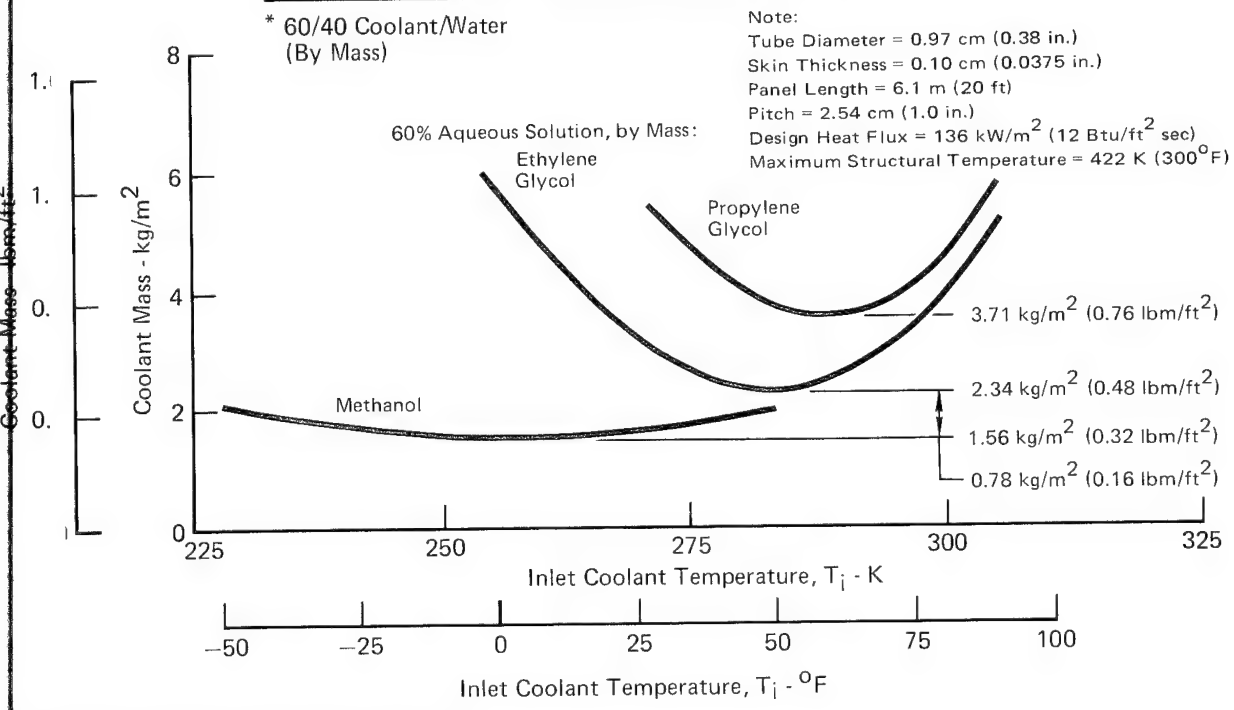

Co lant Mass = APS Plus Coolant Inventory

FIGURE 42
METHANOL/WATER COOLANT MINIMIZES FLUID PENALTY

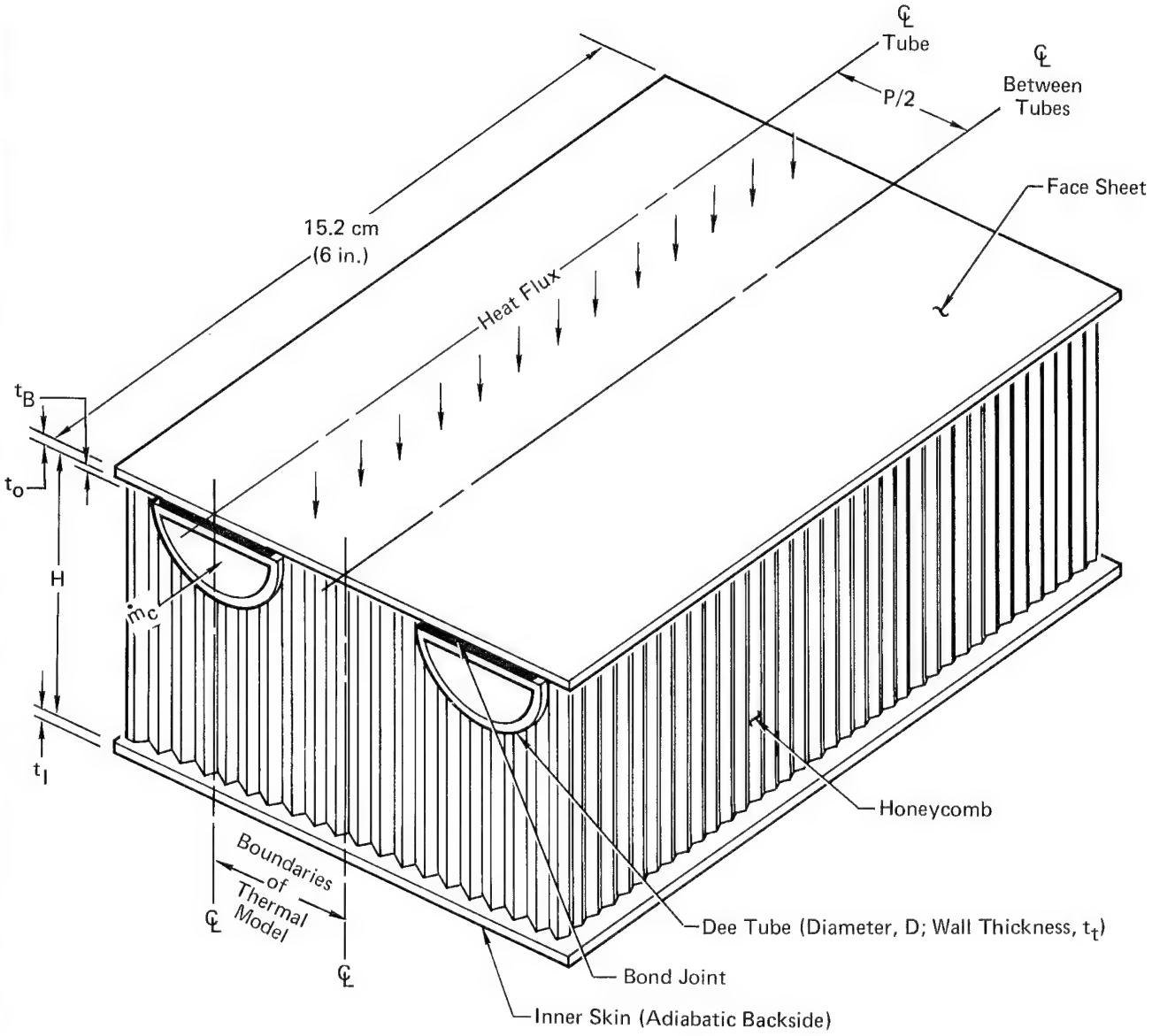

FIGURE 43
ELEMENTS INCLUDED IN PANEL THERMAL MODEL

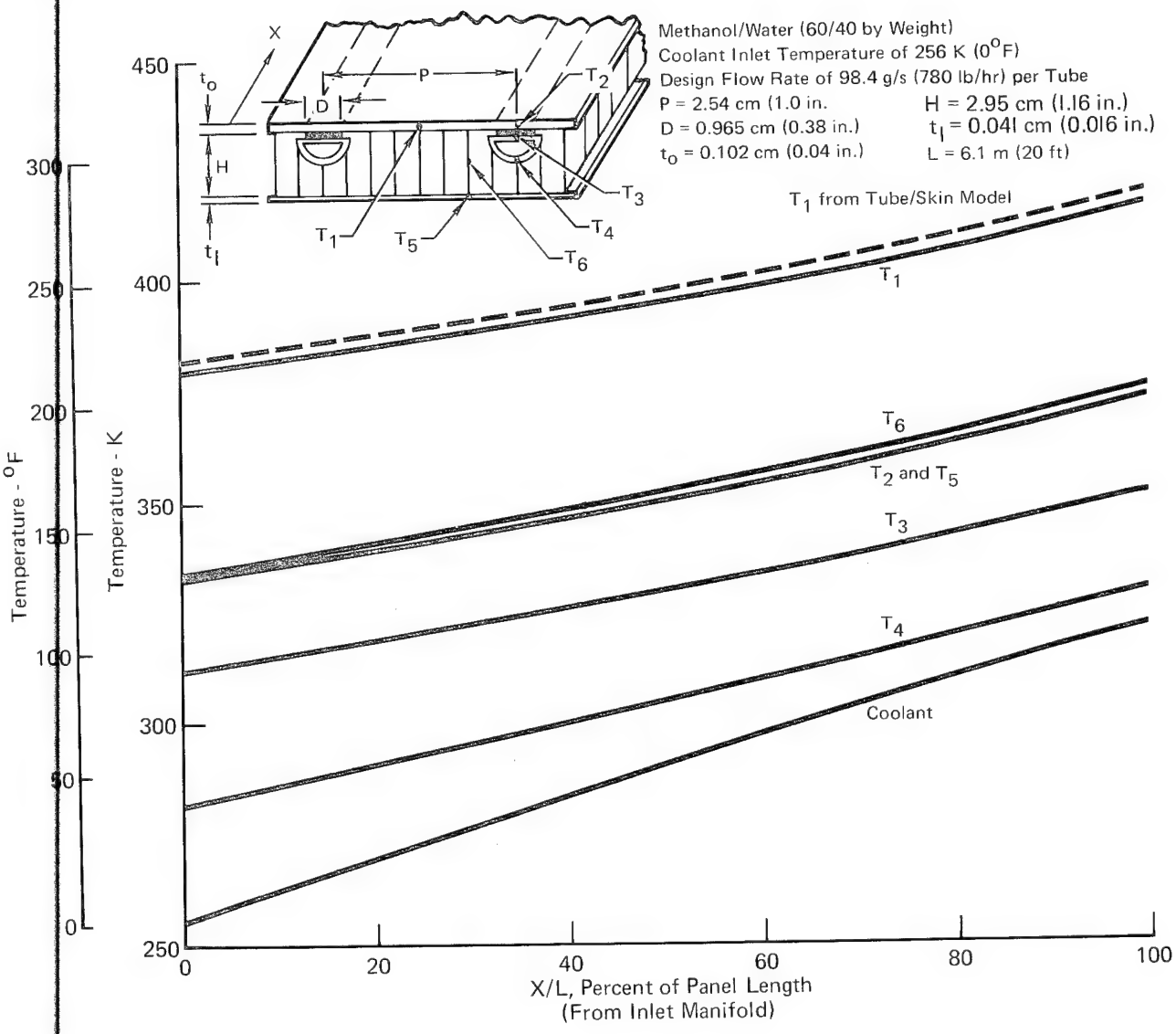

FIGURE 44
ACTIVELY COOLED PANEL TEMPERATURES vs DISTANCE FROM INLET MANIFOLD

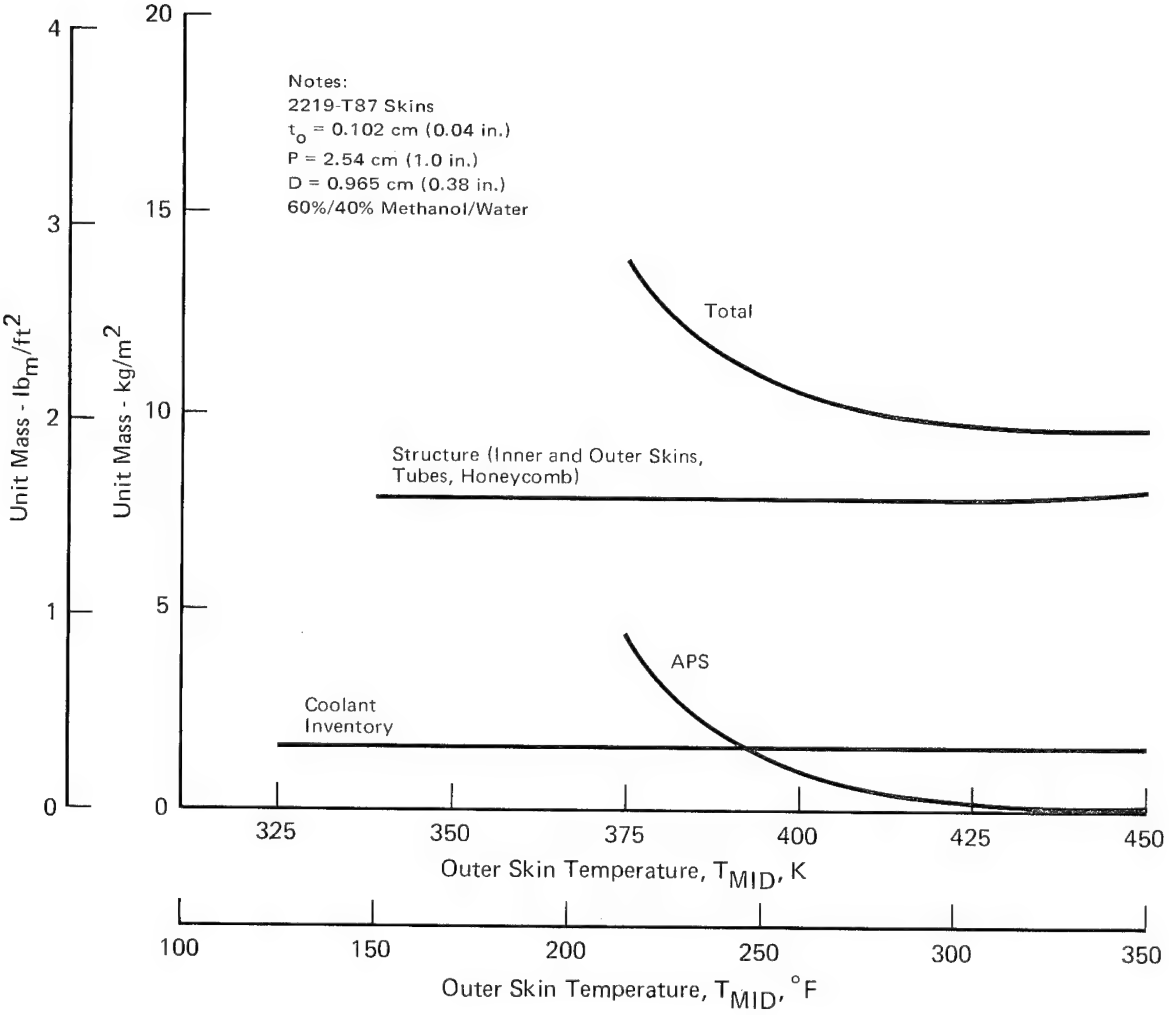

FIGURE 45
SENSITIVITY OF ACTIVELY COOLED PANEL MASS TO MAXIMUM OUTER SKIN TEMPERATURE

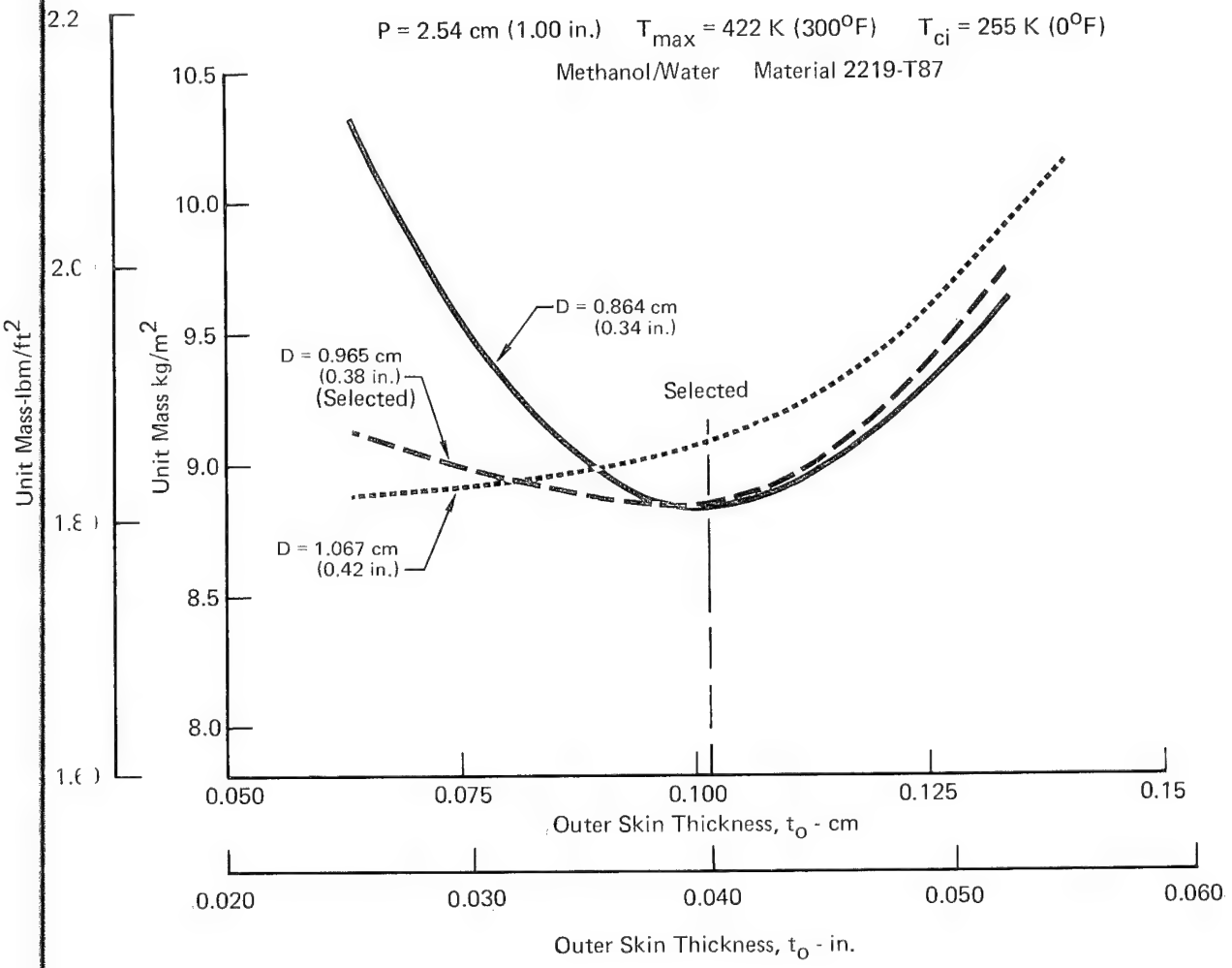

FIGURE 46
PANEL UNIT MASS (STRUCTURAL + APS + COOLANT INVENTORY)
vs OUTER SKIN THICKNESS

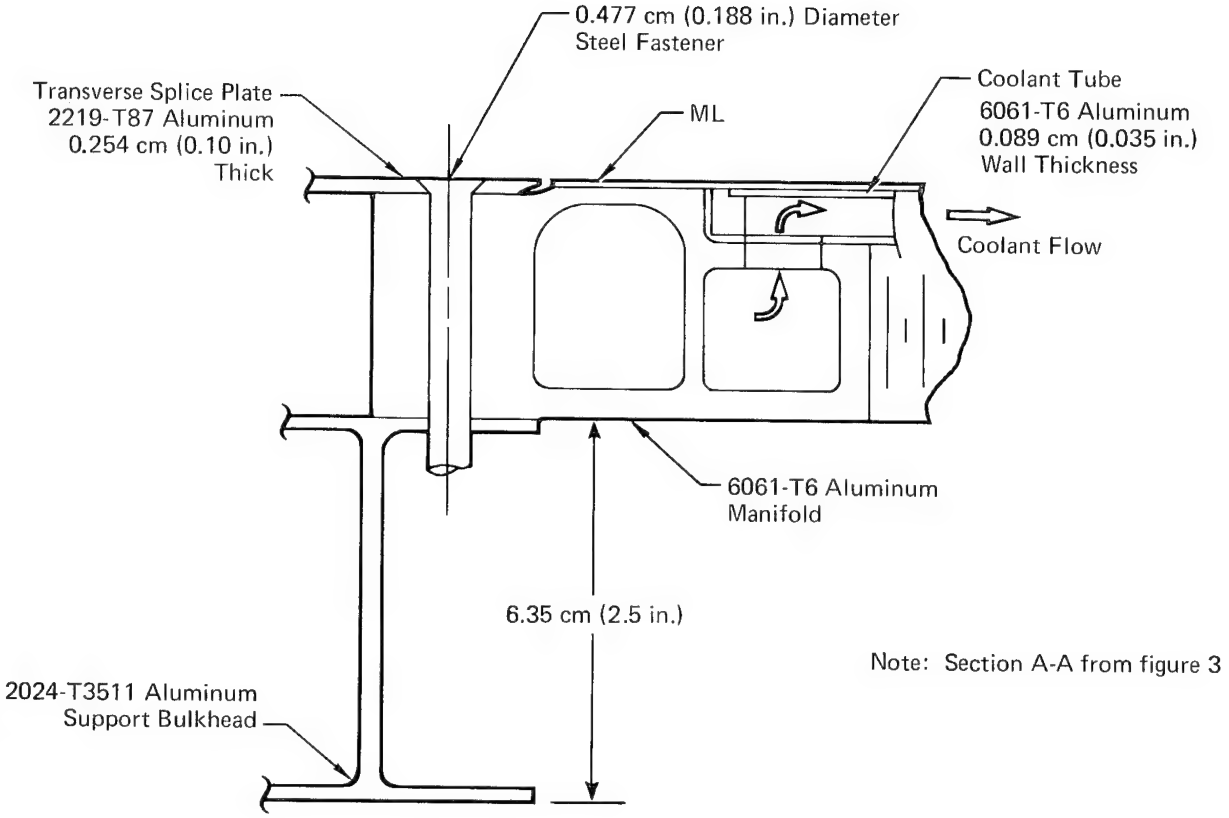

FIGURE 47
MANIFOLD AND TRANSVERSE EDGE SPLICE

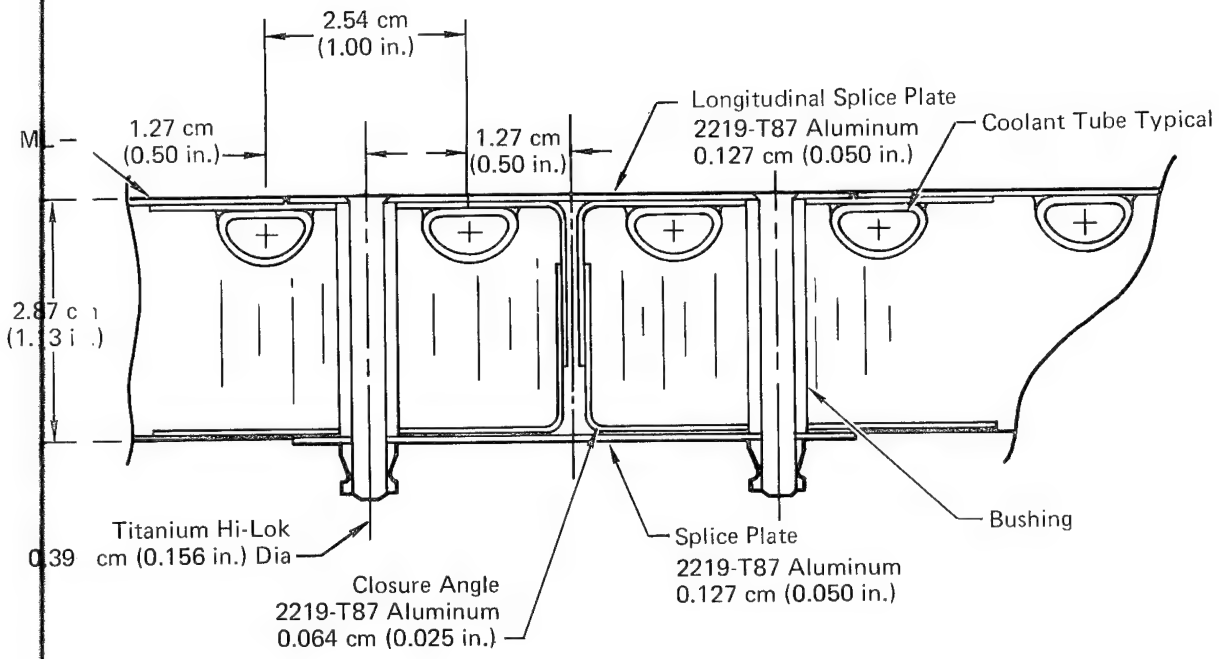

Note: Section B-B from Figure 3

FIGURE 48
LONGITUDINAL EDGE SPLICE

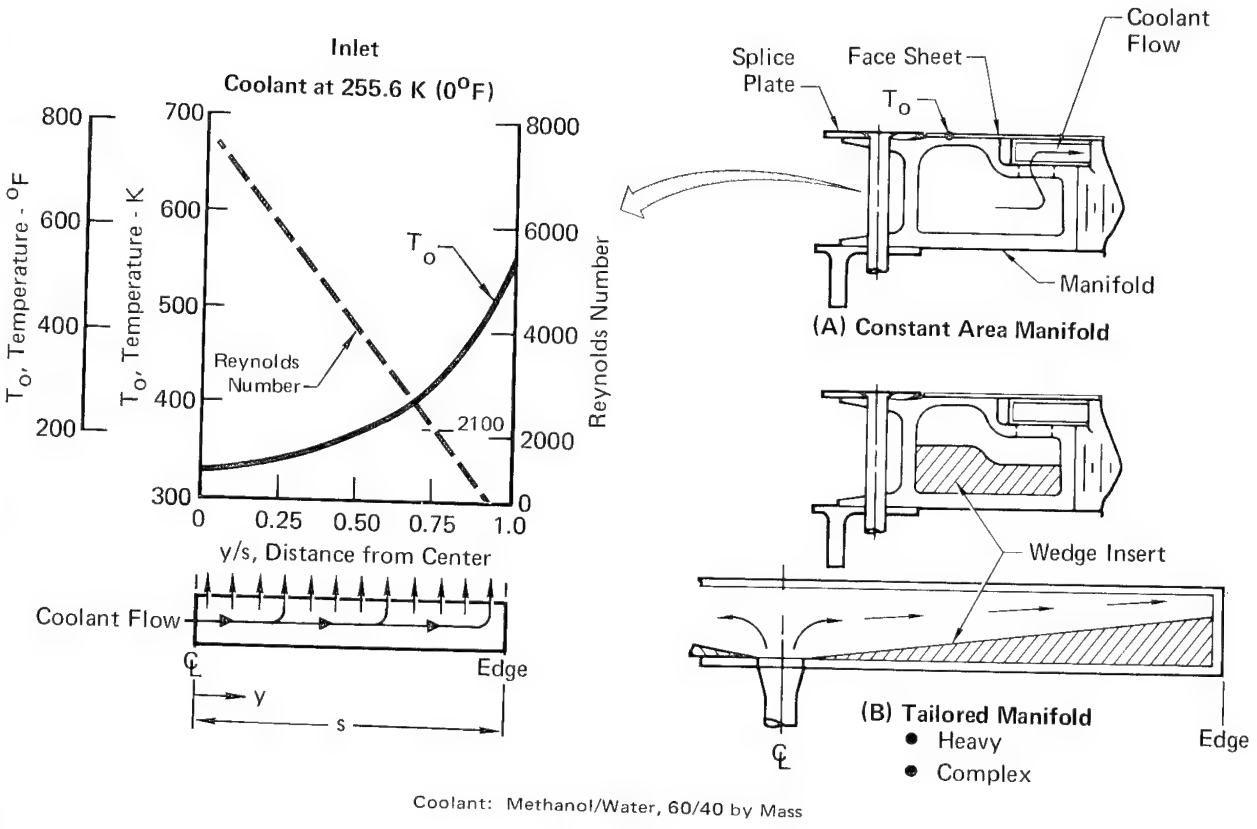

Coolant: Methanol/Water, 60/40 by Mass

FIGURE 49
CONSTANT AREA AND TAILORED MANIFOLD DESIGNS ARE ELIMINATED

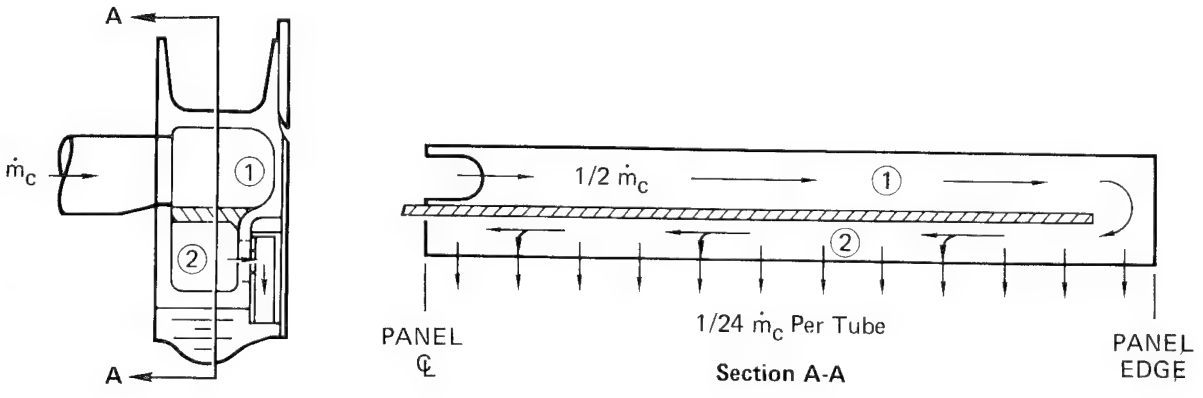

FIGURE 50
COOLANT FLOW IN SELECTED SPLIT MANIFOLD DESIGN

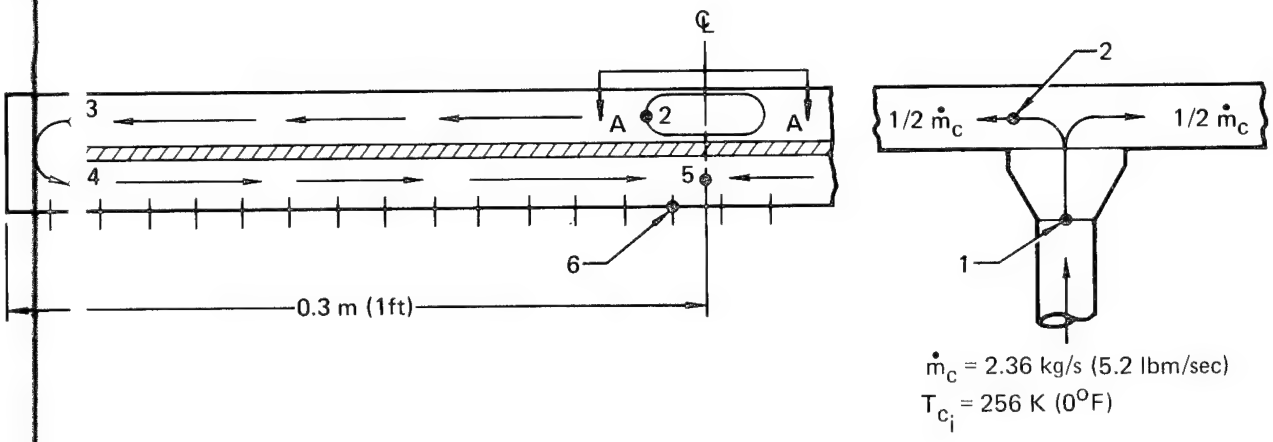

Location	Pressure Drop		APS Mass	
	(kPa)	(psi)	(kg/m^2)	(lbm/ft^2)
1-2, Entrance to Manifold	4.54	0.659	0.0043	0.0019
2-3, Outer Manifold Chamber	2.25	0.327	0.0049	0.0010
3-4, 180° Turn	14.66	2.126	0.0308	0.0063
4-5, Inner Manifold Chamber	2.16	0.313	0.0030	0.0006
6 , Entrance to Coolant Tube	5.43	0.787	0.0112	0.0023
Total	29.04	4.212	0.0542	0.0121

Coolant: 60/40 Mass Solution of Methanol/Water

FIGURE 5I
FULL SCALE PANEL INLET MANIFOLD PRESSURE DROP AND APS MASS

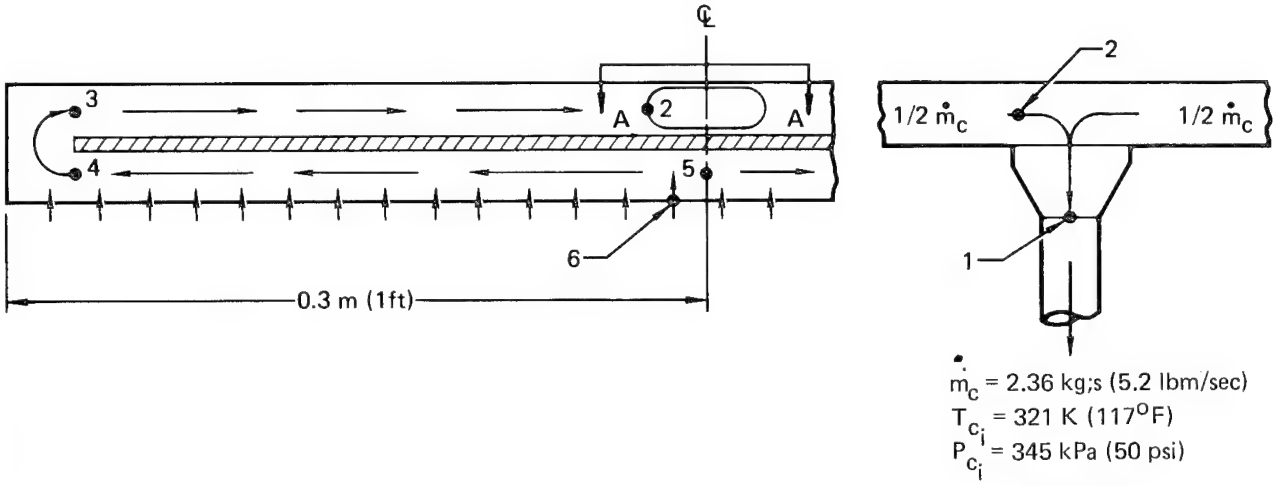

Location	Pressure Drop		APS Mass	
	(kPa)	(psi)	(kg/m^2)	(lbm/ft^2)
6 , Exit of Coolant Tube	3.92	0.568	0.0098	0.0020
5-4, Inner Manifold Chamber	1.47	0.212	0.0015	0.0003
4-3, 180° Turn	6.25	0.907	0.0117	0.0024
3-2, Outer Manifold Chamber	1.54	0.223	0.0034	0.0007
2-1, Exit of Manifold	2.30	0.334	0.0049	0.0010
Total	15.48	2.244	0.0313	0.0064

Coolant: 60/40 Mass Solution of Methanol/Water

FIGURE 52
FULL SCALE PANEL EXIT MANIFOLD PRESSURE DROP

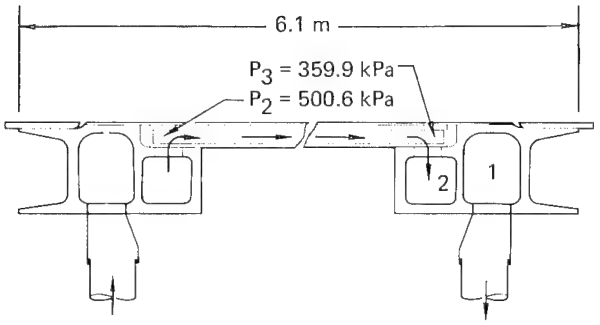

APS Mass	
Inlet Manifold	0.054 kg/m^2 (ΔP = 29.0 kPa)
Panel (24 Tubes)	0.293 kg/m^2 (ΔP = 140.7 kPa)
Exit Manifold	0.031 kg/m^2 (ΔP = 15.5 kPa)
Total APS Mass	0.0378 kg/m^2 (ΔP = 185.2 kPa)
Coolant Inventory	
5.94 kg Per 3.7 m^2	1.61 kg/m^2
Total APS Mass Plus Coolant Inventory	2.0 kg/m^2

a. Metric Units

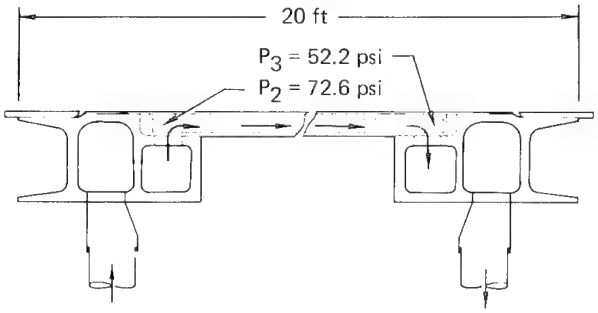

APS Mass	
Inlet Manifold	0.01 psf (ΔP = 4.2 psi)
Panel (24 Tubes)	0.06 psf (ΔP = 20.4 psi)
Exit Manifold	0.01 psf (ΔP = 2.2 psi)
Total APS Mass	0.08 psf (ΔP = 26.8 psi)
Coolant Inventory	
13.1 lb Per 40 ft^2	0.33 psf
Total APS Mass Plus Coolant Inventory	0.41 psf

b. English Units

FIGURE 53
COOLANT PRESSURES AND COOLANT MASS
Methanol/Water (60/40 by Mass)

79 Temperature Nodes
Accounts for: Interface Conductance Between Outer Skin and Tube;
Outer Skin and Manifold; Splice Plate and Manifold; and
Property Variations with Temperature

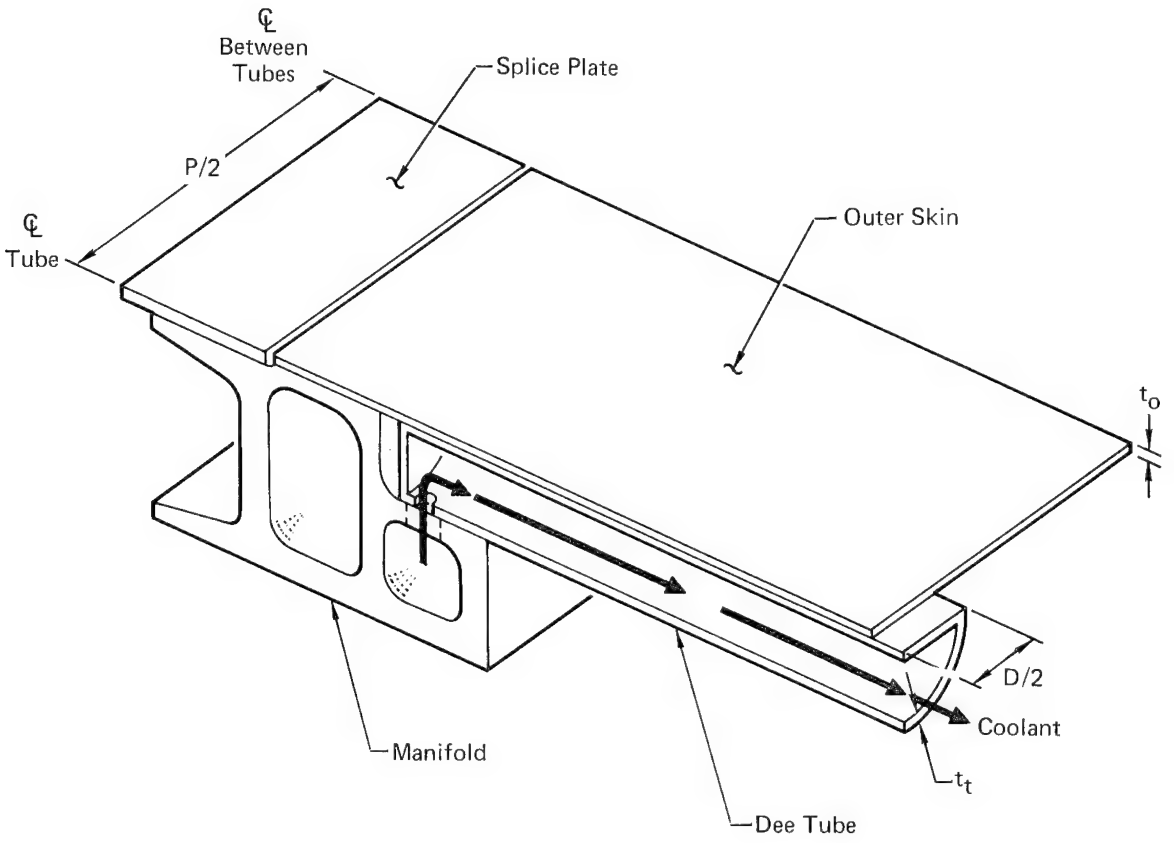

FIGURE 54
THREE DIMENSIONAL MANIFOLD THERMAL MODEL

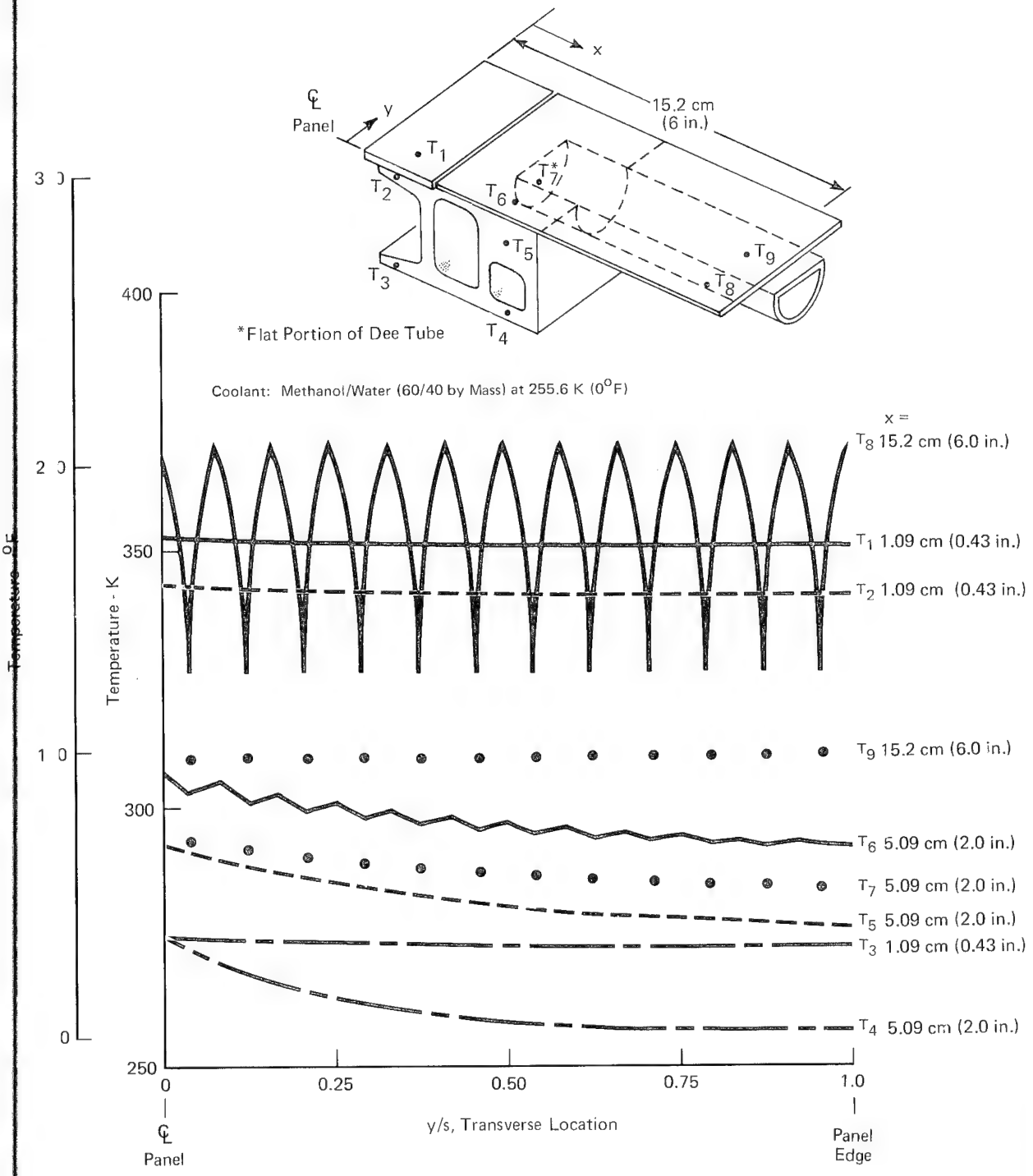

FIGURE 55
TRANSVERSE TEMPERATURE DISTRIBUTIONS AT MANIFOLD INLET

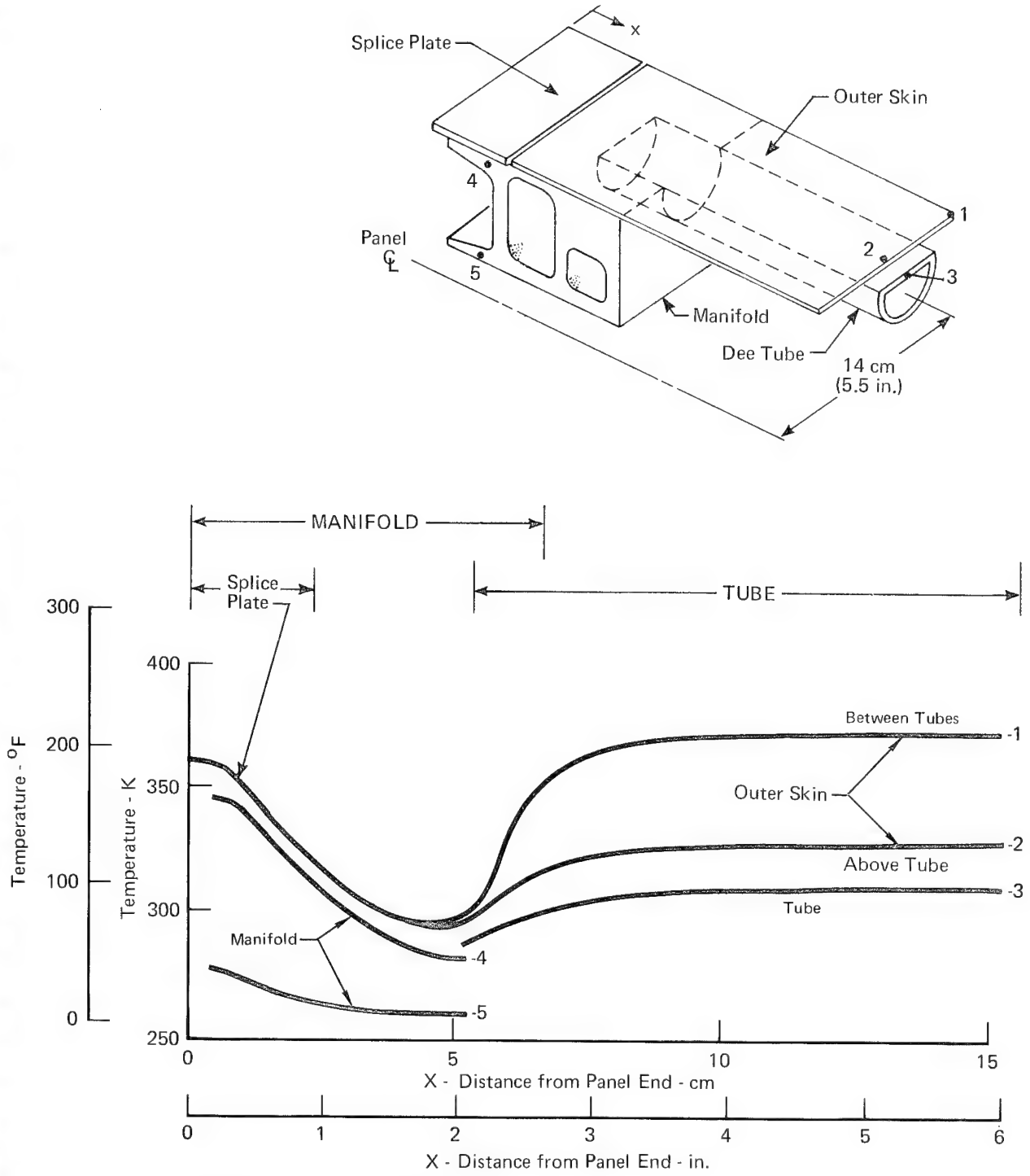

Coolant: Methanol/Water (60/40 by Mass)
at 255.6 K (0°F)

FIGURE 56
LONGITUDINAL TEMPERATURE DISTRIBUTIONS AT PANEL INLET

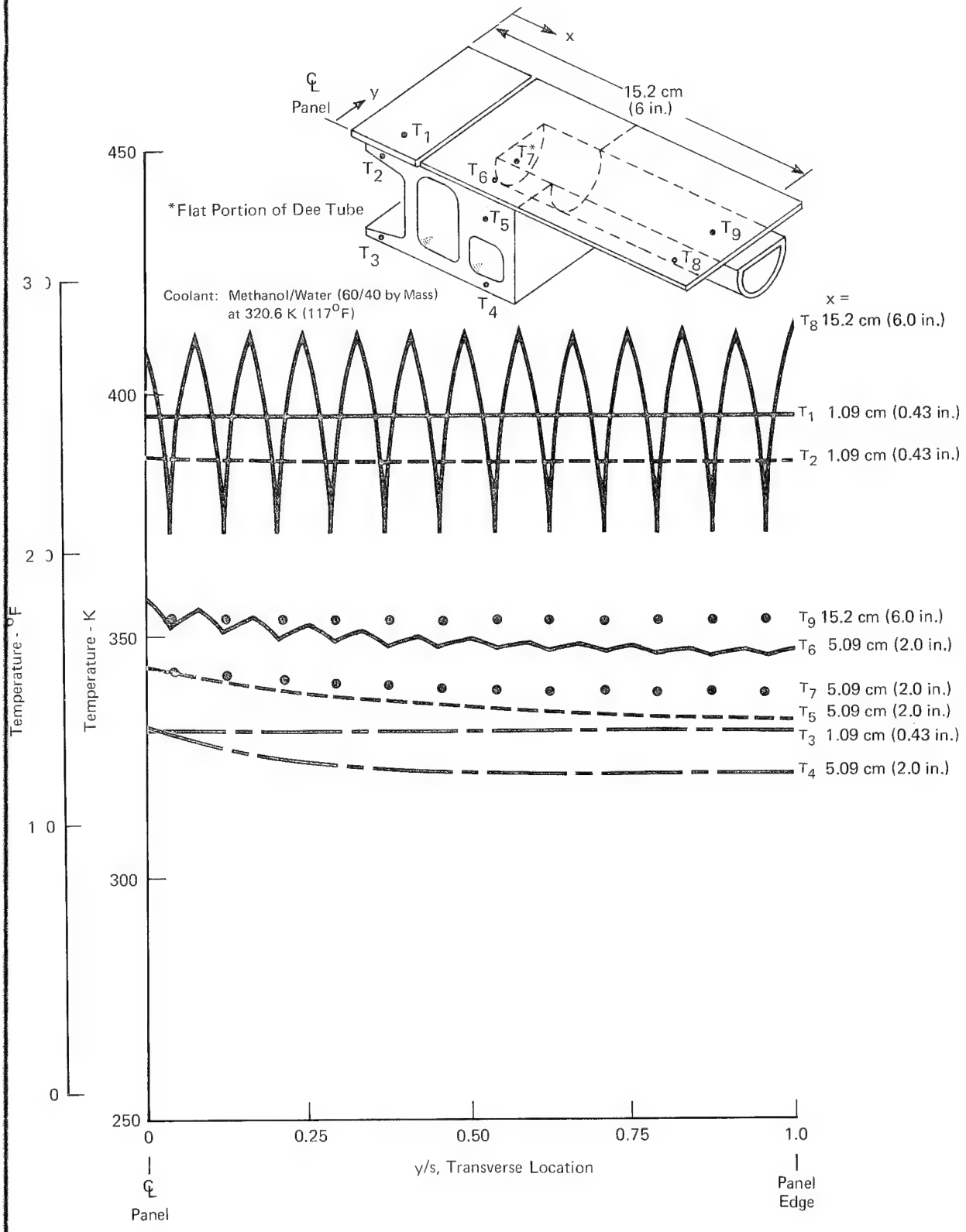

FIGURE 57
TRANSVERSE TEMPERATURE DISTRIBUTIONS AT MANIFOLD EXIT

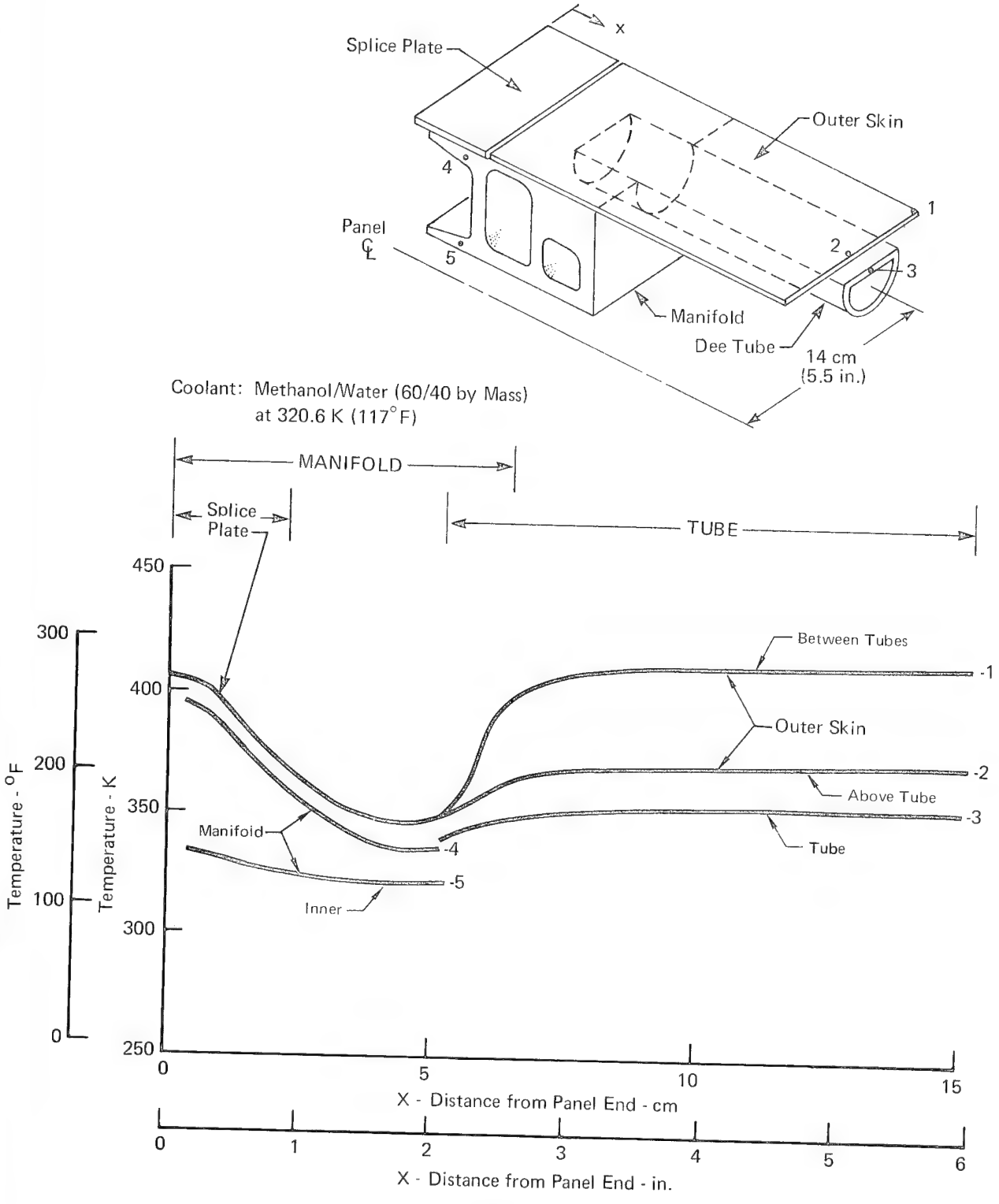

FIGURE 58
LONGITUDINAL TEMPERATURE DISTRIBUTIONS AT PANEL EXIT

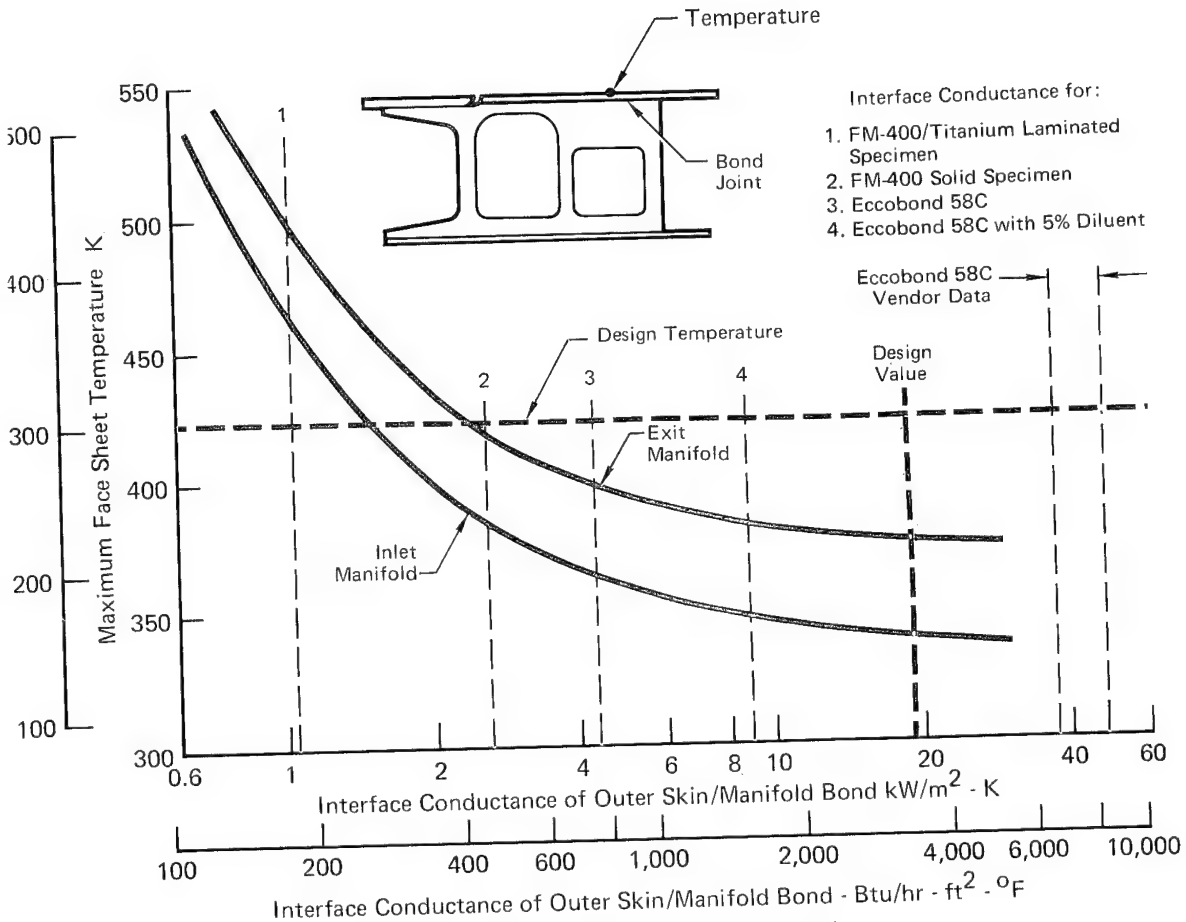

- Bond Joint Thickness is 0.015 cm (0.006 in.)
- Methanol/Water (60/40 by Mass)
- $\dot{m}_c$ = 2359 g/s (5.2 lbm/sec)
- Inlet Coolant Temperature = 256 K (0°F)
- Exit Coolant Temperature = 321 K (117°F)

FIGURE 59
MANIFOLD FACE SHEET TEMPERATURE vs INTERFACE CONDUCTANCE OF BOND JOINT

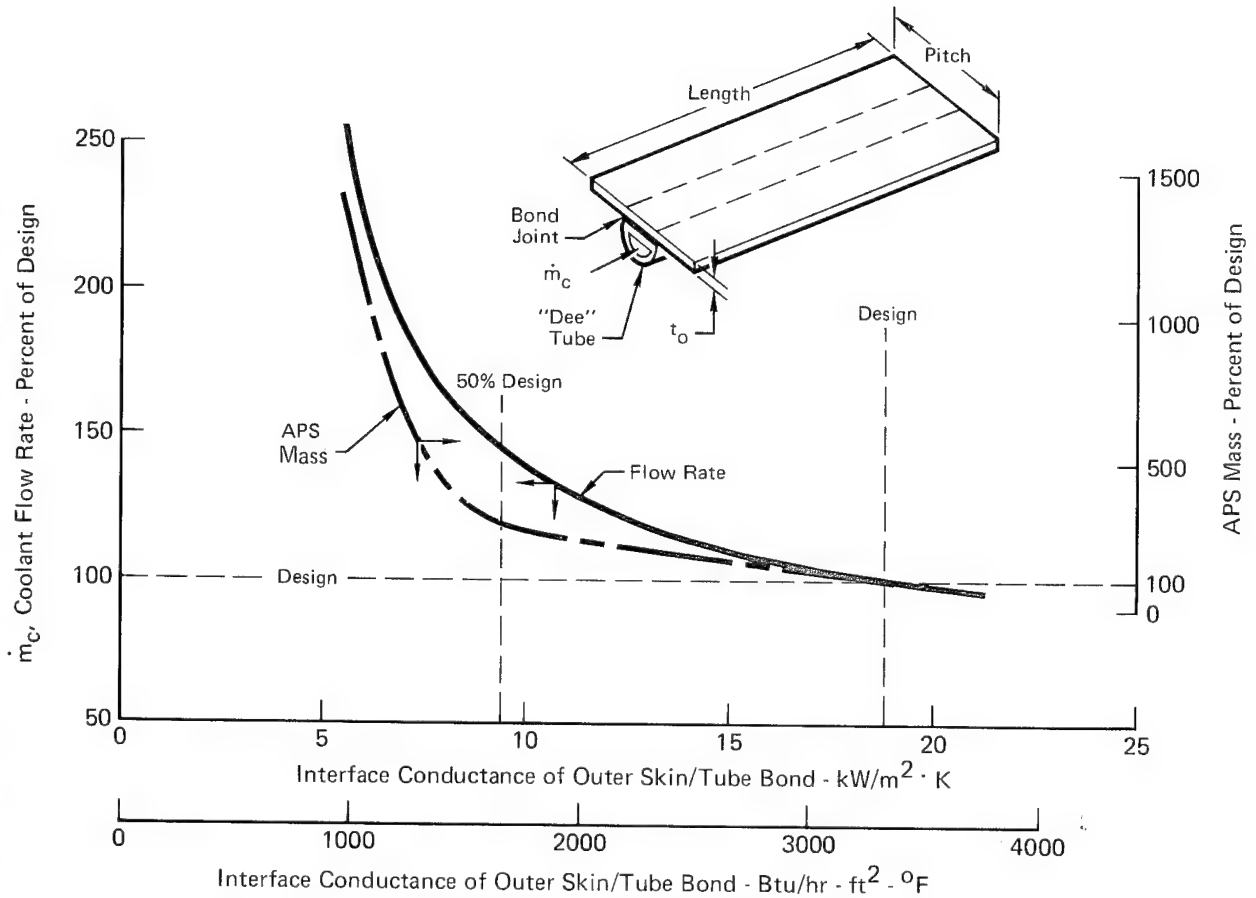

- Design Coolant Flow Rate = 2.36 kg/s (5.2 lbm/sec)
- Design APS Mass = 0.0378 kg/m^2 (0.08 lbm/ft^2)
- Methanol/Water (60/40) by Mass
- Maximum Panel Temperature of 422 K (300^{o}F) (Outer Skin Midway Between Tubes)

FIGURE 60
COOLANT FLOW RATE AND APS FUEL REQUIREMENTS
vs INTERFACE CONDUCTANCE

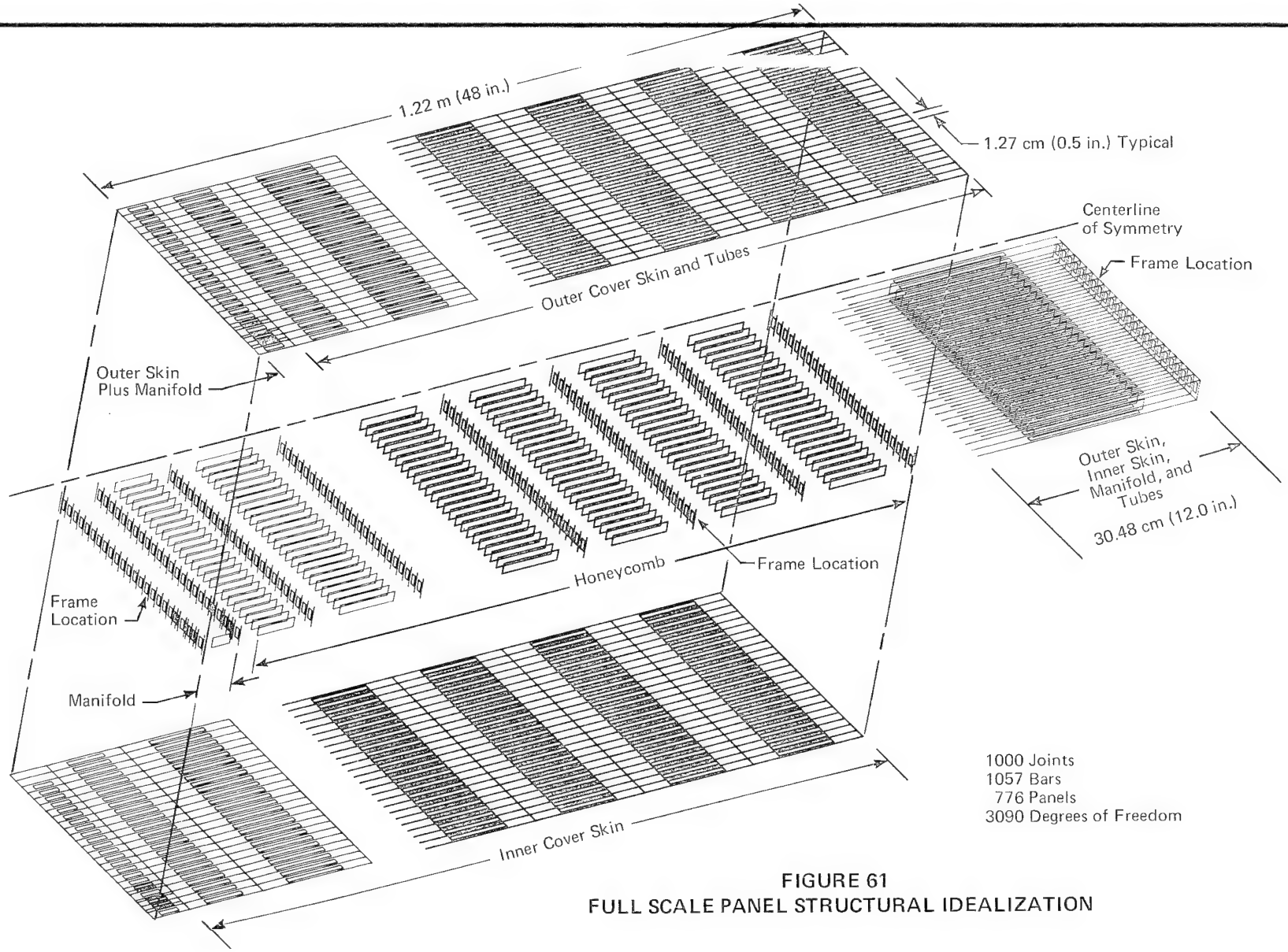

FIGURE 61
FULL SCALE PANEL STRUCTURAL IDEALIZATION

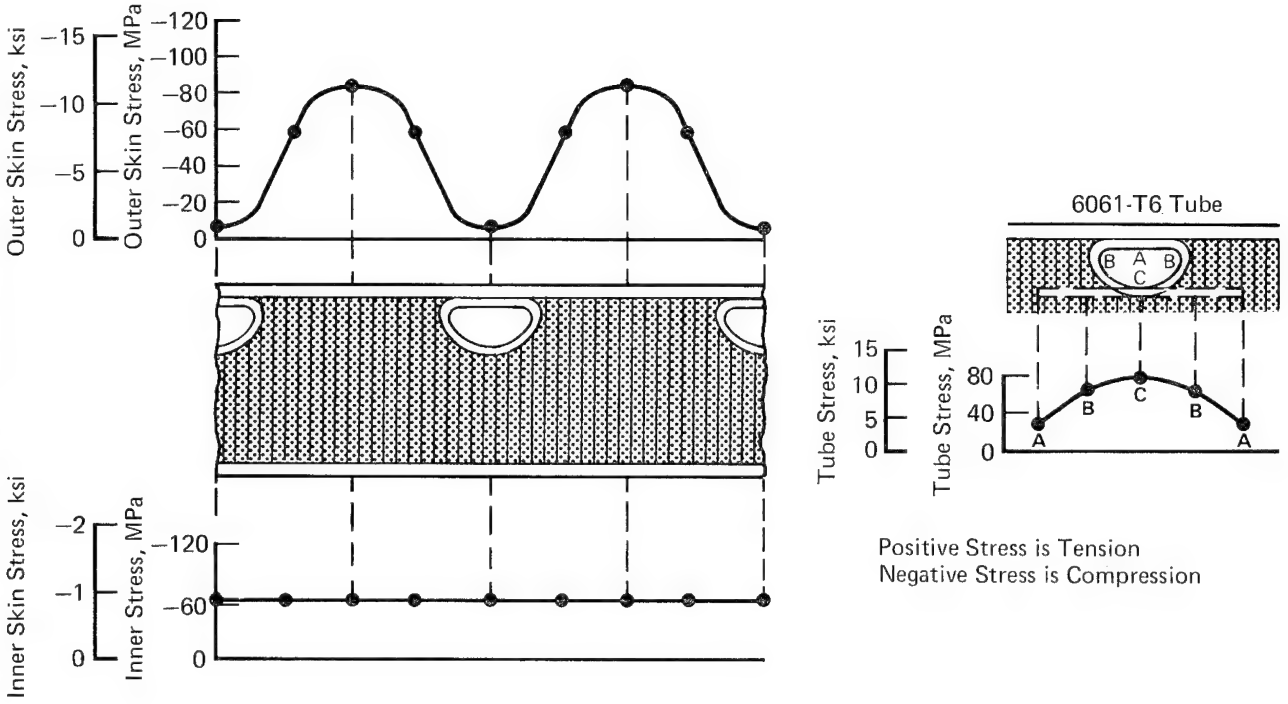

FIGURE 62
ACTIVELY COOLED PANEL THERMAL STRESS

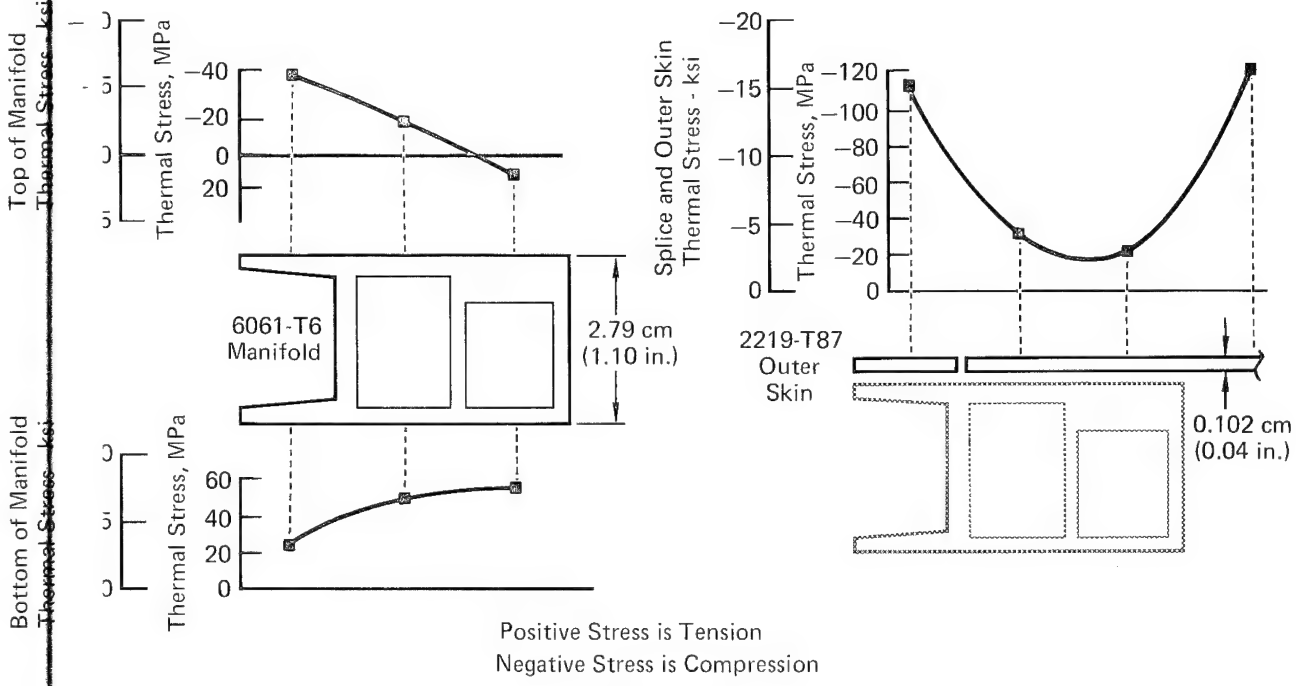

FIGURE 63
ACTIVELY COOLED PANEL INLET MANIFOLD THERMAL STRESS

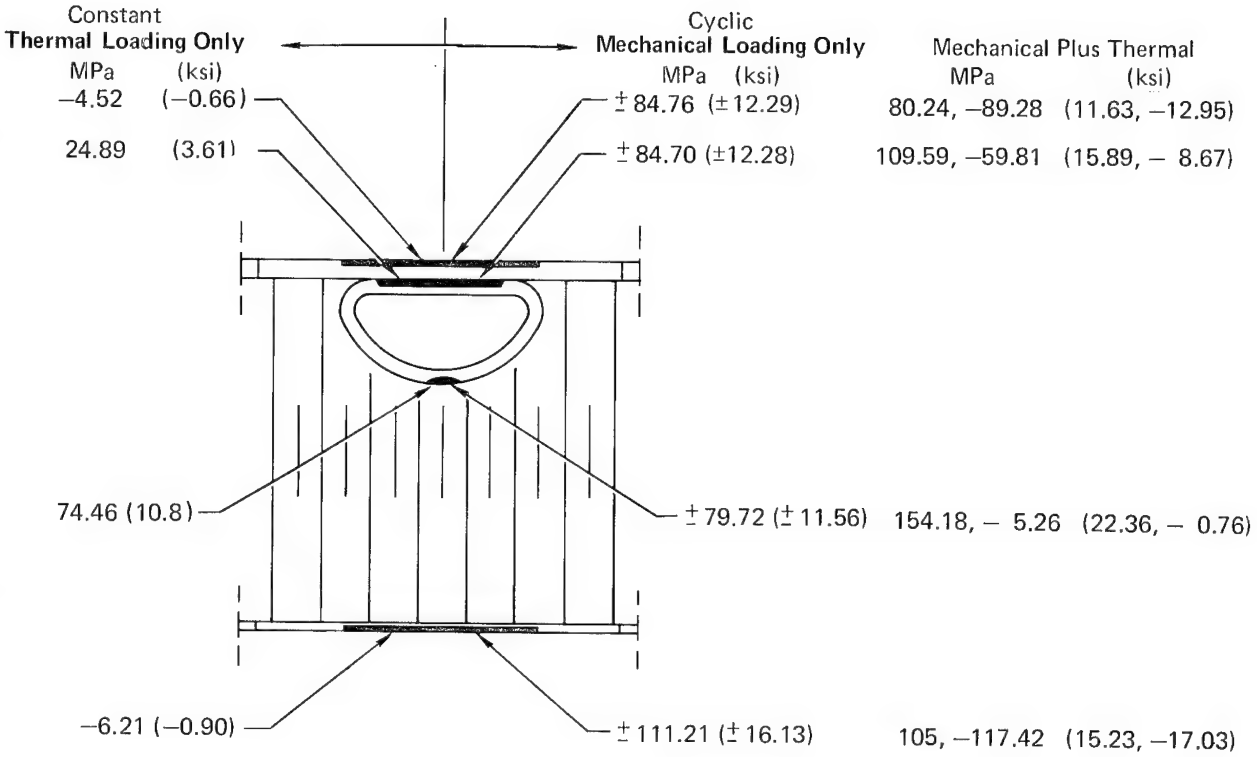

FIGURE 64
STRESS LEVEL AT FLAW

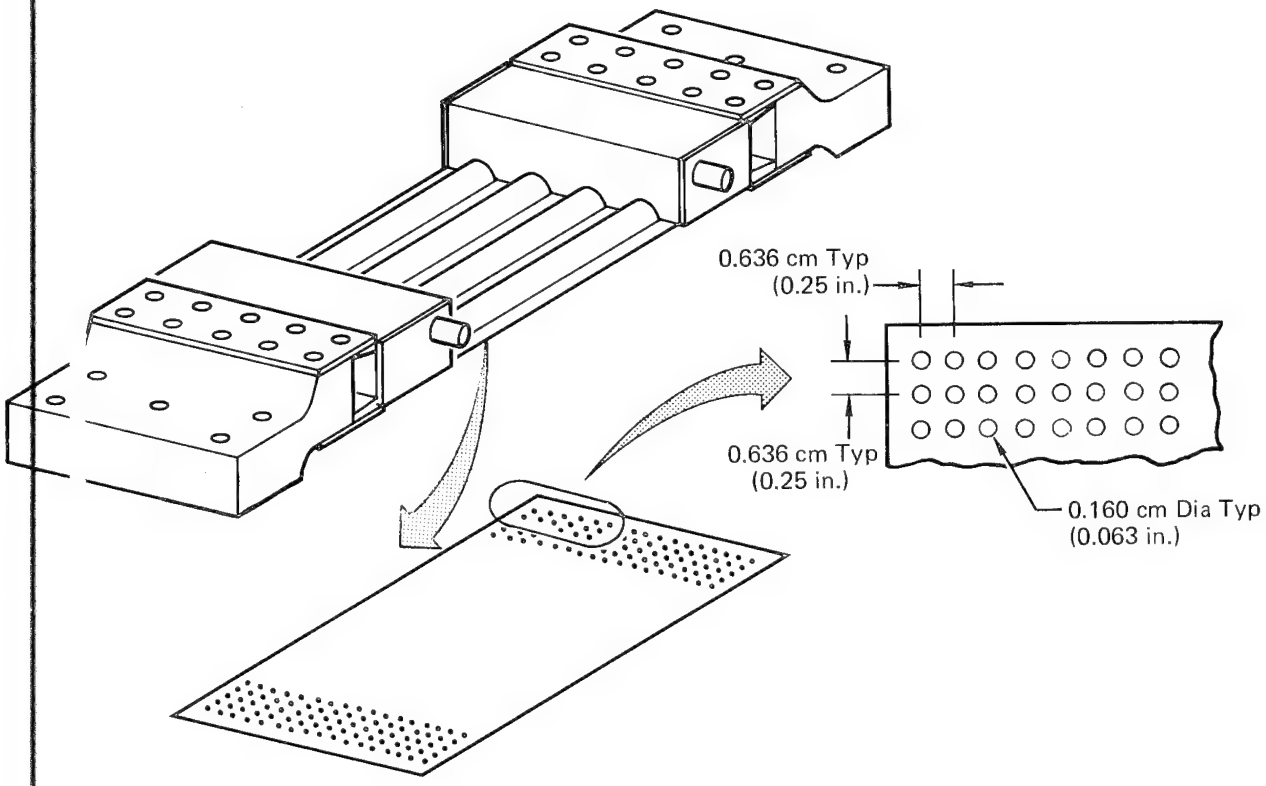

FIGURE 65
PERFORATED SKINS USED TO MINIMIZE SOLDER JOINT VOIDS
(Used on one skin/Dee tube/manifold specimen and first test panel attempt)

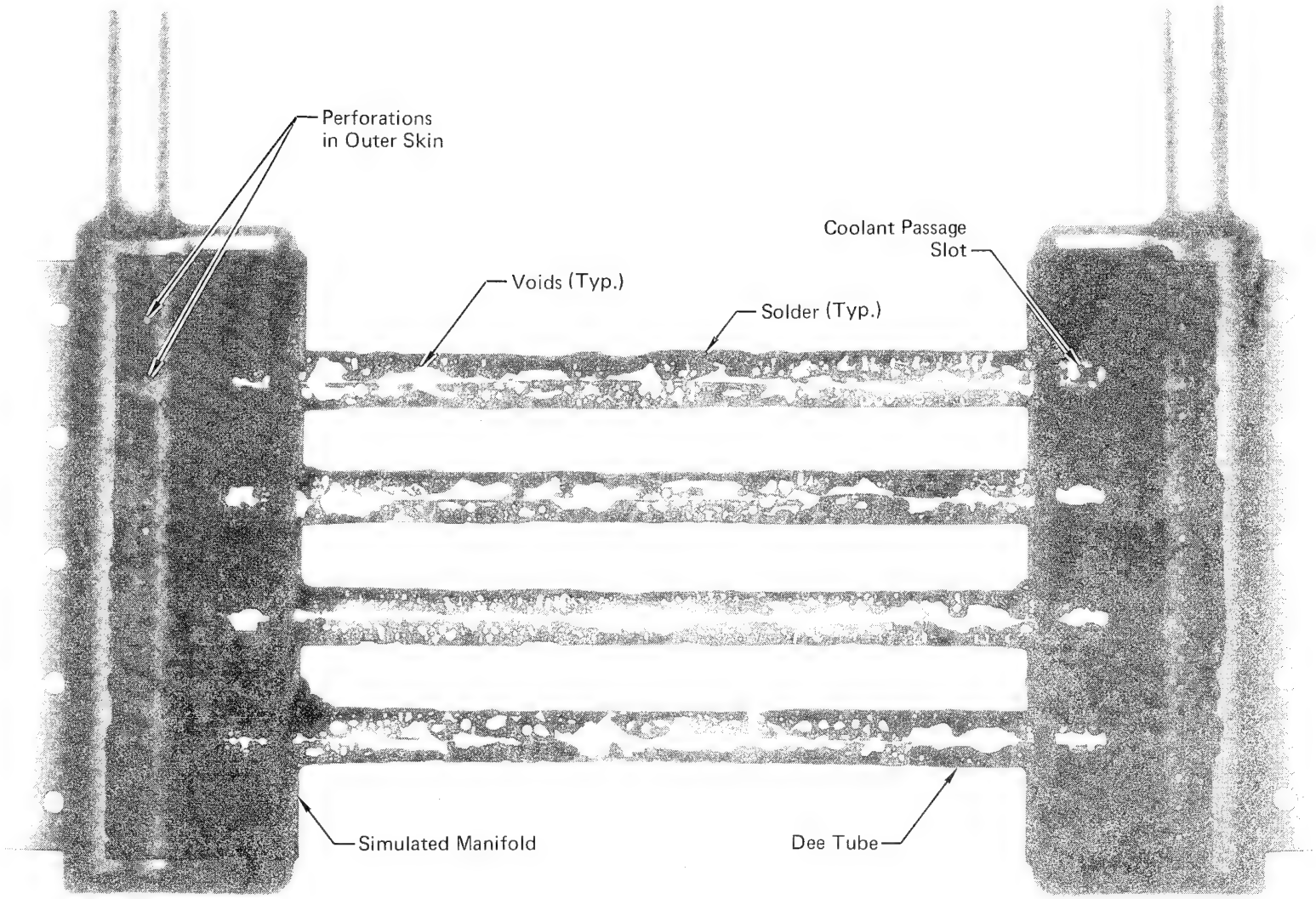

FIGURE 66
RADIOGRAPH POSITIVE OF SOLDERED
SKIN/DEE TUBE/MANIFOLD SPECIMEN

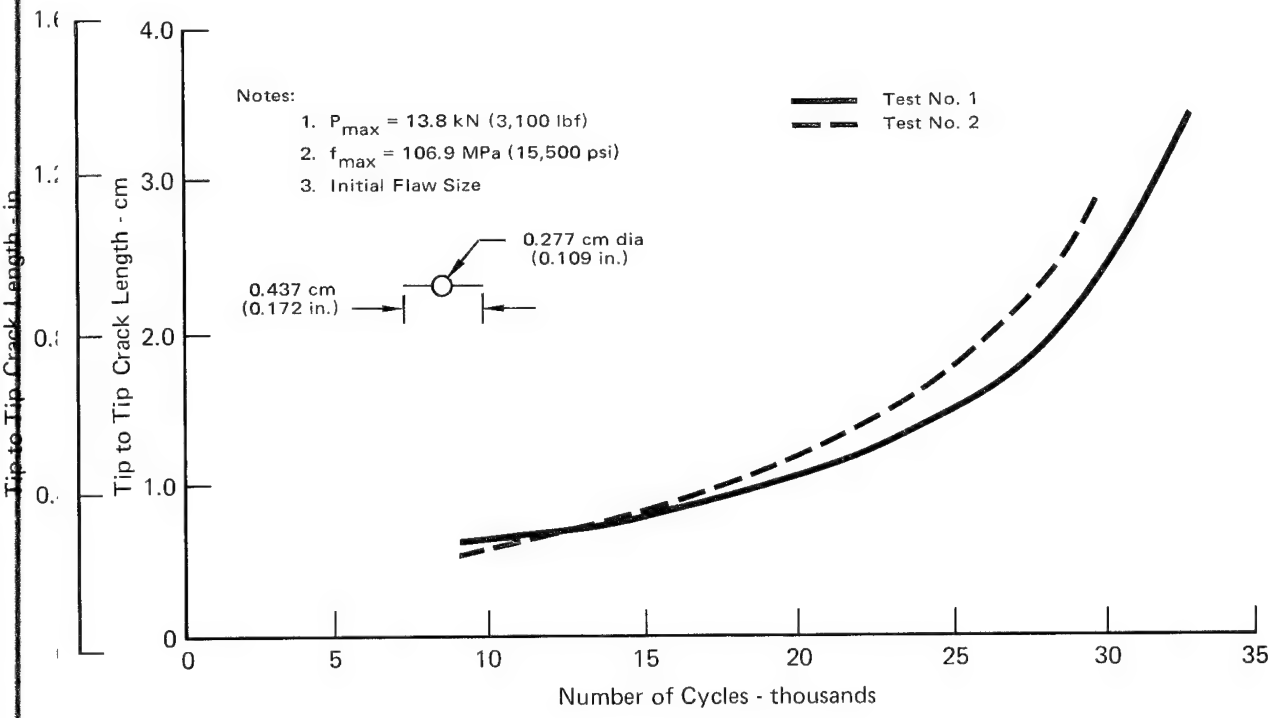

FIGURE 67
BASIC SKIN SPECIMEN - FATIGUE CRACK PROPAGATION

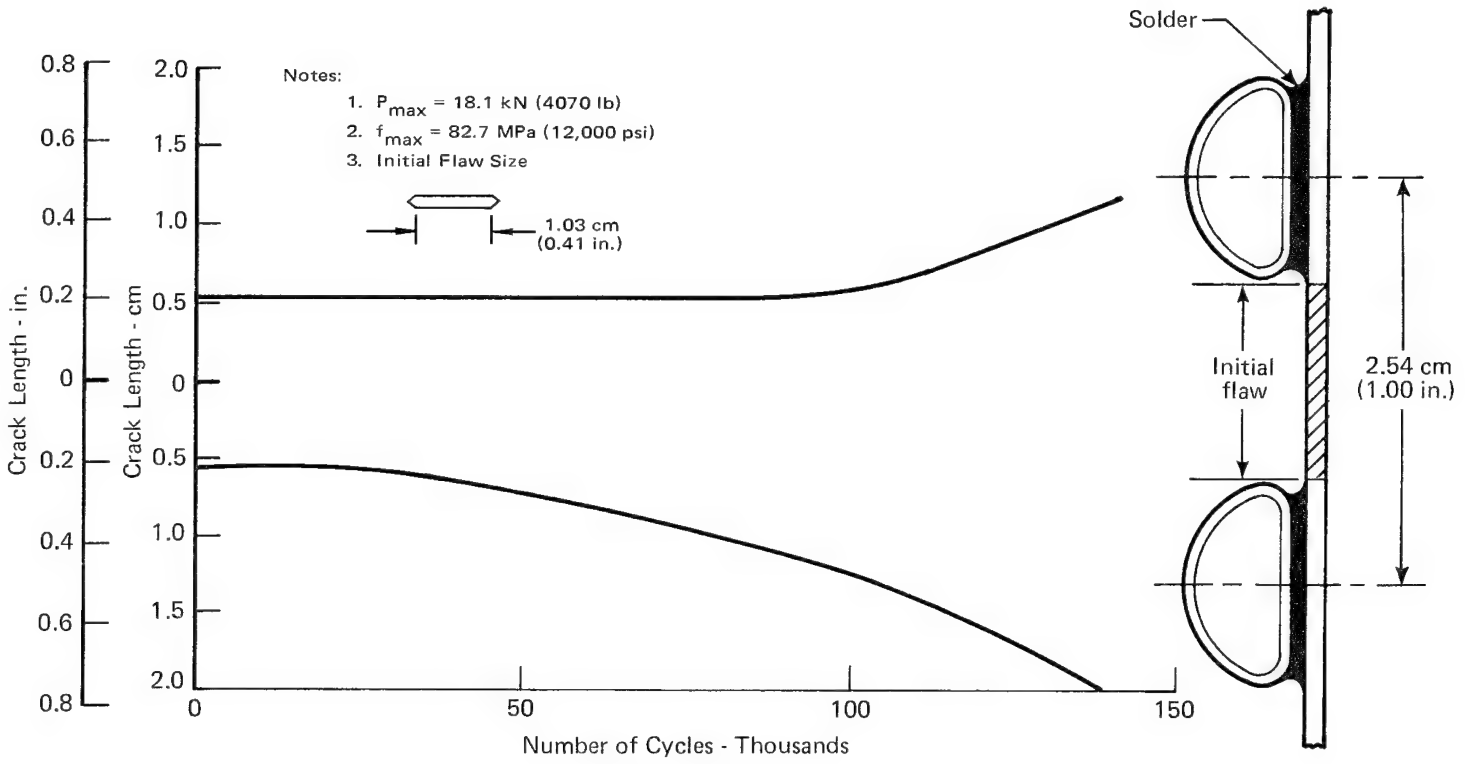

FIGURE 68
SKIN/DEE TUBE/MANIFOLD SPECIMEN FATIGUE CRACK LENGTH
vs CYCLES (SOLDERED SKINS)

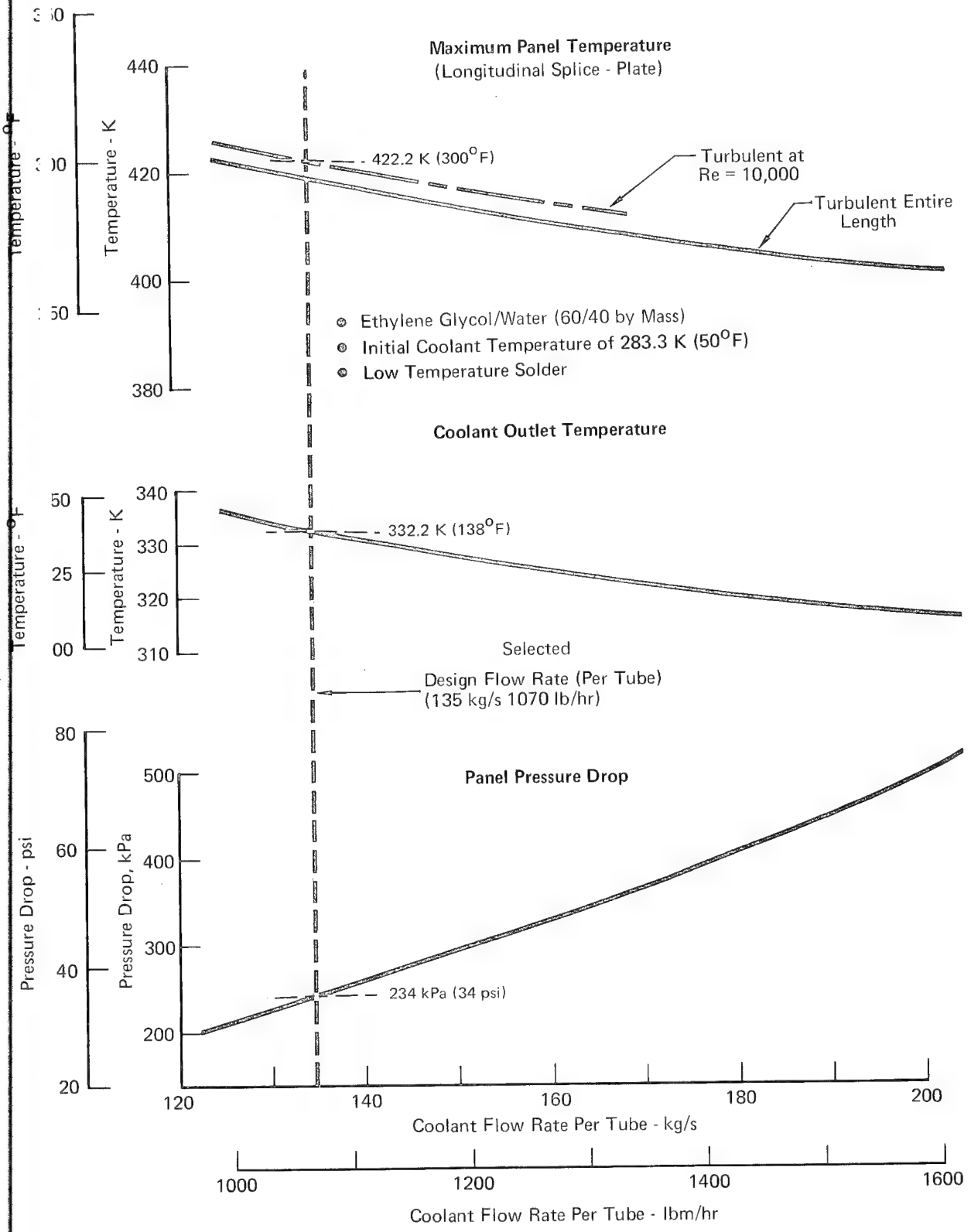

FIGURE 69
GLYCOL/WATER FLOW RATE FOR FULL SCALE PANEL DESIGN

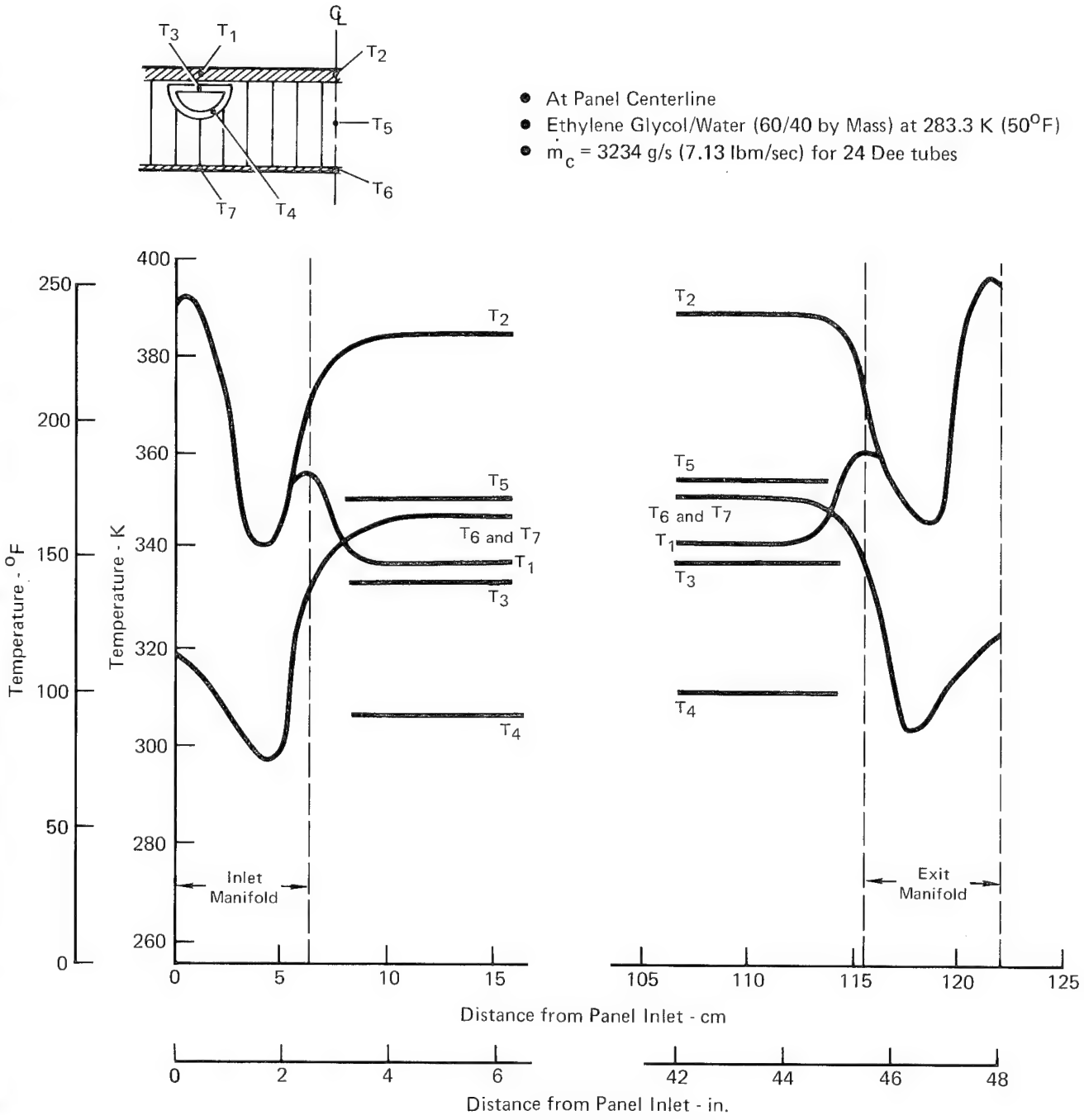

FIGURE 70
ACTIVELY COOLED TEST PANEL TEMPERATURES FOR A SIMULATED FULL SCALE INLET CONDITION

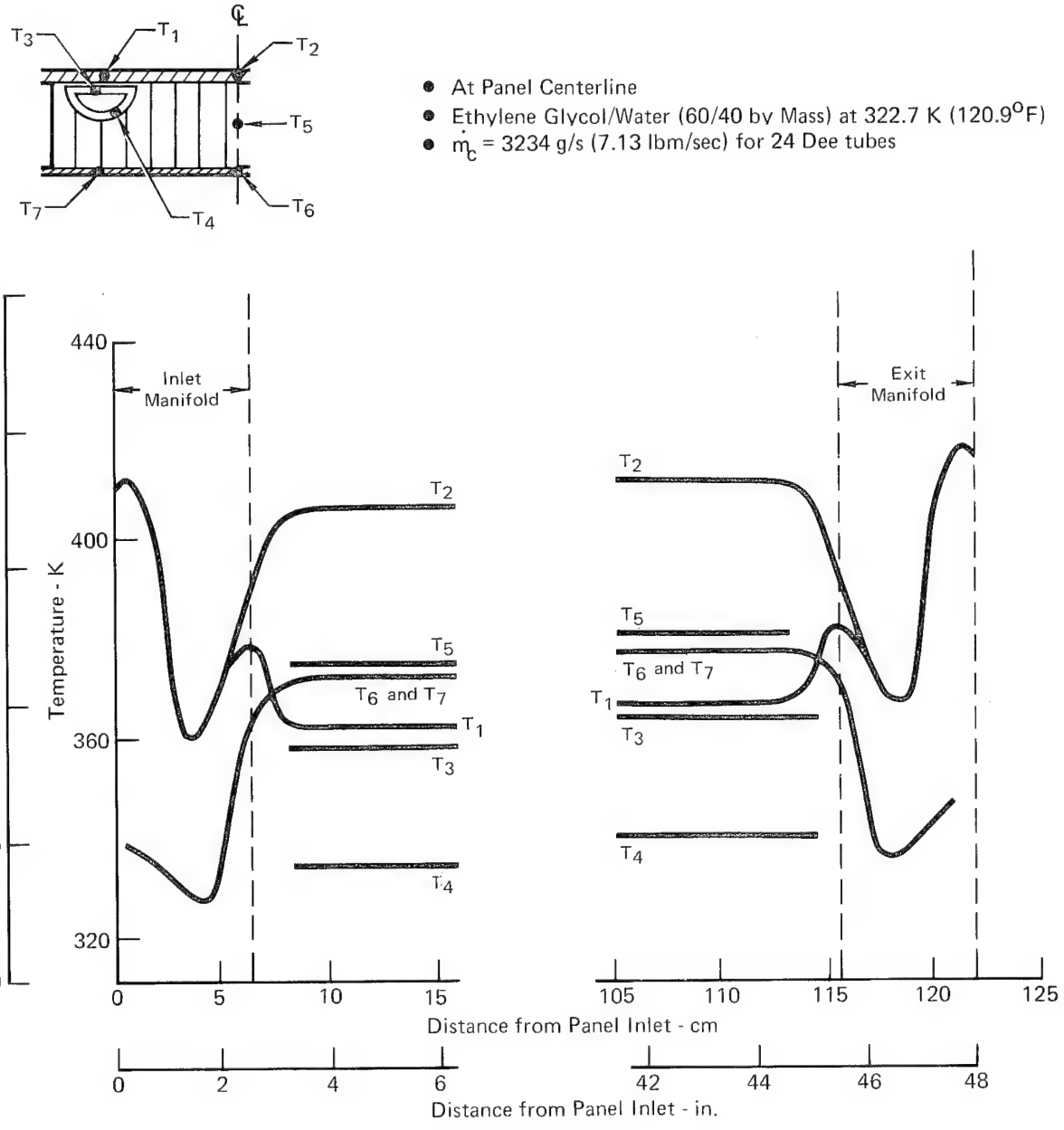

FIGURE 71
ACTIVELY COOLED TEST PANEL TEMPERATURES FOR A SIMULATED FULL SCALE EXIT CONDITION

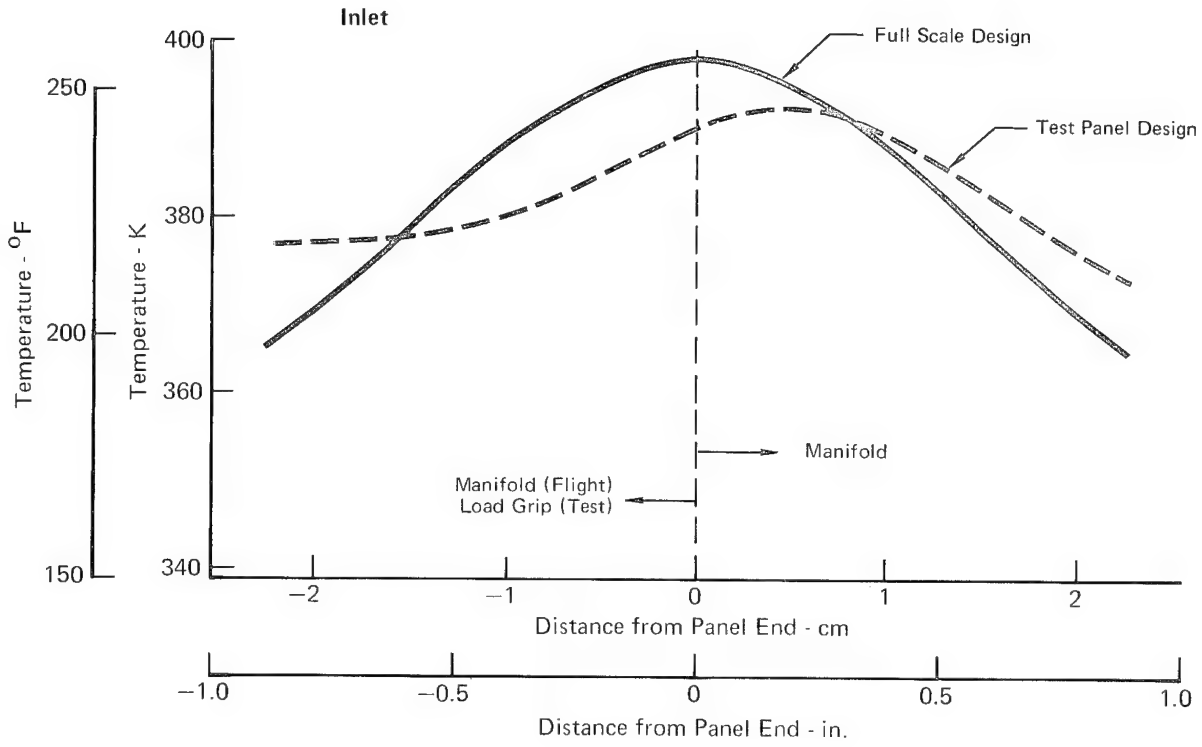

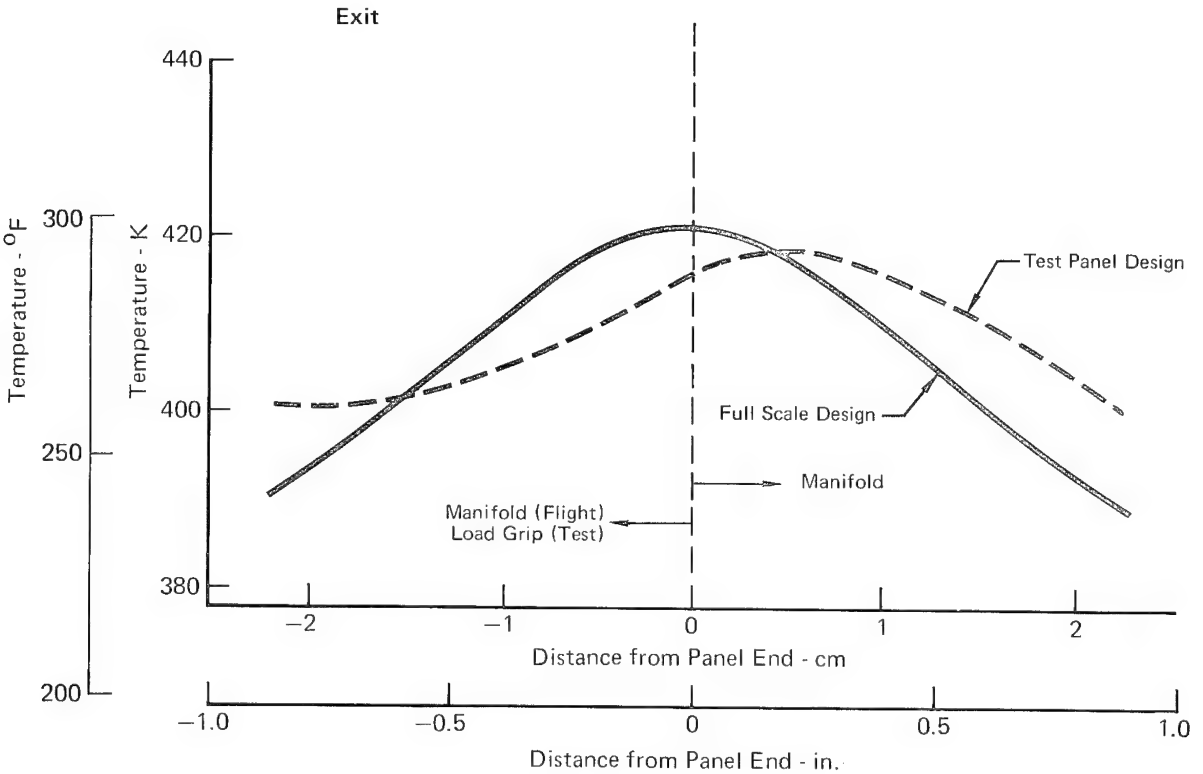

FIGURE 72
STEADY STATE TEMPERATURES OF
TRANSVERSE SPLICE PLATE AT PANEL CENTERLINE

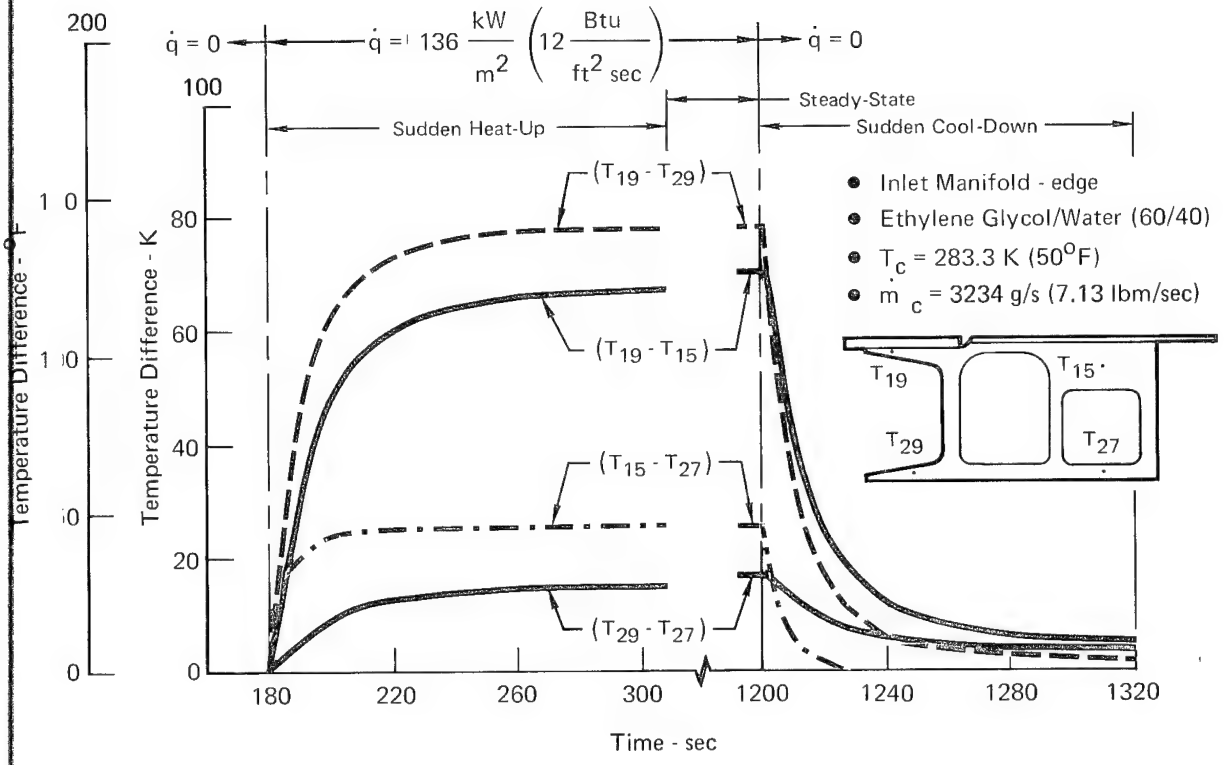

FIGURE 73
MANIFOLD TEMPERATURE DIFFERENCES
FOR A SUDDEN HEAT-UP AND COOL-DOWN

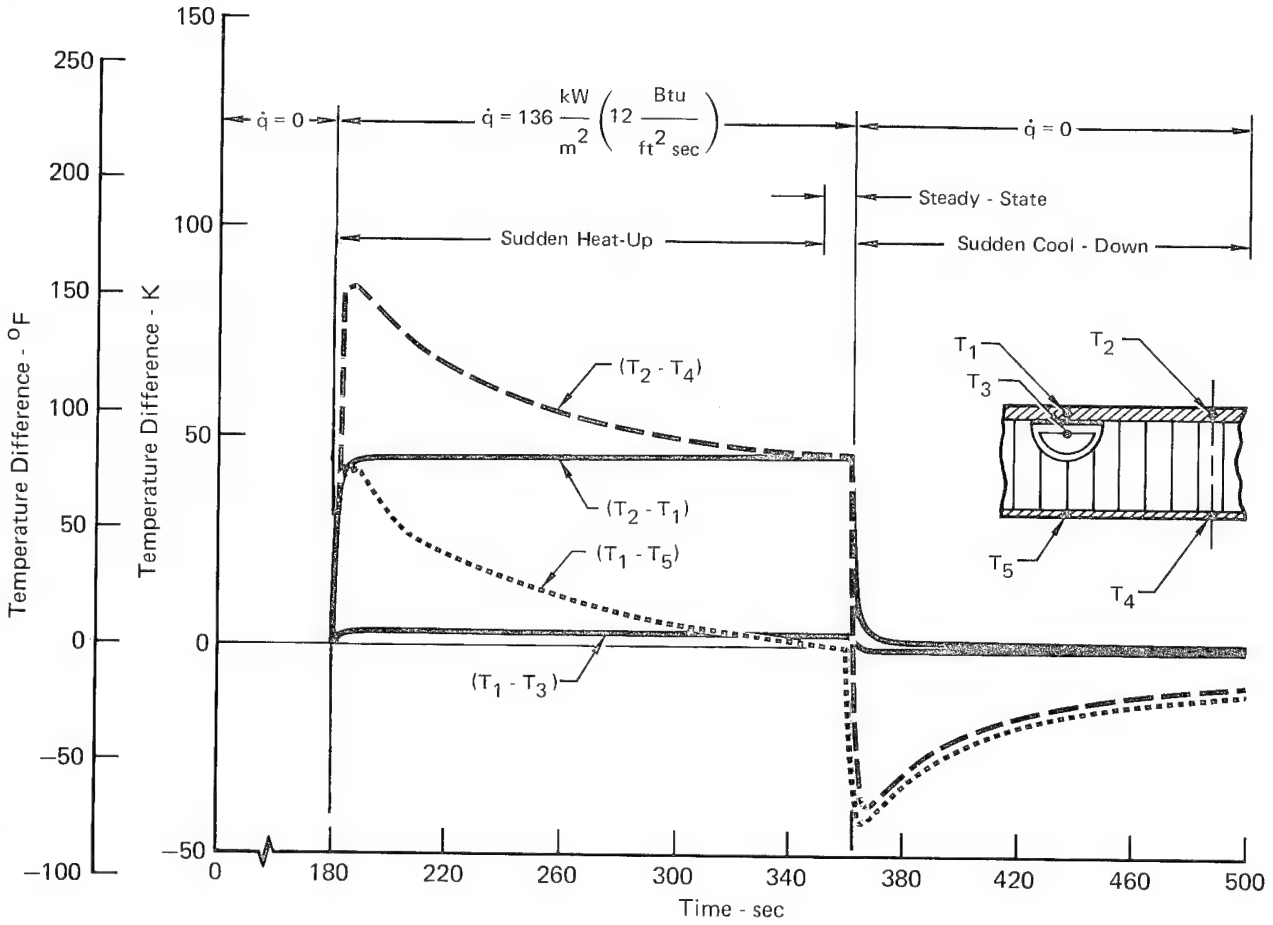

FIGURE 74
PANEL TEMPERATURE DIFFERENCES FOR A SUDDEN HEAT-UP AND COOL-DOWN

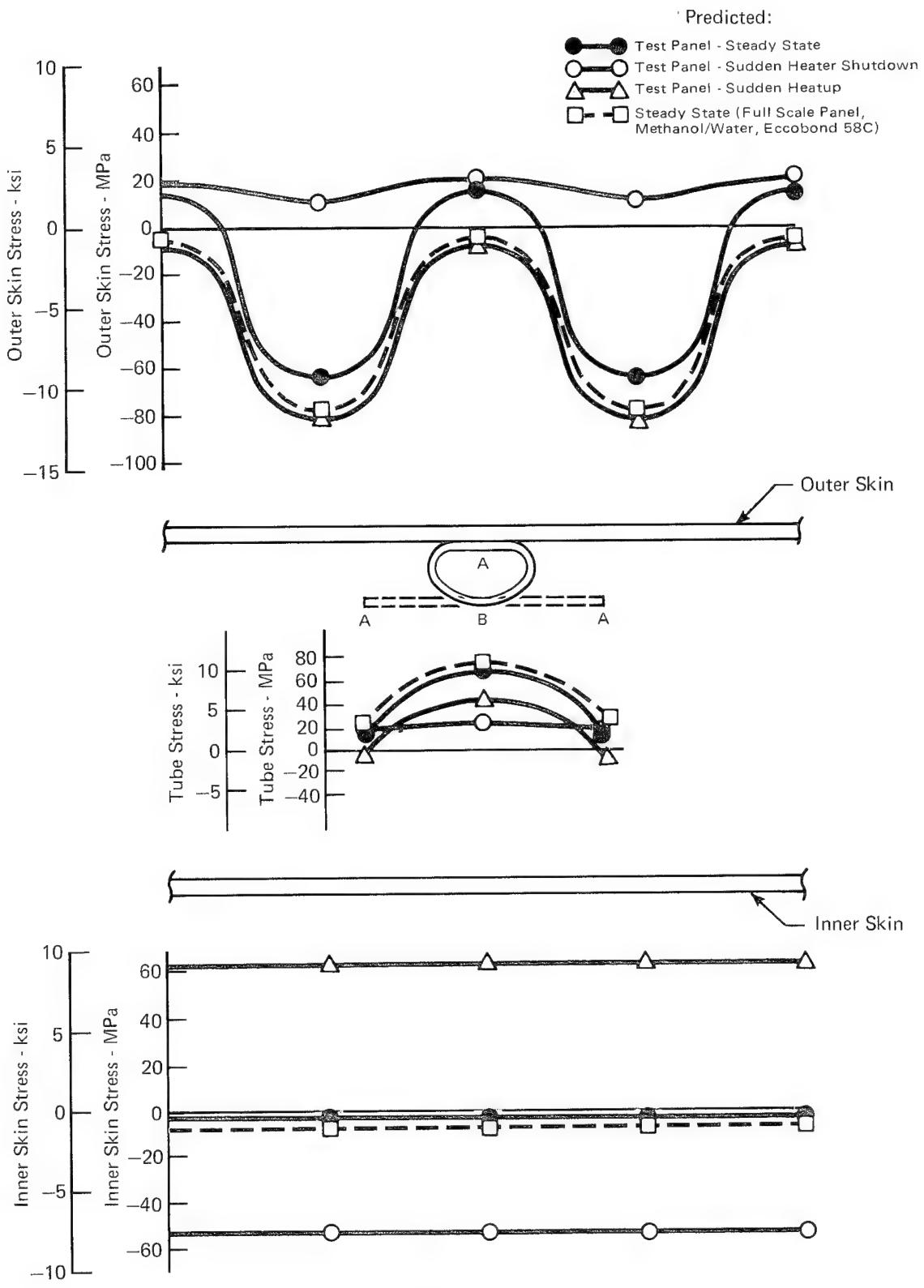

FIGURE 75
TEST vs FULL SCALE PANEL THERMAL STRESSES 7.62 cm (3.0 IN.)
FROM INLET MANIFOLD
Glycol/Water (solder)

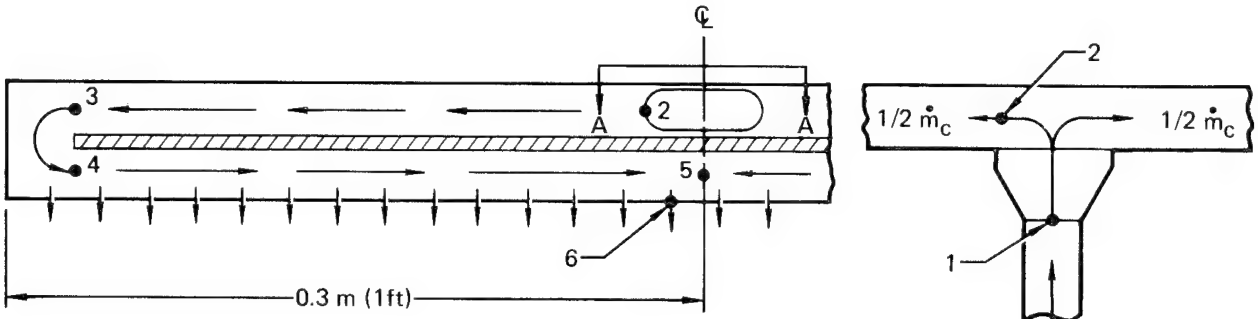

$\dot{m}_c$ = 3.23 kg/s (7.13 lbm/sec)
T_c = 283 K (50°F)

Section A-A

Location	Pressure Drop		APS Mass	
	(kPa)	(psi)	(kg/m^2)	(lbm/ft^2)
1-2, Entrance to Manifold	7.30	1.06	0.0175	0.0036
2-3, Outer Manifold Chamber	3.65	0.53	0.0087	0.0018
3-4, 180° Turn	23.58	3.42	0.0565	0.0116
4-5, Inner Manifold Chamber	3.51	0.51	0.0084	0.0017
6 , Entrance to Coolant Tube	8.69	1.26	0.0208	0.0043
Total	46.73	6.78	0.1120	0.0230

Coolant: 60/40 Mass Solution of Ethylene Glycol/Water

FIGURE 76
TEST PANEL INLET MANIFOLD PRESSURE DROP

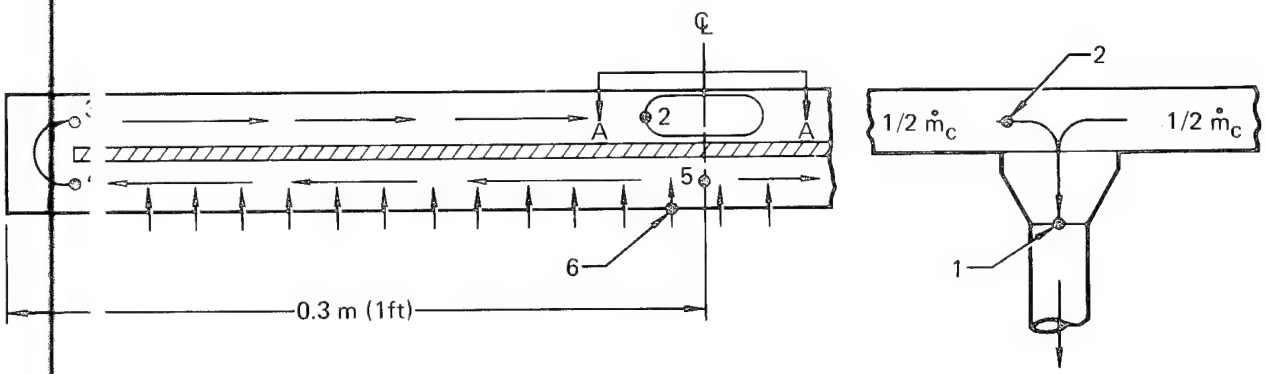

$\dot{m}_c$ = 3.23 kg/s (7.13 lbm/sec)
T_c = 332 K (138°F)
P_c = 345 kPa (50 psi)

Section A-A

Location	Pressure Drop		APS Mass	
	(kPa)	(psi)	(kg/m^2)	(lbm/ft^2)
6 , Exit of Coolant Tube	7.17	1.04	0.0180	0.0037
5-4, Inner Manifold Chamber	2.48	0.36	0.0062	0.0013
4-3, 180° Turn	12.27	1.78	0.0308	0.0063
3-2, Outer Manifold Chamber	2.62	0.38	0.0066	0.0014
2-1, Exit of Manifold	4.34	0.63	0.0109	0.0022
Total	28.88	4.19	0.0730	0.0150

Coolant: 60/40 Mass Solution of Ethylene Glycol/Water

FIGURE 77
TEST PANEL EXIT MANIFOLD PRESSURE DROP

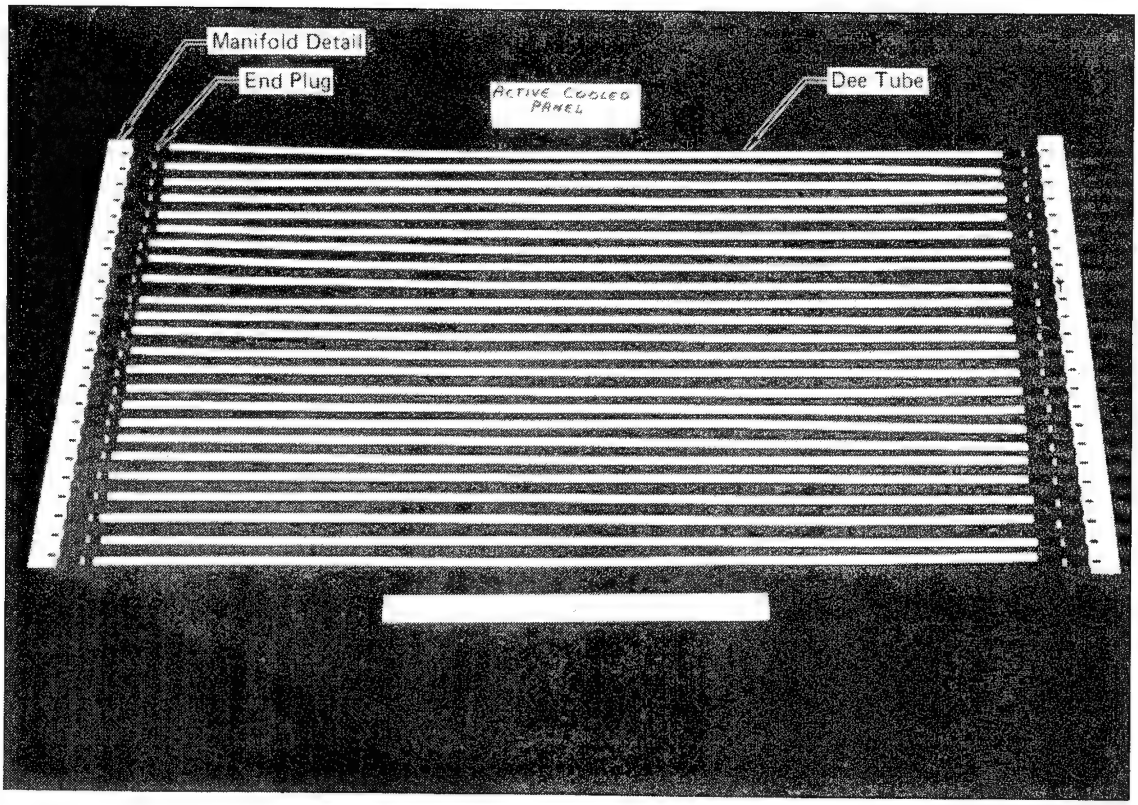

FIGURE 78
DEE TUBES, END PLUGS, AND MANIFOLD DETAIL

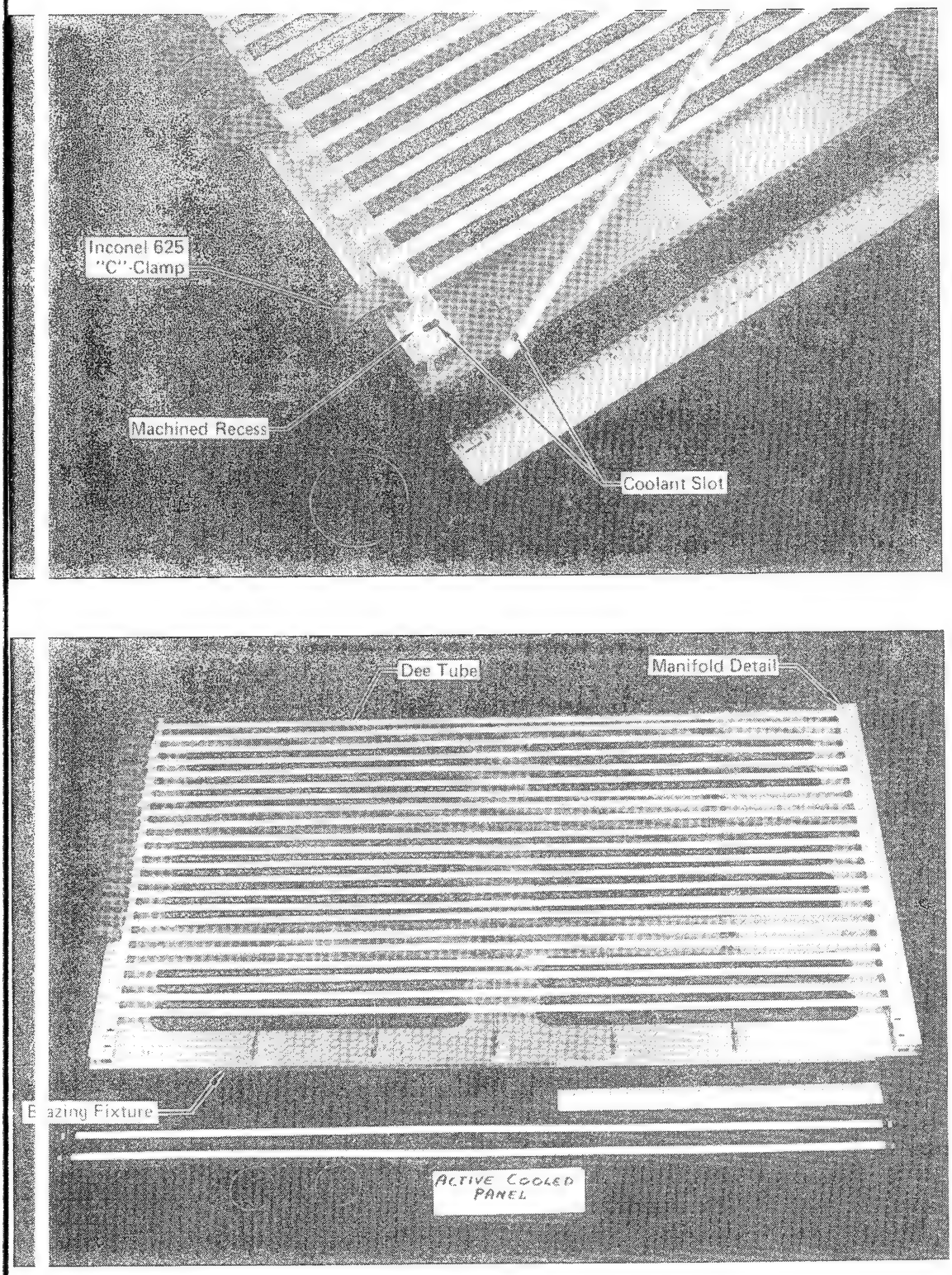

FIGURE 79
TUBES/MANIFOLD DETAIL/BRAZING TOOL AND CLAMPS

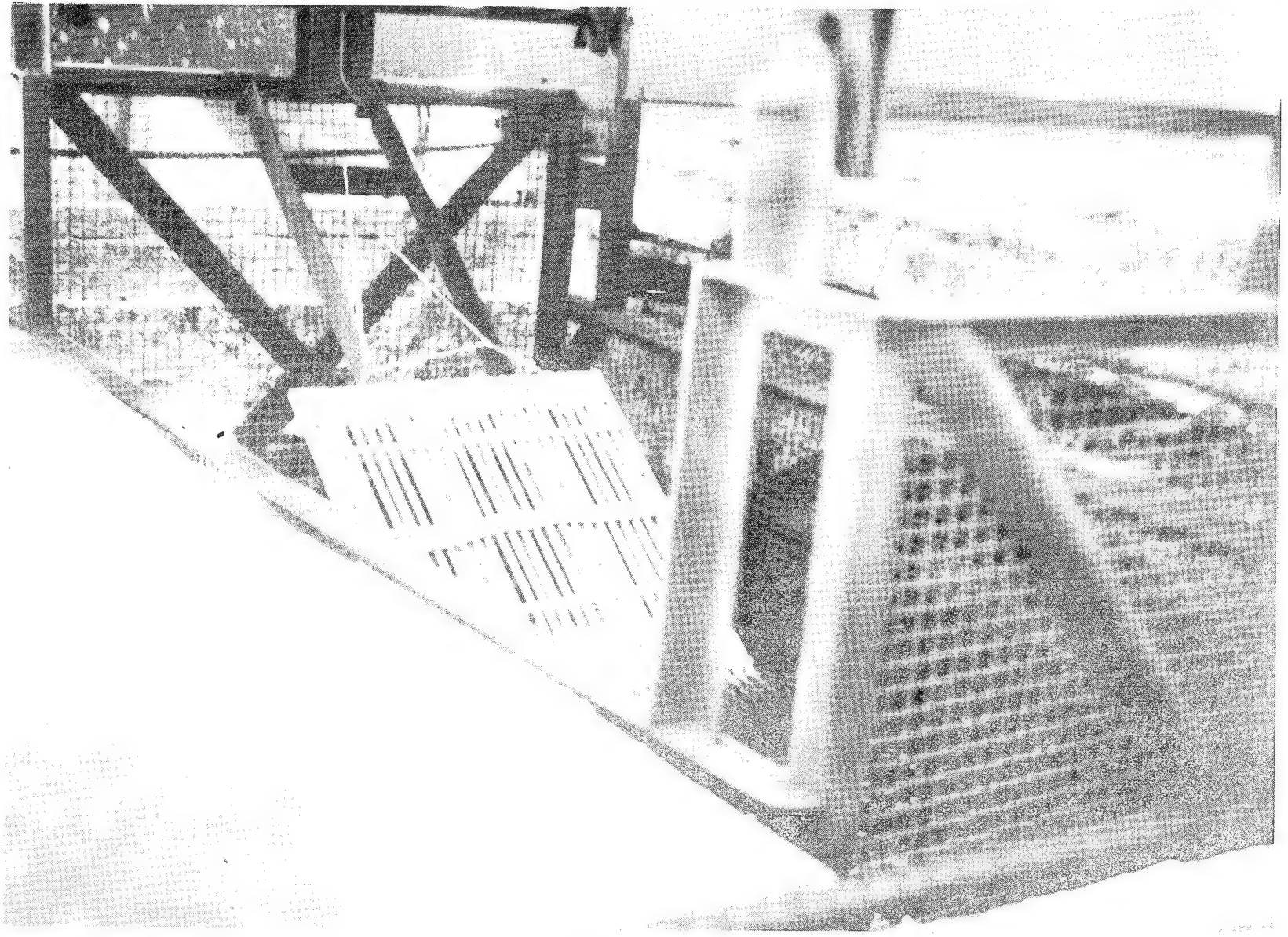

FIGURE 80
TUBE/MANIFOLD BRAZING OPERATION

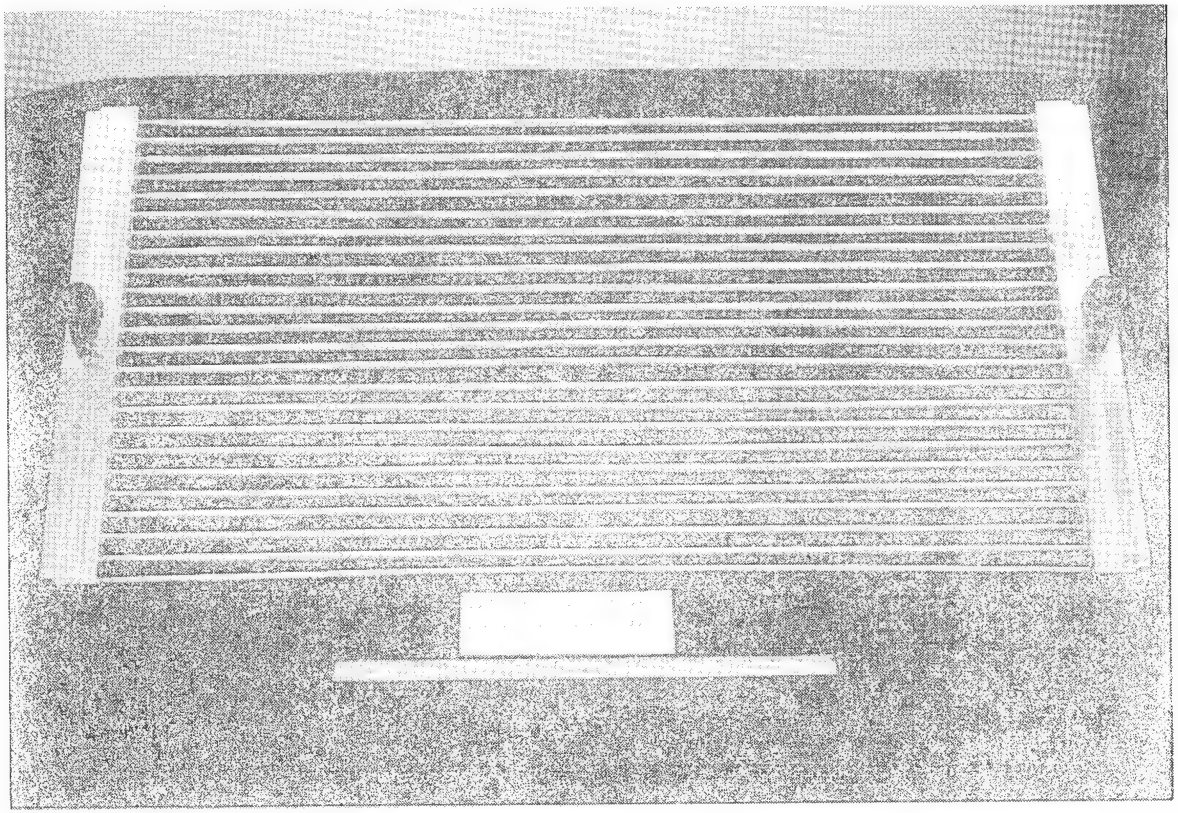

FIGURE 81
TUBE/MANIFOLD ASSEMBLY

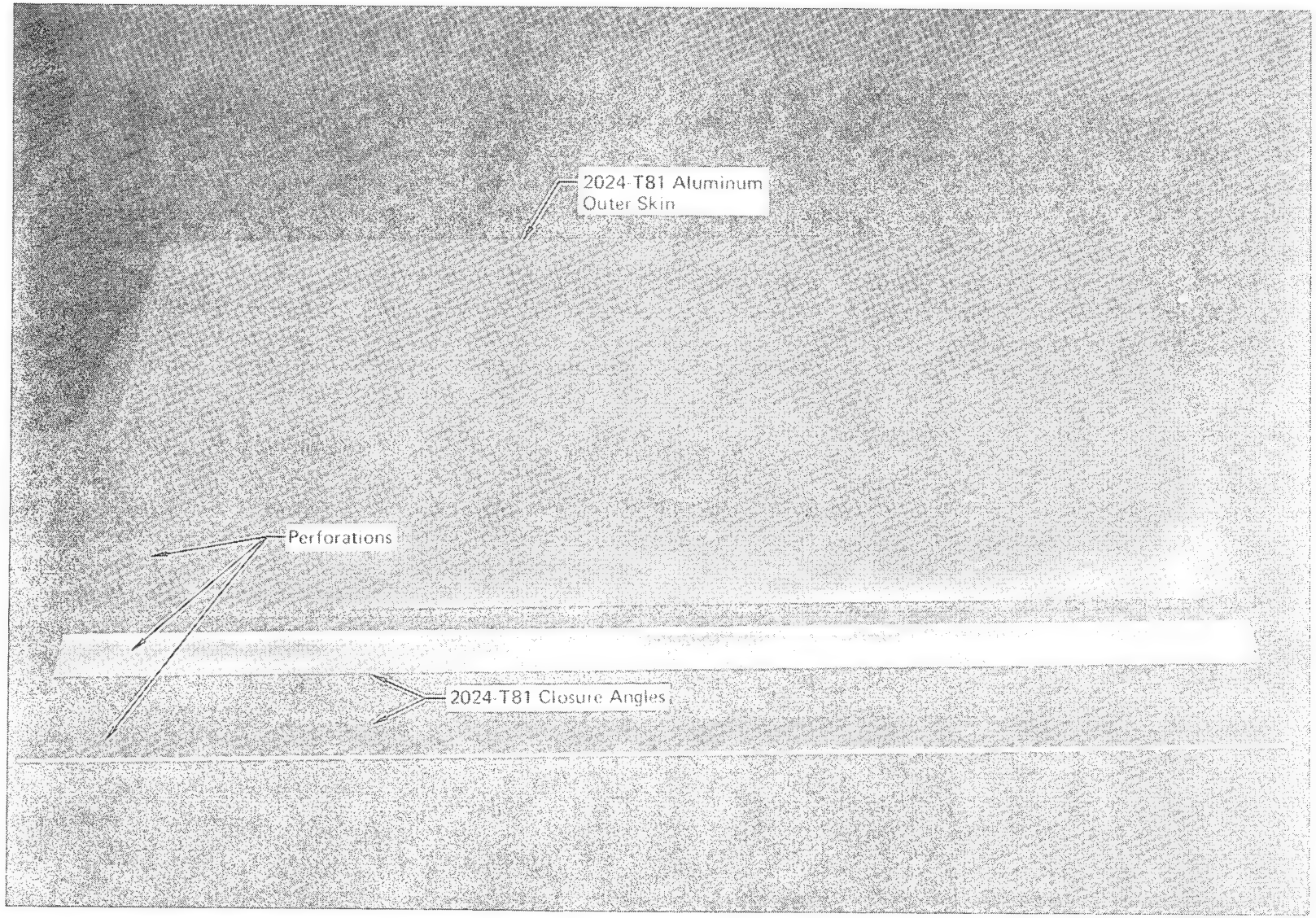

FIGURE 82
PERFORATED OUTER SKIN AND CLOSURE ANGLES

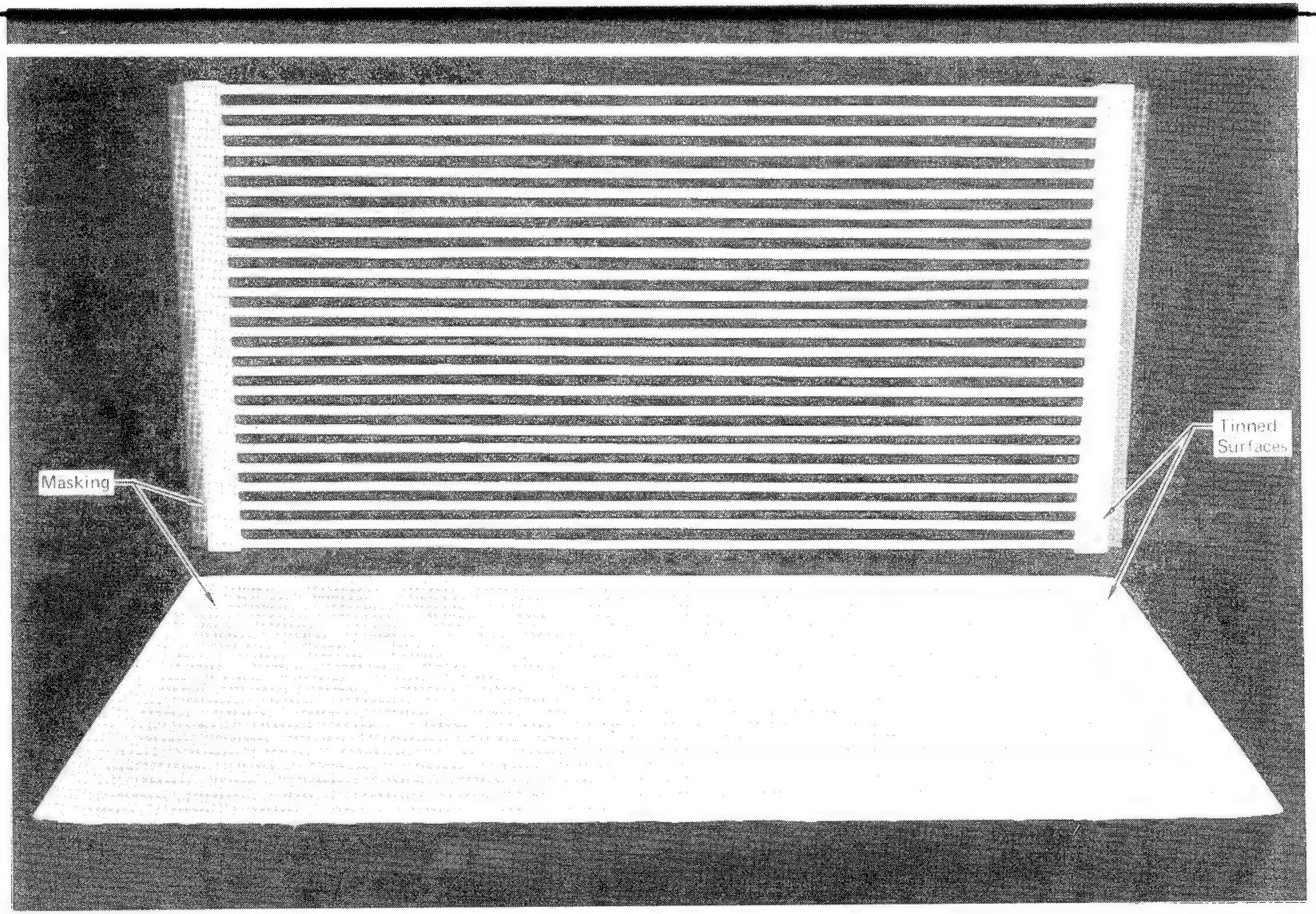

FIGURE 83
TINNED OUTER SKIN AND TUBE/MANIFOLD ASSEMBLY

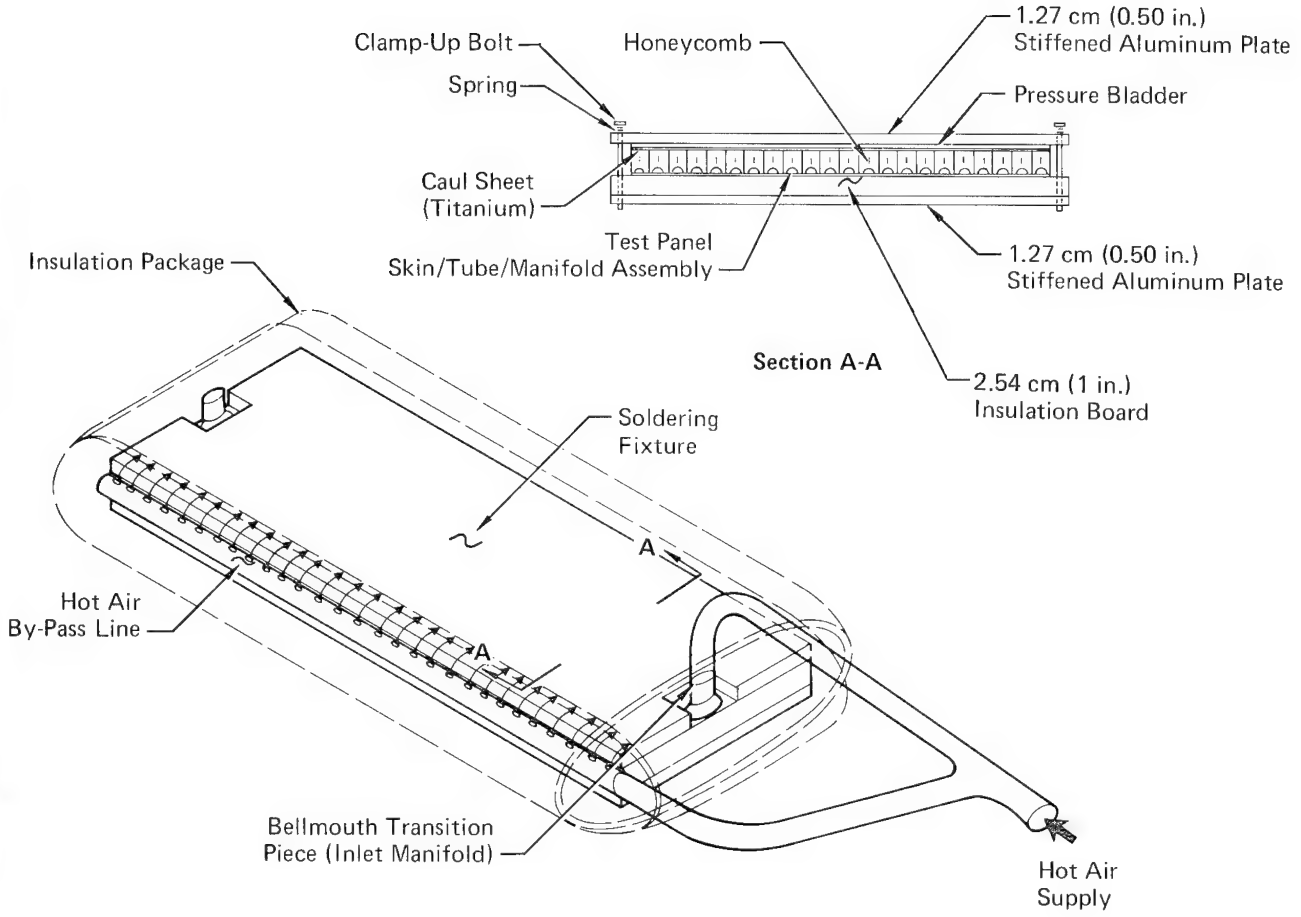

FIGURE 84
SETUP FOR MAINTAINING CORRECT SOLDERING
TEMPERATURE PROFILE

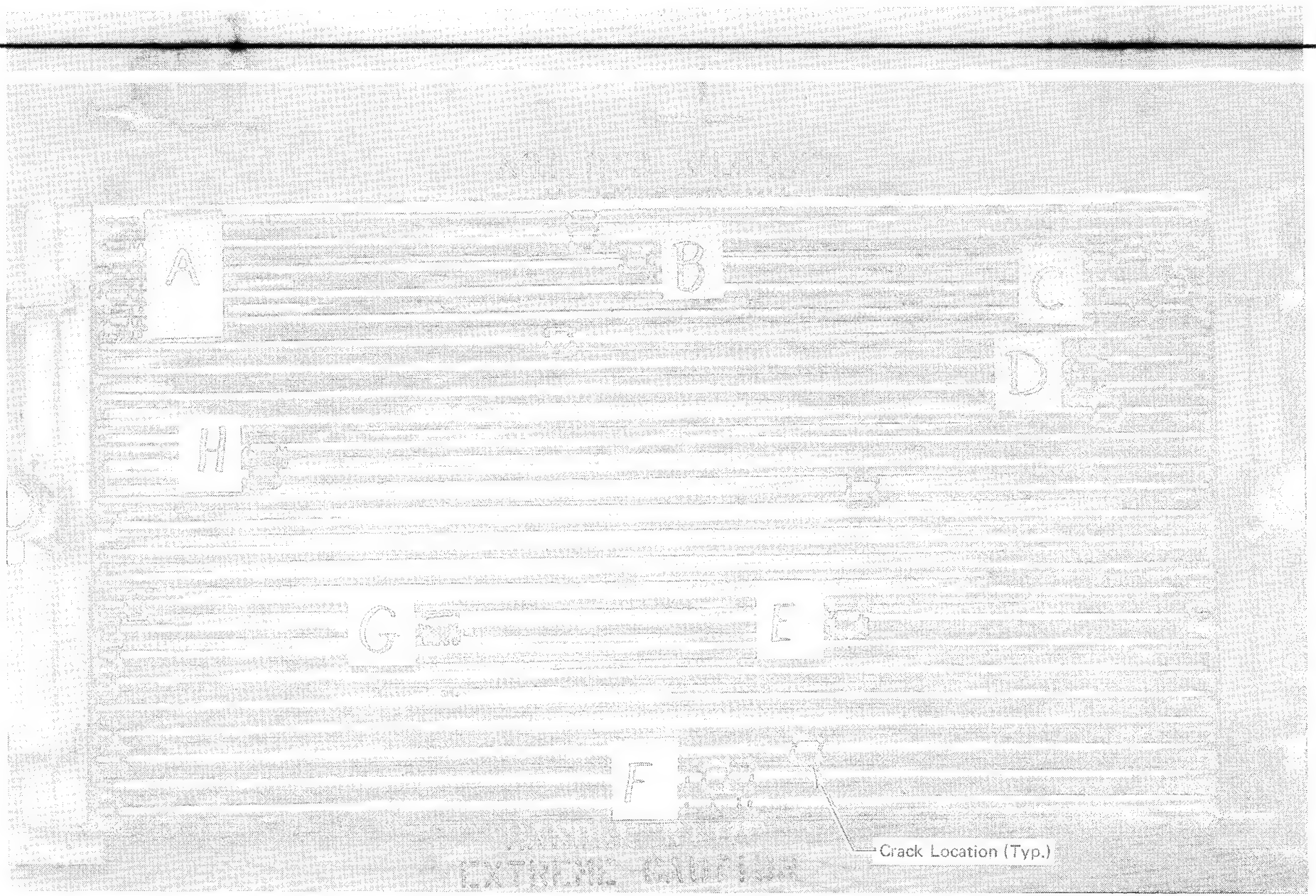

FIGURE 85
LOCATION OF CRACKS AND LEAKS IN TUBE/MANIFOLD ASSEMBLY

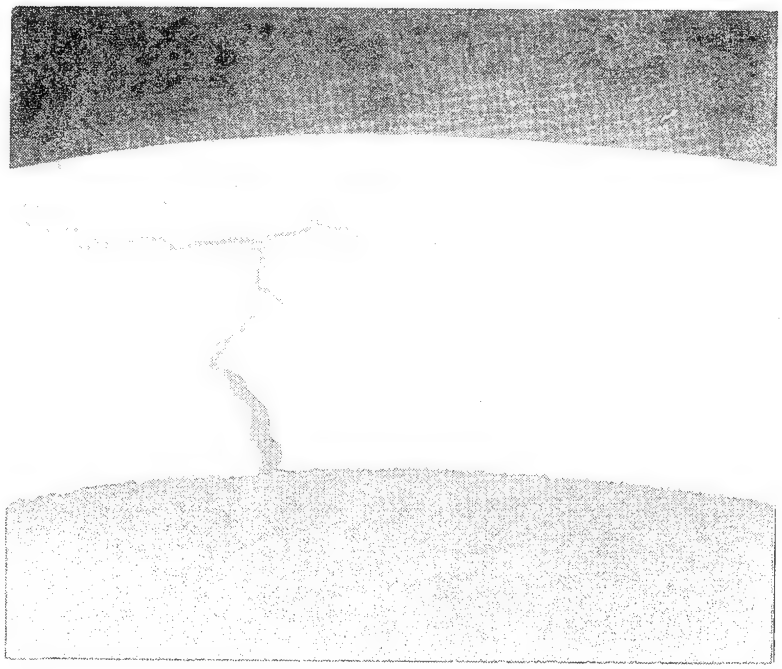

Unetched - 50X

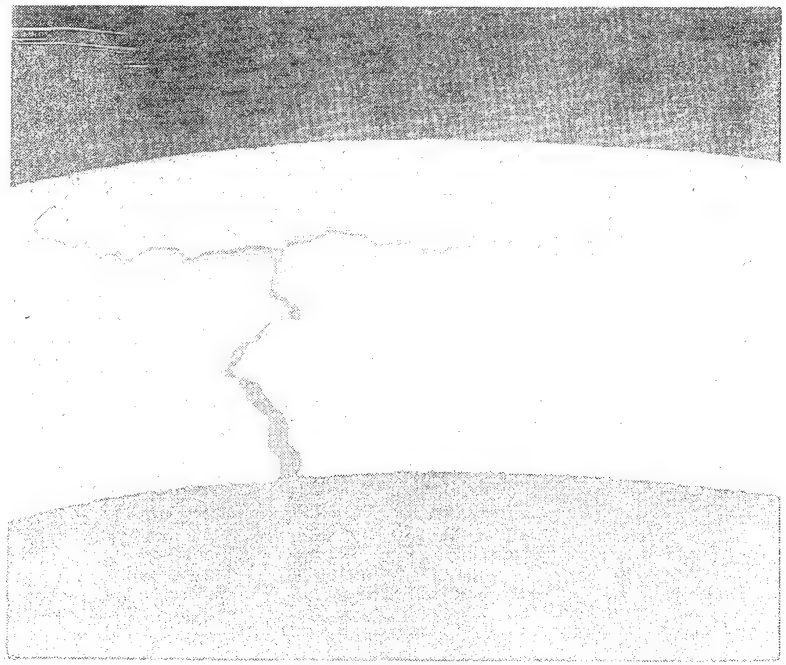

Etched - 50X

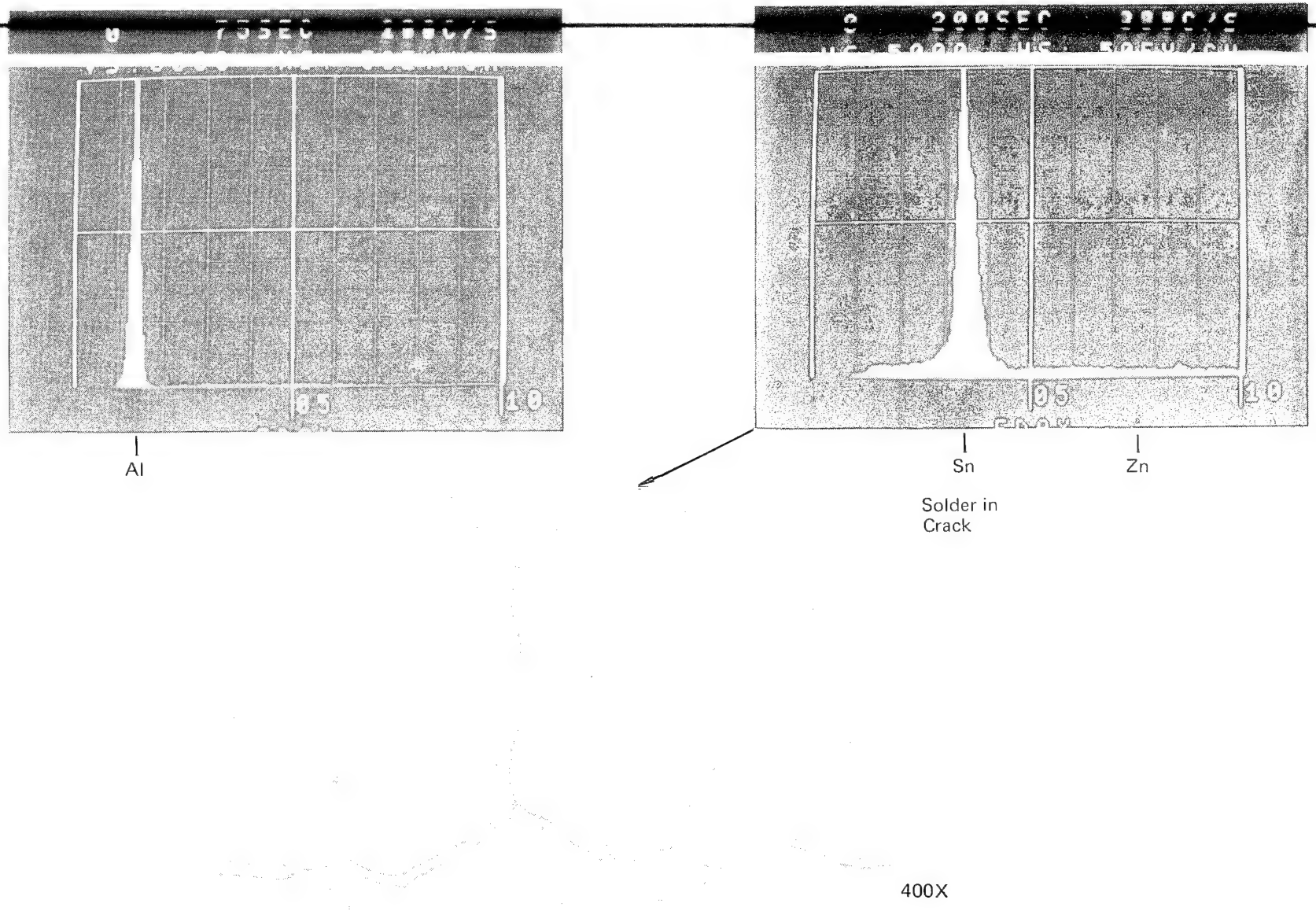

FIGURE 87
MICROSTRUCTURE OF CRACKS IN 6061-T6 TUBE

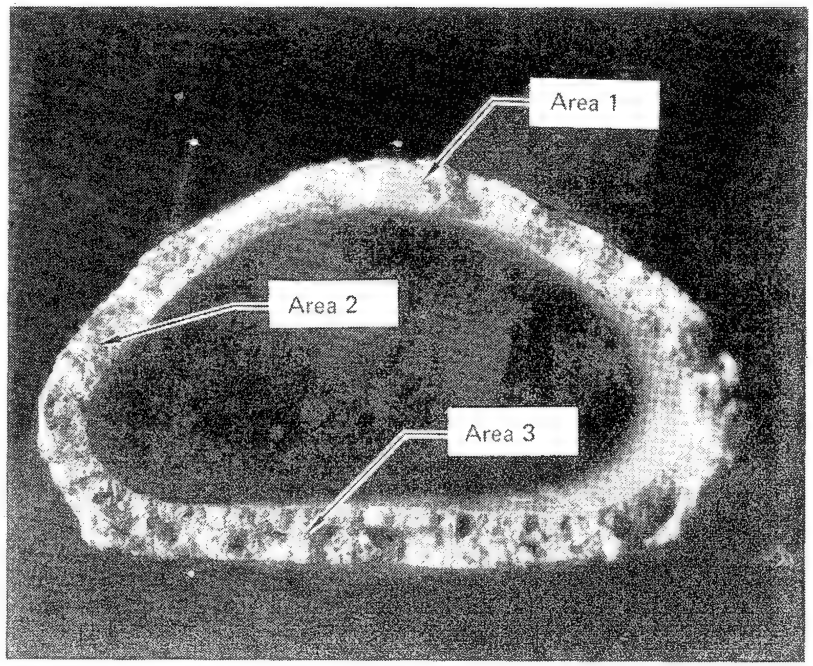

Cross Section - Ruptured Tube

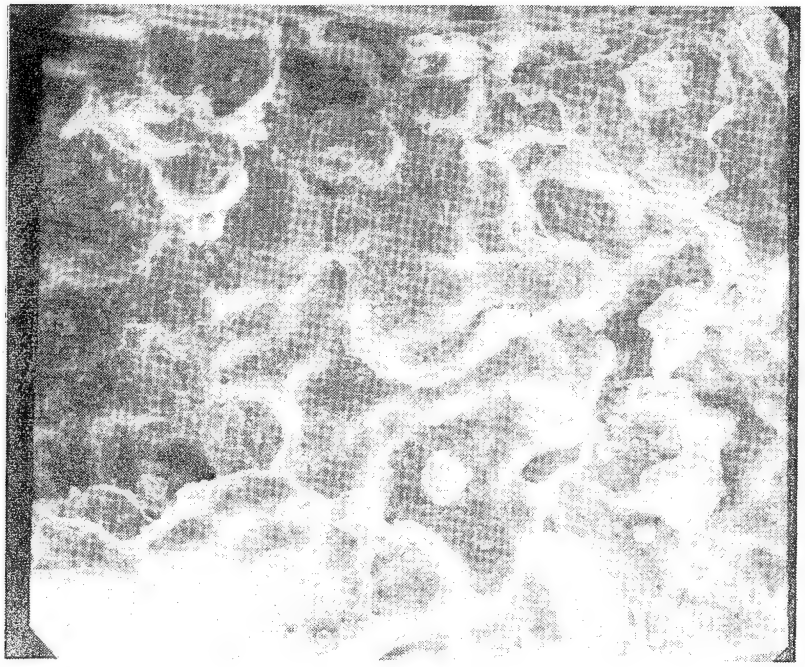

Solder Covered Surface (SEM)
- Area 3 -

Note:
Areas 2 and 3 cracked in processing.
Area 1 mechanically fractured for examination.

FIGURE 88
SOLDER MIGRATED INTO CRACK IN TUBE DURING SOLDERING OPERATION

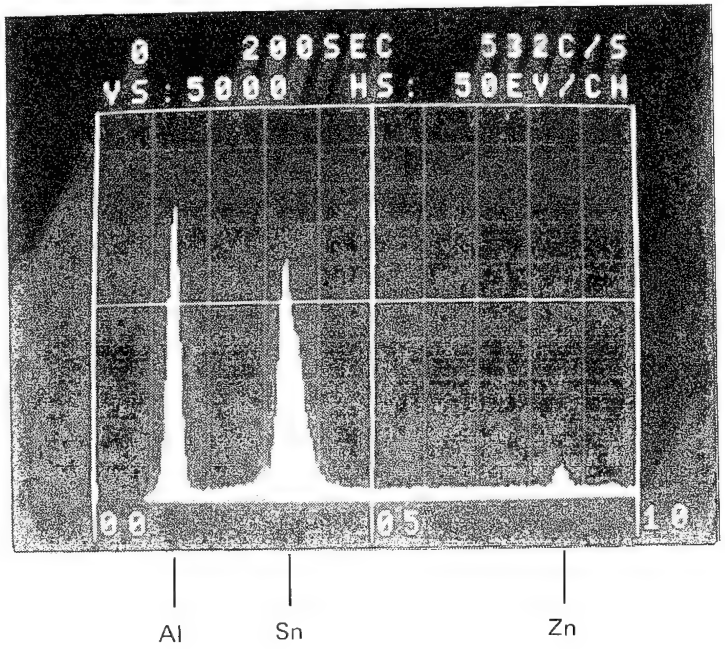

Energy Dispersion Analyzer (X-ray), EDAX, Analysis

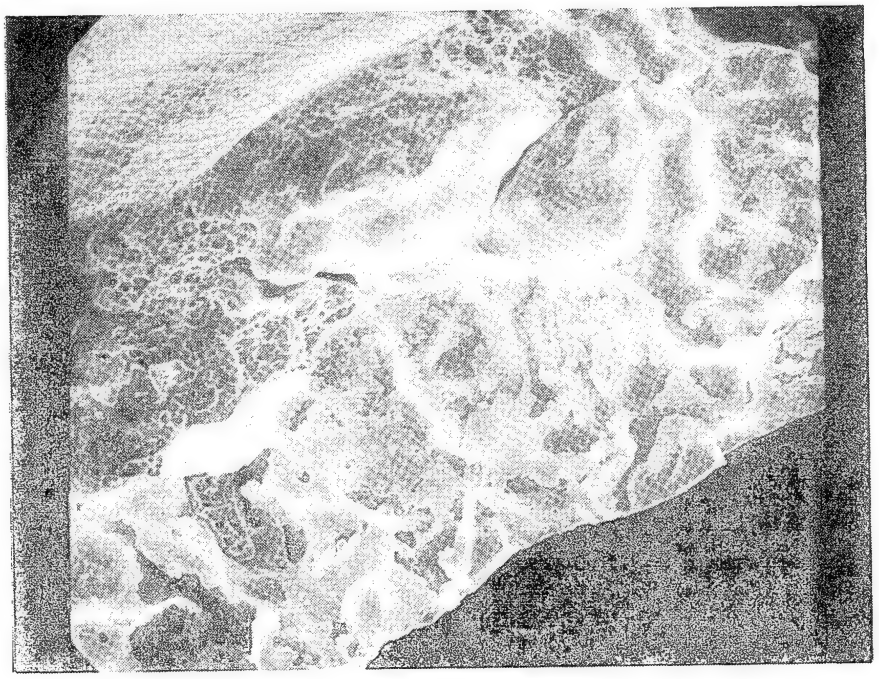

Fracture - Solder Contamination
Area 2 - SEM-100X

FIGURE 89
EDAX INDICATES SOLDER MIGRATED INTO CRACK IN TUBE DURING SOLDERING OPERATION

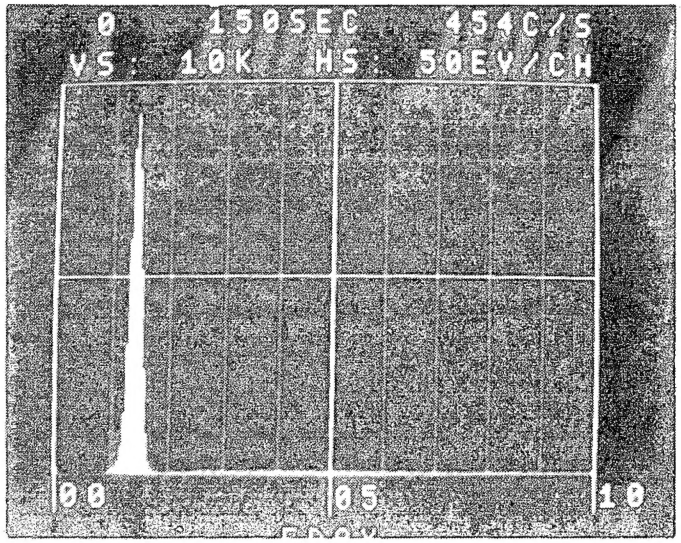

Energy Dispersion Analyzer (X-ray), EDAX, Analysis

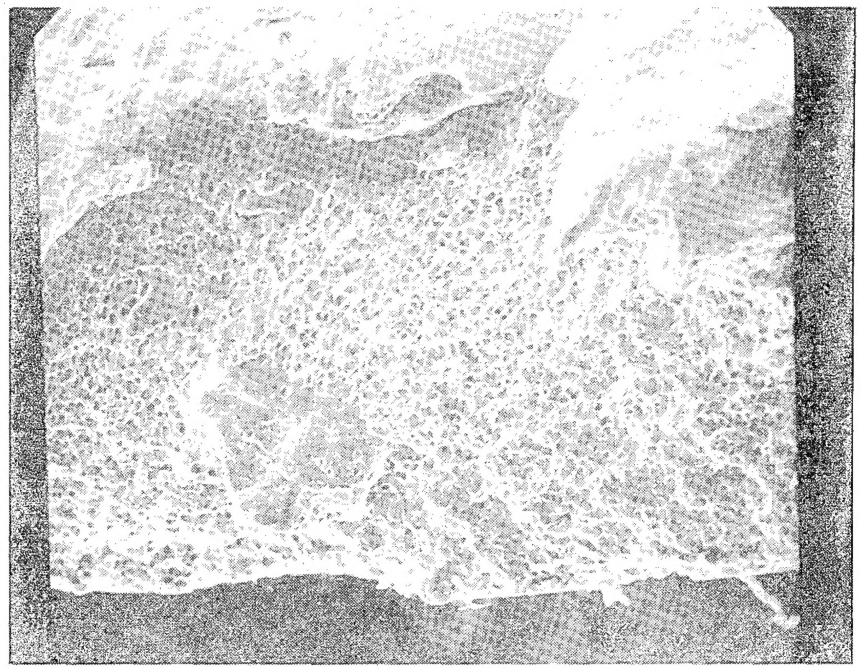

Fracture - No Solder
Area 1 - SEM-100X

FIGURE 90
EDAX INDICATES NO SOLDER ON MECHANICALLY
FRACTURED AREA OF TUBE

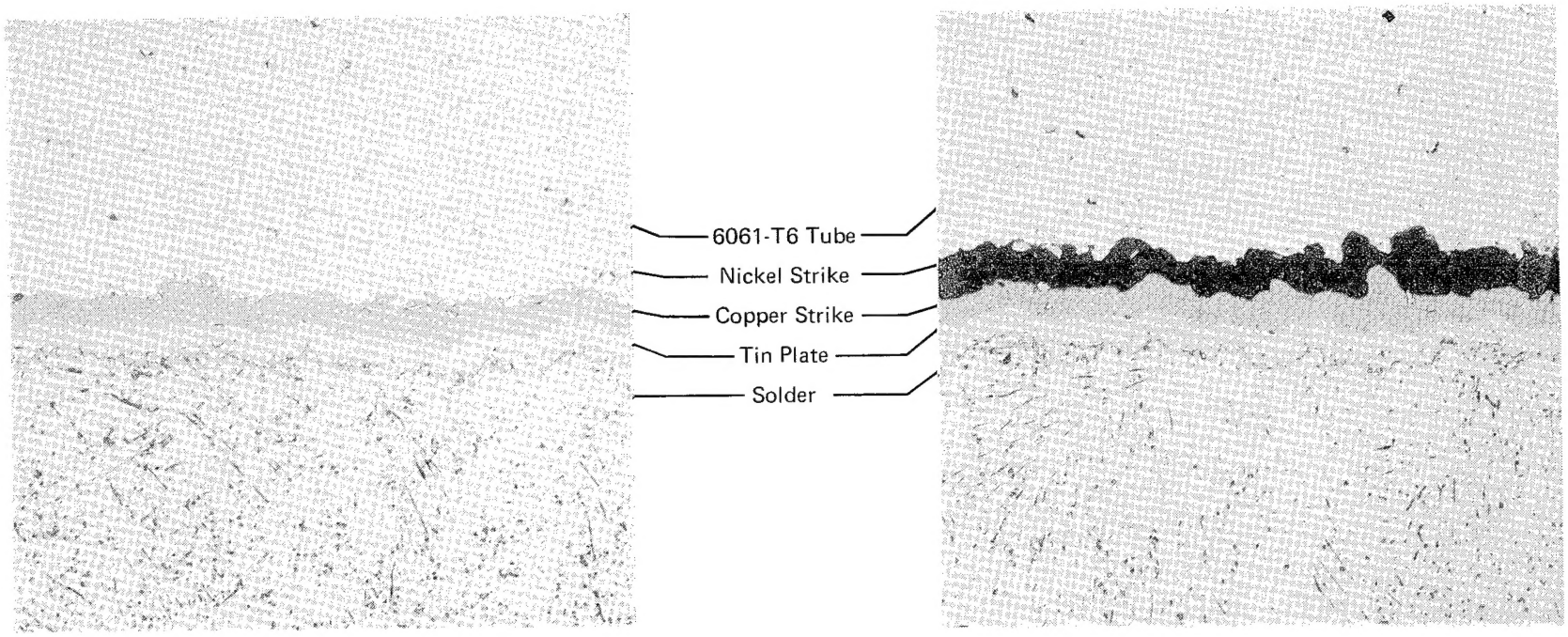

"Sound" Joint
(400X)

Adjacent Area Showing
Separation of Copper
Strike at Tube Boundary

FIGURE 91
NICKEL/COPPER/TIN PLATED AND SOLDERED TUBE END OVER MANIFOLD

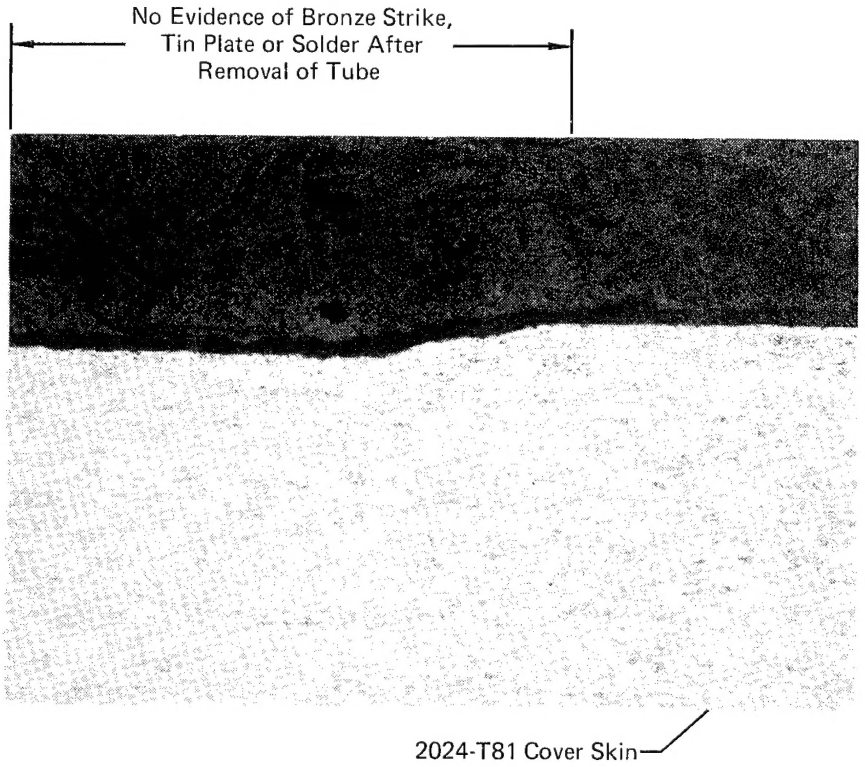

FIGURE 92
INDICATION OF EROSION APPARENTLY DUE TO SOLDER PENETRATING PLATING ON 2024-T81

1. Report No.	2. Government Accession No.	3. Recipient's Catalog No.
NAS CR-2959		

4. Title and Subtitle	5. Report Date
HIGH HEAT FLUX ACTIVELY COOLED HONEYCOMB SANDWICH STRUCTURAL PANEL FOR A HYPERSONIC AIRCRAFT	December 1978
	6. Performing Organization Code
7. Author(s) L. J. Koch and L. L. Pagel	8. Performing Organization Report No.
	10. Work Unit No.
9. Performing Organization Name and Address McDonnell Douglas Corporation P.O. Box 516 St. Louis, MO 63166	11. Contract or Grant No. NAS1-12919
	13. Type of Report and Period Covered Contractor Report
12. Sponsoring Agency Name and Address National Aeronautics and Space Administration Washington, D.C. 20546	14. Sponsoring Agency Code

15. Supplementary Notes

Langley Technical Monitor: Robert J. Nowak
Assistant: James C. Robinson

Final Report

16. Abstract

This report presents the results of a program to design and fabricate an uncooled actively cooled structural panel for a hypersonic aircraft. The design is an all-aluminum honeycomb sandwich with embedded cooling passages sodered to the inside of the outer moldline skin; the coolant is a 60/40 mixture of methanol/water. The panel was mass optimized to sustain 20000 cycles (5000 x scatter factor of 4) of ±210 kN/m (±1200 lbf/in.) inplane loading combined with a 6.9 kPa (±1.0 psi) uniform pressure while subjected to a 136 k W/m^2 (12 BTU/ft^2 sec) uniform heat flux. Six fatigue specimens, of critical panel areas, were fabricated by McDonnell Aircraft Company and tested (at room temperature) by NASA. A representative test panel was not fabricated because of problems with the plating/soldering process. The overall finding is that an actively cooled structure appears feasible for application on a hypersonic aircraft, but the fabrication process is complex and some material and manufacturing technology developments are required. Results from the program are summarized in the body of the report and supporting details are presented in several appendices.

17. Key Words (Suggested by Author(s))	18. Distribution Statement
Actively Cooled Structure High Heat Flux Hypersonic Aircraft Fatigue Specimen Results Fabrication Experience	Unclassified – Unlimited SUBJECT CATEGORY 39

19. Security Classif. (of this report)	20. Security Classif. (of this page)	21. No. of Pages	22. Price*
Unclassified	Unclassified	171	$8.00

* For sale by the National Technical Information Service, Springfield, Virginia 22161

NASA-Langley, 1978